SILICON SHEPHERD

Designing Alicanto, a novel spacecraft for extraterrestrial in-situ biomining
Final Report

AE3200: Design Synthesis

Group 3

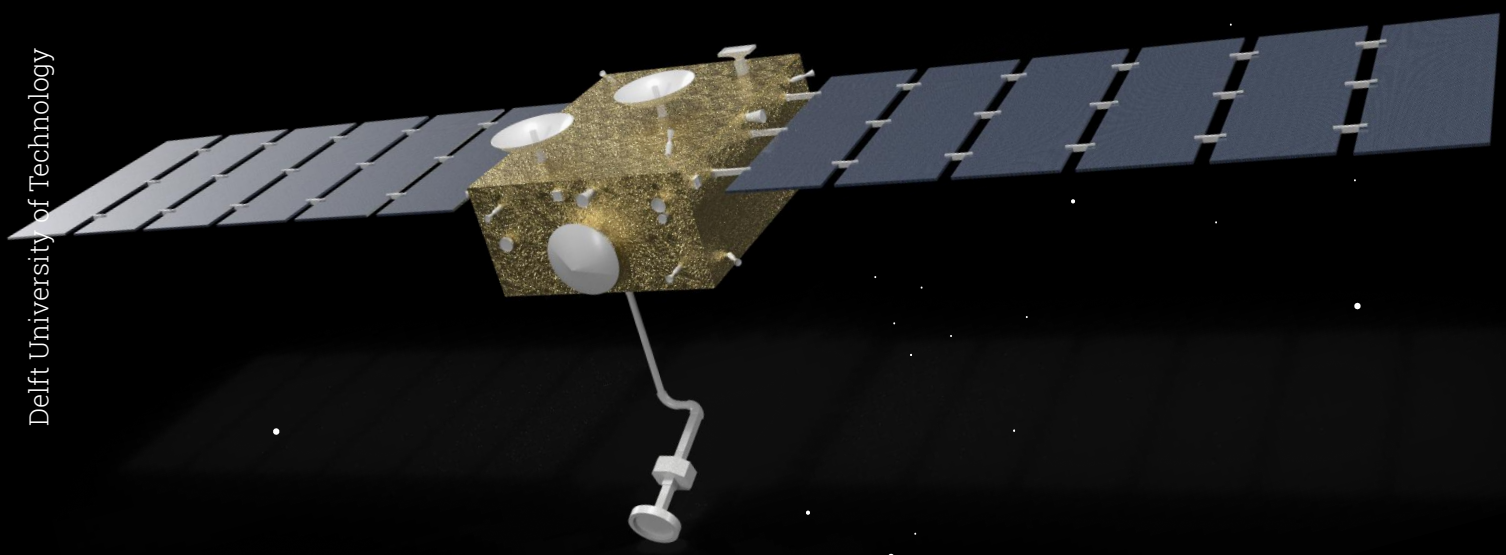

Delft University of Technology

TU Delft

This page has been intentionally left blank

SILICON SHEPHERD

Designing Alicanto, a novel spacecraft for extraterrestrial in-situ biomining
Final Report

by

DSE Group 03

Student Name	Student ID
Roy Cavalini	5974534
Chiem Denen	5923018
Alexis Harvey	5008786
Andries Nusselder	4791363
Theotime Pinchart	5685958
Lucas Puigjaner Montesinos	5907829
Tim Sevenhuijsen	5981387
Nishan Fernando	5002729
Ben Wilson	5564581

Statement on the usage of generative AI

Within this report, generative AI has been used for general research purposes as a means to gather sources. It has also been used to check grammar/spelling in addition to general help with LaTeX formatting for tables and figures.

Tutor:	Niels F.W. Ligterink
Project Duration:	April, 2026 - June, 2026
Faculty:	Faculty of Aerospace Engineering, Delft

Cover:	Render of *Alicanto* Spacecraft in-situ at Itokawa
Style:	TU Delft Report Style, with modifications by Daan Zwaneveld

TU Delft

Table of Contents

Executive Overview

With Rare Earth Elements (REEs) and Platinum Group Elements (PGEs) scarce and critical for modern technology, industrialising the biomining of Near-Earth Asteroids (NEAs) provides a sustainable and scalable alternative to terrestrial extraction. Because global REE mining and refining capacities are heavily monopolised by a single nation, the European supply chain remains highly vulnerable to disruption.

- **Mission Need Statement:** Demonstrate autonomous space-based biomining on a near-Earth asteroid.
- **Project Objective:** Design at Phase 0 an ESA F-class mission utilising an integrated bioreactor spacecraft system to demonstrate autonomous biomining of near-Earth asteroids.

Mission Concept & Strategic Motivation

The Silicon Shepherd Phase 0 study represents a pioneering preliminary design for an autonomous asteroid biomining spacecraft (Alicanto), intended to provide a flight-validated stepping stone toward larger-scale space resource utilisation. Funded under the ESA Science Programme's F-class call, the mission is strictly bounded by a €205 M cost cap (excluding launch) and an Ariane 62 rideshare envelope. Furthermore, the architecture is driven by COSPAR Category V Earth-return planetary protection regulations and BSL-1 organism containment rules. To achieve compliance within an tight schedule up until manufacturing (May 2032), the design philosophy heavily leverages flight-proven heritage architectures.

Rather than acting as a commercial extraction venture, the mission is a technology demonstrator. Its primary value lies in generating space-biomining process heritage and strategic-supply intelligence, maturing a long-term European supply-diversification option. To maximise strategic relevance, the mission targets critical raw materials covered by the EU Critical Raw Materials Act, focusing specifically on Tier-1 magnet REEs (Nd, Pr, Dy, Tb). The ultimate objective is to prove the feasibility of autonomous in-situ biomining by returning a minimum of 5 g of asteroidal material enriched by a factor of at least 50×, guaranteeing the detection of at least five distinct REE species for terrestrial curation.

These strategic drivers and safety constraints directly shaped the scientific baseline. From an initial pool of over 40,000 NEAs, 25143 Itokawa was selected as the target due to its well-characterised S-type silicate composition, which hosts the necessary phosphate phases for REE extraction and is analogous to the L-chondrite substrate used in prior ISS experiments. For the biological payload, the fungus *Penicillium simplicissimum* was selected for its demonstrated high-yield extraction of REEs from meteoritic material in microgravity, alongside its robust tolerance to the deep-space environment and compliance with BSL-1 safety standards.

Mission Development Logic

To translate the mission concept into flight-ready hardware, the project establishes a comprehensive functional architecture that governs both the engineering lifecycle and flight operations. This logic allocates specific functions across the subsystems and defines critical autonomous decision gates, most notably an in-situ mass-verification gate following the Touch-And-Go (TAG) sampling manoeuvre. This allows the spacecraft to autonomously command additional sampling attempts if the required regolith yield is not met before committing to the bioleaching phase.

The post-Phase 0 development logic matures this architecture into a flight-ready mission through Phase A/B detailed design and a strict 48-month Phase C/D implementation cycle, baselined against ESA F-class heritage. To meet this schedule, the Manufacturing, Assembly, and Integration (MAI) plan executes three parallel streams: the spacecraft bus, the payload, and the Sample Return Capsule (SRC).

The spacecraft bus relies heavily on flight-proven hardware, while the SRC is procured as a sealed, pre-sterilised Category-V assembly with its own qualification dossier. The payload stream dictates the critical path, driven by long-lead LMC_{OOL} chip fabrication and heritage-light biological qualification of the bioreactor.

To manage schedule risk, critical payload components are authorised for advance procurement at the start of Phase C. During spacecraft-level integration, the payload is mated to the bus first, while the SRC is mated last to preserve access to the biological loading port. Loading of lyophilised *P. simplicissimum* and sterile media is deferred until after environmental testing under ISO Class 5 laminar flow to prevent culture degradation and respect shelf-life limits.

Mission Operations & Trajectories

Deep-space operations are jointly managed by ESA's European Space Operations Centre (ESOC) for flight dynamics, and the European Space Astronomy Centre (ESAC) for science operations and sampling site selection. Because the one-way light time (tens of minutes to over an hour) to Itokawa precludes real-time ground control, the spacecraft relies heavily on autonomous execution for critical proximity manoeuvres, hazard detection, and the Touch-And-Go (TAG) sampling descent.

Due to Itokawa's negligible and highly irregular gravity field, stable low-altitude orbits are challenging. Instead, proximity operations rely on autonomous station-keeping at distinct altitudes. The spacecraft utilises a Home Position (20 km) as a safe harbour for data downlink and the prolonged 120-day active bioleaching phase. It descends to a Mapping Position (5 km) to compile global shape and thermal models, and a Siting Position (500 m) for high-resolution candidate site screening. Finally, the spacecraft descends to the Sampling Position for the autonomous TAG regolith capture manoeuvre.

To enable this operational campaign, the astrodynamic baseline connects a strict 1300 kg rideshare launch constraint to the heliocentric Earth–Itokawa transfer. To avoid relying on an external kick stage, the spacecraft executes a chemical departure burn from a High-energy Earth-bound Orbit (HEO) to achieve a post-escape energy of $C_3 = 6\ \mathrm{km}^2/\mathrm{s}^2$. The nominal mission spans approximately 3.2 years, divided into a 350-day outbound cruise, a 436-day Itokawa residence phase, and a 365-day return cruise. During the heliocentric transfer phases, the spacecraft relies on highly efficient ion propulsion, requiring a total margined ΔV of 3.86 km/s.

The operational lifecycle concludes with Earth return, where the trajectory safely limits the atmospheric entry speed to a strict 12.9 km/s cap. The spin-stabilised Sample Return Capsule (SRC) is deployed into the entry corridor for recovery at the Woomera Test Range in Australia, operating under strict COSPAR Category V biological containment protocols. Immediately following SRC separation, the main spacecraft bus executes a chemical deflection manoeuvre to enter a passivated, safe heliocentric disposal orbit.

Payload Design

The scientific payload is designed to execute the autonomous biomining objectives, monitor biological integrity, and ensure the safe return of the enriched asteroidal material.

Remote Sensing Suite: A highly miniaturised 10.8 kg instrument suite provides critical optical navigation and supports sample site selection. It features a narrow-angle/wide-angle camera block for stereophotoclinometry (SPC) shape modelling and a laser ranging set. The suite is augmented by two spectrometers: a MERTIS-heritage thermal-infrared spectrometer to map the 10.3 μm absorption band of target phosphates and derive thermal-inertia grain sizing, and a NIRS3-heritage near-infrared spectrometer to map the 3.4 μm band for acid-neutralising carbonates, ensuring a biologically favourable sampling patch is selected.

Sampling Mechanism: To extract the an average of 500 g of bulk regolith per Touch-And-Go (TAG) manoeuvre, the spacecraft uses a 1.4-metre deployable collection arm heavily inspired by the OSIRIS-REx Touch-And-Go (TAG) architecture. During the brief surface contact, pressurised nitrogen fluidises surface debris into a sealed collection head, from which the material is pneumatically transferred directly into the MISAR bioreactor. The system is designed to support up to six independent TAG attempts.

Bioreactor (MISAR): The Microbial Separator of Asteroidal Regolith (MISAR) utilizes a spent-medium, fed-batch architecture to keep the microorganism growth chamber separate from the regolith substrate. Lyophilised *Penicillium simplicissimum* conidia are rehydrated in-situ to produce oxalic acid. This acid leaches the target regolith, while an electro-dialysis unit retains metal ions within the reactor. A dual-filter setup isolates the resulting high-purity Rare Earth Element (REE) oxalate crystals to achieve the required 50× enrichment. The system operates autonomously over a 120-day bioleaching phase, sized at approximately 139 kg with a 20% margin.

Health Monitoring System (HMS): Culture health and containment integrity are tracked via a hierarchical four-tier system to optimise power and consumable usage. Tier 0 and Tier 1 provide continuous hardware and environmental monitoring (pH, dissolved O_2, CO_2, temperature, and biomass). Tier 2 assesses organic acids and metal ions hourly. Tier 3 utilizes the highly sensitive $\mathrm{LMC}_{\mathrm{OOL}}$ chip instrument to perform periodic biological integrity checks by tracking molecular biomarkers, including DNA/RNA oxidative stress, cellular ATP energy status, and specific amino acid profiles, ensuring the culture remains viable for bioleaching.

Sample Return Capsule (SRC): The 46 kg SRC is a passive, parachute-decelerated vehicle built upon Stardust flight heritage. Deployed four hours before atmospheric entry and spin-stabilised to 15 RPM, the SRC protects the enriched samples using a Phenolic-Impregnated Carbon Ablator (PICA) heat shield. The capsule is targeted for a strict $-7.6°$ flight path angle at 12.88 km/s, decelerating under a 40 g structural limit before deploying a 7.66-metre triconic main parachute for a controlled, low-velocity touchdown (<5 m/s) at the Woomera Test Range in Australia.

Spacecraft Bus

The spacecraft bus is designed to operate autonomously in the deep-space environment, providing the necessary power, thermal stability, data routing, and precise manoeuvre authority to support the demanding proximity operations and biological payload requirements.

Structures: The primary structural bus utilizes honeycomb sandwich panels featuring 1 mm CFRP UD tape face sheets and a 10 mm Aluminium 3003 core. This configuration was selected to maximize mass efficiency while surviving the Ariane 62 longitudinal and lateral launch loads, with panel buckling identified as the critical design driver. The structure comfortably maintains strict compliance with the 1300 kg rideshare wet-mass limit.

Propulsion: A highly capable hybrid propulsion architecture drives the mission. The main heliocentric transfer utilizes a 1+1 cold-redundant pair of European ArianeGroup RIT-2X Gridded Ion Thrusters, selected for their power to thrust efficiency. The system is fed by 113.7 kg of Xenon stored in a single-phase supercritical state (150 bar, 20°C) within a spherical Composite Overwrapped Pressure Vessel (COPV) to ensure a static centre of mass. For the high-thrust Earth-departure burn ($\Delta V = 366$ m/s), proximity station-keeping, reaction-wheel desaturation, and the critical post-SRC deflection manoeuvre, a separate green monopropellant Chemical/RCS system is employed. This system utilizes 227 kg of LMP-103S feeding a network of fourteen 22 N Bradford ECAPS HPGP thrusters.

Attitude Determination & Control (ADCS): Three-axis stabilization is provided by four Bradford W18 reaction wheels in a skewed pyramid configuration, specifically dimensioned to counter the dominant Solar Radiation Pressure (SRP) disturbance torques. Precision pointing knowledge ($\leq 0.005°$) is guaranteed by a single-fault-tolerant suite of three ASTRO APS star trackers, augmented by Astrix NS fibre-optic IMUs and coarse Sun sensors. To safely manage asteroid-relative navigation without a stable orbit, a dedicated LiDAR suite (PALT for kilometre-scale approach and TRIS/LRF for terminal Touch-And-Go descent) provides direct altitude and ranging observables to the GNC filter.

Electrical Power System (EPS): Power generation relies on two single-axis articulated solar array wings (38 m^2 total deployed area) utilizing triple-junction GaAs cells. Because solar flux varies drastically, the EPS employs a dynamic throttling strategy: the arrays produce an 8.1 kW surplus at 1 AU (Beginning of Life) to maximize early ion thrust, scaling down to securely deliver the required 3.99 kW at 1.7 AU (End of Life) for simultaneous propulsion and housekeeping. A 1890 Wh Li-ion battery (capped at 30% Depth of Discharge to preserve cycle life) handles LEOP, transient loads, and provides a 2-hour Safe Mode survival buffer.

Thermal Control System (TCS): The mission is heavily cold-biased due to the deep-space environment. The TCS isolates the bioreactor using low-conductivity titanium standoffs and maintains the strict 25 ± 5°C bioleaching setpoint using Kapton heaters, while a 0.3 kg n-heptadecane Phase Change Material (PCM) safely buffers short-term metabolic and sensor transients. Heat rejection is managed via an ammonia Variable Conductance Heat Pipe (VCHP) linked to an Optical Solar Reflector (OSR) radiator, alongside a dedicated radiator for the ion Power Processing Unit (PPU) and a deep-cold 188 K radiator to suppress dark current in the remote sensing VNIRS detector.

Command & Data Handling (C&DH): Operating as the spacecraft's central nervous system, the C&DH utilizes a 1-fault-tolerant, hot/cold redundant pair of radiation-tolerant GR712RC (LEON3FT) processors. Data routing is physically isolated to prevent contention: a MIL-STD-1553B platform bus manages housekeeping, while a SpaceWire Payload network handles high-bandwidth sensor polling. A 64 Gbit Solid State Recorder buffers the massive 1.9 GB proximity science campaign to prevent downlink bottlenecks. The system also hosts a 3-tier autonomous FDIR engine capable of executing a zero-data-loss "Deep Safe" mode if critical anomalies arise during communication blackouts.

Telemetry, Tracking & Command (TT&C): The communication architecture utilizes a resilient X-band and Ka-band switch network mapped to High, Medium, and Low-Gain Antennas. The primary deep-space science downlink relies on a 36 dBi High-Gain Antenna (HGA) requiring precise spacecraft alignment (Comms Mode), seamlessly routing data through a centralized RF-to-baseband bridge linked to the C&DH subsystem.

System Overview & Budgets

With the Payload and Platform subsystems defined, the design conducts a system overview to ensure the spacecraft synthesises accordingly. The external and internal configurations verify compliance with the Ariane 62 rideshare fairing volume, facilitating the placement of all primary subsystems and allowing for preliminary calculation of the spacecraft's Centre of Gravity (CoG). While slight structural asymmetries exist, the CoG deviation is within acceptable limits for Phase 0 and will be refined as design maturity increases.

The system resource budgets, presented in Table 1, consolidate the spacecraft's high-level requirements and cost constraints. Mass is identified as a critical system-level risk due applying a 20% the wet mass pushes to 1273.81 kg, closing with just 26.19 kg remaining against the limit. Mass therefore remains a critical system-level risk requiring strict allocation management. The volume budget closes with ample margin, and the electrical

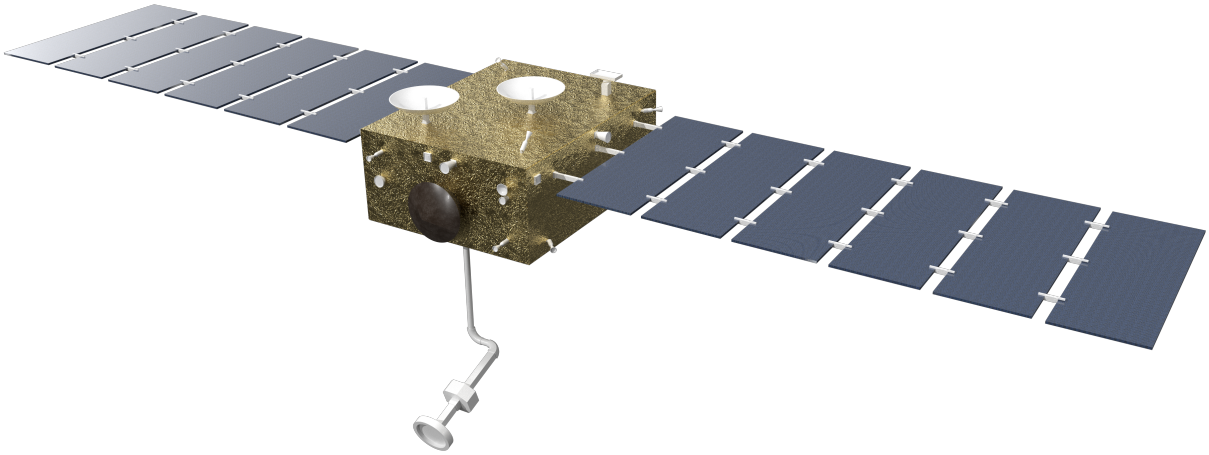

Figure 1: *Alicanto* spacecraft in its deployed flight configuration.

power system is sized to support a peak unmargined load of 3328.0 W, driven primarily by the simultaneous demands of the ion propulsion system and proximity operations.

Table 1: Executive summary of system resource and cost budgets.

Resource	Nominal Value	Margined Total	Limit & Status
Wet Mass	1061.51 kg	1167.66.4 kg (at 10%)1273.81 kg (at 20%)	**1300 kg** allocation. Closes safely at 10%, but leaves only 26.19 kg if the 20% margin is enforced.
Stowed Volume	2061.19 L	2267.31 L (at 10%)	**8800 L** fairing capacity. Non-critical, closes with ample margin.
Peak Power	3328.0 W	3993.6 W (at 20%)	Driven by simultaneous ion propulsion and proximity operations.
Mission Cost	€135–170 M(Base estimate)	€178–224 M(Incl. 20%+10% wraps)	**€205 M** CaC Cap. Target €155 M base successfully closes under cap.

As a single-flight technology demonstrator, the mission's financial return on the ≥ 5 g of REE-enriched material is negligible (−100% ROI based on traded oxide prices). Instead, the primary return is strategic: advancing autonomous space biomining capabilities from TRL 4 to TRL 9 to retire critical process risks and establish a flight-qualified European foothold in the space resources sector.

Verification, Compliance & Design Sensitivity

To ensure the spacecraft satisfies stakeholder needs and mission objectives, a comprehensive Verification and Validation (V&V) framework was established following the systems engineering V-model. Verification relies on a combination of Analysis, Simulation, Review of Design, Inspection, and hardware Testing. Against the current Phase 0 baseline, the system demonstrates strong feasibility: of 112 requirements, 97 are Compliant, 15 are Partially Compliant, and none are Non-Compliant.

Compliance Gaps & Maturation Needs: The 15 Partially Compliant requirements highlight specific areas

requiring maturation in Phase A/B. These include closure of the maximum-range telecommunications link budget, and finalizing payload thermal models.

Design Sensitivity & Robustness: To validate the integrated architecture beyond static compliance, a centralized Monte Carlo sensitivity analysis (10,000 iterations) evaluated interacting uncertainties. The analysis confirmed exceptional margins in the Sample Return Capsule (no structural failure under steep entry dispersions) and the decoupled propulsion strategy. Even when solar array degradation throttles available propulsion power below the 3000 W design point, the system seamlessly trades power for burn duration, securing the trajectory window with a negligible 0.06% trajectory failure rate.

Architectural Vulnerabilities: Conversely, the stochastic model exposed two critical vulnerabilities requiring immediate corrective action. First, compounding dry mass margins create a 15.6% probability of exceeding the launch vehicle capacity if dry mass margins compound aggressively, undermining the baseline design's stability. Second, the nominal 120-day bioleaching timeline possesses zero schedule margin. Because microgravity limits microbial efficiency, the current timeline yielded a 100% probability of schedule failure. To safely proceed into detailed design, a minimum 60-day schedule margin must be formally allocated to the proximity operations phase.

Sustainability, Technical Risks & RAMS

Sustainable Development & Planetary Protection: A screening-tier Life-Cycle Assessment (LCA) confirmed that the Ariane 62 launcher's embedded energy dominates the mission's environmental footprint by two to three orders of magnitude. To minimise launched mass and process hazards, the design leverages electric primary propulsion, CFRP structural facesheets, and LMP-103S green monopropellant, which explicitly eliminates hydrazine toxicity and ground-handling risks. For COSPAR Category V unrestricted Earth-return compliance, the primary containment barrier relies on in-flight biological inactivation. End-of-life debris mitigation is achieved via a non-Earth-intersecting heliocentric divert and full spacecraft passivation. While the energetic cost of returning REEs at demonstration scale is inherently high ($\sim 2 \times 10^{13}$ MJ per kg), the architecture establishes a credible scalability pathway to advance UN Sustainable Development Goals.

Technical Risk Assessment & FDIR: The mission risk framework maps Technology Readiness Levels (TRL) to likelihood probabilities, assign a designated likelihood (A-E) and severity (1-5) providing a risk score (1-25). Pre-mitigation analysis isolated critical vulnerabilities, which are mitigated to acceptable residual levels using specific mitigation strategies. For example, radiation-induced microbial death is mitigated via dedicated radiation shielding; automated regolith-to-bioreactor transfer failures are retired through extensive vacuum life-testing; and biological containment breaches are prevented using dual ground-commandable heat and chemical sterilisation loops. Unforeseen anomalies are managed by an autonomous Fault Detection, Isolation, and Recovery (FDIR) system. The FDIR logic leverages physically reserved contingency buffers (e.g., spare microbial cultures, 25% ΔV margins, and backup survival heater loops) to trigger, isolate, and recover from faults without relying on immediate ground intervention.

RAMS (Reliability, Availability, Maintainability, Safety): The mission establishes an end-to-end reliability target of 0.75 for returning ≥5 g of processed asteroidal material without a containment breach. At the current Phase 0 maturity, system reliability is calculated at 0.55. This shortfall is driven almost entirely by the TRL 4 status of the bioleaching payload and the LMC_{OOL} instruments. Reaching the required threshold dictates the project's critical path: advancing the space bioreactor to TRL 6 through extended microgravity testing and the LMC_{OOL} to TRL 7 prior to the 2032 production start will elevate the integrated post-maturation mission reliability to a compliant 0.754. Safety is strictly anchored by a 2-FT approach against Sample Return Capsule structural disintegration during re-entry.

Roadmap to Phase A

The Silicon Shepherd Phase 0 study successfully demonstrates the preliminary engineering and programmatic feasibility of autonomous asteroid biomining within the ESA F-class envelope. To safely transition this architecture into Phase A detailed design, the project must immediately address the vulnerabilities isolated during the integrated system analysis.

The immediate critical path requires advancing the core payload technologies—specifically, demonstrating the packed-bed bioreactor in a microgravity environment for an extended duration (>120 days) to reach TRL 6, and maturing the LMC_{OOL} instruments to TRL 7 prior to procurement. Simultaneously, system engineering must initiate a strict mass-reduction campaign targeting the over-engineered Sample Return Capsule to confidently secure the 1300 kg rideshare allocation. Finally, the nominal mission operations timeline must be expanded to inject a minimum 60-day schedule margin into the bioleaching phase, protecting the mission against the inherent uncertainties of microbial kinetics in deep space. Addressing these actions will elevate the system reliability to a compliant level and secure the foundation for Europe's first autonomous space resource utilisation mission.

1
Concept and Motivation

Before any subsystem can be sized, the mission has to earn its place: what problem it addresses, why a spacecraft is the right answer, and what that spacecraft is actually meant to do. This chapter sets that foundation. Section 1.1 states the mission concept, fixing the need, the objective, and the top-level architecture against which the rest of the report is designed. Section 1.2 then establishes the case behind it, mapping the stakeholders, segmenting the rare-earth market by strategic criticality, and positioning an F-class biomining demonstrator against terrestrial supply and competing space-resource ventures. Together they explain why ESA would fund the mission and what it is buying.

1.1. Mission Concept
Mission Need & Project Objective

Near-Earth asteroids represent an unexplored yet promising reservoir of high-value elements which would be valuable for terrestrial supply chains that are vulnerable to geographic concentration and geopolitical disruption. In this context, space biomining represents an attractive method to extract desirable metals from mineral substrates. ISS-based experiments have demonstrated microbial ability to perform bioleaching in microgravity environments, establishing feasibility at the laboratory scale. However, a mission has yet to demonstrate the capability to perform these operations autonomously on an asteroid's surface. The SILICON SHEPHERD space mission plans to bridge this gap and further advance the Technology Readiness Level (TRL) of scalable and sustainable required technologies, thus acting as a demonstrator for future commercial and scientific missions.

Mission Need Statement: Demonstrate autonomous space-based biomining on a near-Earth asteroid.

To fulfil this need and secure a development budget, the SILICON SHEPHERD is designed as an ESA F-class mission with a budget of €205 million, launching the *Alicanto* spacecraft on a Ariane 62 rideshare alongside an undetermined M-class system. Developed in tandem with the spacecraft platform to allow for maximal efficiency in satellite design, the core payload of *Alicanto* consists of a microbial bioleaching instrument MISAR (MIcrobial Seperator of Asteroidal Regolith) coupled with TU Delft's origin-of-life life-marker chip (LMC_{OOL}) for in-situ autonomous monitoring of culture health, utilising acid produced by fungi species *Penicillium simplicissimum*, a culture selected through a tradeoff in the baseline report[1]. To balance the scope of mission development, lower technology readiness level (TRL) of the payload, and remain within the F-class cost envelope, extensive use of heritage components will be heavily prioritised during design. The selected mission target is Near-Earth-Asteroid (NEA) Itokawa, selected as explained in the baseline report[1] due to its accessibility, heritage from the HAYABUSA mission [2] and spectral classification as an S-type, promising for REE content and bioleaching heritage from BioAsteroid [3]. The *Alicanto* spacecraft will conduct in situ bioleaching operations and return un/processed material to Earth for a quantitative yield analysis and biological assessment.

Project Objective: Design an ESA F-class mission utilising an integrated bioreactor spacecraft system to demonstrate autonomous biomining of near-Earth asteroids.

Mission Objectives

From the project objective and stakeholder requirements established, a suite of primary mission objectives have been established:

- Rendezvous and proximity operations: Achieve and maintain station-keeping at the target NEA, with attitude knowledge sufficient for surface site characterisation and payload deployment.
- Regolith acquisition: Collect a representative surface sample from the target body and transfer it to the sealed bioreactor assembly under contamination-controlled conditions.

- Autonomous bioleaching: Operate microbial cultures in contact with collected regolith, maintaining viable culture conditions autonomously, using an LMC_{OOL} chip integrated system.
- Sample return and ground analysis: Return at minimum $5g$ of processed and unprocessed regolith to Earth for extraction yield quantification within a planetary protection-compliant containment capsule in accordance with COSPAR category V unrestricted return requirements.

1.2. Market Analysis

Silicon Shepherd is funded by ESA as a technology demonstrator, not as a commercial extraction venture, so its justification rests on strategic value rather than near-term revenue. Rare-earth elements (REEs) are indispensable to permanent magnets, and those lie at the centre of electric traction and wind generation; however, roughly 69 % of mined REE output and close to 90 % of refining capacity are concentrated in a single country [4, 5], and Europe sources almost all of its refined supply from that same country [6, 7]. Moreover, biological REE extraction has never left the laboratory on Earth, and asteroidal biomining has been shown only in a human-monitored, controlled environment aboard the ISS [8, 3]. Flying the process therefore matures a long-term supply-diversification option that currently exists nowhere else, which is the value ESA is obtaining.

This section thus establishes the case and motivation behind the mission. It identifies the stakeholders, segments the REE market by physicochemical group and by strategic criticality, sets out the forecast demand and the mission's deliberately non-commercial market position, and places space biomining against terrestrial supply and competing space-resource ventures. The chapter closes with a SWOT analysis and a ranked REE target list. That target list fixed the element priorities that drove the asteroid and microorganism selections reported in previous reports[1]: the selected target, S-type (25143) Itokawa, and the selected organism, *Penicillium simplicissimum*.

1.2.1. Customer and Stakeholder Identification

Silicon Shepherd is funded by the European Space Agency (ESA) under the Science Programme's F-class call, with a cost cap of €205 M and a launch slot on Ariane 62. ESA is the contracting customer, but not the principal consumer of the mission's outputs. This section identifies the end-users and maps the wider stakeholder landscape.

Stakeholders are placed in a Mendelow matrix in Figure 1.1. The three stakeholders in the Manage Closely quadrant set the dominant constraints on the design: the ESA F-class programme office and Science Programme Committee fix the cost cap, schedule, and technical scope, and the COSPAR Panel on Planetary Protection imposes Category V restricted Earth-return compliance. The remaining stakeholders shape quality-of-output expectations without adding design constraints: the Ariane Group as launcher supplier, the astrobiology and planetary-science community and the European space-resources industry as data and heritage users, the European Raw Materials Alliance (ERMA) as a strategic-supply consumer, and the European public as the funding constituency.

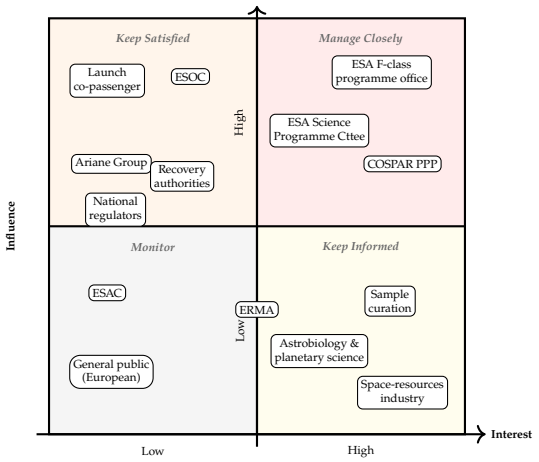

Figure 1.1: Stakeholder Mendelow matrix.

Beyond the strategic stakeholders above, a second tier of implementation and operational stakeholders becomes active during execution and return. ESA's operations centre (ESOC), which conducts deep-space tracking and commanding, holds significant influence over mission execution but limited interest in the strategic REE outcome. At the same time, ESAC, as the eventual science-archive host, sits lower on both axes. The Australian recovery authorities governing the Woomera range can gate physical access to the landing site, giving them high influence over the return phase against an episodic, end-of-mission interest. The launch co-passenger, as the primary Ariane 62 payload, dictates the launch slot and injection conditions yet has no stake in the mission's results. National regulators responsible for re-entry licensing and planetary-protection authorisation can likewise block the return, and are therefore highly influential, moderate-interest. The designated sample-curation organisation is the recipient of the returned material and the arbiter of the curation-acceptance requirement: its interest is high and its influence moderate.

1.2.2. Market Segmentation

The REEs comprise the 15 lanthanides plus scandium and yttrium. They are not equally valuable, scarce, or substitutable, so treating them as a single commodity would misdirect the asteroid and microorganism trade-offs. This section segments the REEs into the categories that matter for the mission: by physicochemical group (light versus heavy) and by strategic criticality.

The industry-standard split separates light rare-earth elements (LREEs: La, Ce, Pr, Nd, Pm, Sm, Eu) from heavy rare-earth elements (HREEs: Gd, Tb, Dy, Ho, Er, Tm, Yb, Lu, plus Y by chemical behaviour) [9]. LREEs are roughly an order of magnitude more abundant in terrestrial ores and dominate production by mass. The 17 elements are also not equally relevant to the mission, so the criticality assessment is restricted to a shortlist built from two filters:

1. **Regulatory relevance.** The element must be covered by the EU Critical Raw Materials Act (CRMA, Regulation 2024/1252) under the LREE group, the HREE group, or as an individually listed material (Sc). Pm is excluded on this basis: it is radioactive and, given its short half-life, is not expected in asteroidal material.
2. **End-use volume.** The element must contribute meaningfully to a high-growth or strategically constrained use. This keeps the permanent-magnet REEs (Nd, Pr, Dy, Tb, Sm), the phosphor-relevant REEs (Eu, Y), and the high-volume LREEs (La, Ce), and excludes the rest on grounds of niche end-use or insufficient accessible abundance.

The resulting shortlist of nine elements, summarised in Table 1.1, drives the ranked target list in Section 1.2.6.

Table 1.1: Criticality drivers for the shortlisted REEs. Global mine concentration is the share of 2024 global mined production held by the largest single producer (China in all listed cases) [4, 6]. EU import dependency is the share of the EU's refined-REE supply sourced from a single non-EU country (also China) [7, 6]. The substitutability tier follows the qualitative classification used in the CRMA criticality methodology [10]: low = no substitute at scale, medium = partial substitution feasible with performance loss, high = readily substitutable.

REE	CRMA group	Global mine conc.	EU import dep.	Subst. tier	Primary end-use
Nd	LREE	~70%	~85%	Low	NdFeB permanent magnets
Pr	LREE	~70%	~85%	Low	NdFeB magnets (co-substituted)
Dy	HREE	~90%	~100%	Low	High-temperature magnet doping
Tb	HREE	~90%	~100%	Low	Magnet doping, phosphors
Sm	LREE	~70%	~85%	Medium	SmCo magnets, defence
Eu	LREE	~70%	~85%	High	Phosphors (legacy lighting)
Y	HREE	~80%	~100%	Medium	Phosphors, ceramics, alloys
La	LREE	~60%	~85%	Medium	Catalysts, NiMH batteries
Ce	LREE	~60%	~85%	High	Catalysts, glass polishing

1.2.3. Demand Outlook

With the relevant REEs scoped, the next question is whether their forecast supply justifies an extra-terrestrial sourcing demonstration, and what role Silicon Shepherd plays in it. This section quantifies the forecast supply gap for the shortlisted REEs and then fixes the mission's intended share of the resulting market.

Forecast demand

Global rare-earth mine production reached 390 000 t of rare-earth-oxide equivalent in 2024 [4]. Demand is forecast to grow at roughly 5 % CAGR through 2035 under decarbonisation scenarios, driven mainly by permanent-magnet demand for electric-vehicle traction motors and offshore wind turbines [5, 7]. The amount is not the concern; the sourcing structure is. Production and refining are concentrated in one supplier, so the gap between forecast magnet-REE demand and credibly committed supply outside that supplier is what makes non-terrestrial sourcing worth maturing as a long-term option, even while terrestrial supply remains far cheaper in the near term.

That gap is greatest for the magnet REEs (Nd, Pr, Dy, Tb) and smallest for the abundant LREEs (La, Ce). This reinforces the criticality filter: the elements most worth demonstrating extraction of are the same ones with the worst forecast supply.

Target market share

Silicon Shepherd is a demonstration mission, not a profit-focused operation, so its target share of the physical REE market is effectively zero. The ≥ 5 g of returned sample is far below any commercial threshold and is

destined for scientific curation, not industrial processing. The mission's market position lies instead in two non-physical markets:

- **Space-biomining process heritage.** The mission targets a first-mover position in autonomous asteroid biomining, building on the crew-tended ISS heritage of BioRock and BioAsteroid [8, 3].
- **Strategic-supply intelligence.** The mission generates first-of-its-kind data on bioleaching of asteroidal mineral phases, of direct value to ERMA and equivalent bodies assessing long-term supply-diversification options. The target share here is, for a defined horizon, monopolistic: no comparable dataset will exist until a follow-up biomining mission flies, plausibly not before the early 2040s. This is a time-bounded first-mover position, not a permanent monopoly.

This reframing is consistent with the mission's role as an F-class technology demonstrator. Success is measured by demonstrated capability, not by tonnes of REE delivered to European refineries.

1.2.4. Competitive Landscape

Silicon Shepherd is positioned against three competitor categories.

Terrestrial REE producers. Conventional mining and refining (Bayan Obo, Lynas, MP Materials, and emerging European refiners such as Solvay and Neo Performance Materials) will dominate REE supply well beyond the mission's lifetime [5]. Silicon Shepherd does not compete on cost or volume, it competes on strategic optionality, providing the process heritage and data that inform EU supply diversification if geopolitical or environmental constraints tighten.

Terrestrial bioleaching. Bioleaching is industrially mature for Cu, Au, U, and Co [11], but no commercial REE bioleaching operation exists; demonstrations on monazite, bastnäsite, phosphogypsum, and red mud remain laboratory-scale [12]. The mission validates biological REE extraction in both terrestrial-analogue and space contexts.

Space-resource demonstrators. Active or near-term ventures such as AstroForge, Karman+, and TransAstra target platinum-group metals or water and use no biological extraction. The closest sample-return missions, Hayabusa2 [13] and OSIRIS-REx [14], return material but do not process it. Silicon Shepherd, therefore, occupies an unfilled niche.

The mission's real competition is for ESA attention and follow-up funding, not for commodity market share.

1.2.5. SWOT analysis

The preceding findings, the stakeholder landscape, the REE criticality shortlist, the demand forecast, and the competitive positioning are synthesised into the SWOT analysis in Figure 1.2, covering the strategic and market positioning of the mission.

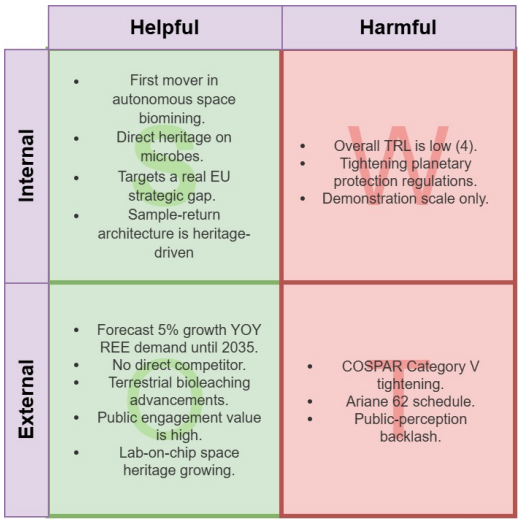

Figure 1.2: Technical and market SWOT analysis.

1.2.6. REE Target List and Hand-off to Design Trades

Combining the criticality drivers of Table 1.1 with the strategic-value tiers of Section 1.2.2 yields the ranked target list in Table 1.2. Tier numbering reflects design-trade priority, not criticality alone.

The target list shaped three design decisions, each now resolved:

Table 1.2: Ranked REE target list and hand-off to design trades.

Tier	REE	Driver	Hand-off
1	Nd, Pr	Magnet demand, low substitutability	Asteroid: silicate/phosphate-rich (S/C); Microbe: Si/P-bound REE leaching
1	Dy, Tb	HREE supply concentration (~90%)	Asteroid: HREE-bearing phases
2	Sm	SmCo magnets, defence end-use	Microbe: tolerance to multi-REE substrate
3	Y, Eu	Phosphor heritage, CRMA listing	Coverage of REQ-MIS-13 (≥5 species)
4	La, Ce	Volume LREEs; chondrite-abundant	Baseline detection check; low strategic weight

- **Asteroid selection.** Tier-1 REEs in chondritic material are hosted mainly in phosphate phases, with a smaller silicate contribution [15], which excludes metal-rich M-types and favours C- and S-types. The target trade-off selected S-type (25143) Itokawa, an ordinary-chondrite analogue directly comparable to the substrate used in the BioAsteroid experiment [16].
- **Microorganism selection.** The dominance of Tier-1 magnet REEs prioritised an organism with demonstrated leaching of mineral-bound REEs from chondritic substrate.*Penicillium simplicissimum* was selected on that basis, having shown REE extraction from meteoritic material in microgravity [3].
- **Payload analytics.** REQ-MIS-13 requires ≥5 distinct REE species in the returned sample. Covering Tiers 1 and 2 (six elements) provides one-element margin against detection failure.

Tier 4 is retained for reference but drives no trade: La and Ce are abundant enough in chondrites that their detection is expected regardless of organism or target.

1.2.7. Implications for Mission Requirements

The market-analysis results translate into design-level constraints through three routes: stakeholder-derived constraints, REE-target-derived capability requirements, and demonstrator priorities. Table 1.3 traces each finding to its downstream impact.

Table 1.3: Traceability from market-analysis findings to mission requirements and downstream design impact.

Market-analysis output	Derived constraint / requirement	Downstream impact
F-class cap and Ariane 62 slot (ESA)	Cost ≤ €205 M (2024), Ariane 62 launcher interface, F-class schedule	System-level cost and mass budgets, launcher compatibility
COSPAR Category V Earth return	Containment architecture and auditable sample chain	Payload containment, sample return capsule, reentry architecture
Sample curation acceptance	≥ 5 g processed and unprocessed asteroidal material returned	Sample interface, sampling mechanism, return capsule sizing
Tier-1 REE list (Nd, Pr, Dy, Tb)	Silicate/phosphate-phase leaching capability required	Excludes M-type asteroids; favours BioAsteroid-heritage organisms
Tier-1 + Tier-2 coverage (6 species)	One-element margin on ≥5 distinct REEs	Analytical sensitivity, organism leaching range
Demonstrator positioning	Reproducibility and full process telemetry	Autonomous operations and data-handling architecture

2
Functional Analysis

The functional analysis translates the mission need into the set of functions the system must perform over its whole life cycle. It is the bridge between the concept of Chapter 1 and the requirements the rest of the report verifies against. The analysis is presented in two complementary views, a time-ordered Functional Flow Diagram (FFD) and a hierarchical Functional Breakdown Structure (FBS), which share a common set of function names and identifiers. In both, the system responsible for each function is tagged in brackets, so the diagrams double as an early allocation of functions to subsystems.

2.1. Functional Flow Diagram

The FFD, given in Figure 2.1 and Figure 2.2, follows the flow of functions from one phase to the next and shows where they run in series, where they run in parallel, and where the mission has to make a decision. It spans the full life cycle, opening with manufacturing, subsystem assembly, and system verification (phases D1-D3) before the flight phases from launch and early operations through outbound cruise, asteroid observation, sampling, in-situ bioleaching, Earth-return cruise, capsule re-entry, disposal, and ground recovery (phases E0-E10, F9). Parallel functions are joined with AND gates, and conditional points are drawn as decision gates with the condition labelled on the branches. Review gates represent checkpoints for the mission throughout production (IRR, ORR, FRR) and utilisation, the 'Itokawa reached?' and 'systems operational?' check during cruise and commissioning, and the captured-mass gate after sampling, which either passes the regolith forward to bioleaching or commands another touch-and-go pass within the budgeted attempts.

2.2. Functional Breakdown Diagram

The FBS, in Figure 2.3, reorganises the same functions by hierarchy rather than by time. It decomposes each top-level function into its sub- and sub-sub-functions down to the system level, reusing the identifiers and names already fixed in the FFD so the two remain consistent.

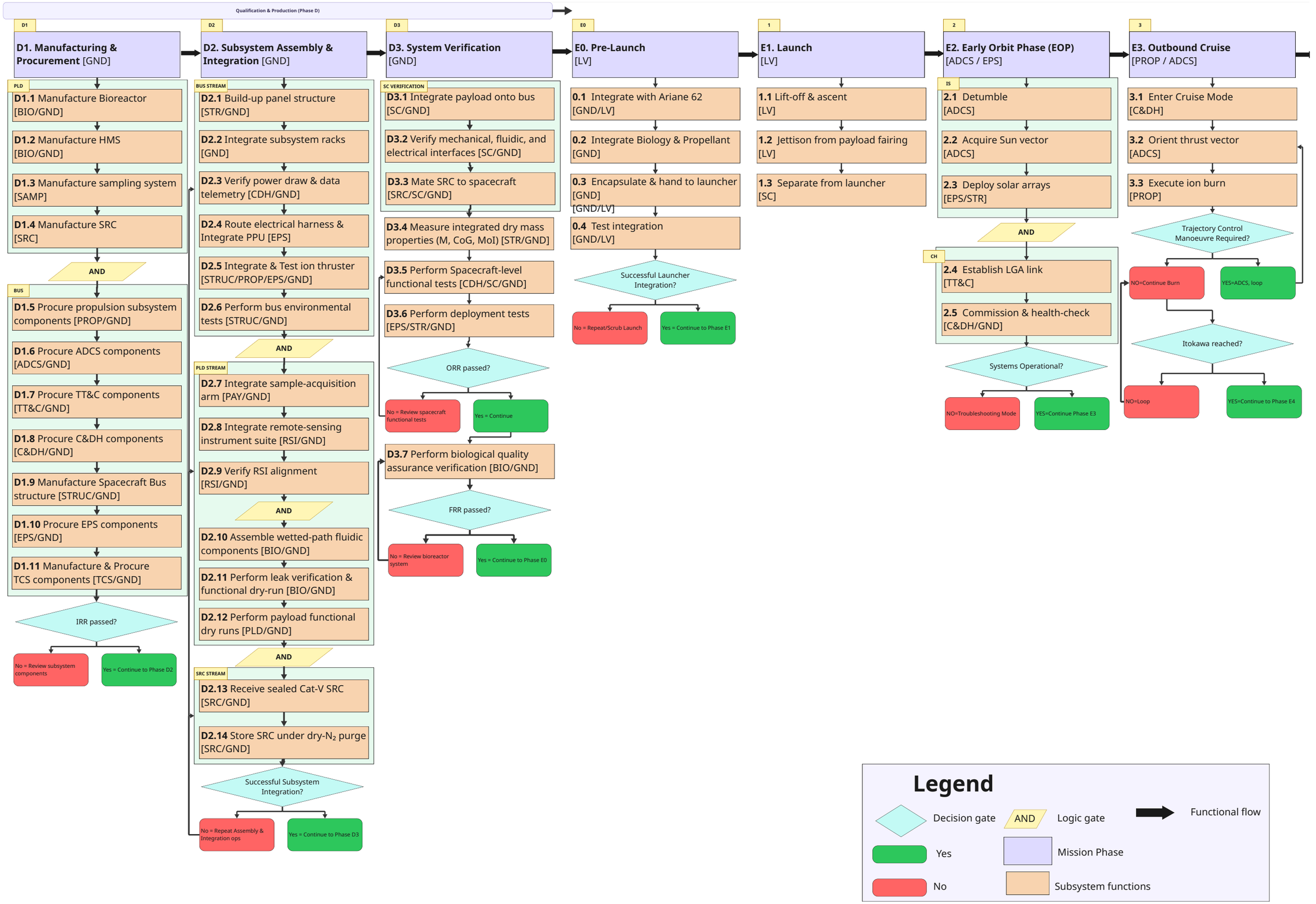

Figure 2.1: Functional Flow Diagram (1/2)

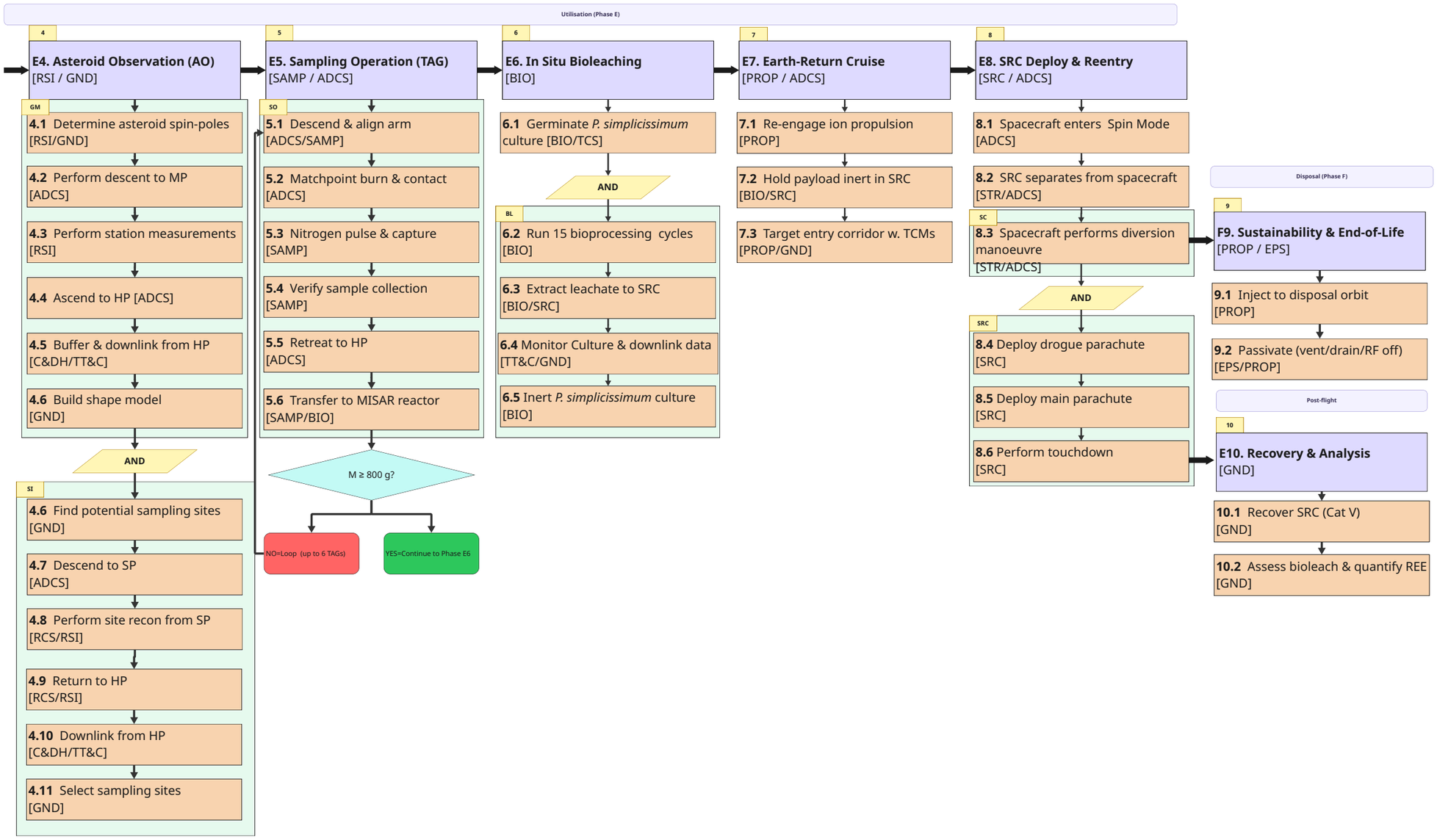

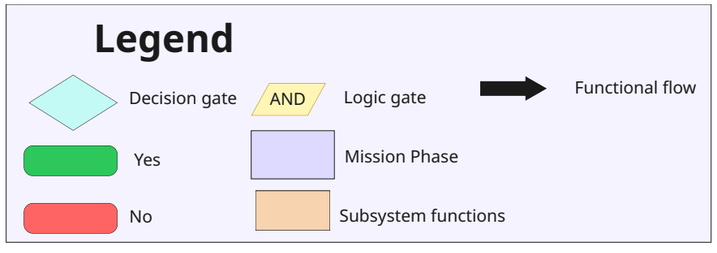

Figure 2.2: Functional Flow Diagram (2/2)

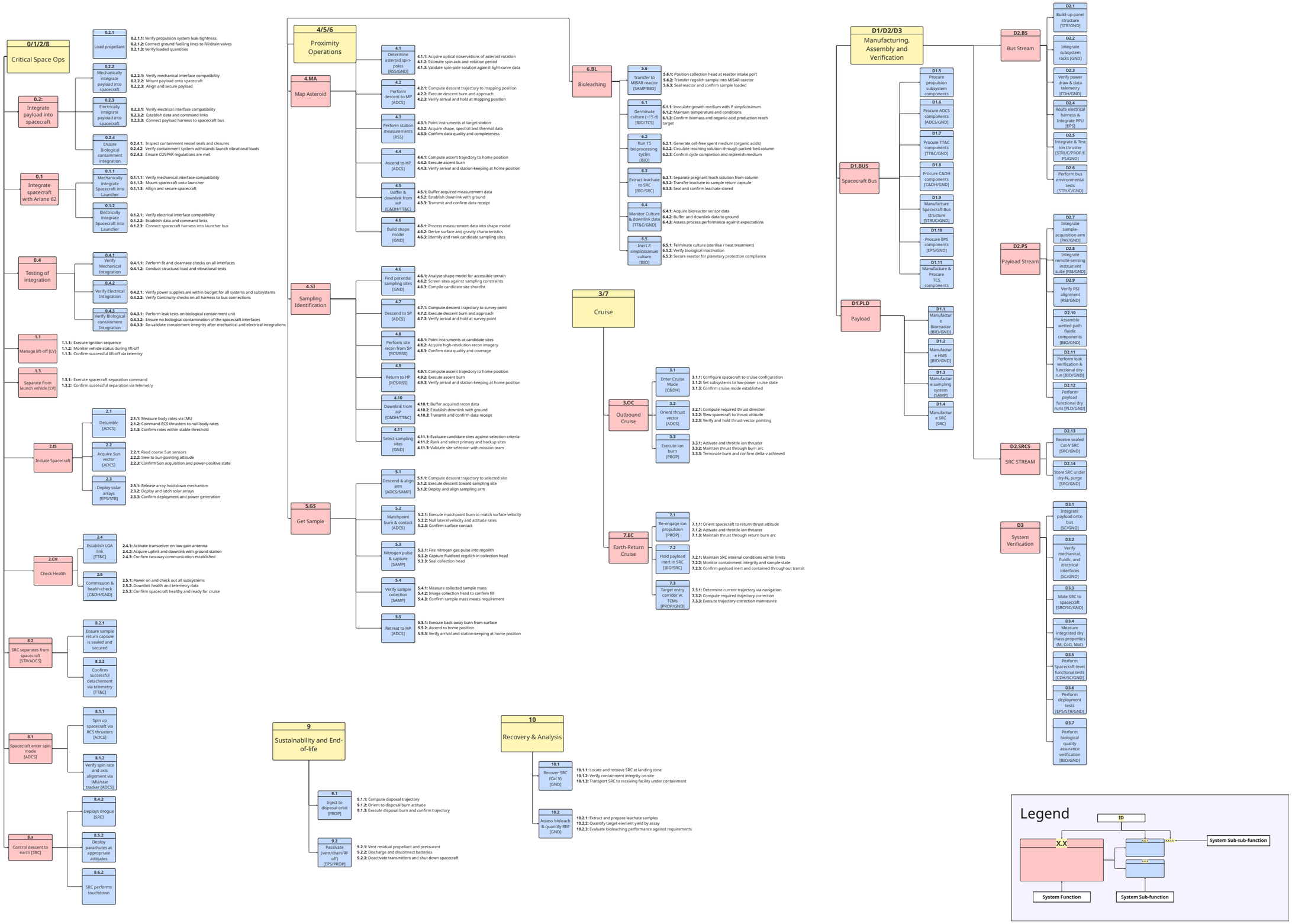

Figure 2.3: Functional Breakdown Structure

3
Project Design and Development Logic

A Phase 0 design is only useful if there is a credible path from it to a flight-ready mission. This chapter lays out that path. Section 3.1 sets the post-DSE development logic, ordering the major activities from feasibility study through operations and end-of-life and marking the review gates and iteration loops that mark progress between them. Section 3.2 places those activities on a timeline, and Section 3.3 expands the production end of that timeline into a manufacturing, assembly, and integration plan for the single flight unit. The three views share one task set: the logic fixes the order, the Gantt fixes the dates, and the MAIP fixes how the hardware is built and verified.

3.1. Post-DSE Development Logic

The development logic in this section shows how the current Phase 0 design would be matured into a flight-ready mission. It is not intended as a schedule; the corresponding timing is given in the project Gantt chart in Figure 3.2, while the cost implications are captured in the Cost Breakdown Structure (Section 8.2). Instead, the purpose of the logic is to show the order of the main post-DSE activities, the review gates between them, and the iteration loops that would be triggered if the design or critical technologies are not mature enough.

As shown in Figure 3.1, the project starts from the DSE Phase 0-equivalent mission-definition study and first enters Phase A, where the mission concept, preliminary requirements, system budgets, interfaces, and technology roadmap are consolidated. For Silicon Shepherd, this early phase is especially important because several mission drivers are still tightly coupled: the closed biomining reactor, $\mathrm{LMC}_{\mathrm{OOL}}$ health monitoring system, sample-return capsule, Category V containment approach, and Itokawa proximity-operations concept all influence the spacecraft architecture. The Preliminary Requirements Review (PRR) therefore acts as the first post-DSE gate. If the mission feasibility or preliminary requirements are not acceptable, the concept and technology roadmap are refined before continuing into Phase B.

After PRR, Phase B develops the preliminary design and raises the maturity of the critical technologies. This includes breadboard and engineering-model testing of the bioreactor and $\mathrm{LMC}_{\mathrm{OOL}}$, early verification of the containment and sterilisation concept, refinement of the sample-chain architecture, and development of the Itokawa mapping, sampling, and abort logic. The System Requirements Review (SRR) takes place during Phase B to verify that the system requirements and interfaces are sufficiently defined. The Preliminary Design Review (PDR) then checks whether the system and payload design are coherent and whether the key technologies have reached a sufficient maturity level, typically around TRL 5–6 for the most critical items. If this is not the case, the project loops back into further Phase B design and testing rather than committing too early to detailed design.

Phase C freezes the detailed design. In this phase, subsystem designs are finalised, interfaces are closed, and the verification, validation, AIT, and planetary-protection implementation plans are defined in detail. The Critical Design Review (CDR) is passed only when the design is mature enough for flight-model manufacturing and the main critical non-conformances have been closed. This is followed by Phase D, which is split in the diagram into hardware qualification and system-level integration. Phase D1 covers the manufacturing and qualification of the flight hardware, while Phase D2 covers spacecraft-level integration, environmental testing, ground-segment preparation, and mission rehearsals. The Qualification Review, Acceptance Review, Operational Readiness Review, and Flight Readiness Review together ensure that both the spacecraft and the operations team are ready for launch.

Phase E starts with launch and covers the actual mission operations: launch and early operations, cruise to Itokawa, asteroid mapping, sampling, biomining, sample isolation, Earth return, and capsule release. A project-specific Earth-return and planetary-protection review, labelled ER/PP in the figure, is included before Earth return is completed. This gate checks that the sample-return capsule, biological containment, recovery plan, and curation chain still satisfy the Category V restricted Earth-return assumptions. If this review is not passed, the mission cannot simply proceed with nominal Earth return; additional mitigation, extended operations, sterilisation, or disposal options would have to be considered. Finally, Phase F covers recovery, curation, scientific analysis of the processed and unprocessed samples, data archiving, and mission close-out.

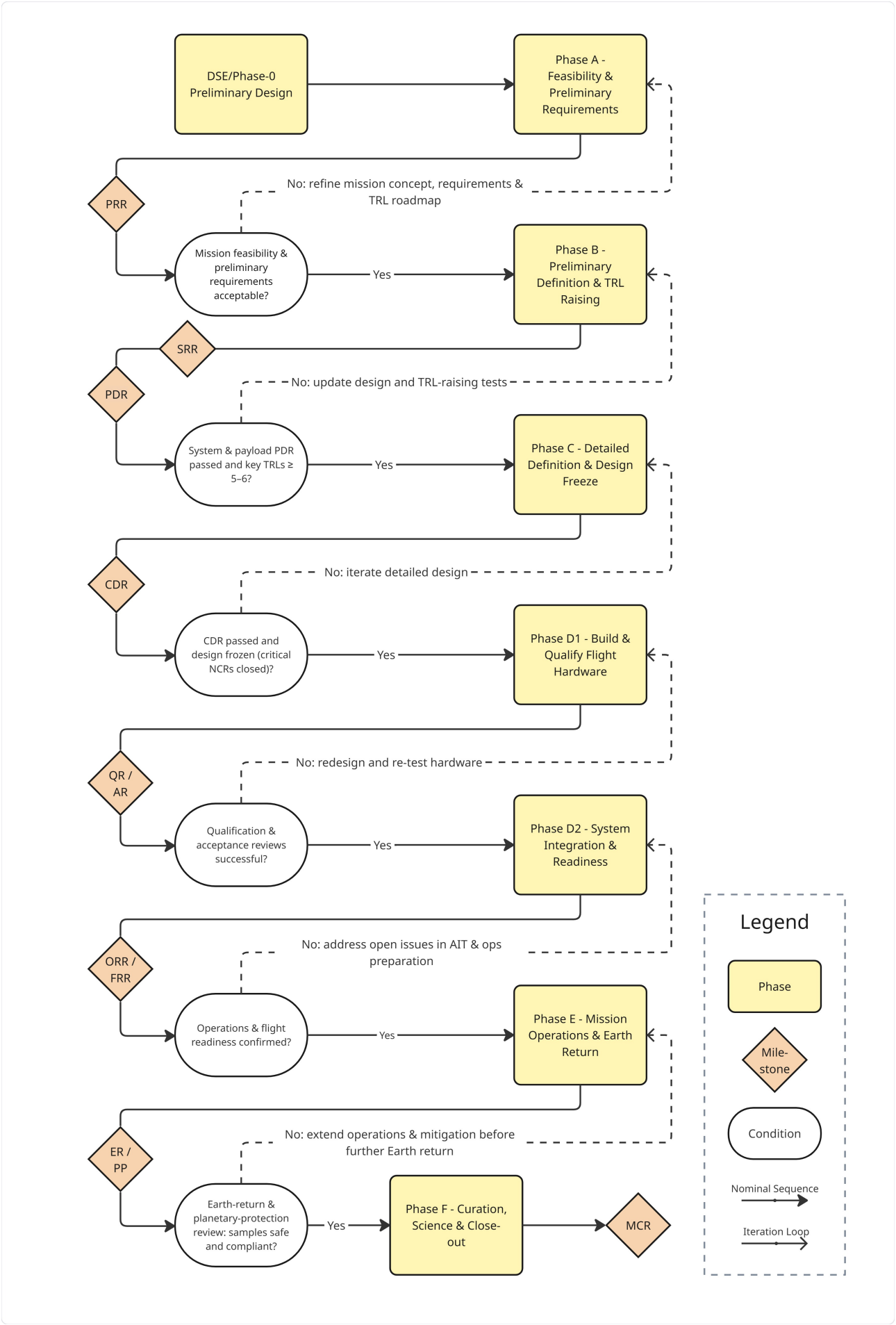

Figure 3.1: Silicon Shepherd project design and development logic.

The same logic also links this section to the rest of the report. The Gantt chart assigns dates and durations to the activities shown here, the CBS attaches costs to the same development blocks, and the MAI/AIT plan expands the Phase D integration and test flow. The V&V plan, risk analysis, and compliance matrix provide the evidence needed to pass each review gate, especially for the high-risk items: biomining performance, LMC_{OOL} maturity, Category V containment, SRC qualification, and Itokawa proximity operations.

Model philosophy and programme risk. The schedule assumes a hybrid model philosophy, since applying a single model approach to all subsystems would either underestimate payload risk or over-qualify heritage hardware. For the low-TRL payload elements, especially the biomining reactor, LMC_{OOL} health-monitoring chain, and regolith-transfer interface, breadboards and engineering models are used during Phase A/B to retire functional and biological risks before committing to flight hardware. The critical containment and return elements then follow a qualification-model plus flight-model philosophy: representative qualification hardware is used to demonstrate environmental robustness, containment integrity, sterilisation compatibility, and interface performance, while the flight model is acceptance-tested and protected from unnecessary qualification-level over-testing. In contrast, heritage spacecraft-bus units may follow a protoflight or acceptance-by-similarity approach where supplier qualification evidence is available.

This model philosophy is deliberately more conservative than a pure protoflight approach for the biological payload and SRC, because a failure in these elements would affect not only technical performance but also planetary protection, schedule, and cost. The consequence is a longer and more expensive Phase B–D development path, but with reduced risk of discovering critical payload or containment failures only after flight-model integration. The resulting critical path is therefore the payload maturation and qualification chain: LMC_{OOL} target freeze, bioreactor engineering-model testing, regolith-transfer validation, payload qualification, late bio-loading, and final spacecraft acceptance. Schedule margin is consequently concentrated near the end of Phase D and within the asteroid-operations allocation.

3.2. Project Gantt Chart

The project Gantt chart in Figure 3.2 translates the post-DSE development logic into an initial programme schedule. Each row represents a high-level work package or review gate, with the corresponding start date, end date, and duration expressed in half-year increments. This level of resolution is considered appropriate for the current design stage, since the objective is to show the overall phasing, sequencing, and major programme dependencies rather than day-level planning.

The calendar dates should be interpreted as a notional implementation schedule anchored to the start of Phase A; the relative phasing and review spacing are the controlling assumptions, and the programme could be shifted to a later ESA call without changing the internal development logic.

The Gantt chart starts at the beginning of Phase A. The DSE final review is treated as the Phase 0-equivalent mission-definition gate and is therefore not shown as a separate half-year activity. The post-DSE programme is shown as beginning in 2027 H1 with Phase A, during which the mission concept, preliminary requirements, interfaces, science case, and technology roadmap are consolidated. Phase A concludes with the Preliminary Requirements Review (PRR). Phase B then runs from 2028 to 2031 and focuses on preliminary definition and TRL raising, with particular emphasis on the biomining reactor, sample-transfer chain, LMC_{OOL} health-monitoring system, and contamination-controlled payload architecture. The System Requirements Review (SRR) is placed during Phase B, while the Preliminary Design Review (PDR) marks the transition from technology maturation into detailed design and advance procurement.

Phase C covers detailed design, interface freeze, verification planning, and long-lead procurement. The CDR marks the transition from detailed definition to flight-model manufacturing and qualification. Phase D then covers flight-model manufacturing, payload and bus qualification, spacecraft-level integration, environmental testing, late biological loading, and launch preparation. The QR, AR, ORR, and FRR gates are therefore placed near the end of Phase D, where payload, spacecraft, SRC, ground-segment, and operations readiness converge.

Phase E covers the flight mission from launch through Earth return, including commissioning, outbound cruise, Itokawa operations, sampling, in-situ bioleaching, Earth-return cruise, ER/PP verification, and SRC release. In the Gantt chart these mission-operations bars are rounded to half-year intervals for consistency with the programme-level resolution; the exact departure, arrival, return, and Earth-encounter dates are defined in the operations and astrodynamics chapters. Finally, Phase F covers recovery, controlled curation, returned-sample analysis, data archiving, and project close-out, ending with the Mission Close-out Review (MCR). The Gantt chart is therefore directly linked to the development logic: the logic diagram shows the order and review dependencies of the post-DSE activities, while the Gantt chart assigns these activities to an initial schedule.

SILICON SHEPHERD High-Level Project Gantt

Phase / Activity	Start Date	End Date	# of Years
Mission phase			
Year			
POST-DSE DEVELOPMENT TO LAUNCH	**2027-01-01**	**2036-06-30**	**9.5**
Phase A mission & technology consolidation	**2027-01-01**	**2027-12-31**	**1.0**
Consolidate mission requirements	2027-01-01	2027-12-31	1.0
Define system and external interfaces	2027-01-01	2027-12-31	1.0
Establish TRL maturation roadmap	2027-01-01	2027-12-31	1.0
Phase B preliminary definition & TRL raising	**2028-01-01**	**2031-12-31**	**4.0**
Mature bioreactor and sample transfer	2028-01-01	2031-12-31	4.0
Mature LMCOOL health monitoring	2028-01-01	2031-12-31	4.0
Refine spacecraft, SRC and operations design	2029-01-01	2031-12-31	3.0
Phase C detailed design & advance procurement	**2032-01-01**	**2033-06-30**	**1.5**
Finalise detailed design and verification plan	2032-01-01	2033-06-30	1.5
Procure long-lead hardware	2032-01-01	2033-06-30	1.5
Phase D build, qualification & system integration	**2033-01-01**	**2036-06-30**	**3.5**
Payload, SRC and bus qualification	2033-01-01	2035-06-30	2.5
Spacecraft-level integration and environmental test	2035-01-01	2035-12-31	1.0
Late bio-loading, ORR/FRR and launch handover	2036-01-01	2036-06-30	0.5
PHASE E MISSION OPERATIONS & EARTH RETURN	**2036-01-01**	**2039-06-30**	**3.5**
Launch, commissioning & outbound cruise	2036-01-01	2037-06-30	1.5
Itokawa proximity campaign & biomining	2037-01-01	2038-06-30	1.5
Earth-return cruise, ER/PP review & SRC release	2038-07-01	2039-06-30	1.0
PHASE F CURATION, SCIENCE & CLOSE-OUT	**2039-07-01**	**2041-06-30**	**2.0**
SRC recovery and containment handover	2039-07-01	2039-12-31	0.5
Returned-sample analysis & science exploitation	2039-07-01	2041-06-30	2.0
Data archive, lessons learned and close-out	2040-07-01	2041-06-30	1.0
REVIEW / MISSION GATES	**2027-01-01**	**2041-06-30**	**14.5**

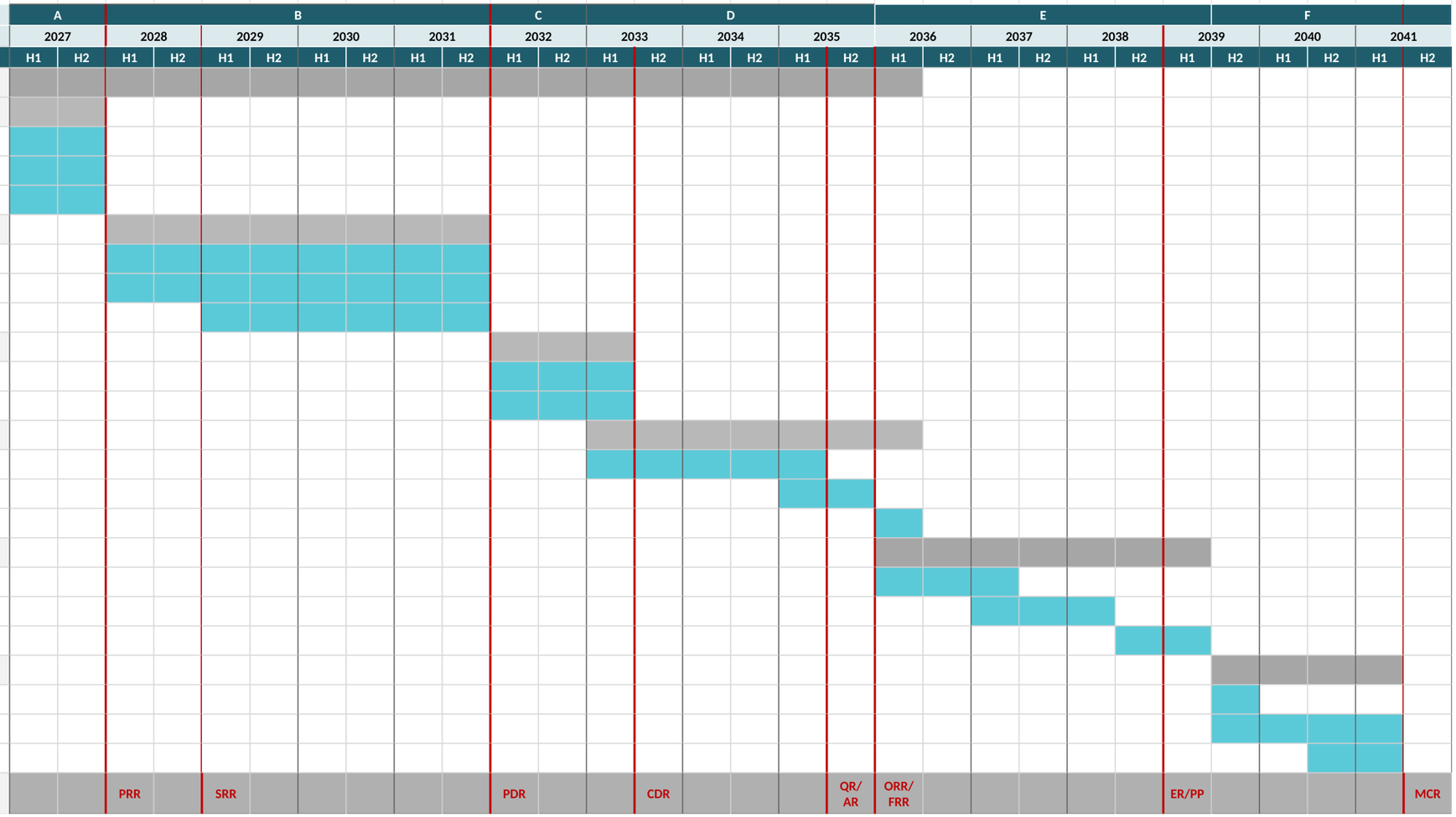

Figure 3.2: Silicon Shepherd project Gantt chart. High-level programme chart with half-year resolution; mission-operations bars are rounded for visual planning and should not be interpreted as exact trajectory dates.

3.3. Manufacturing, Assembly, and Integration Plan (MAIP)

This plan covers the one-off flight-unit Manufacturing, Assembly, and Integration (MAI) of Silicon Shepherd from procurement to launcher handover, corresponding to ESA Phase D. Specialised flight hardware, including the SRC, LMC_{OOL} chip, ion thrusters, and selected mechanisms, is supplied by external contractors. The prime contractor therefore focuses on supplier-interface control and Assembly, Integration, and Testing (AIT) of the delivered subsystems into the final flight model.

The MAI flow is treated as the hardware execution of the Verification Control Document (VCD): inter-stage gates close system and subsystem requirements mainly through Test (T) and Inspection (I) before the Flight Readiness Review (FRR), in line with ECSS-E-ST-10-02C [17]. Integration follows three parallel streams: bus, payload, and SRC, within a 48-month Phase C/D implementation cycle baselined against ESA F-class heritage and the ARRAKIHS timeline [18]. After Phase A/B maturation of the biological payload and regolith-transfer chain to TRL 6, the PDR in May 2032 authorises Phase C and advance procurement of long-lead items by performance specification. Phase D starts after the CDR in May 2033, once the system design is frozen for flight-model manufacturing and integration. The streams, long-lead drivers, and test gates are shown in Figure 3.3; the critical procurements are summarised in Table 3.1.

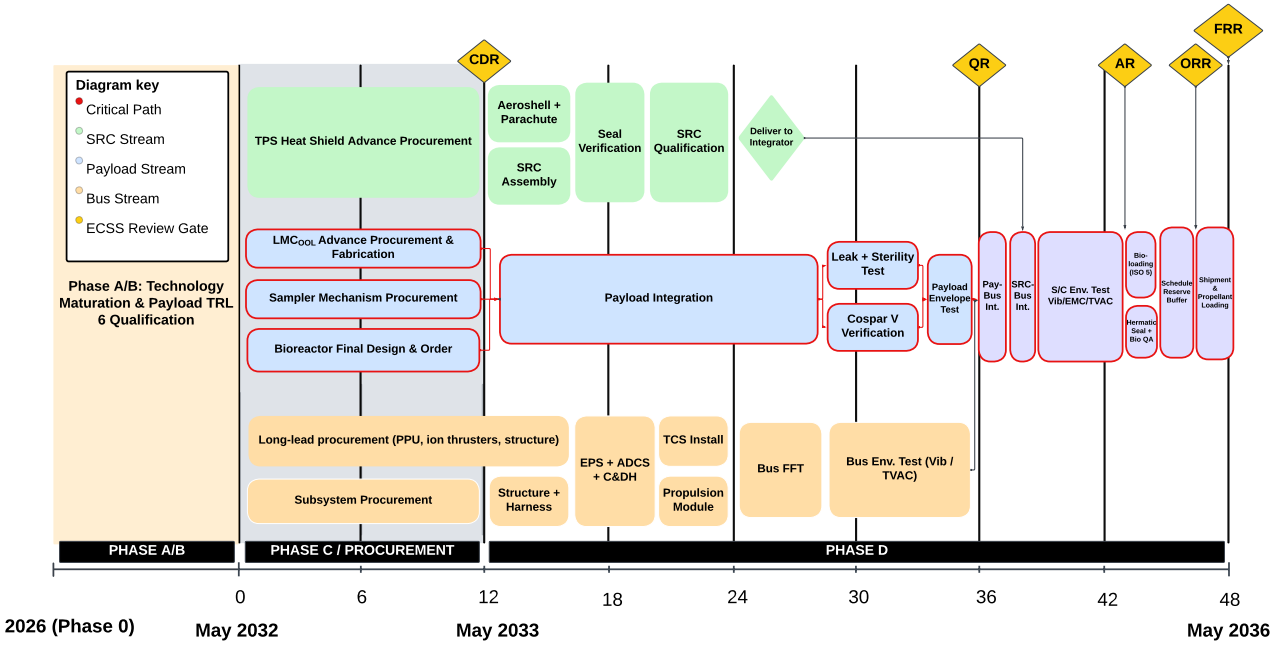

Figure 3.3: Master 48-month Swimlane MAI flow relative to Mission Adoption (May 2032) with ECSS review gates marked in yellow.

Table 3.1: Critical long-lead procurements driving the integration schedule.

Item	Lead time	Driving reason	Gates
LMC_{OOL} chip (multi-analyte build)	10-14 Mths	Each analyte adds ~1 month of qualification [19]. Biomarkers must be frozen before procurement.	Payload integration gate
Bioreactor pressure vessel Wetted Surfaces	10-12 Mths	Acid-compatible wetted surfaces (e.g., Ti-alloy/PEEK) for pH 2-6. Cleanliness and biocompatibility verification extend machining times.	Payload integration gate
SRC ablative heat shield	10-14 Mths	Custom layup, Category-V compliance, sterilisation of the return seal, and 12 km s^{-1} qualification by similarity to Stardust/OSIRIS-REx	SRC delivery to integrator
Ion thruster & Power Processing Unit (PPU)	14-18 Mths	Uncompressible >5000 h vacuum endurance qualification. PPU integration is the secondary schedule driver.	Bus electrical integration
Sample acquisition arm	10-12 Mths	Custom mechanism requiring deployment and contact-loads qualification on a representative test article.	Payload integration gate

Bus stream. The bus carries the structure, hybrid propulsion, ADCS, EPS, TT&C, and thermal hardware. Mechanical build-up of the panel structure is performed by the prime contractor in an ISO Class 8 high bay. Subsystem racks are integrated and run through "Aliveness Tests" to verify basic power draw and data telemetry before complete electrical harness routing. The long-lead Ion Thruster and PPU are scheduled for Just-In-Time (JIT) delivery to support these functional tests. After full electrical integration, the bus undergoes integrated environmental testing: vibration testing verifies structural compliance against launcher load spectrums, while Electromagnetic Compatibility (EMC) ensures PPU transients do not interfere with sensitive harnesses. Thermal Vacuum (TVAC) cycling verifies thermal control limits and includes critical bake-out procedures to prevent outgassing from contaminating optical sensors. Propellant loading is held until after spacecraft-level integration for safety and to ensure an accurate pre-shipment dry mass is recorded.

Payload stream. The payload comprises the bioreactor, LMC_{OOL} health-monitoring chain, sample acquisition arm, and the remote-sensing instrument suite. Mechanical integration of the arm and Tier-1/2/3 sensors is performed under ISO Class 8 conditions, with the final assembly of wetted-path fluidic components performed under strict laminar flow to prevent particulate and microbial contamination. After full assembly, the reactor undergoes leak verification, sterility verification, and a functional dry-run. This dry-run acts as the final subsystem-level validation gate before spacecraft convergence.

SRC stream. The SRC—aeroshell, ablative heat shield, parachute system, sample canister, and ground-commandable seal—is procured as a sealed assembly. Category-V sterilisation of the return-side seal interface is performed by the supplier before delivery. The SRC is delivered with its own qualification dossier (vibration, shock, thermal soak). Upon early delivery, the hardware is placed into controlled cleanroom storage (e.g., a dry nitrogen purge cabinet) to preserve its Category-V sterility and degrade-sensitive ablative materials until spacecraft-level mating at Month 37.

Convergence and spacecraft-level integration. The three streams converge in a defined order. The payload integrates onto the bus first, constituting the Integration Readiness Review (IRR) gate at Month 36 (May 2035). Here, mechanical, fluidic (sample-feed and gas-recycle lines), and electrical interfaces are verified to ensure the Command & Data Handling (C&DH) subsystem can successfully handshake with the payload. The SRC joins next, after the payload-to-bus integrated functional checkout. Mating the SRC last ensures physical access to the payload's biological loading port is preserved during late activities. Spacecraft-level environmental testing follows the mate. Biological loading of lyophilised *P. simplicissimum* and sterile media reservoirs is deferred to a late-access activity under ISO Class 5 laminar flow. Placing this loading after full spacecraft-level environmental testing is a mandatory quality assurance step to prevent culture degradation from extreme system-level test stresses and to respect strict biological shelf-life limits. Finally, a dedicated two-month schedule reserve buffer is maintained to absorb unforeseen delays before the fully integrated and verified article is packed into an environmentally controlled container. It is then shipped to the launch range for Launch operations: propellant loading, encapsulation, and launcher handover.

Critical path and schedule margin. The payload stream drives the critical path. The dominant constraint is set by the LMC_{OOL} multi-analyte fabrication and qualification activity. While actual spacecraft manufacturing is gated by the Critical Design Review (CDR) at Month 12 (May 2033), the 48-month schedule necessitates the tailored ECSS application of Advance Procurement; therefore, long-lead manufacturing for the LMC chip and Ion Thruster must be explicitly authorised via specification immediately at the start of Phase C in May 2032. With the Integration Readiness Review (IRR) gate at Month 36 (May 2035), the payload stream consumes nearly all available schedule margin. Because the mission targets a specific orbital launch window to Itokawa, the overall schedule holds minimal float. Heritage-light biological qualifications [8, 3] provide only short-duration analogues, meaning any payload-side slip propagates directly to the FRR. Any supplier-side delays in this critical path will necessitate utilising emergency schedule reserves such as the 2-month pre-shipment buffer or transitioning to 24-hour AIT shift work to prevent a slip in the launch date. The bus and SRC streams carry less schedule risk as they rely on flight-proven hardware bounded by procurement rather than extensive qualification, allowing them to complete early and await integration.

4
Operations & Logistics

This chapter presents the operations and logistics of Silicon Shepherd across Phases E and F, spanning from critical pre-launch operations – such as loading of the fuel tanks and coupling with the Ariane 62 launch system – to end-of-life passivation operations. Mission phases are first outlined in Section 4.1, with the spacecraft's ground support system described in Section 4.2 and the array of operational modes given in Section 4.3. This information is then brought together in Section 4.4, where mission operations are further detailed, leading to the establishment of a preliminary mission timeline.

4.1. Mission Phases

The Silicon Shepherd mission spans 11 distinct phases, tracking the spacecraft from final Earth integration through to spacecraft disposal and sample recovery and analysis.

Table 4.1: Summary of Silicon Shepherd operational mission phases.

Phase	Description
0: Pre-launch	Final Assembly, Integration, and Testing (AIT), operational reviews (ORR/FRR), propellant/biological loading, and launcher encapsulation.
1: Launch & Early Orbit Phase (LEOP)	Lift-off, atmospheric ascent, fairing jettison, spacecraft separation, initial telemetry lock, autonomous detumbling, and solar array deployment.
2: In-Orbit Commissioning	Commissioning of spacecraft, with final verification of spacecraft bus and check on payload subsystems.
3: Outbound Cruise	Primary propulsion engaged, ESA's European Space Operations Centre (ESOC) commands periodic Trajectory Correction Manoeuvres (TCMs) to target Itokawa.
4: Asteroid Observation	Spin-pole determination, global mapping from the $\sim$ 6 km Mapping Position (MP), and recon of candidate sites from the $\sim$ 500 m Siting Position (SP). The SOC analyses data transmitted back after each stage to select sampling sites.
5: Sampling Operation	Autonomous Touch-and-Go (TAG) manoeuvre to capture regolith, immediately retreating to the stable 20 km Home Position (HP). Up to six attempts are possible.
6: In Situ Bioleaching	Regolith is injected into the active bioreactor at HP. Leachate is extracted, transferred to the SRC, and the biological culture is chemically fixed.
7: Earth-Return Cruise	Primary propulsion re-engaged. ESOC continuously monitors the trajectory to target the precise atmospheric entry corridor.
8: SRC Deployment & Reentry	SRC is spin-stabilised and released for atmospheric entry. The main bus immediately executes a deflection manoeuvre to avoid Earth impact.
9: End-of-Life (EOL)	Main spacecraft enters a heliocentric disposal trajectory and undergoes full passivation (venting lines, draining batteries, cutting RF power) to prevent uncontrolled Earth return.
10: Sample Recovery	Ground recovery of the SRC by international partners. Samples are returned to ESA/SOC to evaluate microgravity bioleaching efficacy.

4.2. Ground Segment

Ground segment responsibilities are divided into mission operations, science operations, and sample recovery, each assigned to a centre or partner with the relevant expertise.

Mission Operations Centre (MOC) ESA's European Space Operations Centre (ESOC) acts as the Mission Operations Centre and is the central node of the ground segment. It receives all satellite data via ESA's Estrack tracking-station network, relays payload data to the SOC, and translates the SOC's science decisions into actionable instructions uplinked to the spacecraft. Nominally, ESOC manages overall system and mission parameters over the course of the mission. It carries the highest level of ground attention during the operationally critical phases: LEOP, Sampling Operation, SRC deployment, and EOL passivation.

Scientific Operations Centre (SOC) ESA's European Space Astronomy Centre (ESAC) makes the key science decisions for the mission, particularly during proximity operations (Phases 4 to 6). As was done at Itokawa by Hayabusa, global mapping data from the remote sensing instruments is used to build a shape model of Itokawa by stereophotoclinometry [20]. This model is then used to select candidate sampling sites, with detailed site data locally refining the surface model and high-resolution spectrometer data driving the final site selection. Following the sampling operation, the SOC is responsible for reinoculating the microbial culture and monitoring live bioreactor telemetry through the bioleaching phase.

Ground Recovery Europe has no sufficiently large, unpopulated inland landmass for a hard landing, so SRC recovery is conducted with international partners at the Woomera Test Range, South Australia. The recovery team will operate under full COSPAR Category V biological containment protocols from retrieval onwards. The capsule is placed in a sealed containment bag immediately on the range before any transport, as by REQ-MIS-24b. Following retrieval, the SRC is repatriated to Europe and handed over to the designated ESA curation partner, where the sample is opened under controlled conditions, the bioleaching efficacy is assessed, and final REE quantification is performed.

4.3. Modes of Operations

To execute the mission phases effectively, the on-board software transitions through a set of operational modes, reconfiguring power allocations, thermal baselines, and ADCS rules. Table 4.2 maps each mode to its active subsystems, which drives the worst-case concurrent EPS sizing. Of particular note for the proximity campaign, Sensing Mode and Comms Mode are mutually exclusive: science-rate downlink requires the spacecraft to return to the HP and rotate to align the body-fixed HGA with Estrack, so observation data is buffered locally to mass memory and downlinked on return.

Table 4.2: Silicon Shepherd operational modes and active subsystems.

Operational Mode	Primary Description	Active Subsystems
LEOP Mode	Post-separation autonomous detumbling, array deployment, sun acquisition, first contact.	ADCS, TCS, EPS, TT&C (LGA), C&DH
Cruise Mode	Interplanetary transfer, focused on propulsion, periodic TCMs when required.	Propulsion, ADCS, TCS, EPS, C&DH, TT&C
Sensing Mode	Proximity science operations. Remote sensing instrument suite pointed at Itokawa. High-bandwidth raw data is buffered locally to mass memory.	Remote Sensing Suite, ADCS, TCS, EPS, C&DH
Comms Mode	Store-and-Forward downlink. Spacecraft returns to HP and rotates to align HGA with Estrack.	TT&C (HGA), ADCS, TCS, EPS, C&DH
Manoeuvre Mode	Translational thruster firings to relocate the spacecraft during proximity operations (e.g., 20 km to 6 km).	ADCS (RCS & sensors), TCS, EPS, C&DH
Bioprocessing Mode	Biological activation/monitoring at HP. Operates concurrently with Comms Mode, mutually exclusive with Cruise Mode.	Bioreactor, TCS, EPS, TT&C (HGA/MGA), C&DH, ADCS
Sampling Mode	Highly autonomous execution of the Touch-and-Go (TAG) manoeuvre.	Sampling Mechanism, ADCS, Remote Sensing Suite, EPS
Spin Mode	Execution of spacecraft spinning manoeuvre imparting 15 RPM to the SRC after deployment.	ADCS, TCS, EPS, TT&C (LGA), C&DH
Standby Mode	Nominal idling and station-keeping. Passive attitude control and minimal housekeeping telemetry generation.	EPS, ADCS (reaction wheels + RCS) C&DH, TT&C (LGA)
Troubleshoot Mode	Commanded by MOC to isolate faults. Executes sequential diagnostic testing of redundant hardware strings.	C&DH, TCS, Targeted Subsystem under test
Safe Mode	Emergency survival mode. Non-essential payloads/engines powered down. ADCS maintains rigid sun-pointing; omnidirectional LGA await ground intervention.	TCS, EPS, ADCS (Sun-pointing), TT&C (LGA), C&DH (Minimal)

The 11 modes fall into three groups by the autonomy they demand. Ground-commanded Cruise, Comms, and Troubleshoot modes execute against a sequence defined prior to the start of the mission. Autonomous proximity modes: Sensing, Manoeuvre, and Sampling must run open-loop between contacts, since the one-way light time to Itokawa (tens of minutes to over an hour depending on the heliocentric geometry) precludes joystick control of any time-critical manoeuvres. Survival and housekeeping modes: Safe, LEOP, Spin, Standby, and Bioprocessing hold a defined safe configuration with minimal or no ground dependence. This grouping, rather than the chronological phase order, is what sets the fault-tolerance requirements on each mode: the autonomous proximity modes carry the burden of on-board hazard detection and abort logic, because no ground operator can intervene inside the event.

Mode transitions are commanded by the on-board software against the active phase, with two exceptions that any mode can preempt: a fault that exceeds the FDIR thresholds forces an immediate transition to Safe Mode, and a completed contingency diagnostic returns control to Troubleshoot Mode. The nominal proximity cycle alternates between the autonomously maintained stand-off positions: the spacecraft descends under Manoeuvre Mode, holds station and collects data in Sensing Mode, then climbs back to the HP under Manoeuvre Mode and transitions to Comms Mode to clear the buffer, Standby Mode ensuing while the ground segment analyses the data and establishes the following course of action. Sampling Mode is entered only after a candidate site has been validated across the full reconnaissance campaign, and it is the single most autonomy-intensive mode, executing the TAG descent, contact, and ascent without ground in the loop.

4.4. Mission Timeline

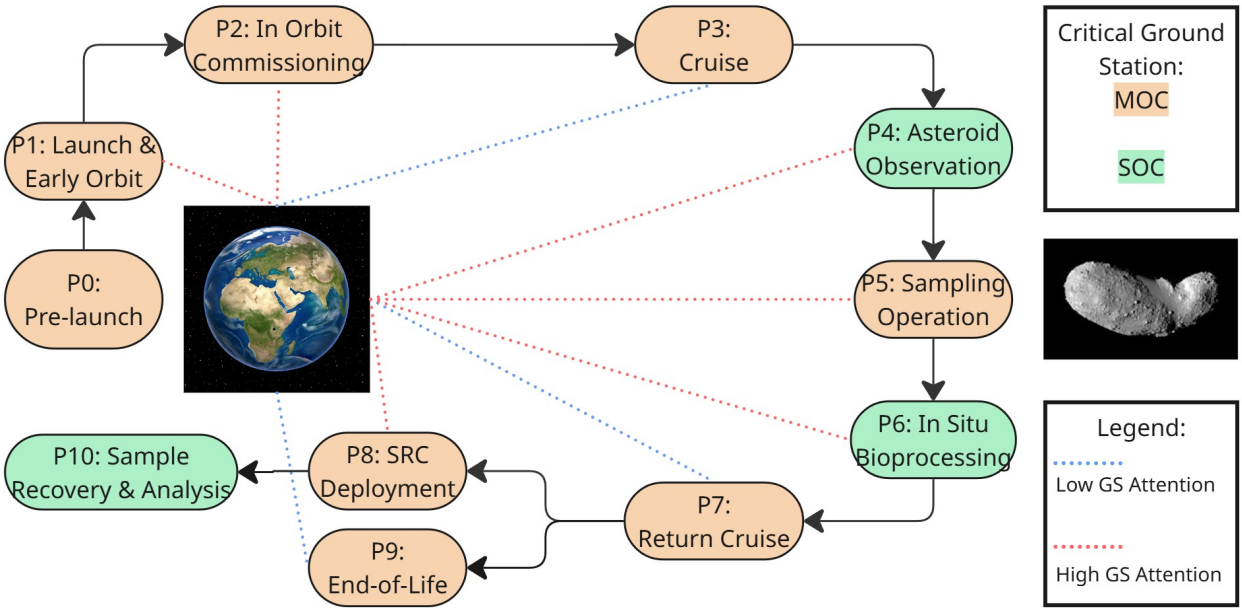

Figure 4.1: Silicon Shepherd ConOps diagram.

Figure 4.1 and Table 4.3 combine the mission phases, operational modes, and estimated durations into the preliminary mission timeline. Durations are based on comparable mission timelines, except for the in situ bioleaching phase, which follows MISAR sizing in Section 6.1.

4.4.1. Launch & Early Orbit Phase

LEOP covers the transition from the encapsulated launch configuration to a power-positive, ground-commandable spacecraft ready for cruise.

Launch: The launch stage delivers the encapsulated spacecraft onto its Earth-escape trajectory aboard an Ariane 62. After powered ascent, the fairing is jettisoned once aerothermal flux falls below the spacecraft's exposure limit, and the upper stage completes the escape burn before release. The spacecraft remains in Standby Mode on internal power, guided by the launch vehicle for approximately one hour to separation, which marks *Alicanto*'s handover to ESOC.

Table 4.3: Silicon Shepherd mission duration.

Title	Primary Mode(s)	Estimated Duration	Key Operational Milestones
LEOP	Standby → LEOP	~ 6 Hours	Lift-off, atmospheric ascent, fairing jettison, spacecraft separation, initial telemetry lock, autonomous detumbling, and solar array deployment.
In-Orbit Commissioning	Troubleshoot, Standby → Cruise	~ 75 Days	Commissioning of spacecraft, with final verification of spacecraft bus and check on payload subsystems.
Outbound Cruise	Cruise	350 Days	Primary propulsion manoeuvres, periodic ADCS TCMs.
Asteroid Observation	Sensing ↔ Comms → Standby	157 Days	Pole determination, global mapping, site identification, detailed reconnaissance, and site selection.
Sampling Operations	Manoeuvre, Sampling	7 Days	Final descent, Autonomous TAG execution, regolith capture (< 1 min sampling), ascent to HP, SRC regolith transfer.
In Situ Bioleaching	Bioprocessing ↔ Comms	120 Days	Active bioreactor operations at HP, SRC leachate transfer, biological fixation.
Earth-Return Cruise	Cruise, Spin	365 Days	Bioreactor deactivated. Primary propulsion departure manoeuvres, SRC re-entry targeting.
SRC Deployment	Cruise	~ 24 Hrs	Mechanical separation of SRC, spin-stabilisation, spacecraft deflection manoeuvre.
EOL	Safe → Passivation	~ 7 Days	Injection to disposal orbit, venting of propellants, battery discharge, RF deactivation.
Recovery & Analysis	–	Years	SRC ground recovery, biological efficacy assessment, final REE quantification at the SOC and partner laboratories/institutes.

Early Orbit: The early-orbit stage is the most critical survival phase: its objective is to reach a safe, power-positive state. Following separation, the ADCS damps the residual tip-off rates and acquires the Sun vector, and the solar arrays deploy to establish a power-positive attitude. The spacecraft then opens its first Estrack telemetry link through the low-gain antennas; the stage lasts ~3 hours.

4.4.2. In-Orbit Commissioning

Once the spacecraft is safe and power-positive, commissioning progressively verifies every subsystem from its post-LEOP configuration to a cruise-ready state. It proceeds bus-first: the EPS, TCS, C&DH, and ADCS are checked against nominal performance, the high-gain antenna is exercised to confirm the high-rate downlink, and the primary propulsion chain is verified ahead of the first cruise manoeuvre. The remote sensing instruments receive a power-on functional check only, as the payload is not commissioned for science until asteroid arrival, consistent with the deep-space profile. The bioreactor remains dormant until Phase 6, though the Health Monitoring System's functioning is verified. The stage is conducted under ESOC oversight and concludes with the transition to Cruise Mode once the bus is confirmed nominal, spanning approximately 75 days.

4.4.3. Cruise

The outbound and inbound cruise phases are both conducted in Cruise Mode, during which the primary propulsion executes the bulk transfer manoeuvres while the ADCS maintains the thrust vector. ESOC downlinks telemetry periodically and commands the TCMs required to target Itokawa on the outbound leg and the atmospheric entry corridor on the return leg. During the return cruise the bioreactor is deactivated, and the biological payload is held chemically inert inside the sealed Sample Return Capsule (SRC).

4.4.4. Proximity Operations

Proximity operations comprise the asteroid observation, sampling operation, and in situ bioleaching phases. Because Itokawa's negligible and highly non-spherical gravity field admits no stable low-altitude orbit, the spacecraft does not orbit the body; instead maintaining its position relative to Itokawa by autonomous station-keeping while co-orbiting the Sun on Itokawa's heliocentric trajectory. A consequence used throughout the characterisation campaign is that the spatial scan required for mapping is provided by Itokawa's ~ 12.1 h rotation sweeping the surface past the instruments, rather than by orbital motion.

Asteroid Observation
This phase proceeds with 3 remote sensing stages during which the spacecraft enters Sensing Mode: spin-pole determination, global mapping, and detailed recon. Each campaign is being buffered to the solid-state recorder and downlinked when the spacecraft returns to the HP and enters Comms mode, followed by a waiting stage in Standby mode while the SOC performs sampling site identification and selection.

Spin-pole determination: Following optical acquisition of Itokawa during approach, a short imaging arc from the HP recovers the spin-pole orientation and rotation period with the narrow-angle camera. This precursor is required because the latitude-station geometry of the mapping campaign is referenced to the spin axis. Together with the establishment of nominal station-keeping capabilities, spin-pole determination is expected to take ~5 Days.

Global mapping: Global mapping produces the shape model and the mineralogical and thermal context needed to identify candidate sites. From the homing position to the 6 km MP, the spacecraft works through seven sub-spacecraft latitude stations (the equator, ±30°, ±60°, and the two poles). At each station, Itokawa's ~ 12.1 h rotation sweeps the surface past the held-attitude instruments, providing the spatial scan for three concurrent products: an SPC shape model from single-filter narrow-angle imaging, seven-band multispectral colour context, and a thermal-inertia map from the thermal-infrared spectrometer-radiometer. The spacecraft will spend a minimum of 42 orbit periods in Sensing Mode (3 sidereal days at each latitude for single-filter narrow-angle imaging and 7 more at 3 different stations to cycle through the 7 colour filters of the camera system and obtain global spectral context), representing 508 hours (~21 days). As seen in Section 7.6, the spacecraft will spend a total of 648 hours (27 days) in manoeuvre mode to descend and return to the HP and transit between the 7 global mapping stations. This brings the duration of the global mapping stage to a total of 48 days.

Site Identification: The spacecraft is then allocated 5 days for data downlinking, as 100 hours would be sufficient at the expected data rate of 32 kbps in Comms Mode with the HGA and in proximity of Itokawa. This will be followed by 50 days the spacecraft spends in Standby Mode allocated to the ground segment for building the Itokawa shape model and identifying 10 candidate sampling sites.

Detailed Reconnaissance: In this stage, each of the 10 candidate sampling sites are examined individually from the 500 m SP. Each is imaged at high resolution for boulder and geometry screening and spectrally mapped in the near and thermal infrared, respectively for carbonate avoidance and for phosphate-band confirmation. The altimeter provides ranging on approach, the laser range finder closes the altitude loop through the terminal descent below the altimeter floor, and natural-feature tracking from the wide-angle cameras provides lateral guidance. The spacecraft spends 2 sidereal days in Sensing Mode above each site, with proximity manoeuvres of ~1 hour each and ascent and descent taking 4 days each, bringing the stage to 392 hours (~16 days).

Site selection: The SOC weighs each candidate against the geometry, grain size, and phosphate-to-carbonate criteria and commands the final site selection, a decision of about one month. The buffered observation data is fully returned, with total downlink estimated to 3 days, after which the spacecraft is ready to begin the sampling operation.

Sampling Operation
Once a target site is selected, the spacecraft initiates phase 5 with a series of braking manoeuvres that decelerate it from cruise to proximity-operation velocities and stabilise it into a low-altitude proximity state. The GNC system navigates during final descent via natural-feature tracking, comparing real-time images against the high-resolution reconnaissance maps to establish a local coordinate frame and maintain precise positioning where GPS is unavailable. In the final approach the spacecraft sends a status transmission and performs its final Go/No-Go check before the following sequence:

- **Checkpoint Manoeuvre T-20 min** The spacecraft descends to about 125 m above the sampling point and matches the rotation rate of the asteroid. Then starts descending at about $10 cm/s$
- **Matchpoint Manoeuvre:** The final targeting manoeuvre places the spacecraft on a trajectory for contact with the sample site at ≤ 2 cm/s relative velocity.
- **Touch-and-Go:** At the moment of contact, the sampling arm is extended and the nitrogen pulse is triggered. This initiates regolith fluidisation into the collection head for immediate pneumatic transfer to the MISAR instrument.

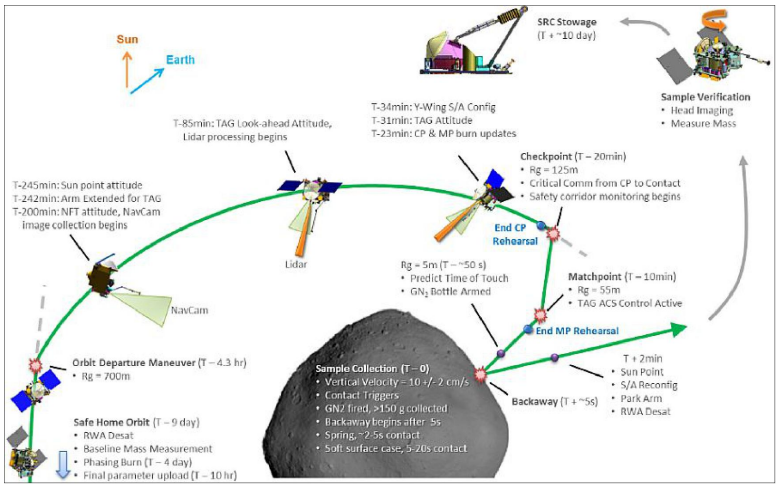

Figure 4.2: The landing sequence for OSIRIS-REx [21]

In Situ Bioleaching

After collection of the targeted 800 grams of regolith and spacecraft return to stable HP have been confirmed by the MOC, the spacecraft will enter bioprocessing mode and begin the in situ bioleaching, which can broken down into the following stages.

Germination: The fermenter is filled with medium, and the temperature of the MISAR instrument is increased to 25 °C, germinating the microbes. Germination takes 15 days [22].

Leaching operations: During leaching operations, the microbes will start producing acid, which will be fed to the regolith reactor. 15 cycles of acid production will be conducted, each with 52 cycles of regolith leaching. A cycle of acid production can take up to 7 days [23], meaning a total of 105 days of bioleaching. The precise breakdown of flow around the MISAR instrument is shown in Table 6.7, Table 6.8 and Table 6.9.

Leaching termination: Leaching terminates after 15 cycles have been conducted. The regolith and microbe reactor are filled with nitrogen gas, and the leached precipitates are filtered out and captured in the SRC.

4.4.5. End-of-Life

The end-of-life operations span SRC deployment and Earth flyby, followed by spacecraft passivation and disposal.

SRC Deployment & Earth flyby

At the conclusion of the Earth-return cruise, ESOC targets the SRC onto the atmospheric entry corridor derived in Section 6.5. Approximately four hours before entry interface, the capsule is spring-released and spun up to 15 RPM for attitude stability through the rarefied-flow regime, after which *Alicanto* executes a chemical RCS divert burn to a safe miss distance from Earth, satisfying the COSPAR Category V unrestricted Earth-return obligation. The SRC enters passively, decelerating under the PICA heat shield before deploying its drogue and main parachutes for low-velocity touchdown. The sequence is fully autonomous, consistent with the Stardust and OSIRIS-REx heritage on which the capsule is based [24, 25].

Decommissioning

The recovery phase adopts the operational framework validated by JAXA's Hayabusa2 mission [26]. After main parachute deployment, an onboard UHF beacon and ground-based radar provide trajectory tracking for helicopter-borne recovery teams. Following touchdown in the Woomera Prohibited Area, operators safe the vehicle against unactivated pyrotechnics and seal the capsule to prevent terrestrial contamination of the REE-enriched regolith before it is transported to a local containment facility and prepared for transit to the curation laboratory.

Following separation and the deflection manoeuvre, the main spacecraft uses its remaining propellant to inject it onto a stable, non-Earth-intersecting heliocentric disposal trajectory. Once ESOC has verified the final trajectory, passivation operations are performed and render the vehicle inert: pressurised propellant lines are vented, the batteries are drained and isolated, and power to the RF transmitters is cut, in compliance with the applicable space-debris-mitigation and planetary-protection requirements.

5
Astrodynamics and Trajectory

This chapter defines the Silicon Shepherd trajectory baseline and the astrodynamic interfaces used by the rest of the design. Section 5.1 introduces the driving requirements, launch allocation and modelling assumptions; Section 5.2 defines the Earth-departure and outbound low-thrust transfer; Section 5.3 covers Itokawa residence and Earth return; and Section 5.4 consolidates the resulting timeline, ΔV budget, thrust inputs, Earth arrival v_∞, capsule entry speed and remaining open work.

5.1. Design Problem, Requirements and Modelling Assumptions

Astrodynamics is used here as an interface discipline. It does not close propellant masses directly; instead, it provides the ΔV, thrust and timing inputs used later by the ion-propulsion, chemical-propulsion, EPS, ADCS, operations and SRC sections.

5.1.1. Driving Requirements and Launch Allocation

The trajectory design is mainly constrained by requirements on Itokawa access, launcher compatibility, propulsion capability, navigation, sample return and planetary protection. The full requirement wording is given in the V&V and compliance chapter. Table 5.1 summarises only the requirement groups that directly drive the astrodynamic design.

Table 5.1: Main requirement groups driving the astrodynamic design.

Requirement group	Relevant IDs	Trajectory implication
Itokawa access and operations	REQ-STK-03, REQ-MIS-02, REQ-MIS-10, REQ-SYS-04	Reach 25143 Itokawa, arrive in rendezvous, and support safe proximity operations and the sample-return mission at Itokawa.
Sample return, disposal and planetary protection	REQ-STK-04, REQ-STK-10, REQ-STK-11, REQ-MIS-13	Target an Earth atmospheric encounter for SRC release while keeping the main spacecraft on an Earth-avoidance/disposal path.
Launcher and resource compatibility	REQ-STK-08, REQ-MIS-14, REQ-MIS-15, REQ-SYS-01, REQ-SYS-02	Remain compatible with Ariane 62 rideshare launch, $M_{\text{launch}} \leq 1300$ kg, and $V_{\text{stowed}} \leq 8.8$ m^3.
Mission schedule, propulsion and navigation	REQ-STK-09, REQ-MIS-06, REQ-MIS-07, REQ-PROP-01, REQ-PROP-02, REQ-PROP-04	Define transfer windows, C_3, ΔV, thrust class, burn duration and cruise-TCM inputs; the outbound thrust estimate remains to be reconciled with REQ-PROP-04.

The active launch allocation is $M_{\text{launch,max}} = 1300$ kg and $V_{\text{stowed,max}} = 55.7$ m^3. These values are treated as rideshare allocations, not as the full Ariane 62 capability. For the high-energy HEO reference used here, an Ariane 62 capability of approximately 3300 kg is retained from the launcher-performance screening based on the Ariane 6 User's Manual [27]. To estimate a realistic secondary-passenger mass allocation, the Ariel–Comet Interceptor rideshare was used as reference: Ariel is quoted with a launch mass of approximately 1300 kg, while early Comet Interceptor constraints placed the spacecraft wet mass in the 850−900 kg range [28, 29]. Using the conservative 850 kg value gives $f_{\text{RS}} = 850/(850 + 1300) \approx 0.395$, and therefore $M_{\text{alloc}} \approx 0.395 \times 3300 \approx 1300$ kg.

The stowed-volume allocation is updated from the earlier preliminary value to $V_{\text{stowed,max}} = 55.7$ m^3. This is based on the study of analogous Ariane 62 rideshare concepts, including the Ariel-Comet Interceptor mission [30]. Within the design of Comet Interceptor, a similar stakeholder requirement as REQ-STK-08 was constraining which lead to the division of the ride-share parters to the two distinct payload areas under the Ariane 62 fairing. Additionally, the smaller F-Class Comet Interceptor was placed in the upper compartment [30]. Following this philosophy, the smallest constraining geometric volume in the upper fairing as defined by the Ariane user guide

[27] is 55.7 m^3. This value is still a project-level allocation rather than a formal launcher-interface limit, since the final usable envelope will depend on the dispenser, adapter, co-passenger layout, separation clearances and launcher-interface definition. The 1300 kg launch-mass allocation is the intended convention for the final report. Some trajectory and thrust quantities were generated before this update and still use the previous 1100 kg trade mass. These values are flagged where they appear and should be rerun once the final propulsion and system budgets are frozen.

5.1.2. General Modelling Assumptions

The transfers are modelled heliocentrically with the Sun as central body in the ECLIPJ2000 frame, using Earth and 25143 Itokawa as the modelled bodies. Lambert scans are used for first transfer-window screening, while the selected outbound case is refined with TudatPy hodographic shaping and PyGMO optimisation. Earth arrival is treated as an atmospheric encounter for SRC release rather than as spacecraft rendezvous with Earth; Earth-arrival v_∞ is therefore passed to the SRC design and is not counted as capture ΔV. Propellant masses are not final outputs of this chapter, preventing double-counting with the ion- and chemical-propulsion sections.

5.2. Earth Departure and Outbound Transfer Design

This section defines the path from the rideshare injection state to Itokawa rendezvous. The Earth-departure part selects the post-escape C_3 condition. The outbound-transfer part then connects that state to Itokawa using ion propulsion.

5.2.1. Earth-Departure Architecture

A direct launcher injection onto the Earth–Itokawa transfer is not assumed. Instead, Silicon Shepherd is treated as a rideshare spacecraft delivered to a high-energy Earth-bound orbit, after which the spacecraft performs its own chemical departure burn.

The reference departure state is an HEO-like orbit with low perigee and very high apogee, of order $r_a \sim 1.5 \times 10^6$ km, close to the Earth–Moon/L2 energy regime. This reference is consistent with high-apogee L2-transfer rideshare geometries discussed for Ariel–Comet Interceptor-type launches [31]. It keeps the spacecraft close to escape energy while still allowing a perigee kick that benefits from the Oberth effect.

The escape burn is not assumed to occur immediately after launcher separation. After separation, the spacecraft is assumed to use one full HEO revolution for early-orbit operations: detumbling, communications acquisition, Sun acquisition, initial health checks and commissioning. For the reference $r_a \sim 1.5 \times 10^6$ km HEO, this corresponds to an order-of-magnitude coast time of about 75 days. The chemical Earth-departure burn is then performed at the next perigee passage, giving the spacecraft time to confirm a healthy post-separation state before committing to escape while preserving the intended perigee-kick geometry.

The resulting perigee-kick ΔV values are ideal trajectory-interface values. The exact delivered orbit, one-orbit coast duration, separation state, phasing, finite-burn losses and outgoing asymptote direction still need to be closed with the launcher and propulsion interfaces.

The main Earth-departure options considered during the design are summarised in Table 5.2. The HEO perigee-kick architecture was selected because it keeps the final escape targeting under spacecraft control without requiring a custom external kick stage.

5.2.2. Selected C_3 Interface

Once onboard chemical departure was selected, the post-escape characteristic energy C_3 was traded. Higher C_3 lowers the outbound ion-propulsion burden, but increases the chemical kick required before ion cruise can begin. Lower C_3 does the opposite.

The heliocentric post-escape state is represented as

$$\mathbf{r}_{SC,0} \approx \mathbf{r}_\oplus(t_0), \qquad \mathbf{v}_{SC,0} = \mathbf{v}_\oplus(t_0) + \mathbf{v}_{\infty,\oplus}, \qquad |\mathbf{v}_{\infty,\oplus}| = \sqrt{C_3}.$$

The selected practical value is

$$C_3 = 6 \text{ km}^2/\text{s}^2, \qquad v_{\infty,\oplus} = 2.45 \text{ km/s}.$$

For the ideal HEO-reference perigee kick after one HEO revolution, this gives the nominal trajectory value

$$\Delta V_{\text{kick,HEO,nom}} \approx 0.293 \text{ km/s}.$$

To remain consistent with the Chemical/RCS sizing convention in Section 7.4, this nominal value is converted into the departure design interface by applying the trajectory-design margin at astrodynamics level:

Table 5.2: Condensed Earth-departure concept screening.

Concept	Principle	Outcome
Direct launcher escape	Launcher injects directly onto the Earth–Itokawa transfer.	Rejected as baseline; weakly compatible with rideshare launch.
External kick stage	Additional stage supplies Earth-escape energy.	Useful in principle, but adds mass, adapter, separation and procurement/interface risk.
HEO perigee kick, onboard chemical departure	Spacecraft performs a high-thrust burn from a high-energy Earth-bound orbit.	Selected architecture; good balance of transfer usefulness, rideshare compatibility and spacecraft control.
True Sun–Earth L2 staging	Separation near an L2-bound trajectory, then ion departure.	Rejected for baseline; loss of Oberth benefit led to an ion-equivalent requirement of about 4.27 km/s.
Lunar-transfer/flyby branch	Lunar rideshare plus lunar flyby for escape.	Rejected; valid flybys were possible but the post-flyby geometry was poor for Itokawa.
GTO chemical or ion escape	Start from GTO and supply escape energy onboard.	Rejected for baseline; even $C_3 = 0$ requires about 772 m/s, with additional radiation and eclipse concerns for ion spiral.

$$\Delta V_{\mathrm{dep,design}} = 1.25\,\Delta V_{\mathrm{kick,HEO,nom}} \approx 0.366\ \mathrm{km/s}.$$

This 366 m/s value is the Earth-departure input used by the Chemical/RCS propellant sizing. It already includes the astrodynamic trajectory margin and is therefore not given an additional propulsion-side ΔV margin. Hardware, tank, residual and system-level mass margins are applied separately in the propulsion and budget chapters.

The $C_3 = 5\ \mathrm{km^2/s^2}$ case remains a lower-energy comparison case, while $C_3 = 9\ \mathrm{km^2/s^2}$ is retained as a high-energy comparison. The $C_3 = 6\ \mathrm{km^2/s^2}$ case is carried forward because it gives a more balanced split between the chemical departure burn and the outbound ion-thrust demand.

Table 5.3: Post-escape C_3 trade summary. Design kick values include the astrodynamic trajectory margin used by the Chemical/RCS sizing.

Case	C_3	$v_{\infty,\oplus}$	Nom. kick	Design kick	Interpretation
Low-energy comparison	$5\ \mathrm{km^2/s^2}$	2.24 km/s	≈ 0.248 km/s	≈ 0.310 km/s	Lower chemical demand, but higher outbound ion-thrust requirement.
Practical baseline	$6\ \mathrm{km^2/s^2}$	2.45 km/s	≈ 0.293 km/s	≈ 0.366 km/s	Selected compromise and Chemical/RCS sizing interface.
High-energy comparison	$9\ \mathrm{km^2/s^2}$	3.00 km/s	≈ 0.425 km/s	≈ 0.531 km/s	Lower ion burden, but larger chemical departure burn.

No chemical propellant mass is reported here. The chemical-propulsion section sizes the green-monopropellant load from the departure design ΔV and applies the project margin philosophy.

5.2.3. Outbound Earth–Itokawa Transfer

The outbound trajectory starts from the $C_3 = 6\ \mathrm{km^2/s^2}$ post-escape state and ends in rendezvous with Itokawa. Lambert scans were used to identify suitable transfer windows, and the selected case was then refined with hodographic shaping to represent the transfer as a continuous low-thrust arc.

The thrust-class metric used for preliminary engine sizing is

$$T_{80} \approx \frac{m\Delta V}{0.8\,t_{\mathrm{TOF}}},$$

where m is the representative spacecraft mass during the low-thrust leg. This is a mean-thrust estimate for an 80% duty cycle, not a fully thrust-constrained optimal-control result.

The selected outbound case departs the Earth post-escape state on 6 May 2036 and arrives at Itokawa around 21 April 2037, giving a transfer time of 350 days. The trajectory is shown in Figure 5.1 and summarised in Table 5.4.

The outbound ion ΔV includes Itokawa rendezvous. It does not include the chemical departure burn used to reach the post-escape C_3 state.

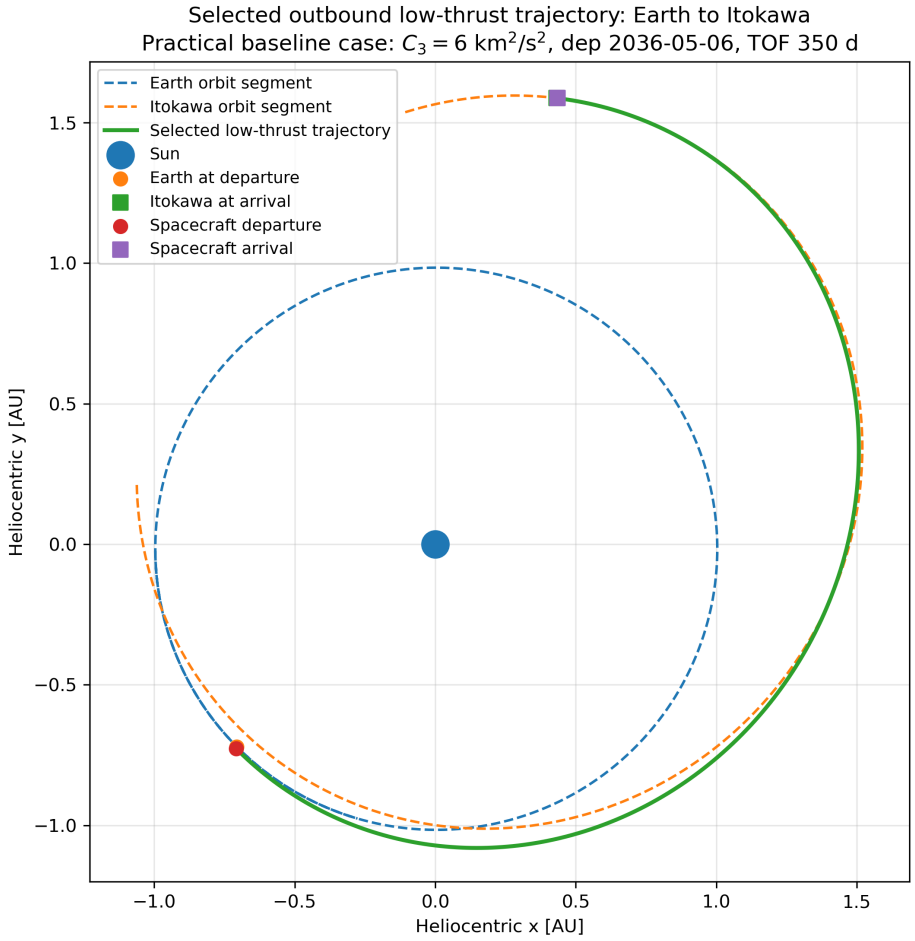

Figure 5.1: Selected $C_3 = 6$ km^2/s^2 outbound low-thrust trajectory from Earth to Itokawa in the heliocentric $x - y$ plane.

5.3. Itokawa Operations and Earth Return

This section gives the asteroid residence time, the proximity-operations hand-off, and the selected Earth-return trajectory. Detailed proximity-operation ΔV is not closed in astrodynamics because it depends on the final GNC and operations design.

5.3.1. Itokawa Residence and Proximity-Operations Interface

The outbound trajectory arrives at Itokawa around 21 April 2037. With the selected return departure on 1 July 2038, the asteroid residence time is approximately

$$t_{\text{stay}} \approx 436 \text{ days}.$$

The spacecraft is not assumed to fly a continuous low-altitude orbit around Itokawa. Instead, operations use stand-off positions, mapping observations, staged descents and short proximity manoeuvres. This is better suited to Itokawa's weak and irregular gravity field, where solar radiation pressure, navigation uncertainty and surface hazards make conventional low-altitude orbiting unattractive.

No fixed proximity-operations ΔV is allocated in this chapter. Station-keeping, disturbance rejection, sampling support and descent/rehearsal manoeuvres are assigned to ADCS and operations, where they can be assessed together with attitude-control authority, disturbance torques, navigation performance and the final sampling concept.

5.3.2. Itokawa–Earth Return Transfer

The return leg is an Itokawa-to-Earth atmospheric-encounter problem. The spacecraft does not rendezvous with Earth. Instead, Earth arrival v_∞ is passed to the SRC design as an entry driver and is not counted as spacecraft capture ΔV.

Candidate return arcs were screened using Lambert solutions from Itokawa to Earth. The approximate capsule entry speed is computed as

Table 5.4: Selected practical outbound low-thrust baseline.

Quantity	Value
Post-escape C_3	6 km^2/s^2
Post-escape $v_{\infty,\oplus}$	2.45 km/s
Earth post-escape departure	2036-05-06
Itokawa arrival	≈2037-04-21
Outbound time of flight	350 days
Approximate outbound ion ΔV	≈ 3.10 km/s
Itokawa arrival condition	Rendezvous, $v_\infty \approx 0$
T_{80}, legacy 1100 kg run	125.0 mN
Linear 1300 kg estimate for T_{80}	≈ 148 mN
Status of thrust value	To be rerun with final 1300 kg mass budget.

$$v_{\text{entry}} \approx \sqrt{v_\infty^2 + \frac{2\mu_\oplus}{R_\oplus + h_{\text{entry}}}}, \qquad h_{\text{entry}} = 125 \text{ km}.$$

The lowest-ΔV return found in the scan required 0.489 km/s at Itokawa departure, but it gave an approximate entry speed of 13.209 km/s. This exceeds the adopted 12.9 km/s entry-speed limit, which is retained as a Stardust-class sample-return reference value [32]. The selected entry-capped case therefore uses a slightly higher Itokawa departure ΔV of 0.608 km/s, reducing the approximate entry speed to 12.878 km/s.

Table 5.5: Selected Earth-return baseline.

Quantity	Selected value
Itokawa departure date	2038-07-01
Earth encounter date	2039-07-01
Return time of flight	364.763 days
Nominal return ΔV	0.608 km/s
Design return ΔV	0.760 km/s
Earth arrival v_∞	6.566 km/s
Approximate entry speed at 125 km	12.878 km/s
Entry-speed limit	12.9 km/s

The design return ΔV applies the same astrodynamics-level trajectory-margin convention used in the current system-level interface tables. Final return-leg xenon mass, thrust operating point and power compatibility are closed in the propulsion and EPS sections.

5.4. Consolidated Astrodynamic Characteristics and Interfaces

This section collects the trajectory timeline, manoeuvre interfaces, cruise-TCM estimate, subsystem hand-offs and remaining work.

5.4.1. Timeline, Manoeuvre Interfaces and TCMs

The selected outbound and return cases give the timeline in Table 5.6. The total post-escape mission duration is approximately 3.2 years, excluding launch campaign and recovery operations.

The manoeuvre hand-off is summarised in Table 5.7. The table separates nominal trajectory values from the values currently passed to propulsion sizing. These margins are not meant to be multiplied again in the propulsion chapter; subsystem hardware, tank, residual and system-level mass margins are handled in the relevant budget sections.

Table 5.6: Current trajectory timeline and phase durations. All dates and durations are approximate.

Event / phase	Date	Duration
Launch / HEO insertion	2036-02-21	–
HEO checkout coast	–	75 days
Earth post-escape departure	2036-05-06	–
Outbound cruise	–	350 days
Itokawa arrival	2037-04-21	–
Asteroid residence	–	436 days
Itokawa departure	2038-07-01	–
Return cruise	–	365 days
Earth encounter	2039-07-01	–
Total post-escape duration	–	3.2 years

Table 5.7: Consolidated trajectory-level manoeuvre interfaces for the selected baseline.

Manoeuvre / interface	Nominal value	Sizing value	Owner / use
Chemical C_3-setting burn, ideal HEO reference	≈ 0.293 km/s	≈ 0.366 km/s	Chemical/RCS propulsion; performed at perigee after one HEO revolution.
Outbound ion rendezvous transfer	≈ 3.10 km/s	≈ 3.10 km/s	Ion propulsion; includes Itokawa rendezvous.
Return ion departure manoeuvre	0.608 km/s	0.760 km/s	Ion propulsion; Earth arrival is atmospheric encounter, not capture.
Cruise trajectory-correction manoeuvres	0.015 km/s	0.01575 km/s	Chemical/RCS and operations; 5% navigation margin applied in propulsion sizing.
Itokawa proximity operations and disturbance rejection	From ADCS section	From ADCS section	ADCS and operations.
SRC release targeting and bus Earth-avoidance divert	From SRC section	From SRC section	Return Capsule section and Chemical/RCS propulsion.
Main ion subtotal	≈ 3.71 km/s	≈ 3.86 km/s	Outbound plus return ion ΔV; excludes chemical Earth departure and non-cruise manoeuvres.
Known mixed-propulsion subtotal	≈ 4.02 km/s	≈ 4.24 km/s	Chemical departure, main ion and cruise TCM only; excludes proximity and bus-divert values.

The cruise-TCM value comes from a first-order Monte Carlo estimate. Initial states were perturbed in the local RTN frame, propagated to candidate correction epochs, and corrected using a finite-difference sensitivity matrix. The 10 day correction opportunity was retained because it gave low, well-conditioned correction magnitudes for both cruise legs.

Table 5.8: Cruise TCM estimate from the single-correction Monte Carlo analysis.

Contribution	TCM epoch	$\Delta V_{95\%}$ [m/s]
Outbound cruise	10 d after departure	5.20
Return cruise	10 d after departure	2.63
Combined p95 sum	–	7.83
Rounded cruise-TCM allocation	–	15.0

The retained cruise-TCM allocation is therefore

$$\Delta V_{\mathrm{TCM,cruise}} = 15 \text{ m/s}.$$

This value covers deterministic heliocentric cruise corrections only.

5.4.2. Astrodynamic Characteristics and Derived Interfaces

The main astrodynamic characteristics and subsystem hand-offs are collected in Table 5.9.

Table 5.9: Summary of astrodynamic characteristics and derived subsystem interfaces.

Characteristic / interface	Current baseline treatment
Launcher resource allocation	Ariane 62 rideshare-compatible; $M_{\text{launch,max}} = 1300$ kg, $V_{\text{stowed,max}} = 8.8$ m^3.
Current mass-status note	Active system mass convention is 1300 kg. Some legacy thrust results still use 1100 kg and must be rerun.
Target body	Near-Earth asteroid 25143 Itokawa.
Dynamical model	Sun-centred heliocentric transfer model in ECLIPJ2000, with Earth and Itokawa as modelled bodies.
Earth-departure architecture	Spacecraft-controlled chemical C_3-setting burn from a high-energy HEO-like state, performed at perigee after one HEO revolution for commissioning and post-separation checkout.
Selected post-escape energy	$C_3 = 6$ km^2/s^2, corresponding to $v_{\infty,\oplus} = 2.45$ km/s.
Chemical departure interface	Ideal HEO-reference kick of approximately 0.293 km/s nominal; 0.366 km/s Chemical/RCS sizing value.
Outbound transfer	Low-thrust Earth–Itokawa transfer from 2036-05-06 to approximately 2037-04-21.
Outbound ion requirement	Approximately 3.10 km/s, including Itokawa rendezvous.
Outbound thrust class	Legacy $T_{80} = 125.0$ mN for 1100 kg; linear 1300 kg estimate is ≈ 148 mN. This exceeds the current REQ-PROP-04 range of 80−120 mN, so the thrust interface is partially compliant and must be rerun or re-traded.
Itokawa arrival condition	Rendezvous; arrival $v_\infty \approx 0$.
Asteroid residence	Approximately 436 days, with proximity-operation ΔV assigned to ADCS and operations.
Return transfer	Itokawa-to-Earth atmospheric encounter from 2038-07-01 to 2039-07-01.
Return ion requirement	0.608 km/s nominal; 0.760 km/s sizing value.
Cruise TCM allocation	15 m/s, covering deterministic heliocentric TCMs for outbound and return cruise.
Earth arrival condition	$v_{\infty,\oplus} = 6.566$ km/s, giving an approximate entry speed of 12.878 km/s at 125 km.
SRC and bus divert	SRC entry handled by the Return Capsule section; post-release bus divert is also taken from the Return Capsule section.
Mission duration	Approximately 3.2 years from Earth post-escape departure to Earth encounter.
Coverage and visibility	Surface coverage follows the operations concept; Earth visibility and ground-station coverage remain to be checked with TT&C and operations.

5.4.3. Limitations and Future Work

The current trajectory is a preliminary sizing baseline, not a final flight trajectory. The main remaining work is:

- **Mass update:** rerun thrust, burn-duration and propellant-interface calculations with the active 1300 kg launch-mass allocation and final propulsion budget.
- **Earth departure:** replace the ideal HEO-reference perigee kick with a finite-burn trajectory including gravity losses, outgoing asymptote constraints, one-orbit phasing, launcher separation dispersions and commissioning timeline.
- **Low-thrust optimisation:** check the outbound and return designs with a thrust-constrained optimal-control or direct-collocation method.
- **Navigation:** update the 15 m/s cruise-TCM allocation once launcher injection accuracy and orbit-determination performance are available.
- **Proximity operations:** quantify Itokawa station-keeping, disturbance rejection, descent/rehearsal and sampling-support manoeuvres in ADCS and operations.
- **SRC interface:** refine the Earth entry corridor, landing dispersion and post-SRC bus Earth-avoidance divert in the Return Capsule section.
- **Coverage and timeline:** harmonise astrodynamics dates with the operations timeline, TT&C visibility and surface-coverage plan.

The practical baseline departs Earth on 6 May 2036, arrives at Itokawa around 21 April 2037, departs Itokawa on 1 July 2038, and encounters Earth on 1 July 2039. The selected $C_3 = 6$ km^2/s^2 post-escape interface and entry-capped return case give a credible preliminary Itokawa sample-return trajectory. The remaining priority is to propagate the 1300 kg mass update through the final propulsion and EPS sizing.

6
Payload

The following chapter will outline the design of the scientific payload. It is the component of the mission that enables fulfilment of the scientific objectives of the mission. First, the design of the leaching instrument MISAR (Microbial Separator of Asteroidal Regolith) will be outlined in Section 6.1. Next the design of the concurrent health monitoring system (HMS) will be presented in Section 6.2. Afterwards, the sensing payload will be explained in Section 6.4. Following, the design of the sampling mechanism will be presented in Section 6.3, and lastly, the sampling return capsule's design will be outlined in Section 6.5.

6.1. MISAR Bioleaching Instrument

In the following section, MISAR will be outlined in more detail. First, requirements and assumptions are stated, followed by a scope definition in Section 6.1.1. Next the design of MISAR will be outlined, explaining the architecture selection in Section 6.1.2, defining microorganism handling in Section 6.1.3, REE extraction in Section 6.1.4, and presenting a hypothetical architecture in Section 6.1.5. Next, the instrument will be preliminarily sized in Section 6.1.6 and the design will be summarised in Section 6.1.8.

The bioleaching instrument has been given the name MISAR (Microbial Separator of Asteroidal Regolith).

6.1.1. Requirements, Assumptions and Scope Definition

Assumptions

All assumptions made in the design process are collected and stated in Table 6.1. They are numerous while the design heritage and scope of the MISAR design is very limited. The conservatively chosen assumptions help preliminary sizing of a low TRL instrument.

Table 6.1: Consolidated Design Assumptions for the Bioreactor System.

Assumption ID	Description
ASS-BIO-00	Fluid transport by pressurised nitrogen gas
ASS-BIO-01	Atmospheric conditions are maintained inside the reactor.
ASS-BIO-02	All dissolved iron ions in the system are assumed to be ferric ions.
ASS-BIO-03	Neodymium (Nd) is representative of all Rare Earth Elements (REEs) in the system.
ASS-BIO-04	The sample composition is assumed to be identical to the BioAsteroid composition.
ASS-BIO-05	Every metal is leached with equal efficiency during the process.
ASS-BIO-06	The leaching efficiency is representative of the expected performance.
ASS-BIO-07	100% of the oxalic acid is consumed in the regolith reactor.
ASS-BIO-08	The liquid is assumed to be kept clean through electrodialysis.
ASS-BIO-09	Electrodialysis operates at 100% efficiency.
ASS-BIO-10	Acid production scales linearly with the number of microbes.
ASS-BIO-11	The system undergoes 15 operational cycles to constrain the operations of the system.
ASS-BIO-12	The fermenter is assumed to be made of glass, while all liquid tanks are assumed to be made of stainless steel (SS).
ASS-BIO-13	Water is maintained at atmospheric conditions throughout the process.
ASS-BIO-14	Tank load is assumed to be atmospheric pressure times the launch load.
ASS-BIO-15	All tanks are assumed to be spherical in shape.
ASS-BIO-16	All tanks are sized following thin-walled assumption
ASS-BIO-17	A 20% safety factor is applied to the wall thickness of all tanks.

Continued on next page

Table 6.1 – continued from previous page

Assumption ID	Description
ASS-BIO-18	The regolith reactor wall thickness is assumed to be 5 mm.
ASS-BIO-19	The medium is assumed to have the density of water (1 kg L^{-1}).
ASS-BIO-20	The fermenter has an additional mass factor of 2.
ASS-BIO-21	Fermenter beads are assumed to be solid polyester.
ASS-BIO-22	The void fraction in fermenter and regolith reactor is assumed to be 0.46 [33].
ASS-BIO-23	Commercial N2 pressure vessels are used as referenced in [34].
ASS-BIO-24	Spores assumed stored under N2 instead of vacuum
ASS-BIO-25	Linear scaling of acid production for amount of microbes
ASS-BIO-26	Total ion displacement demand on ED twice oxalic acid
ASS-BIO-27	Desalination ED power consumption representative. [35]
ASS-BIO-28	A Margin of 50 % is taken for N_2 gas required.
ASS-BIO-29	Condiditia stored under N_2 gas under transport.

Requirements

The primary requirements driving the design of MISAR are collected and evaluated. Their target, baseline, and rationale is shown in Table 6.2:

Table 6.2: Synthesis of mission, payload, and bioreactor requirements for the Silicon Shepherd mission.

Requirement ID	Subject / Target	Design Baseline	Rationale & Resolution
REQ-MIS-01	REE/PGE extraction	Bioleaching in microgravity.	Demonstrate bioleaching on a NEA, MISAR system
REQ-MIS-12	Sample composition	≥ 5 distinct REEs in returned samples.	Show broad applicability of leaching, S-type asteroid selection with ≥ 5 distinct REEs present
REQ-MIS-13	Sample mass	≥ 5 g of processed and unprocessed asteroid regolith.	Bioreactor sizing driver
REQ-PAY-01	Bioreactor inclusion	Spent-medium bioreactor in payload.	As from tradeoff in [36]
REQ-BIO-01	*P. simplicissimum* dormancy	Dormancy maintained until Phase 6.	For safe transport. Kept dehydrated and refrigerated ($2 - 10^\circ$ C) until Phase 6
REQ-BIO-02	*P. simplicissimum* germination	Controlled germination/activation.	Fermenter hydrated and temperature increased
REQ-BIO-03	Contamination control	Closed fluid and gas exchange system.	Out of Phase 0 scope, important for reliability
REQ-BIO-04	Microbe activity sustainability	Activity sustained for bioprocessing duration.	Microbe fed-batch fed, kept at hydrated and 25 ° C conditions. Microbe degredation out of scope
REQ-BIO-05	Bioleaching enrichment	Enrichment factor ≥ 50×.	Bioreactor sizing driver
REQ-BIO-DER-01	LMC_{OOL} sample flow	5–20 μL/min, ≤ 100 μL per cycle.	Exact LMC_{OOL} integration out of scope

Scope definition and design goal

The scope of the MISAR design is defined as follows; first, an improved estimation of payload system demands over the preliminary study [36]. Secondly, the design should demonstrate technical feasibility that a bioreactor subsystem can be made and included on a space mission capable of reaching the enrichment requirements **REQ-MIS-12** & **REQ-PAY-15**. To this extent the following technicalities will be discussed; design architecture, life support demands, operational lifecycle, and subsystem sizing. Technicalities excluded from the study are discussed in Section 6.1.8.

6.1.2. MISAR Architecture Selection

The architecture present in MISAR follows from a preliminary investigation [36] in which a spent-medium bioreactor architecture was selected that utilises a packed-bed bioreactor type as a design scope. The main outcomes of the trade-off analysis is discussed as follows.

The spent-medium architecture was selected largely as the separated nature of the bioleaching procedure enables

an improved environmental tolerance and improved leaching efficacy to other methods[37]. A packed-bed reactor style was selected as the design scope against other membrane based space-tested reactor types and other typical terrestrial types for several reasons. Firstly, the gravitational requirement posed by typical terrestrial reactors[38] or the rotating nature [39] of other systems poses clashes with the spacecraft simplicity philosophy in accordance with **REQ-STK-01**. Additionally, with respect to membrane-based bioreactor these have space heritage having been tested on the BioAsteroid and BioRock missions [40]. However, a packed-bed reactor also has space-heritage [41] and a simplified structure [42] that lends itself to microgravity performance.

6.1.3. Microorganism Handling

Storage

In the preliminary design, it has been established that *P. simplicissimum* species will be transported in the form of lyophised conidia. [36] This is the most stable form for long term storage and best compatible with the space environment, and led to **REQ-BIO-01**. To keep dormant, coniditia have to be stored under vacuum or an inert gas at low above-freezing temperatures $4 - 10\,^{\circ}$ C [43] . From this follows a **REQ-TCS-DER-07**. No tradeoff has been conducted onto storage under vacuum or nitrogen gas, so is has been mass-conservatively assumed to be under N_2 gas (**ASS-BIO-29**).

Germination

To germinate the freezedried fungi, they need to be brought to a temperature of 25 degrees. Also, they need to be hydrated and kept at a pH of around 5 [22]. It was shown simplicimum germinates optimally at a water activity of 98 and above [44]. To wake the microbes, it is thus sufficient to fill the bioreactor with medium (at pH 5) and increase the temperature from cruise temp (4 to $10\,^{\circ}$ C) to bioleaching temp ($25\,^{\circ}$ C) to start germination. pH control will be required [22] to keep microbes, something kept out of scope.

Nutrition strategy

Five nutrition strategies have been analysed, as outlined in [45]. Their compatibility with the selected bioreactor architecture [36] is assessed in Table 6.3:

Table 6.3: Compatibility of feeding strategies outlined in Fike [45] with a spend-medium packed-bed acid producing fermenter

Feeding strategy	Compatible with production cycles	Compatible with packed-bed fermenter
Batch		X
Fed-batch	X	X
Continuous		
Perfusion culture		
Controlled fed-perfusion	X	

Only a fed-batch feeding strategy is compatible with the selected bioreactor design. It also offers benefits in terms of culture longevity, product concentration and complexity [45]. Most heritage into bioleaching is done through batch or fed-batch feeding strategies [23, 46]. From heritage, it can be determined that a feed needs a sugar source, nitrogen source, sulfur source and phosphate source [23]. Exact determination of the batch composition and sizing is excluded from the design scope.

6.1.4. REE extraction

One of the significant design challenges for MISAR is achieving a 50× enrichment despite other metal ion contaminants, as the expected composition of the target regolith is more than 2 % other metals [3]. A mechanism needs to be found to both extract the solved REE ions from the medium such that they can be collected in the SRC, and to purify this content to include relatively more REEs. Extraction of REEs with other metal contaminants has been point of multiple researches. Literature points to oxalic acid as a promising tool in high-purity REE extraction through selective precipitation [47]. Leaching of LL chondrite rich in other metals than REE, mainly iron [3] may provide difficulties when Ferric ions occupy and precipitate with oxalates, a problem that can be solved through pre-removal with sulphuric acid [48] or an excess of oxalates, which reduces ferric ions to ferrous ions, which are more soluble with oxalic acid [49]. Conveniently, it is one of the acids produced by *P. simplicissimum* [40, 23]. Next to the option of using a microbe-origin chemical to collect REE ions, other possibilities have been considered. First, selective precipitation using ammonium-hydroxide is an option, able to selectively precipitate REEs while ions like ferric stay soluble with citric acid [50]. Additionally, separation through electrolysis is considered. To select a REE extraction method, the options have been analysed, as shown in Table 6.4:

Table 6.4: REE extraction design option analysis and outcome

Option	Analysis	Outcome
Oxalate extraction	Shows credible scaling by precipiation with microbe-origin chemical	Selected
Ammonium Nitrate	Leaching chemical of inorganic origin that is not feed, no show of credible scalability, breach of **REQ-STK-14**	Not selected
Electrolysis	No REE deposition possible, water deterioration before REE isolation [51]	Not selected.

Of the three options analysed, only oxalate extraction, which is of microbe-origin, is a viable option to stay within user requirements. Hence it is selected and design and sizing is continued upon its selection.

As per the mechanisms explained in [49], a excess of oxalic acid is required to prevent iron ions from leaching. To keep the metal ions in the regolith reactor, after moving out of the regolith reactor, the medium is first transferred to a demineralisation (demi) tank, where through electrodialysis the medium is de-ionised, and the ions are retransported to the regolith reactor. This way, all metal ions stay in the regolith reactor, while simultaneously a excess of oxalic acid builds up in the regolith reactor.

To extract the precipitates from the medium, they are filitered out. For this, a 2-filter setup is selected, to prevent regolith particles from reaching the SRC filter that captures the final sample. Exact filter sizing is not conducted, but the regolith filter has been given a placeholder 20 µm and the capture filter 1 µm. This is deemed sufficient, as oxalates form crystals in between this range [52], letting the large regolith particles get filtered out by the first, and the oxalate crystals captured by the second. To prevent clogging of the capturing filter, a bypass filter will be used during cycle leaching operations.

Washing operations may also need to be conducted to suspend oxalate crystels in the regolith reactor, such that they do not get trapped in the regolith. This is left for forward work.

6.1.5. Hypothetical architecture

With the microbe handling and REE extraction outlined, a hypothetical architecture has been generated, from which MISAR will be sized. Fluid handling has been left for forward work, but for accurate sizing estimations a nitrogen tank is included by **ASS-BIO-00**. The architecture includes five liquid tanks; Volume control, Fermenter, Acid tank, Regolith reactor and Demi Tank. The architecture is shown in Figure 6.1. In the schematic Ω refers to volume capacity (how much liquid fits inside the tank), whereas V is used as a symbol for occupation volume (how much space the tank occupies).

6.1.6. Sizing

In the following subsection MISAR will be preliminarily sized according to the assumptions in Table 6.1.

Mass and volume sizing

To comply with a 50×enrichment (**REQ-PAY-15**) for a 5 g returned sample (**REQ-PAY-15**) 630.5 µg should be in the returned sample. This was calculated through taking the 2.522 µg g^{-1} REE content of the bioasteroid LL Chondrite, and multiplying with the required enrichment $5 \times 50 \times 2.522 = 630.5$ µg. The efficiencies of the extraction process were taken 95 % for both filters, in line with modern micron-size filters [53], 95 % for the precipitation efficiency [49], and 75 % leaching efficiency from particles >0.5 mm [54]. Additionally an additional 50 % efficiency is taken to account for losses in regolith flushing, electrodialysis and unforeseen losses. The required regolith can be computed as:

$$m_{\text{req,regolith}} = \frac{m_{\text{req,REE}}}{\eta_{\text{safety}} \cdot \eta_{\text{filter,2}} \cdot \eta_{\text{filter,1}} \cdot \eta_{\text{precipitation}} \cdot \eta_{\text{leaching}} \cdot w_{\text{REE}}} = 777.6\text{g}$$

According to Nawab, Yang, and Honaker [49], 80 g L^{-1} of oxalic acid are sufficient to saturate 0.6205 g L^{-1} of dissolved ferric ions. For a sample of 777.6 g, with a 75 % leaching efficiency and a sample composition as in BioAsteroid [3], 8.472 kg Oxalic Acid will be required:

$$m_{\text{Acid}} = \frac{w_{\text{acid}}}{w_{\text{ferric}}} \cdot m_{\text{req,regolith}} \cdot w_{\text{Iron,sample}} = \frac{80}{0.6205} \cdot 777.6 \cdot 0.084502 = 8.472\text{kg}$$

Using [23] where *P. simplicissimum* was capable of producing 2.6 g L^{-1} of oxalic acid. A total of 3243 L of medium would be required. This is too large for a Ariane 62 rideshare, well outside the mass budget. From **ASS-BIO-11** and the fact that packed-bed reactors can house up to a order of magnitude more microbes [42], the total amount of acid required, with 10^8 microbes L^{-1} is 324 L. By **ASS-BIO-11** for 15 cycles, this means

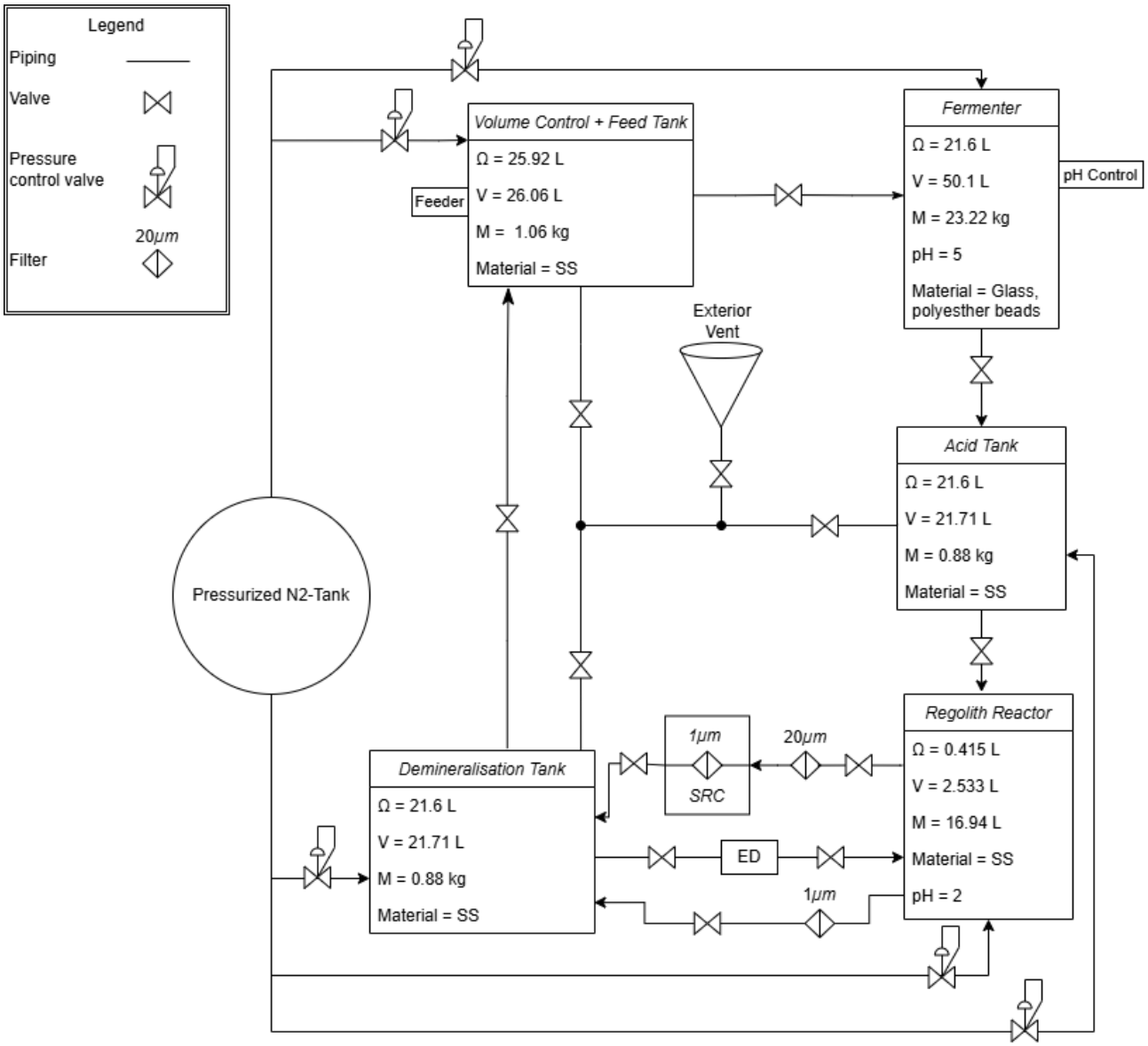

Figure 6.1: Schematic viewing of MISAR

batches of 21.6 L, which will be the volume capacity of the fermenter and acid tank. The volume of the regolith reactor will be determined by the void fraction of a packed-bed reactor, which can be assumed 0.46 [33]. The regolith is of density $\rho = 3.5\,\mathrm{g\,cm^{-3}}$ [16], occupying a volume of $\frac{777.6}{3.5} = 0.222\,\mathrm{L}$. The tank would thus be 0.411 L. This is rounded to 0.415 L to perform 52 cycles of acid leaching for each cycle of acid production. Only the bioreactor needs to be continuously in water, therefore, twice 21.6 L, or 43.2 L is required. A safety factor of 10% is included, sizing the volume control tank to 25.92 L, and a total medium loaded of 47.52 L.

The tanks have to sustain a pressure difference of 1 atmosphere. Tank thicknesses for the volume controll, acid, regolith and demi-tank have been calculated using the formula for a thin-walled spherical tank (**ASS-BIO-17, ASS-BIO-16, ASS-BIO-15, ASS-BIO-14**) Equation 6.1:

$$t = k\frac{p}{2}\sqrt[3]{\frac{3}{4}\frac{\Omega}{\pi}} \tag{6.1}$$

Where Ω is the volume capacity, in line with the thin-walled assumption, and $k = 1.2$ the safety factor. Pressure is taken as 6 (launch loads) times the atmospheric conditions, this pressure far exceeds the load of the water weight at the same load factor, it is hence considered a conservative estimation. The regolith tank is assumed a thickness of 5 mm to protect against regolith damage.

Mass can be calculated:

$$m = \rho \cdot t \cdot 4\pi\sqrt[3]{\frac{3}{4}\frac{\Omega}{\pi}}^{2} \tag{6.2}$$

The fermenter is sized by taking borosilicate glass [55] for the same load case. Also, the mass of beads are added, with a packing fraction of 0.54 [33] and made of polyester, have a mass of $0.54 * 21.6 * 1.45 = 16.9$ kg, and a occupational volume accordingly.

The required N_2 volume to displace the fluids (assume atmospheric conditions **ASS-BIO-01**) is 735.23 L from the bioreactor operations Section 6.1.7. A safety factor of 50% is taken to arrive to 1103 L of N_2. The mass is estimated using an AirLiquide N_2 bottle of 1400 L [34].

The full volumetric and mass breakdown is shown in Table 6.5. A volume margin of 10% and mass margin of 20% is included to encompass tubing, Electrodialysis device and other supporting equipment.

Table 6.5: MISAR Mass and volume budget breakdown per tank and fluid

Component	Volume capacity (Ω) [L]	Occupational Volume [L]	Dry mass [kg]	Material
Volume control + feed tank	25.92	26.06	1.06	Stainless Steel
Fermenter	21.6	50.10	33.28	Glass, polyester
Acid tank	21.6	21.71	0.88	Stainless Steel
Regolith reactor	0.415	2.533	16.94	Stainless Steel
Demi-tank	21.6	21.71	0.88	Stainless Steel
N_2 pressure tank	1103 (1 atm)	8.60	14	Steel
Medium	n.a.	47.52 (not added to total)	47.52	
N_2 gas	n.a.	1103 (pressurised, not added to total)	1.38	
Total	91.14	129.72	115.94	
Margin		10%	20%	
Total with margin		142.69	139.13	

Power sizing

The thermal management is taken under the thermal system power budget. The figure for the midterm report is therefore terminated. Instead, the identifiable power sources are taken, namely, electrodialysis and operations (valving and dispensers) is considered.

For fluid operations, the 18 W figure is retained from midterm design [36], as exact detailing is out of scope. Added is the power consumption of the electrodialysis unit. Its power can be estimated by taking the 94.13 mol oxalic acid produced, and by **ASS-BIO-26** the demand on the ED is 0.075 mol h^{-1}, well below the capacity of the desalination ED plant from [35]. 33 W is therefore considered a conservative estimation. Still, an additional 50 % growth margin is taken to take into account to arrive at a power figure of 76.5 W.

6.1.7. Operations

In the following section the broad operational outline of MISAR is presented.

First, Table 6.6 shows MISAR's operations along the mission timeline. The species is kept dormant until it is germinated before initialising bioleaching procedures, and terminated after bioleaching procedures are completed. The bioleaching phase will be outlined in more detail in the rest of the section.

Table 6.6: MISAR operational phases

Mission Phase	Leaching Phase	Operation
0 through 4	Cruise	Lyophised coniditia kept dormant
5	Sample collection	Regolith disposed in regolith reactor
6 (15 days (4.4))	Germination	Rehydration and warming of spores to germinate
6 (106 days (4.4))	Leaching	Repetition of leaching cycles under acid production
7 and onward	Return cruise	Termination of leaching procedures

For each tank included in the hypothetical architecture, the usage has been outlined for each leaching phase and shown in Table 6.7. *Empty* is used as a placeholder where it it yet to be determined whether vacuum or N_2 gas should be used.

Table 6.7: MISAR tank usage for each leaching phase

Leaching Phase	Medium tank	Fermenter	Acid tank	Regolith reactor	Demi- tank
Cruise	Medium Storage	Lyophilised conditia under N_2	Empty	Empty	Medium storage
Sample collection	Medium Storage	Lyophilised conditia under N_2	Empty	Regolith under gas	Medium storage
Germination	Medium Storage	Filled with medium, spores germinating	Empty	Regolith under gas	N_2 gas
Leaching	Medium replenishment and volume control	Microorganism producing acid	Acid volume control	Regolith leaching	Demineralisation
Return cruise	Medium	N_2 + dehydrated microorganism	Medium	N_2	N_2

Next, Table 6.8 displays MISAR's operations during an acid production cycle. After an initial period of acid production, following ASS-BIO-11; 15 7-day mining cycles of bioleaching and acid reproduction are performed.

Table 6.8: Tank usage for an acid production cycle

Phase	Medium tank	Bioreactor	Acid tank	Regolith reactor	Demi- tank
First Acid production	Medium storage	Microorganism producing acid	N_2	Regolith + N_2	N_2
Mining Cycle	N_2	Microorganism producing acid on new medium	Acidic medium produced in previous batch	Regolith under acidic medium with ion return	Medium demineralisation
Re-nourishment	Medium renourishment	Fungi producing acid on same medium	N_2	Regolith + acid + ions	N_2

Each of the 15 acid production phases constitutes 52 regolith leach cycles to concentrate the acid and metal ions. Table 6.9 shows details the operations of a regolith leaching cycle.

Table 6.9: Tank usage for a regolith leaching cycle

Phase	Acid tank	Regolith reactor	Filters and ED	Demi- tank
Pre-leaching	Acidic medium	N_2 + regolith	–	N_2
First leach	Acidic medium + N_2 driving gas	Regolith + acid	–	N_2
Repeated 52× *per acid production cycle:*				
Acid renewal	415 ml acid moves to regolith reactor	Old acid moves to Demi- tank, new acid flows in	1 micron filter used to prevent precipitates escaping	415 ml spent acid moves in
Leaching	Acid + N_2 driving gas	Regolith + new acid + ion return	ED returning ions	Spend acid demineralisation
Last leach per acid batch	N_2	Last acid flows out, replaced with acid from new batch	1 micron filter used to prevent precipitates escaping, ED returning ions	Demineralised medium to Medium tank for renourishment

6.1.8. MISAR Design Summary

The design of the MISAR has successfully completed its goal as stated in Table 6.1.1. Potential is shown that an instrument can be constructed to comply with the requirements as outlined in Table 6.2. The design summary and budgets are outlined in Table 6.10. Additional derived requirements to be imposed upon the thermal control system (TCS) are detailed in Table 6.11.

Table 6.10: Full MISAR design breakdown

Parameter	Value
Mass	139.13 kg
Volume	142.69 L
Power	76.5 W
Cost	Donated by scientific community and member states
TRL	Lowest: 4, as a system: 3
Fermenter type	Packed bed
Regolith reactor type	packed bed
Feeding strategy	Fed-batch
REE extraction	Filtered Oxalate crystals

Table 6.11: Derived requirements from MISAR

Requirement ID	Subject/ Target	Requirement	Rationale
REQ-TCS-DER-02	TCS	The TCS shall ensure the bioreactor operates within the 20–30°C range.	Inoculation of spores
REQ-TCS-DER-07	TCS	The TCS shall ensure a $2 - 10$ ° C of the fermenter during cruise phase	Storage of spores

Forward work

Since MISAR is a novel design and the field of extraterrestrial bioleaching is in its infancy, significant forward work is necessary to ensure suitable design maturity before operation. These work recommendations are described below in Table 6.12

Table 6.12: Future work recommendations and subsystem detailing requirements.

Required Work	Description
Exact acid production profile	The acid production figures used are terrestrial values, ideally values should be verified and calculations reiterated using microgravity-based values.
Feed detailing	Optimal nutrient feed composition and amount should be investigated for microgravity-based oxalic acid production. Additionally, the feed dispensing mechanism should be detailed.
Electrodialysis unit detailing	The ED unit has to be accurately detailed in terms of size, voltage, architecture, integration and power usage.
Piping detailing	Connecting the tanks requires piping, which needs to be design for mass and challenges, including microbial waste and clogging due to flagella
Fluid handling demands on S/C	Fluid handling may put demands on the spacecraft like degassing and sloshing. An analysis into these effects should be conducted and mitigating measures implemented when necessary.
Aeration of the fermenter	*P. simplicissimum* is an aerobic organism requiring oxygen to survive and produce acid. Future design of MISAR should analyse and detail oxygen demands and select a suitable aerating mechanism.
Exact LMC_{OOL} integration	by **REQ-BIO-DER-01** a flow rate is required on the LMC_{OOL} interface. An exact integration should be made which meets this demand from the HMS.
Microbe degradation	The degradation of microbes, both in number and in efficacy of acid production should be quantified and analysed, and the instrument should be sized accordingly.
Filter sizing	The exact efficiency of filters and size of precipitate crystals should be analysed and filter should be selected and sized accordingly.
Regolith washing	Regolith cleaning may be desired by the system to enable suspension of precipitated. A detailed design of this process is necessary.
pH control of fermenter	The fermenter requires pH control, but this is yet to be detailed. It should be analysed and sized.
Nitrogen or Vacuum trade off	The transport of dormant spores under vacuum or nitrogen-gas requires a detailed trade-off.

The overall scientific maturity of this field still poses the largest challenge for future design maturity. All technologies used in the bioreactor are space-proven, as outlined in Section 12.6, except the space bioreactor technology. More in-depth bioleaching experiments in space are required to improve design maturity. Specifically, research into acid production of microbes under microgravity and fed-batch feeding should be conducted to mature space bioreactor technology. Technology maturation is further detailed in Section 12.6.1.

6.2. Health Monitoring System

This section presents the detailed design of the Health Monitoring System (HMS), which is responsible for continuous direct microorganism and environmental monitoring. Section 6.2.1 presents and assumptions and driving requirements of the HMS, followed by Section 6.2.2 in which the design objectives and methodologies are detailed. Section 6.2.3 continues through a description of the selected instruments and overviews the overall subsystem architecture, and Section 6.2.4 outlines the biomarkers selected for monitoring. Finally, Section 6.2.5 presents the overall technical budget before Section 6.2.6 and discusses notes for future study.

6.2.1. Driving Assumptions and Requirements

Table 6.13: Consolidated Design Assumptions for the Health Monitoring System (HMS).

Assumption ID	Description
ASS-HMS-01	HMS operates autonomously throughout active bio-leeching phase.
ASS-HMS-02	Anomalous threshold values established and accounted for pre-launch
ASS-HMS-03	Tier 0 flags hardware faults and wont allow subsequent tier escalation until hardware faults addressed
ASS-HMS-04	All instruments used are qualified for space conditions, if not they are under development and will be at acceptable TRL prior to Silicon Shepherd launch
ASS-HMS-05	Resource budgets for some instruments are classified and are proprietary data and are best guess estimates based on similar reference instruments found online
ASS-HMS-06	Calibration intervals are sufficient for correct functionality through entire mission duration without manual recalibration
ASS-HMS-07	Leak detection sensitivity is adequate to detect biological leaks before any sterilisation protocols are initiated
ASS-HMS-08	Nominal *P. Simplicissimum* culture states are characterised pre-launch and anomalous threshold values are defined
ASS-HMS-09	Molecular Imprinted Polymers (MIPs) can be developed for each bio-marker
ASS-HMS-10	All 20 bio-marker receptors are developed and verified for use prior to launch - Most time & cost intensive process for HMS
ASS-HMS-11	LMC_{OOL} reliability decrease from effects such as degradation and radiation is considered to be neglegible.
ASS-HMS-12	A buffer solution of PBS (phosphate-buffered saline) with concentration of 5mg/L is used and is assumed compatible with *P. Simplicissimum*
ASS-HMS-13	The LMC_{OOL} receptor are weak binding so the buffer solution washes before and after sample introduction will prevent cross-contamination

Table 6.14: Consolidated Design Requirement for the Health Monitoring System (HMS).

Assumption ID	Description
REQ-BIO-03	The bioreactor shall implement a closed, contamination-controlled fluid and gas exchange system
REQ-MIS-16	The bioreactor containment system shall prevent any release of biological material to the asteroid environment under all credible failure modes.
REQ-MIS-17	The cell culture health shall be continuously monitored during bioprocessing operations.
REQ-HMS-01	The health state of the *P. simplicissimum* shall be monitored continuously throughout all active bioreactor phases.
REQ-HMS-02	The system shall provide sufficient information on the microorganism state for autonomous C&DH decision-making.
REQ-HMS-03	The cellular integrity of the *P. simplicissimum* shall be monitored primarily using LMC_{OOL} chips.
REQ-HMS-04	The system shall detect and assess potential indications of life in asteroid samples using LMC_{OOL} chips.
REQ-HMS-05	The system shall provide information on the containment status of the microorganism.
REQ-HMS-06	The system shall characterise the effects of prolonged cosmic radiation exposure on the microorganism.
REQ-HMS-07	The system shall implement redundancy for all instruments including LMC_{OOL} chips to ensure data reliability.

6.2.2. Objectives and Methodology

The primary objective of the HMS, **PO-1**, is to provide continuous data on the state of the culture and to enable autonomous decision-making based on the biological condition of *P. simplicissimum* throughout the active bioreactor phases, ensuring the culture remains viable and capable of performing the biomining process.

Secondary objectives further define the depth and scope of the HMS. Each is outlined below alongside the methodological approach adopted within the HMS architecture to address it.

Table 6.15: Scientific and operational objectives and their verification methods.

Objective ID	Description
SO-1	Contribute to the broader scientific case for the mission by characterising biological activity in an extreme extraterrestrial environment. The presence of amino acids on asteroidal surfaces, such as Bennu, was confirmed by NASA's OSIRIS-REx mission [56]; even though Itokawa itself may not host such compounds, demonstrating sustained microbial activity under these conditions provides scientific data that strengthens the justification for the Silicon Shepherd mission.
SO-2	Detect deviations from nominal culture conditions at the earliest possible stage, before anomalies become irreversible. This is achieved through continuous Tier 1 physicochemical monitoring (temperature, pH, dissolved O_2/CO_2), which responds fastest to environmental upsets and triggers escalation to higher tiers for diagnosis.
SO-3	Confirm biological integrity prior to sample return, providing the go/no-go evidence required to initiate processed sample collection. This is achieved by requiring confirmatory Tier 2 and Tier 3 data, rather than Tier 1 data alone, before a positive containment and viability status is reported to CD&H.
SO-4	Preserve LMC_{OOL} consumables by deploying Tier 3 only when necessary. This is achieved through the tiered escalation logic itself: Tier 3 biomarker detections are only triggered by a Tier 1 or Tier 2 flag, rather than running continuously, directly limiting consumable usage.
SO-5	Ensure all biological measurements are trustworthy by verifying containment and instrument integrity before biological data is processed. This is achieved through the Tier 0 hardware-fault gate (ASS-HMS-03), which blocks escalation to biological measurement tiers until any underlying hardware fault is resolved, preventing corrupted or false biological readings from reaching CD&H.
SO-6	Characterise the radiation stress environment experienced by *P. simplicissimum* in space, contributing scientific data on the effects of cosmic radiation on fungal culture health, addressing REQ-HMS-06. This is achieved by correlating Tier 3 biomarker trends against mission elapsed time and known radiation dose accumulation.

6.2.3. Instrumentation and System Architecture

The Health Monitoring System (HMS) employs a four-tier instrumentation architecture, illustrated in Figure 6.2, that progressively escalates from continuous hardware verification to targeted biological diagnostics. Tier 0 safeguards the physical integrity of the system itself, ensuring that pumps, filters, and sensors are functioning correctly before any biological data is trusted. Tier 1 then provides continuous, real-time monitoring of core environmental parameters within the bioreactor. Tier 2 builds on this by periodically assessing the metabolic state of the culture, while Tier 3 performs the most resource-intensive checks, conducting daily biological integrity assessments. Each tier can trigger the next out of sequence in response to anomalies, allowing the system to allocate monitoring resources proportionally to risk while keeping nominal operations lightweight. The following subsections detail the instrumentation, operating cadence, and rationale for each tier.

Tier 0 — Containment and System Integrity

Tier 0 operates continuously and functions as a pre-condition for all subsequent tiers. It does not monitor biological parameters directly, instead it verifies that the physical and instrumentation of the HMS is functioning correctly. Four functions are monitored: pump status by flow rate verification via a miniature flow sensor, filter integrity via differential pressure monitoring across each filter present, leak detection via pressure drop monitoring and trace gas sensing, and lastly automated bio-reactor sensor calibration checks.

In accordance with ASS-HMS-03, hardware faults identified by Tier 0 suspend higher-tier measurements until resolved. This provides continuous active verification of biological containment. Tier 0 instruments are mentioned in Table 6.17 and will be integrated around the bio-reactor and along the connected piping systems, all instrument commands and intervals are executed through the C&DH subsystem.

Tier 1 — Environmental Monitoring

Tier 1 provides continuous, real-time monitoring of six core environmental parameters via inline sensors that require no sample extraction: pH, dissolved oxygen, and dissolved carbon dioxide. Temperature is monitored via a resistance temperature detector (RTD) probe, while biomass concentration is tracked through an optical backscatter sensor mounted externally to the bioreactor vessel, avoiding any contact with the culture medium.

While continuous monitoring is a mission requirement, true continuous sampling would generate data volumes that place a significant strain on the overall system. Following recommendations from external sources, a measurement interval of once every 30-60 minutes was therefore adopted as a practical compromise between data fidelity and system load.

Tier 1 instruments are listed in Table 6.17 and are located inside the bioreactor itself; all instrument commands and intervals are executed through the C&DH subsystem.

Tier 2 — Culture State Assessment

Tier 2 operates hourly (2-4 hours) or is triggered by a Tier 1 anomaly event. Metal ion concentrations that might be present in the bioreactor such as Ca^{2+}, K^{+} and Na^{+} are monitored via solid-state ISFET sensors [57], and require no consumables.

Identifying an exact instrument that can measure sucrose concentrations proved to be the most time consuming task, but instruments that can measure glucose such as [58] are widely available and the molecular structure of both is similar so investing on developing an instrument that could measure exclusively sucrose concentration is a valid option.

An increase in metal ions confirm active bio leaching, and sucrose depletion show the culture is consuming its food source and together they provide a complementary pair of events that can help in understanding the overall state of the culture. Tier 2 instruments are mentioned in Table 6.17 and are located inside the bio reactor itself, all instrument commands and intervals are executed through the C&DH subsystem

Tier 3 — Biological Integrity Check

Tier 3 operates from a daily measurement cycle under nominal conditions or is brought forward due to a Tier 1 and Tier 2 anomaly event. A sample flow rate of 5–20 μL/min with a minimum of 100 μL per cycle is required to pass through the LMC_{OOL} chamber to get valid readings. A PBS buffer solution at 5 mg/L concentration is flushed through all chips both before and after sample introduction for approximately 10 mins whilst the sample has to run through the housing for approximately 20 mins. As stated from ASS-HMS-13, washing receptors clears them of residual analytes from the previous cycles thus decreasing cross-contamination events.

Tier 3 consists of: 14 units of LMC_{OOL} chips, 7 chips in series operating as 2 sets in parallel for redundancy purposes, and will be operating inside a separated chip housing chamber, a container of about $\sim$ 250 mL to store the PBS solution, and a waste chamber of $\sim$ 500 mL to store both discarded PBS buffer solution and the bio reactor samples.

6.2.4. Biomarker Selection

The Tier 3 biological integrity compliance requires the LMC_{OOL} chip sensing surfaces to be fitted with selective bio marker receptors prior to launch. Each chip at a size of 5x10x3mm^3 and combined requiring less than 10 W to operate, each accommodates six receptors, five of which are allocated to active target molecules and the final receptor is used as a comparative reference check. Receptors are engineered using Molecularly Imprinted Polymers (MIPs) [59], which provide synthetic binding sites complementary to each target molecule's geometry, these molecules are cheaper to produce and can work over a larger range of both temperatures and pH levels when compared to naturally occurring receptor bodies.

The target molecule panel is distributed across six distinct chips, each addressing an aspect related to the health of the culture: DNA and RNA oxidative integrity (Chip A), Cellular energy status (chip B), 20 amino acids (Chip C,D,E and F), and 5 nucleobase profiles (Chip G) .

The full target molecule panel and associated justifications are presented in Table 6.16

Table 6.16: LMC_{OOL} target molecule panel for bioreactor culture health monitoring.

Slot	Molecule	Justification
Chip A — DNA/RNA Oxidative Stress Responses		
1	8-oxo-dG	Primary oxidative DNA lesion formed by stress events on guanine. Persistent dose-dependent increases reported in bio-fluids following high-LET radiation exposure, directly relevant to the deep space cosmic radiation environment. [60]
2	8-oxo-G	RNA equivalent of 8-oxo-dG. The ratio between 8-oxo-dG/8-oxo-G provides a complete picture of oxidative damage across both DNA and RNA. [61, 62]
3	Hypoxanthine	Adenine deamination product formed in both DNA and RNA by reactive nitrogen species. Produced during ATP degradation via AMP → IMP → Hypoxanthine, provides an indication on both DNA damage and energy status signal [63, 64].

Continued on next page...

Table 6.16: LMC_{OOL} target molecule panel for bioreactor culture health monitoring.

Slot	Molecule	Justification
4	5-HMU	Thymine oxidation product formed by ionising radiation and reactive oxygen species. Provides a more complete picture of radiation-induced cell damage [65].
5	8-OH-Gua	Base excision repair product of guanine oxidation. Its presence in the culture confirms not only that DNA damage is occurring but also that the cell is actively mounting a repair response, a strong indicator of genetic integrity [66].
Chip B — Cellular Energy Status		
1	ATP	Universal energy currency in the fungal world and most direct indicator of cell viability. ATP depletion is known to precede cell death and is a standard culture viability parameter across all aerobic organisms [67].
2	ADP	Pairs with ATP as part of the adenylate pool. Rising ADP/ATP ratio signals declining metabolic capacity and reduced energy regeneration rate before total ATP depletion occurs, providing an even earlier warning compared to ATP.
3	AMP	Completes the adenylate pool alongside ATP and ADP, enabling calculation of the Adenylate Energy Charge: $$AEC = \frac{[\text{ATP}] + 0.5[\text{ADP}]}{[\text{ATP}] + [\text{ADP}] + [\text{AMP}]}$$ AEC ≈ 0.9 under healthy exponential growth; values below 0.5 indicate severe metabolic stress or signs of cell death [68, 69].
4	NADH	Redox cofactor involved in over 700 reactions related to the species in the same category as *P.simplicissimum*. Acts as a metabolic readout of the overall cell redox state [70].
5	NAD^+	Pairs with NADH for the NADH/NAD^+ ratio calculation. A rising NADH/NAD^+ ratio signals accumulation of reducing agents faster than the cell can process them, an early indicator of metabolic stress preceding ATP depletion [71].
Chip C, D, E & F— Amino Acid Profile		
1–20	**Alanine, Arginine, Asparagine, Aspartic acid, Cysteine, Glutamic acid, Glutamine, Glycine, Histidine, Isoleucine, Leucine, Lysine, Methione, Phenylalanine, Proline, Serine, Threonine, Tryptophan, Tyrosine, Valine:** Common amino acids can be utilized for monitoring nutrient depletion and protein synthesis, as amino acids are a crucial element protein synthesis. These molecules can also be used to check for signs of life on the asteroid.	
Chip G — Nucleobase Profile		
1–5	**Adenine, guanine, Xanthine, Hypoxanthine, Purine:** Canonical nucleobases to track nucleic acid turnover and availability. These nucleobases similar to the amino acids have been shown to be found on asteroidal surfaces, therefore the same reasoning stands as to why these are included in the LMC_{OOL} panel [56].	

6.2.5. Technical Budgets

Based on the Tiers mentioned above, some commercial instruments have been chosen as representative of actual instruments to be used in the mission, conservative values have been used for all parameters included as for most of the used instruments there are no definitive values, Table 6.17 shows the consolidated components with all the respective values with a overall 80% design margin to account for the extra components supporting the sensors.

Table 6.17: Health Monitoring System Consolidated Component, Mass, Power, and Volume Budget Estimate.

Instrument / Component	Unit [kg]	Qty [-]	Total [kg]	Unit [W]	Total [W]	Unit Vol. [L]
Tier 0 — Containment & System Integrity						
Pump status / micro-flow sensor [72]	0.08	2	0.16	0.25	0.50	~0.005
Differential pressure sensor [73]	~0.05	2	0.10	0.01	0.02	~0.002
Leak / trace gas sensor [74]	~0.05	2	0.10	0.10	0.20	~0.003
Tier 1 — Environmental Monitoring						
pH sensor [75]	0.12	2	0.24	0.10	0.20	~0.025
Dissolved O_2 sensor [76]	0.35	2	0.70	0.15	0.30	~0.024
Dissolved CO_2 sensor [77]	0.28	2	0.56	0.20	0.40	~0.014
Temperature sensor [78]	~0.03	2	0.06	<0.01	<0.02	~0.002
Pressure sensor [79]	~0.05	2	0.10	0.01	0.02	~0.003
Biomass concentration sensor [80]	0.15	1	0.15	0.50	0.50	~0.040

Continued on next page

Table 6.17 – continued from previous page

Instrument / Component	Unit [kg]	Qty [-]	Total [kg]	Unit [W]	Total [W]	Unit Vol. [L]
Tier 2 — Culture State Assessment						
Metal ion concentration sensor [57]	<0.01	2	~0.02	0.05	0.10	<0.001
Sucrose concentration sensor [58]	0.04	2	0.08	0.10	0.20	~0.004
Tier 3 — Biological Integrity Check						
LMC_{OOL} chips ×7	~0.26	2	~0.53	0.50	1.00	~0.020
PBS Analytical Buffer Solution	~0.124	1	~0.124	–	–	~0.124
HMS Grand Total			**~2.9 kg**	**~3.46 W**		**~0.267 L**
HMS Total (with 80% Margin)			**~5.229 kg**	**~4.2 W**		**~0.4806 L**

6.2.6. HMS Design Summary

The culture health monitoring system presented in this section constitutes a four-tier hierarchical architecture covering containment integrity, environmental monitoring, culture state assessment, and biological integrity confirmation across the 310-day Silicon Shepherd mission timeline. The estimated total system mass is ~ 5.22 kg, with an overall volume of ~ 0.4806 L and a total power consumption of ~ 4.2 W .

Several areas of the design remain at low maturity and represent the primary development priorities for subsequent mission phases:

Table 6.18: Further work recommendations and testing requirements.

Further work	Description
CGQ BioR validation for *P. simplicissimum*:	The optical backscatter biomass sensor should be validated specifically for the morphology of *P. simplicissimum* to increase reliable data acquisition and correlations prior to launch.
ISFET microgravity drift characterisation:	Long-duration ISFET sensor drift under microgravity and space radiation conditions is not well characterised in literature and represents a Tier 2 reliability risk that must be addressed through dedicated testing prior to launch.
NADH/NAD^+ detectability:	The presence of NADH and NAD^+ at detectable concentrations in the culture has not been confirmed for *P.simplicissimum*. This is the most uncertain biomarker in the Tier 3 panel and should be validated experimentally before receptor development is initiated.
Supporting structure and harness mass characterisation:	The current 5.22 kg estimate captures sensor instruments only, with an 80% margin applied as a placeholder for structural mounts, wiring harnesses, connectors, and enclosures. A detailed design phase should replace this blanket margin with component-level estimates for each tier.
Pre-launch Testing and Qualifications:	Testing of overall HMS with integration with MISAR bioreactor. Following that, an adequate testing phase encompassing tests such as vacuum/thermal cycling (TVAC), shaker testing, etc. have to be performed to ensure the HMS functions as expected and can handle the mission duration.

The HMS as designed represents a credible and mass-efficient architecture for autonomous biological integrity monitoring in a resource-constrained space environment. At an estimated total mass of 5.2 kg, it compares favourably against heritage life-detection instruments such as the ROSINA mass spectrometry package at 34.8 kg [81] and the MOMA instrument at approximately 12 kg [82], demonstrating the significant mass advantage of an LMC_{OOL}-centred architecture. The outstanding development items identified above are recommended as the primary focus of the next design phase, with biomarker validation representing the highest-priority actions given their direct impact on the Tier 3 biological integrity assessments.

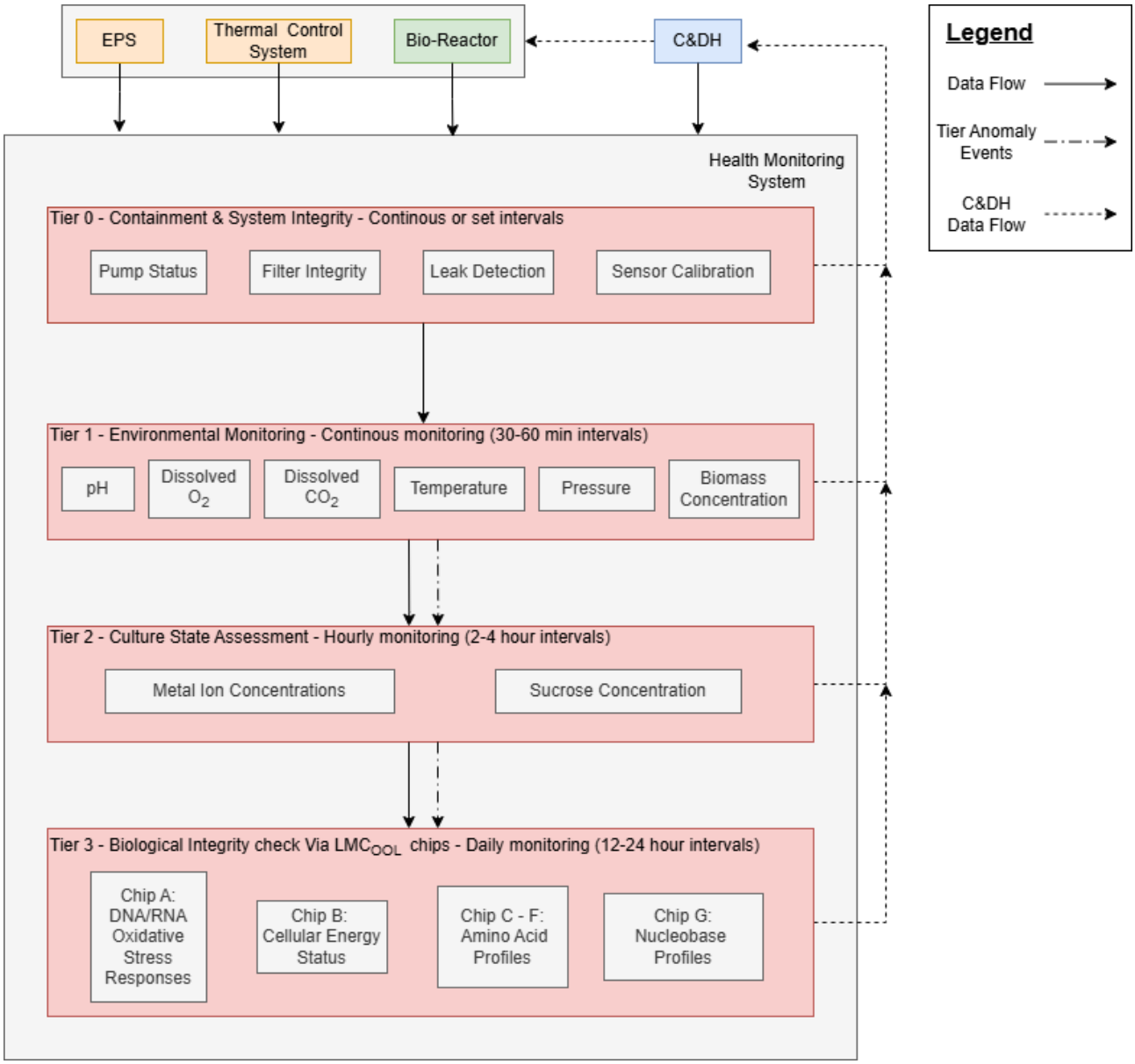

Figure 6.2: Health Monitoring System Architecture

6.3. Sampling System

The sampling system is responsible for the acquisition of asteroidal regolith and transferring to the MISAR bioreactor. This section outlines the operations , guidance sequence, interfaces, and performance parameters of the Touch-and-Go (TAG) manoeuvrer. The discussion is structured as follows: Section 6.3.1 defines the mission objectives and sampling strategy; Section 6.3.2 consolidates design assumptions and derived requirements; Section 6.3.3 details the four-stage acquisition sequence and subsystem interfaces; Section 6.3.4 presents the operational performance envelope, sizing budget, and integration parameters. Finally, Section 6.3.5 summarizes the baseline architecture and identifies forward-work priorities for subsequent design phases.

6.3.1. Objectives and Methodology

The primary objective of the sampling system is to collect about of 500 g of asteroidal regolith per acquisition visit, with sufficient particle size distribution compatibility for pneumatic ingestion into MISAR. The methodology leverages a gas-assisted collection architecture derived from the OSIRIS-REx TAGSAM heritage [83]. A shoulder-elbow-wrist articulated arm extends 1.4 m from the spacecraft bus, terminating in a 0.55 m diameter collection head. During operation, a pressurised nitrogen pulse adjutants the surface regolith into the head; the modified head seals material gas-tight and pneumatically transfers it upward through the arm to the MISAR bioreactor inlet manifold Section 6.1.2. The system has a total of six independent TAG attempts during proximity operations.

6.3.2. Assumptions and Requirements

The sampling architecture is constrained by heritage-derived performance baselines, payload integration limits, and MISAR feed specifications. Consolidated assumptions and derived requirements are synthesised in Table 6.19.

Table 6.19: Consolidated Design Assumptions and Requirements for the Sampling System.

ID	Description
ASS-SAMP-01	OSIRIS-REx TAGSAM heritage provides baseline fluidisation, sealing, and transfer performance for S-type/LL-chondrite regolith analogues.
ASS-SAMP-02	N_2 pulse achieves instantaneous regolith fluidisation and full head ingress within 0.5 s.
ASS-SAMP-03	Collection head hermetic seal maintains integrity during vacuum/low-gravity transition and pneumatic transfer; working gas is fully recaptured for recycling.
ASS-SAMP-04	Arm articulation operates within the 1.4 m reach envelope without bus interference at the $-z$ panel interface.
REQ-SAMP-01	The sampling system shall perform up to six independent TAG acquisition cycles per mission campaign.
REQ-SAMP-02	The sampling system shall collect 300–700 g of regolith per TAG, with particle size distribution compatible with MISAR pneumatic feed requirements.
REQ-SAMP-03	Visual verification of successful capture and seal integrity shall be provided via imaging with a monitoring camera before arm retraction.

6.3.3. Architecture and Operational Sequence

The sampling operation is executed in four distinct phases, leveraging heritage navigation logic and automated pneumatic handling to ensure robustness in microgravity.

Stage 1: Approach and Target Alignment Utilising reconnaissance mapping data from Section 6.4.3, the GNC system aligns the spacecraft such that the sampling arm's reach envelope covers the selected landing patch. The vehicle maintains a safe-home orbit until the final proximity phase, at which point station-keeping transitions to targeted descent planning.

Stage 2: Contact (Touch-and-Go) Following the Matchpoint trajectory correction, the spacecraft executes a brief contact phase. At < 1 km altitude, the sampling arm is deployed and a calibrated nitrogen pulse triggers simultaneously with physical surface contact to fluidise and capture regolith into the collection head.

Stage 3: Capture Verification Gas flow is reversed or terminated to seal the collection chamber. A visual inspection via a wrist-mounted camera (analogous to OSIRIS-REx's SamCam) confirms material ingress and head integrity before arm retraction initiates. If insufficient mass is detected, the system loops back to Stage 1 for subsequent TAG attempts, supporting up to six independent cycles per campaign.

Stage 4: Retrieval and Feed Transfer The arm retracts into its stowed configuration. An internal pneumatic pump engages to transfer captured regolith through dedicated feed lines directly into the MISAR regolith reactor Section 6.1.4. Upon successful injection, the system logs campaign completion, recycles working gas back to the spacecraft tank, and awaits GNC cueing for Earth-return insertion.

Subsystem Interfaces The acquisition arm integrates with three primary subsystems:

- **Mechanical:** Pivoted at the $-z$ panel of the spacecraft bus, providing structural mounting and deployment/stowage rails while maintaining clearance during articulation.
- **Electrical:** Communicates with the C&DH subsystem for actuator commanding, joint position feedback, and sampling-camera imagery downlink.
- **Fluidic:** Interfaces directly with the MISAR bioreactor inlet manifold via hermetically sealed quick-disconnect fittings, ensuring leak-tight pneumatic transfer under low-gravity conditions.

6.3.4. Performance Envelope and Sizing

The sampling system operates as a discrete, high-thrust phase within the broader payload timeline (Table 6.6). Key performance parameters are consolidated in Table 6.20, with operational envelope details below.

Table 6.20: Sample acquisition arm sizing and performance parameters.

Parameter	Value
Stowed dimensions	$140 \times 75 \times 30$ cm (315L)
Volume (assumed cube)	315 cm
Collection head diameter	55 cm
Mass (estimated, ~ 5 % of OSIRIS-REx dry)	~ 44 kg
Peak power (servos, solenoids, camera)	~ 10 W for ~ 10 min per visit
Working gas	N_2 (recycled to spacecraft tank)
Target sample mass per visit	> 500 g

Operational Envelope

- **Cycle Duration:** Each TAG sequence (approach to retraction) is designed for ~ 120 s operation, fitting within the Leaching phase timeline.
- **Nitrogen Consumption:** ≈ 2.5 kg per cycle for fluidisation and purge sealing; total campaign allocation scales with attempted cycles ($N_{\text{cycles}} \leq 6$). Recycling efficiency targets > 90% gas recovery per transfer.
- **Power Draw:** Peak loads of ~ 10 W during valve actuation, joint servoing, and camera illumination. Steady-state consumption remains < 5 W.
- **Mass Allocation:** The ~ 44 kg dry mass is integrated within the payload structural envelope, with distribution of stowed volume aligned to $-z$ panel clearance constraints.

6.3.5. Sampling System Summary and Forward Work

The sampling architecture leverages OSIRIS-REx TAGSAM heritage, shoulder-elbow-wrist articulation, and closed-loop pneumatic transfer to deliver a robust, multi-cycle acquisition capability directly coupled to the MISAR bioreactor. The design satisfies **REQ-SAMP-01** through **REQ-SAMP-03** while maintaining compatibility with the payload mass/power budget and spacecraft interface constraints.

Several areas require maturation prior to detailed design:

- **Microgravity Fluidisation Validation:** Ground testing under reduced gravity must confirm nitrogen pulse efficacy across expected regolith cohesion ranges (ASS-SAMP-01).
- (ASS-SAMP-03).
- **Arm Kinematics and Stowage:** Monte Carlo simulations of shoulder-elbow-wrist joint actuation limits must confirm 1.4 m reach clearance at the $-z$ panel without bus interference during stowed/operational transitions (ASS-SAMP-04).
- **GNC Navigation Covariance:** NFT tracking error and descent dispersion must be validated to guarantee the ≤ 2 cm contact tolerance across six independent TAG attempts.

These validation campaigns will be prioritised in the subsequent phase to retire sampling-specific risks, freeze mechanical/electrical/fluidic interfaces, and confirm hardware packaging ahead of prototype development.

6.4. Remote Sensing Suite

The remote sensing suite enables target identification during Phase 3, but also characterisation and sampling-site selection by Silicon Shepherd during Phase 4. This section presents the detailed design of the instrument suite. Section 6.4.1 first establishes the observation objectives, the ensuing subsystem requirements, and finally the requirements derived for other subsystems. Section 6.4.2 presents the selected instruments and the rationale for their selection, Section 6.4.3 summarises the operational concept, and Section 6.4.4 closes the mass, power, volume, thermal, and data budgets. The section concludes with a summary of the suite baseline and the forward-work roadmap in Section 6.4.5.

6.4.1. Driving Assumptions and Requirements

The remote sensing suite must enable the collection of Itokawa surface data allowing for the selection of a sampling site simultaneously satisfying three criteria.

- acceptable surface geometry for TAG acquisition
- majority regolith grain size in the approximate range 0.5–5 mm, compatible with pneumatic ingestion
- high abundance of desired phosphates and low carbonate presence in surface regolith

Phosphates are targeted because REEs sought are concentrated in the calcium-phosphate accessory minerals of ordinary chondrite material [15], resembling Itokawa's confirmed LL-chondrite composition [16]. Conversely, carbonates are avoided, as their alkalinity will neutralise the acid on which the downstream bioleaching depends, suppressing leaching efficiency. Obtaining remote sensing data from the various positions, stations, and rotation-driven scans described in the operations subsection sets the pointing performance the suite demands of the ADCS. Three quantities are distinguished and detailed in Section 6.4.3: absolute pointing control, pointing knowledge, and pointing stability.

Table 6.21: Consolidated design assumptions.

ID	Description
ASS-RSI-01	The remote sensing instruments required for a given phase can operate concurrently, with their fields of view simultaneously satisfiable from a single spacecraft attitude.
ASS-RSI-02	Instrument performance does not degrade over the asteroid-observation and reconnaissance phase.
ASS-RSI-03	The 10.3 μm phosphate band is resolvable against the S-type silicate emission background at the spectral SNR of the TIR spectrometer.
ASS-RSI-04	The 3.4 μm carbonate band is resolvable against the S-type silicate emission background at the spectral SNR of the VNIR spectrometer.
ASS-OPS-01	The spatial scan required for mapping is provided by Itokawa's 12.1 h rotation sweeping the surface past the held-attitude instruments, rather than by spacecraft motion.

Table 6.22: Part I — Characterisation requirements met by the suite.

ID	Requirement	Design baseline / resolution
REQ-MIS-11	The mission shall perform pre-sampling characterisation of the surface of Itokawa.	Parent requirement; decomposed into REQ-RSI-01 through REQ-RSI-04.
REQ-RSI-01	Provide a morphology characterisation of Itokawa's surface accurate to 1 m.	Stereophotoclinometry (SPC) using imaging and LiDAR altimetry data. [20]
REQ-RSI-02	Provide grain-size magnitude on Itokawa's surface down to 5×5 m patches.	Grain sizing using surface thermal-inertia data from a thermal infrared spectrometer [84].
REQ-RSI-03	Measure relative surface phosphate abundance from the 10.3 μm P–O band.	Ground analysis of thermal infrared spectra of Itokawa surface.
REQ-RSI-04	Measure relative surface carbonate abundance from the 3.4 μm band.	Ground analysis of visible-to-near-infrared spectra of Itokawa surface.

Table 6.23: Part II — Derived subsystem requirements.

ID	Design baseline	Rationale
REQ-ADCS-DER-01	Pointing control $\leq 0.008^\circ$ about each axis during Phase 4.	Place instrument footprints on the desired patch.
REQ-ADCS-DER-02	Pointing knowledge $\leq 0.005^\circ$ during Phase 4.	Keep accurate knowledge of coordinates for topography during shape modelling.
REQ-ADCS-DER-03	Pointing stability $\leq 0.004^\circ/\mathrm{s}$ during Phase 4.	Limit smear over instrument integration time.
REQ-TCS-DER-03	NIRS3 thermal control.	Suppress dark current and preserve sensitivity in the 3 μm region.
REQ-TCS-DER-04	TIR spectrometer thermal control.	The uncooled microbolometer must be kept in operating temperature range.
REQ-TCS-DER-05	MERTIS thermal stability.	The uncooled microbolometer requires tight temperature control.
REQ-CDH-01	Data storage.	Remote sensing data is buffered to SSR during observation and downlinked upon return to Home Position.

6.4.2. Instrument Selection and Rationale

The selected suite comprises an optical camera block, a near-infrared point spectrometer (NIRS), a thermal-infrared spectrometer–radiometer (TIRS), and a two-element ranging set. Heritage is drawn preferentially from flight-proven asteroid sample-return and rendezvous missions.

Table 6.24: Remote sensing suite instrument selection, primary function, and heritage.

Instrument	Primary function	Heritage
Narrow-angle camera (AFC)	Optical navigation, shape-model imaging, seven-band visible–NIR colour screening	Dawn FC / Hera AFC [85, 86]
Wide-angle cameras (SMC)	Wide-field mapping, sampling and feed monitoring	Hera SMC, Hayabusa2 ONC [86]
VNIR spectrometer (NIRS3)	Carbonate-avoidance mapping (~3.4 μm band)	Hayabusa2 NIRS3 [87]
TIR spectrometer-radiometer (MERTIS)	Phosphate detection (~10.3 μm band) and thermal-inertia grain sizing	BepiColombo MERTIS [88]

The optical functions are baselined on the Hera mission instrument line (AFC, SMC) in preference to Hayabusa heritage since this substitution reduces mass without affecting the spectral detection chain by using more modern sensors and electronics [86]. The primary science camera (narrow-angle telescopic Hera AFC), is flown with the heritage eight-position filter wheel it flew with on the Dawn mission [85]. This wheel is populated with a seven-band visible-near-infrared set spanning $0.44 - 0.97\mu m$. The colour bands straddle the $1\mu m$ mafic absorption diagnostic of Itokawa's olivine-pyroxene S-type surface, recovering spectral slope and silicate context for site screening and geological mapping at negligible cost, since the wheel is intrinsic to the instrument. This band set is functionally equivalent to the ECAS-derived filters flown on Hayabusa's AMICA at Itokawa, and thus retained here. It is not intended for the carbonate- and phosphate-detection objectives, whose features lie far beyond the silicon detector's $\sim 0.9\mu$m cut-off; those are carried by the infrared spectrometers. The carbonate-avoidance and phosphate-detection functions are split between two instruments because their diagnostic features lie in different spectral regions. Carbonates present a near-infrared absorption near 3.4 µm, accessible to the NIRS3 point spectrometer; this approach is directly preceded by the detection of carbonate features on a near-Earth asteroid with a comparable near-IR point spectrometer [89]. Phosphates have no comparable near-IR feature; their diagnostic signature is the phosphate-group fundamental near 10.3 µm in the thermal infrared, which requires the MERTIS TIR spectrometer [88]. Hera's TIRI thermal IR imager was considered for this role and rejected: a small set of fixed-band filters cannot resolve the narrow phosphate feature against the dense silicate emission background, and the limitation is spectral rather than radiometric, so it is not relieved by operating at a lower altitude. The same instrument provides the surface thermal-inertia measurement used for grain-size screening since thermal inertia maps onto effective grain size across the $\tilde{0}$.05–5 mm regime and has flight heritage for surface mapping at rubble-pile asteroids [90, 91]. The grain-size-to-thermal-inertia calibration is material-dependent, so the carbonaceous-asteroid calibrations are not transferred directly to the S-type Itokawa case [84].

The selected spectrometers are iterative with respect to Hayabusa2 and miniaturised relative to instruments flown on OSIRIS-REx, which together perform the equivalent carbonate, phosphate, and thermal-inertia measurements. OTES is explicitly designed to resolve features of silicates, carbonates, sulphates, phosphates, oxides, and hydroxides, establishing a direct precedent for the phosphate-detection objective [92]. The capability traded away in the miniaturised baseline is spectral range and spectral SNR. The residual risk associated with resolving a shallow phosphate band with a mass-constrained instrument is carried in the technical risk register and in the forward-work roadmap and is the subject of ongoing consultation with mission-heritage subject-matter experts.

6.4.3. Remote Sensing Operations

Three stand-off positions structure the suite's use, consistent with the operations and logistics concept: a Home Position (HP) at 20 km (downlink, standby, and bioprocessing), a Mapping Position (MP) at 6 km, and a Siting Position (SP) at 500 m for sampling-site validation. Because stable bound orbits do not exist at Itokawa's negligible gravity, the spacecraft maintains these positions by autonomous station-keeping while co-orbiting the Sun on Itokawa's heliocentric trajectory. Two consequences follow: the spatial scan required for mapping is provided by Itokawa's 12.1 h rotation rather than by spacecraft motion, and diurnal thermal coverage requires a moderate Sun–spacecraft–asteroid phase angle so that the terminator and night side fall within the instrument field of view. The suite is exercised across three sequential proximity phases from these positions.

A short imaging arc from the HP recovers Itokawa's spin-pole orientation and rotation period before the characterisation geometry is defined. This precursor is required because the latitude-station geometry of the global phase is referenced to the spin axis.

Global characterisation is conducted from a set of sub-spacecraft latitude stations spanning the equator to both poles, reached by a single descent from the HP, followed by translations parallel to the spin axis. At each station, Itokawa's rotation sweeps the surface past the instruments, providing the spatial scan for three

concurrent products: an SPC shape model from single-filter narrow-angle imaging, multispectral colour context from the seven-band filter set [20], and a thermal-inertia map from the MERTIS radiometer. Thermal inertia is derived by fitting the diurnal temperature variation, which the rotation supplies, provided the station geometry keeps the terminator in view, from which a grain size map of Itokawa can then be obtained by the SOC [84]. The campaign is buffered to the solid-state recorder and downlinked on return to the HP, as science-rate downlink and asteroid pointing cannot be performed simultaneously.

A set of candidate sampling sites is examined at the siting altitude with high-resolution imaging for boulder and geometry screening, NIR spectroscopy for carbonate avoidance, and TIR spectroscopy for phosphate-band confirmation. Direct imaging resolves the coarse block population to be avoided, while the effective fine-fraction grain size in the 0.5–5 mm band of interest is screened from the global thermal-inertia map and confirmed post-mission by returned-sample analysis. The laser range finder provides closed-loop altitude through the terminal descent below the altimeter floor, and natural-feature tracking from the cameras provides lateral guidance; ranging and lateral guidance are complementary functions and are not interchangeable.

6.4.4. Mass, Power, Volume, Thermal, and Data Budget

The preliminary suite resource budget is given below. Values are first-order estimates scaled from the heritage instruments and are consistent with the system-level payload budget.

Table 6.25: Mass, power, and volume estimates for the remote sensing suite.

Instrument	Mass [kg]	Peak power [W]	Volume [L]
AFC	1.5	1.3	2.0
SMC ×2	1.7 (0.85 each)	8 (4 each)	1.6 (0.8 each)
VNIR spectrometer (NIRS3)	∼2.0	∼10	2.0
TIR spectrometer–radiometer (MERTIS)	3.1	∼10	4.0
Total instrument suite	**∼8.3**	**∼30**	**9.6**

The suite imposes one driving thermal requirement and two secondary ones, formalised as **REQ-TCS-DER-03**, **REQ-TCS-DER-04**, and **REQ-TCS-DER-05**. The NIRS3 detector requires cooling to ∼188 K (−85°C) by a dedicated passive radiator to suppress dark current and preserve sensitivity in the 3 μm region; this deep cold sink is distinct from the warm, heater-biased payload zones and competes for cold-facing radiator area with the bus radiator. The MERTIS instrument is uncooled but requires tight detector-temperature stability and a radiometric calibration reference. The cameras operate over a broad envelope (−60 to +40°C) accommodated within the bus cold-bias range, with reduced sensitivity if the detector runs warmer than its optimum of −60°C; this is treated as a performance trade rather than a hard thermal requirement.

The preliminary data generation for the proximity campaign is summarised below. The dominant contributor is the multispectral imaging of the global phase. The total campaign volume buffers comfortably within the solid-state recorder (**REQ-CDH-01**). Downlink is the binding operational constraint: at the X-band capability of the selected telecommunications architecture, and because science-rate downlink and asteroid pointing cannot be performed simultaneously with the body-fixed HGA, the campaign requires an extended sequence of ground-station passes spread across the asteroid-observation phase allocation; data compression is identified as a mitigation and is deferred to detailed design.

Table 6.26: Data-generation estimates for the proximity campaign (first-order, uncompressed).

Phase	Product	Volume
Global	Shape-model imaging (single-filter)	∼0.33 GB
Global	Multispectral context (seven-band)	∼0.98 GB
Global	Thermal-inertia mapping	∼0.07 GB
Global	Altimetry (ranging)	negligible
Recon	Site imaging (multi-band)	∼0.49 GB
Recon	Spectroscopy (NIR + TIR)	small
Campaign total		**∼1.9 GB (∼15 Gbit)**

The remote sensing suite is represented in the system-level power budget by two active states. The navigation-only state is used during sampling and proximity manoeuvres, where camera-based optical navigation and laser ranging are required. The full-science-sensing state is used during global mapping and site reconnaissance when the camera block, laser-ranging set, and both spectrometers are assumed available.

Table 6.27: Power-state assumptions for the remote sensing suite.

Power state	Active instrument configuration	Power
Navigation only	Camera block	~10 W
Full science sensing	Camera block + Spectrometer block	~30 W

Per-frame sizing assumes the narrow-angle camera detector format at its quoted bit depth; the multispectral total scales with the number of full colour coverages, and the thermal and spectroscopic volumes are driven by the scan-line and per-pointing counts. All figures are preliminary and will be refined once the detailed observation plan and instrument operating parameters are fixed.

6.4.5. Remote Sensing Suite Summary and Forward Work

Because the preliminary design relies on heritage performance data and on calibrations established at bodies of different taxonomy, several assumptions must be investigated in further design:

- **Phosphate-band detectability (ASS-RSI-03):** A quantitative band-depth and SNR analysis must be performed for the MERTIS spectrometer. This is the highest-risk element of the suite.
- **Thermal-inertia grain-size calibration (REQ-RSI-02):** An S-type, LL-chondrite-specific grain-size-to-thermal-inertia calibration must be derived, since heritage calibrations on carbonaceous-asteroid (Bennu, Ryugu) do not transfer directly.
- **Pointing-budget closure (REQ-ADCS-DER-01, REQ-ADCS-DER-03):** The narrow-angle camera and spectrometer integration and scan-line times must be fixed to confirm the stability allocation.
- **Data volume and downlink (REQ-CDH-01):** A data-compression assumption and a detailed observation plan must be adopted to refine the $\tilde{1}.9$ GB estimate and to confirm closure against the X/Ka-band downlink across the asteroid-observation phase allocation.
- **Instrument and interface maturation:** The AFC seven-band filter complement must be confirmed at build level, the NIRS3 cold-radiator interface (**REQ-TCS-DER-03**) must be sized against the available cold-facing radiator area.
- **SNR Verification:** The SNR of heritage instruments from mission calibration and measurements for their respective missions and environments must be cross-examined to obtain SNR for operation at Itokawa and validate instrument selection.
- **Dark current:** The effect of dark current on measurements and methods to minimise it during operations from the remote sensing suite must be investigated.

6.5. Sample Return Capsule

This section presents the detailed design of the Sample Return Capsule (SRC), the passive Earth-return that delivers the regolith through entry, descent, and landing. It starts by consolidating the design assumptions, as well as the payload, mission, and newly derived subsystem requirements. Section 6.5.2 then establishes the entry corridor and the gyroscopic stability that fixes the flight path angle and spin rate, which Section 6.5.3 then brings into the calibrated aerothermal environment. Section 6.5.4 sizes the thermal protection system and capsule geometry, after which Section 6.5.5 presents the separation kinematics and the Earth-avoidance manoeuvre. Section 6.5.6 closes the passive descent and parachute chain, and Section 6.5.7 selects the landing site. The section concludes with a summary of the SRC baseline and the forward-work roadmap (Table 6.5.8).

6.5.1. Assumptions and Requirements

The primary payload and mission requirements have been evaluated against the baseline design, heritage data, and as-flown parameters. Furthermore, the detailed design of the SRC imposes new critical constraints on the primary spacecraft to ensure successful delivery. Table 6.29 synthesises these conflicts, establishes the updated design baselines, and explicitly outlines the derived requirements that must be adopted by the respective spacecraft subsystems.

Table 6.28: Consolidated Design Assumptions for the Sample Return Capsule (SRC).

Assumption ID	Description
ASS-SRC-01	Total entry mass is strictly locked at 46.0 kg (Stardust heritage) [93, 32].
ASS-SRC-02	The internal payload canister fits within the heritage volume without requiring outer mold line modifications [93, 14].
ASS-SRC-03	The 32 g biological deceleration limit is retired due to the payload being inactivated/dead.
ASS-SRC-04	Hypersonic drag coefficient (C_D) is constant at 1.50 across the continuum regime [94, 24].
ASS-SRC-05	Peak dynamic pressure is calculated utilizing the recessed "Ablated Geometry" profile [94].
ASS-SRC-06	A 15 RPM longitudinal spin provides sufficient transient gyroscopic stiffness to survive the 15-second unstable rarefied flow transit [95, 94].
ASS-SRC-07	The spacecraft inertia tensor (I_{xx}/I_{yy}) inherently satisfies oblate major-axis spinner stability criteria [95].
ASS-SRC-08	The U.S. Standard Atmosphere 1976 profile accurately represents the entry corridor without day-of-entry localized variations [96].
ASS-SRC-09	Empirical scaling factors (K_q, K_Q) sufficiently capture both radiative heating and convective bias, and remain valid extrapolated to the slightly lower entry speed [24, 97].
ASS-SRC-10	E-4 hour separation passively mitigates deep-space cross-track drift perturbations [95].
ASS-SRC-11	The $\approx$ 34.7 m/s Earth Avoidance Manoeuvre (EAM) utilises a small-angle divert approximation
ASS-SRC-12	Angular momentum from the 15 RPM spin effectively suppresses unmodelled spring force tip-off rates [32, 95].
ASS-SRC-13	The 1.6% atmospheric density deficit at Woomera (170 m ASL) is negligible for parachute sizing [96].
ASS-SRC-14	Linear scaling of the OSIRIS-REx delivery footprint conservatively bounds Woomera cross-wind and aerodynamic dispersions [14, 25].

Table 6.29: Synthesis of resolved payload/mission requirements and derived spacecraft subsystem requirements.

Requirement ID	Subject / Target	Design Baseline	Rationale & Resolution
Part I: Payload & Mission Resolutions (Capsule Internal Limits)			
REQ-SRC-01	Orig: $\geq$ 32 g deceleration	**40 g** design limit.	Nominal entry generates 35.2 g, and steep limit generates 37.5 g. The 32 g biological limit is retired (manifest is inert). A standard FoS must be explicitly defined against 40 g.
REQ-SRC-02	Orig: $\geq$ 12 km/s.	**12.9 km/s** entry.	Heritage Review of Design (RoD) is invalid above 12.9 km/s. Verification must shift to analysis and testing, utilising a 1.15 to 1.20 uncertainty factor for recession scaling.
REQ-SRC-03	Orig: $V_{td} \leq 5$ m/s.	Parachute **D** $\approx$ **7.66** m.	A 7.3 m canopy at $C_D = 0.65$ yields $\approx$ 5.25 m/s, violating the requirement. Hence, a 7.66m parachute has been selected, instead of the heritage 7.3m.
REQ-SRC-04 **REQ-MIS-13**	Orig: $\geq$ 5 g processed & unprocessed.	Clarification pending.	Current wording conflates biomass, asteroidal material, and the REE-loaded electrode. The definition of "processed" must be fixed to align with the payload manifest.
Part II: Derived Subsystem Requirements (Mothership Interfaces)			
REQ-ADCS-DER-04	ADCS	Orient vector & spin SRC to **15 RPM**.	Provides the SRC with transient gyroscopic stiffness to prevent pitch divergence (tumbling) during the brief 15-second transit through unstable, rarefied flow.

6.5.2. Entry Corridor and Flight Dynamics

The objective of the entry corridor analysis is to define a safe geometric window where the sample return system may enter the Earth's atmosphere, satisfying both structural and thermal survivability.

Trajectory Model

The corridor analysis originates from a simplified version of the six-degree-of-freedom atmospheric flight dynamics analysis from NASA[98]. It is sized with a three-degree-of-freedom point-mass integrator, written

in Python and solved with an explicit Runge–Kutta scheme (`solve_ivp`, RK45). The state is the radius, the Earth-relative speed, and the flight path angle γ, propagated in the vertical plane from the 120 km interface to the surface:

$$\dot{V} = -\frac{\rho V^2 C_D A}{2m} - g\sin\gamma, \qquad \dot{\gamma} = \left(\frac{V}{r} - \frac{g}{V}\right)\cos\gamma, \qquad \dot{h} = V\sin\gamma, \tag{6.3}$$

with altitude-varying gravity $g = \mu/r^2$ and an exponential atmosphere $\rho = \rho_0 e^{-h/H}$ ($\rho_0 = 1.225\,\mathrm{kg/m^3}$, $H = 7.2\,\mathrm{km}$). The vehicle is the Stardust aeroshell: $m = 46\,\mathrm{kg}$ (**ASS-SRC-01**), $C_D = 1.50$ (**ASS-SRC-04**), and the ablated reference diameter $d = 0.81\,\mathrm{m}$ (**ASS-SRC-05**) [94, 32], for a ballistic coefficient $\beta = m/(C_D A) \approx 59\,\mathrm{kg/m^2}$. Entry is fixed at the Itokawa return speed $V_E = 12.88\,\mathrm{km/s}$.

Corridor Logic and Result

The model runs as two nested sweeps. The first step, γ from shallow to steep, integrates each trajectory to the ground, and records the peak deceleration $n_g = D/(mg_0)$. A steeper descent spends less time in the atmosphere and lowers the integrated heat soak, so the trajectory is biased as steeply as the structure permits. The steep (undershoot) bound is the $40\,g_0$ qualification load, set to match OSIRIS-REx once the inert manifest retires the original $32\,g_0$ biological limit (**ASS-SRC-03**, **REQ-PAY-01**) [25], with the aeroshell failure limit at $50\,g_0$. The shallow (overshoot) bound is the thermal-soak ceiling carried from the aerothermal model in Section 6.5.3.

Together these close a narrow window at $\gamma = -7.6° \pm 0.2°$, levied back on the spacecraft as a navigation requirement. The steep edge ($-7.8°$) peaks at $37.5\,g_0$ and is g-limited, the shallow edge ($-7.4°$) peaks at $32.9\,g_0$ and is heat-limited. Finally, the nominal $-7.6°$ sits at $35.2\,g_0$. Every case clears the design load with a margin.

Spin Rate

A capsule in this band is statically unstable. Above ~ 85 km the rarefied flow pushes the centre of pressure ahead of the centre of gravity ($C_{m_\alpha} > 0$), so any disturbance grows, and the vehicle tends to tumble backward [94]. The second sweep tests longitudinal spin against this. Across 120 km to 90 km it forms a gyroscopic stability ratio $S_g = (I_{xx}\omega)^2/(4I_{yy}M_{\mathrm{aero}})$, with $M_{\mathrm{aero}} = qAd\,C_{m_\alpha}$, and raises the spin until $S_g \geq 1.1$ everywhere in the band. Held to that steady-state criterion, the model returns a spin above 50 RPM (≈ 52 RPM at the 12.88 km/s state), which is expensive in terms of spacecraft control authority.

That requirement is unnecessary, because the instability does not persist. The capsule crosses the unstable band in 10 s to 15 s, and once it drops below ~ 85 km the bow shock forms, the centre of pressure returns behind the centre of gravity, and the vehicle damps back to $\alpha \approx 0°$ on its own [95]. The spin only has to slow pitch divergence over that short window and absorb the spring tip-off at release (**ASS-SRC-06**, **ASS-SRC-12**), not hold $S_g \geq 1$ throughout. The steady-state figure is therefore dropped, and the flight-proven Stardust release of ~ 13.5 RPM is adopted as a 15 RPM baseline (**REQ-ADCs-DER-04**,**ASS-SRC-07**).

6.5.3. Aerothermal Analysis

The entry heating environment is established with a 3-DOF ballistic-entry integrator coupled to a stagnation-point heating model, written in Python and exercised across the full $\gamma_E = -7.6° \pm 0.2°$ corridor at the return entry state $V_E = 12.88\,\mathrm{km/s}$ derived in Section 6.5.2. The point-mass equations of motion are integrated in the vertical plane:

$$\dot{V} = -\rho V^2 C_D A/(2m) - g\sin\gamma, \dot{\gamma} = (V/r - g/V)\cos\gamma, \dot{h} = -V\sin\gamma \tag{6.4}$$

with altitude-varying gravity $g = g_0(R_E/r)^2$ and the U.S. Standard Atmosphere 1976 density profile [96] (**ASS-SRC-08**), using an Runge-Kutta (RK45) scheme and an entry interface at 120 km. The convective stagnation-point flux follows the Sutton-Graves correlation [99],

$$q_c = C\sqrt{\rho_\infty/R_n}\,V^3 \tag{6.5}$$

with $C = 1.7415 \times 10^{-8}$ and output in $\mathrm{W/cm^2}$, and the integrated load is $Q = \int q\,\mathrm{d}t$.

The drag coefficient is fixed at $C_D = 1.5$. This value reproduces the published Stardust ballistic coefficient of $\sim 60\,\mathrm{kg/m^2}$, validating our method. The C_D also places the modelled peak-heating altitude near the heritage flight values (Stardust and OSIRIS-REx, ~62 km), which validates the trajectory phasing independently of the heating model.

Radiative heating is deliberately not evaluated by a closed correlation. The Tauber-Sutton relation [97] was fitted for nose radii of order 1 m to 23 m, and at our $R_n = 0.22\,\mathrm{m}$, it lies an order of magnitude outside its validity range and returns an unphysical $2\,\mathrm{W/cm^2}$ to $3\,\mathrm{W/cm^2}$. Because the SRC is geometrically a Stardust flight twin, the total environment is instead anchored empirically to the Stardust post-flight CFD reconstruction ($942\,\mathrm{W/cm^2}$ peak, $27.6\,\mathrm{kJ/cm^2}$ load) [24]: the bare model, run at the Stardust geometry and entry state, is scaled by geometry-matched factors $K_q \approx 1.16$ on peak flux and $K_Q \approx 1.27$ on integrated load that force agreement

with the CFD, and the same factors are applied to the Silicon Shepherd cases. This calibration folds both the radiative contribution and the convective-correlation bias into one flight-traceable factor (**ASS-SRC-09**).

The calibration anchor is the Stardust entry at 12.9 km/s, Silicon Shepherd enters marginally slower, at 12.88 km/s, where the radiative fraction is smaller. K_q and K_Q are therefore mild lower bounds, assuming empirical scaling extrapolated up remains valid (**ASS-SRC-9**). A higher-fidelity reanalysis should replace the empirical anchor with a radiative correlation validated for small nose radii in the future.

The calibrated corridor results are summarised in Table 6.30 and Figure 6.3. Across the ±0.2° dispersed corridor the peak flux is 854 W/cm^2 to 899 W/cm^2 (25-29% below the 1200 W/cm^2 PICA qualification ceiling) and the integrated load is 28.79 kJ/cm^2 to 30.26 kJ/cm^2 (16-20% below the 36 kJ/cm^2 Stardust design envelope). The shallow edge ($\gamma_E = -7.4°$) is heat-load (TPS) limited while the steep edge ($\gamma_E = -7.8°$) is g force limited, consistent with the corridor construction in Section 6.5.2. At the −7.6° nominal the margins are balanced, load 18%, g-force 12%, flux 27%.

Table 6.30: Calibrated aerothermal results for the Silicon Shepherd SRC entry corridor ($V_E = 12.8$ km/s, $C_D = 1.5$). Deceleration is reproduced from Section 6.5.2.

Case	q_{peak} [W/cm^2]	Q [kJ/cm^2]	$n_{g,\max}$ [g_0]	$h_{q,\text{peak}}$ [km]
Shallow, $\gamma_E = -7.4°$	854	28.8	32.9	63.9
Nominal, $\gamma_E = -7.6°$	877	29.5	35.2	63.4
Steep, $\gamma_E = -7.8°$	899	30.3	37.5	63.0
Stardust (post-flight CFD) [24]	942	27.6	32	—
Design limit [100][25]	1200	36	40	—

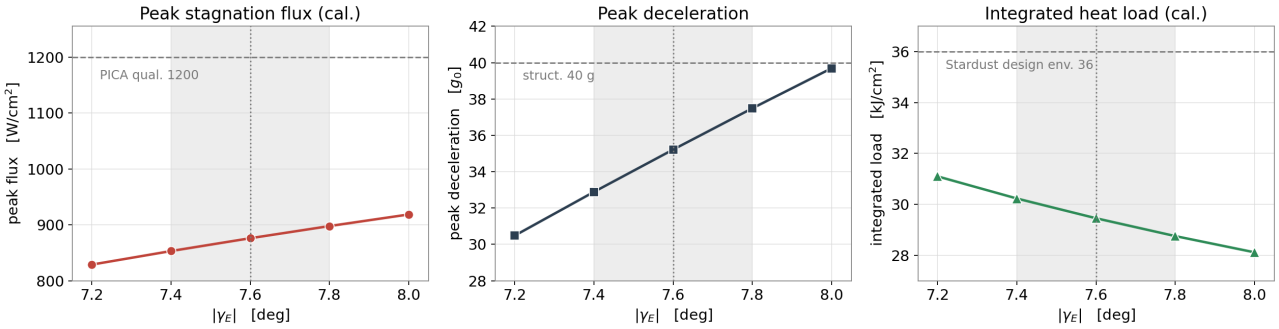

Figure 6.3: Calibrated entry-corridor sensitivity over $|\gamma_E| = 7.2°$-$8.0°$: peak stagnation flux (left, vs the 1200 W/cm^2 PICA qualification ceiling), peak deceleration (centre, vs the 40 g_0 structural limit), and integrated heat load (right, vs the 36 kJ/cm^2 Stardust design envelope). The shaded band is the ±0.2° corridor about the −7.6° nominal (dotted).

6.5.4. TPS Sizing and Capsule Geometry

The aeroshell is build-to-print Stardust class: a 60° half-angle sphere-cone forebody of base diameter $d = 0.8128$ m and nose radius $R_n = 0.2202$ m, with a 30° afterbody cone [93]. The complete geometry is shown in Figure 6.4. The governing constraint on the outer mould line is the aeroheating environment, not internal volume. The Silicon Shepherd return capsule will return the REE-enriched regolith plus the reference regolith. This would require a sealed canister of order 1 L to 2 L and 1 kg to 3 kg, which occupies a small fraction of the existing internal volume, so no outer geometry change is required to house the payload (**ASS-SRC-02**). Additionally, OSIRIS-REx returned regolith in greater quantities than this mission (120 g); hence, no internal volume increase is expected.

The forebody thermal protection system (TPS) is a phenolic-impregnated carbon ablator (PICA), the material developed for and flown on Stardust [101, 93], with an SLA-561V afterbody as on the heritage vehicle. The Stardust forebody is qualified PICA at a stagnation thickness of 5.82 cm, sized against a design environment of ~1200 W/cm^2 peak flux and ~36 kJ/cm^2 heat load [93, 102]. The calibrated Silicon Shepherd environment (Table 6.30) sits inside this box at every point, peak flux ≤ 899 W/cm^2 and load ≤ 30.3 kJ/cm^2, so on an envelope basis, the build-to-print PICA is adequate.

Moreover, given that the entry heat load is expected to be greater than the heritage anchor, the recommendation is to carry the build-to-print 5.82 cm as the baseline thickness with an explicit aerothermal uncertainty factor of ×1.15–1.20, and to close a dedicated recession-and-bondline analysis as an open item. In summary, while the SRC is within the qualified environment, further analysis is still needed.

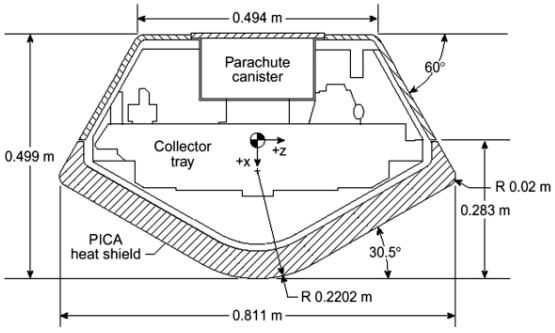

Figure 6.4: Exact geometry of the Stardust SRC [103].

Table 6.31: SRC mass basis (build-to-print Stardust SRC). The sample canister is accommodated within the heritage internal payload allocation and does not add to the heritage total.

Item	Mass [kg]
Build-to-print Stardust SRC[93]	45.6-46
Silicon Shepherd sample canister (REE electrode + regolith reference)	1-3
Modelled entry mass (aerothermal)	46

6.5.5. Separation Kinematics

Separation Architecture

The SRC utilizes a passive, heritage-derived Spring-Loaded V-Band system for ejection [104]. To satisfy the longitudinal spin requirement without introducing internal rotating mechanisms (which present critical single-point failures), the rotational momentum is imparted externally by the Spacecraft, similar to Stardust [32].

Prior to separation, the Spacecraft utilizes its ADCS to orient the combined stack along the final $-7.6°$ entry vector and physically spins the entire vehicle (**REQ-ADC-01**). Once stabilized at the target rotation, redundant pyrotechnic cutters sever the V-Band tension bolts. This releases calibrated helical compression springs positioned between the mating rings, actively pushing the SRC away from the Spacecraft. The capsule cleanly carries the angular momentum away, effectively suppressing any transverse tip-off rates imparted by minor spring force asymmetries [32].

Separation Timing Architecture

A heritage-driven timeline is adopted for the separation sequence to mitigate the complex modelling of deep-space environmental perturbations, such as Solar Radiation Pressure (SRP) cross-track drift (**ASS-SRC-10**). Mirroring the established flight profile of the Stardust mission, the SRC is commanded to separate at precisely **E-4 hours** (four hours prior to the 120 km atmospheric interface) [95]. This V-band release at T–4 hours, imparting a separation $\Delta V \approx 0.25$ m/s, is levied on the mothership as the derived mechanisms requirement

Flight telemetry confirms that a spin-stabilised capsule released at E-4 hours passively maintains its trajectory well within the required $\pm 0.2°$ flight path angle tolerance [95]. Furthermore, this specific time window guarantees the Spacecraft possesses sufficient distance to execute the necessary lateral Earth avoidance manoeuvre without requiring an excessively massive propulsion system.

Earth Avoidance Manoeuvrer

To comply with planetary protection and Earth impact avoidance protocols, the unsterilised Spacecraft must physically divert from the atmospheric entry trajectory immediately following separation [32]. Assuming a baseline planetary protection lateral miss distance requirement of 500 km and utilising the small-angle divert approximation (**ASS-SRC-11**), the required lateral ΔV for the EAM is calculated as:

$$\Delta V = \frac{\text{Target Miss Distance}}{\text{Time to Entry}} \tag{6.6}$$

For a $500,000$ m divert executed at the established E-4 hours ($14,400$ s) boundary, the required impulsive manoeuvre is the following:

$$\Delta V = \frac{500,000}{14,400} \approx 34.7 \text{ m/s} \tag{6.7}$$

Because this manoeuvrer is time-critical and must be executed immediately after the separation recoil and de-spin sequence, it cannot be executed by low-thrust electric propulsion. The spacecraft's propulsion architecture must therefore allocate sufficient chemical RCS propellant to deliver this impulsive 34.7 m/s burn

6.5.6. Descent and Parachute Deployment

The descent system is a dual-stage, unguided sequence built to print from Stardust/OSIRIS-REx heritage: a Disk-Gap-Band (DGB) drogue for transonic stabilisation followed by a triconic main for terminal descent [14]. It is passive throughout, so the design problem reduces to sizing each canopy, checking the drogue opening shock against the structural limit, and fixing the trigger logic. All figures below are for the nominal corridor ($\gamma = -7.6°$) at the working SRC mass $m = 46$ kg, originating from Stardust's 45.6 kg, plus the marginally heavier payload.

Drogue Parachute

The drogue deploys at Mach 1.4 ($\sim$ 33 km, T+134 s in the integrated profile) to damp the transonic angle-of-attack instability [14]. The sizing driver is not drag but the opening (snatch) load $F = C_x\, q_\infty A_d$, which must stay inside the 40 g_0 structural design load. At the deploy dynamic pressure and the heritage 0.80 m DGB ($C_D \approx 0.55$), the computed opening load is 2–3 g_0, an order of magnitude below the limit, so the build-to-print 0.80 m drogue is adopted unchanged and is not a structural driver.

Main Parachute

The main parachute is sized to the touchdown target requirement, REQ-SRC-03:

$$V_{td} \leq 5\,\mathrm{m/s} \tag{6.8}$$

Additionally, the main parachute deploys when decelerating the capsule to ~Mach 0.5, where it can open safely, derived from heritage [14]. Following that, the terminal-descent equilibrium $mg = \frac{1}{2}\rho V_{td}^2 C_D \frac{\pi}{4} D^2$ rearranges to

$$D = \sqrt{8mg/(\pi\rho C_D V_{td}^2)} \tag{6.9}$$

at the Woomera surface density $\rho = 1.205\,\mathrm{kg/m^3}$ (**ASS-SRC-13**) with a conservative triconic $C_D = 0.65$, the nominal 46 kg case needs $D_{\mathrm{main}} = 7.66$ m. That lands within 5 % of the OSIRIS-REx 7.3 m main. Additionally, given that Osiris-Rex used a smaller parachute to land at a slower touchdown speed, it implies they used a greater effective C_D, hence, the 7.66 m canopy is a viable conservative build-to-print baseline. This upsizing of the heritage main from 7.3 m to 7.66 m is the resolution carried for REQ-SRC-03: the $V_{td} \leq 5$ m/s target is met without having to prove an effective $C_D \approx 0.8$ on the smaller heritage canopy.

Trigger Logic

The drogue is equipped with redundant g-switches and a backup timer, and the main follows on drogue cut and spring ejection. This directly inherits the Genesis lesson: the Genesis SRC was lost during capture (2004) because all four g-switches were installed inverted, so the deceleration-sensing function never triggered [105]. Silicon Shepherd therefore mandates independent trigger paths (g-switch *and* pressure-transducer/timer), an explicit verification step, and an end-to-end deployment test under representative deceleration.

Integrated profile

Figure 6.5 traces the full three-phase descent: ballistic deceleration to drogue deploy (Mach 1.4, $\sim$ 33 km), drogue-stabilised transonic descent to main deploy (3.0 km, T+533 s), and terminal descent under the 7.66 m main to touchdown at 5.0 m/s (T+1066 s). Peak heating and peak deceleration both fall in the ballistic phase, well above drogue deploy, confirming that the parachute sequence operates entirely outside the aerothermal and structural design envelopes.

6.5.7. Landing Site Selection

Evaluation of ESA and International Landing Sites

Selecting a terrestrial landing site for a high-energy hyperbolic return capsule ($V_E = 12.88$ km/s) requires matching the lander's unguided footprint with an appropriate recovery zone. Existing European ranges, such as the Esrange Space Center in Sweden or the Salto di Quirra range in Sardinia, are physically too small to safely accommodate the projected 60–100 km landing ellipse [106]. Furthermore, facilities like Kourou are optimized for lifting-body vehicles utilizing guided parafoils for runway recoveries, making them incompatible with a passive, ballistic sphere-cone capsule [107]. International ranges must therefore be considered. The Utah

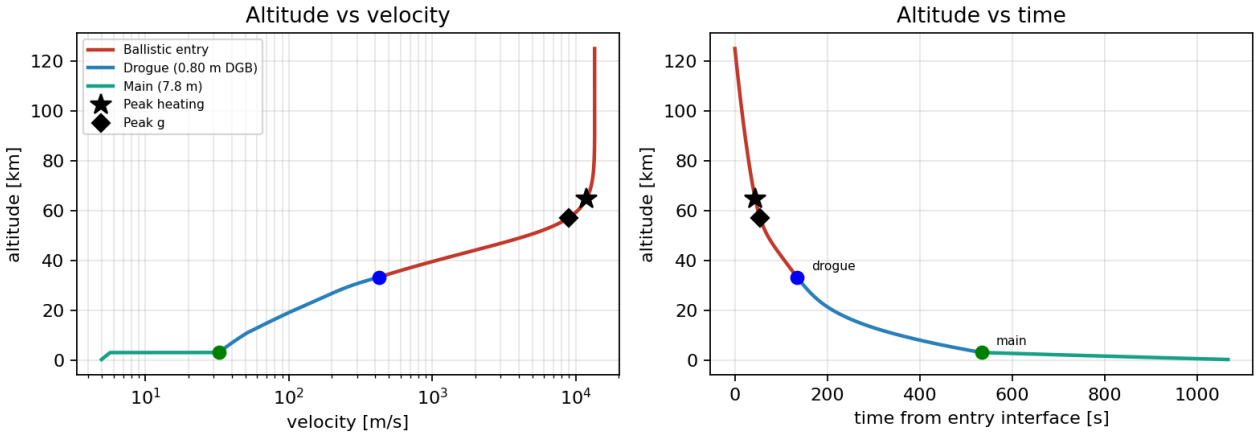

Figure 6.5: Integrated SRC descent for the nominal $\gamma = -7.6°$, 46 kg case: altitude versus velocity (left, log scale) and altitude versus time (right). Markers denote peak heating (★), peak deceleration (⧫), drogue deploy, and main deploy.

Test and Training Range (UTTR) offers established recovery infrastructure for ballistic capsules [25]. However, because UTTR is a US Department of Defense facility, an ESA-led recovery operation would require complex, treaty-level bilateral approvals that currently do not exist [108]. Conversely, the Woomera Prohibited Area (WPA) in South Australia presents a well-established regulatory pathway for international civil space agencies, supported by extensive deep-space sample return heritage [26].

Site Characterization and Landing Ellipse

The WPA consists of an arid, flat desert spanning approximately 127,000 km^2 at an average elevation of 170 m above sea level. At this altitude, the atmospheric density is modelled at $\rho = 1.205$ kg/m^3 based on the U.S. Standard Atmosphere, representing a minor 1.6% deficit relative to sea-level conditions that does not alter parachute sizing [96] (**ASS-SRC-13**).

The capsule landing footprint is estimated by scaling the performance of the OSIRIS-REx mission, which serves as a direct architectural analogue (a 60° sphere-cone employing a dual-stage parachute sequence). OSIRIS-REx demonstrated a 84×20 km (3σ) landing ellipse [14]. For an unguided ballistic entry, the major axis (downrange dispersion) is dominated by the delivery accuracy at the entry interface and variations in the vehicle's ballistic coefficient and atmospheric density profile. The minor axis (cross-track dispersion) is almost entirely driven by horizontal wind drift during the subsonic parachute descent from an altitude of 3 km. To account for Phase A uncertainties in Woomera's day-of-landing wind profiles and minor aerodynamic deviations, the heritage baseline is conservatively expanded, bracketing the Silicon Shepherd landing ellipse at 60-100 $\times$ 15-25 km (**ASS-SRC-14**). This footprint easily fits within the WPA boundaries without risking populated areas.

Recovery Concept of Operations

The baseline recovery phase is modelled on the JAXA Hayabusa2 recovery operations [26]. Upon parachute deployment, tracking relies on an onboard UHF beacon for direction-finding triangulation. Ground teams deployed via recovery helicopters are tasked with visual localisation, initial environmental monitoring, and secured transport of the capsule to a mobile containment laboratory stationed on-site.

6.5.8. SRC Design Summary

The preliminary design of the SRC successfully closes through heavily leveraging the heritage of the Stardust and OSIRIS-REx capsules. By accepting a steeper entry corridor, the design trades higher deceleration loads (which easily fit within the non-biological structural limits) for reduced thermal soaking, protecting the heritage 46 kg mass budget and the PICA heat shield.

Table 6.32 synthesises the final derived parameters, limits, and operational setpoints that define the SRC architecture.

Forward Work

Because this design relies heavily on empirical scaling and heritage performance data from missions with slightly lower energy states, several key assumptions must be explicitly investigated and retired in next phase. Table 6.33 outlines open items for future work.

Table 6.32: Synthesis of SRC baseline parameters and operational setpoints.

Parameter	Baseline Value	Notes / Bounding Limits
System Mass & Geometry	46.0 kg	0.811 m diameter, 60° sphere-cone.
System Volume	170 L	Heritage
Entry Velocity (V_E)	12.88 km/s	At 120 km atmospheric interface.
Peak Deceleration	32.9–37.5 g	Nominal deceleration at 35.2 g (structural yield set at 50 g).
Landing Site	Woomera (WPA)	[60-100] × [15-25] km footprint.
Cost	20M€	Calculated using Cost Estimation Methods (CER) based on Osiris-Rex and Stardust.

Table 6.33: Future work recommendations

Future work	Description
Aerodynamics and Radiative Heating Models:	The baseline hypersonic drag coefficient (C_D = 1.50) and the aerothermal flux scaling factors (K_q, K_Q) are entirely anchored on empirical post-flight Stardust Computational Fluid Dynamics (CFD) [24]. Because the Tauber-Sutton correlation [97] is invalid for the SRC's small nose radius, Phase B must conduct vehicle- and velocity-specific CFD.
Recession and Bondline Analysis:	The current TPS validation is an envelope assessment confirming that Silicon Shepherd sits inside the Stardust qualification box [100]. A coupled material-response simulation (e.g., FIAT) is required to dynamically model the PICA ablation, calculate exact recession depths, and verify that the internal bondline temperature limits are respected.
6-DOF Flight Dynamics and Inertia Modeling:	The 15 RPM separation spin is derived from steady-state approximations and transient survival assumptions [95]. Detailed internal CAD modeling is necessary to ascertain the exact inertia tensor (I_{xx}/I_{yy}) to confirm oblate-spinner stability. Furthermore, a full 6-Degree-of-Freedom (6-DOF) Monte Carlo trajectory simulation is required to verify pitch damping and angular rates during the rarefied-to-continuum transition.
Navigation Covariance and Landing Dispersion:	The Woomera landing ellipse was sized via linear scaling of OSIRIS-REx delivery metrics [25]. The next design phase must integrate site-specific Woomera wind profiles and explicit deep-space navigation delivery covariances (from the approach B-plane) to generate a rigorous, mission-specific Monte Carlo landing footprint.
Mass Budget Closure:	The 46.0 kg mass is a fixed assumption based on heritage [93]. The packaging of the internal sample canister, and avionics must be detailed to officially close the mass budget and confirm that the $V_{td} \leq 5.0$ m/s requirement holds with the 7.66 m main parachute.

7
Spacecraft Platform

This chapter will explain the design of the spacecraft platform. It will follow from requirements set by the payload as presented in Chapter 6. The design of the bus will include structural design in Section 7.1, TT&C design in Section 7.2, C&DH design in Section 7.3, propulsion subsystem design in Section 7.4, thermal control subsystem design in Section 7.5, ADCS design in Section 7.6, and finally the EPS design in Section 7.7.

7.1. Structures

The structural design concerns the compliance of the system to enable its operational envelope. Section 7.1.2 details the external structural design of the spacecraft bus, while the interface with the Ariane 62 launch vehicle is specified in Section 7.1.3. Section 7.1.5 summarises the structural design; presenting an overview of the subsystem budget, and highlights additional structural considerations to be clarified in a later design phase.

7.1.1. Assumptions and Requirements

In order to facilitate the structural analysis presented in this section, the following assumptions are defined in Table 7.1. The are requirements the structural subsystem must meet are defined as follows in Table 7.2 In

Table 7.1: Structural Subsystem Design Assumptions.

Assumption ID	Description
ASS-STRUC-01	Launch loads are design critical.
ASS-STRUC-02	Launch loads are applied axially.
ASS-STRUC-03	Earth gravitational acceleration is assumed constant at 9.80665 m/s^2.
ASS-STRUC-04	External sizing does not account for internal reinforcement.
ASS-STRUC-05	External shape is assumed to be rectangular cubic.
ASS-STRUC-06	A safety factor of 1.25 is applied to all loading conditions.
ASS-STRUC-07	Loads are introduced at the corners of structural elements.

Table 7.2: Requirements for Structural Analysis

Requirement ID	Requirement	Structural relevance
REQ-STK-08	The mission shall be launched on Ariane 62 in compliance with the Ariane 62 User's Manual.	Defines structural limitations.
REQ-MIS-15	The mission shall ensure volume compatibility with the Ariane 62 launcher.	Drives maximal structural size.
REQ-STRUC-01.1	The structure shall withstand longitudinal launch loads ≥ 6g.	Derived from REQ-STK-08 and places constraints on material choice and structural architecture.
REQ-STRUC-01.2	The structure shall withstand lateral launch loads ≥ 2g.	Derived from REQ-STK-08 and places constraints on material choice and structural architecture.
REQ-STRUC-05	The structure shall enable compatibility with the payload adapter of the Ariane 62 launcher	Derived from REQ-STK-08 and places constraints on material choice and structural architecture.

addition to the assumptions above in Table 7.1, the main external structural element is assumed to be honeycomb sandwich panels. This is driven to improve the mass efficiency of previously selected solid structured panels in an earlier design phase and also to improve the TRL of the mission. Honeycomb sandwich panels are a flight-demonstrated technology, having served as the primary structural element of previous mission including Osiris-Rex [109]and Rosetta [110]. Furthermore, relating to ASS-STRUC-01 the honeycomb sandwich panels must be sized to be compatible with launch conditions under the Ariane 62 launch vehicle. Derived from the user manual [27], the critical load cases are defined to be the subsequent longitudinal/lateral structural loading in additional to the vibrational requirements regarding spacecraft-launch vehicle interface are considered. Further constraints are further discussed in Section 7.1.5, but are not included in structural calculations. Within all considerations a range of thicknesses will be evaluated of the skin panels and internal thicknesses, the limits driven by manufacturability constraints.

7.1.2. Structural Characteristics

With respect to the Ariane 62 launch vehicle, the overall critical load envelope is presented below in Figure 7.1a. To perform a complete analysis, the combined load-case is considered to ensure a conservative design is presented. Using the load envelope, sizing will be conducted to ensure structural integrity against failure modes including panel buckling, material yielding, shear crimping, skin wrinkling and intra-cell buckling[111]. First sizing will be done will respect to loading on the cross section of the sandwich panel before analysis is continued through loading on directly on the face sheet. In both cases the honeycomb sandwich panels are sized to have a margin of safety to ensure compliance with ASS-STRUC-06. The margin of safety is defined as follows in Equation 7.1 where a margin of 0 infers exact alignment with ASS-STRUC-06.

$$MoS = \frac{AllowableStress}{UltimateStress} - 1 \tag{7.1}$$

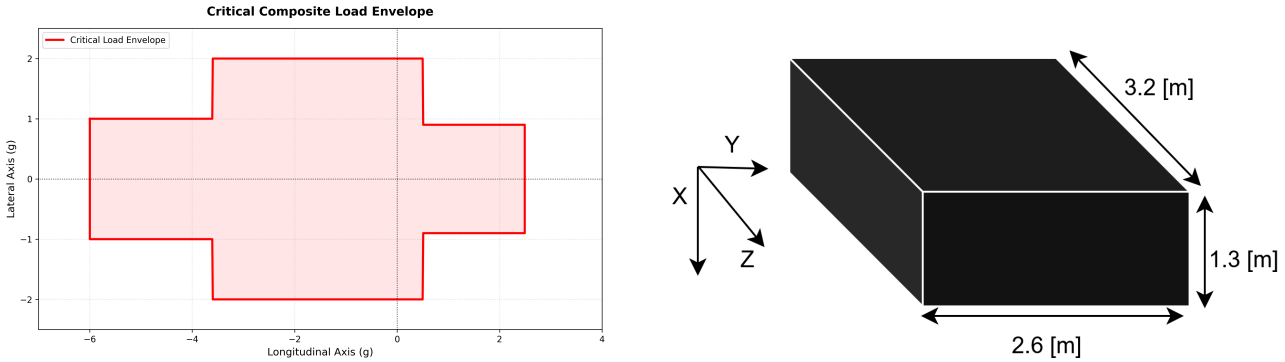

(a) Ariane 62 Critical Loading Envelope

(b) External Structural Geometry and Coordinate System

Figure 7.1: Ariane 62 Load Envelope and Spacecraft Structural Geometry

Following from ASS-STRUC-07, the primary load path is defined through the corners of the panels. Therefore assuming a nominal configuration as defined in Figure 7.1b, the four vertical panels of the spacecraft are sized to support the full load case. The sizing defined for these four panels will be used for the remaining 2 panels.

Considering the combined load case, the limit load is thus described:

$$P_{\text{limit}} = m\, n\, g = 1300\,\text{kg} \times \sqrt{6^2 + 1^2} \times 9.81\,\text{m/s}^2 = 77.573\,\text{kN}, \tag{7.2}$$

and the ultimate load follows by applying the safety factor as defined by ASS-STRUC-06.

$$P_{\text{ult}} = \text{SF} \cdot P_{\text{limit}} = 96.966\,\text{kN}. \tag{7.3}$$

The assumption is made to assume that this load to applied uniformly across the sizing panels, resulting in an ultimate uniform distribution as follows:,

$$q_{\text{ult}} = \frac{P_{\text{ult}}}{\sum_i w_i} = \frac{96.966\,\text{kN}}{11.6\,\text{m}} = 8.36\,\text{kN/m}. \tag{7.4}$$

Using methods from Hexcel Composites[111], analysis was conducted of the honeycomb sandwich panels considering the load case above.

To facilitate this analysis the panel bending stiffness (D) is further defined[111]:

$$D = \frac{1}{2} E_f \, t_f \, h^2 \, b \tag{7.5}$$

where E_f is the panel face elastic modulus, t_f the panel face thickness, h the panel face spacing, and b the overall panel width[111].

Further analysis of an additional loading condition is necessary to determine the critical failure mode. To facilitate this analysis, the geometry defined from the End Loading analysis will be utilised. If load compliance with this geometry is achieved, then this will be the panel sizing used.

Face Loading

With respect to direct face loading, the same P_{ult} is used as defined under End Loading. However, in the case of direct face loading, the uniform distribution of the load is distributed across the entire plate cross-sectional area. Therefore, the uniform distributed load is defined per cross-sectional areas as defined in Figure 7.1b and is presented below in Table 7.3

Table 7.3: Cross-sectional face dimensions and ultimate line loads.

	Cross-sectional Face [i [m] $\times$ j [m]]		
	2.6 $\times$ 1.3	**3.2 $\times$ 1.3**	**2.6 $\times$ 3.2**
$\mathbf{q_{ult}}$ [kN/m]	28.678	23.301	11.650

Using the loading as defined in Table 7.3, failure is evaluated using methods from Hexcel [111].

In both loading cases, a list of varying face and core materials were considered in addition to varying face and core thicknesses. The results of the overall analysis is presented in Table 7.1.2 and the lightest face-core combination that meets the loading constraints is selected for design. This combination is presented in Table 7.4 and the margins of safety are presented in Table 7.5.

Sizing Evaluation

Through evaluating both face and end-loading of the sandwich panels, both loading cases were found to be design limiting and an optimised (lightest) panel configuration is presented for both cases. The honeycomb skin panel configuration is described below in Table 7.4 with the margin of safety compliance described in Table 7.5

Table 7.4: Skin Panel Configuration

Parameter	Value
Facing material	CFRP UD tape (0°)
Facing thickness t_f	0.50 mm
Core material	Aluminium 5052 (37 kg/m^3)
Core thickness t_c	10.00 mm

Table 7.5: Margins of safety at ultimate load for the sized wall.

Failure mode	MoS at ultimate during End Loading
Facing compression	+154.517
Panel buckling	+1.18
Shear crimping	+132.984
Skin wrinkling	+93.892
Intracell buckling	+166.936

7.1.3. Launch Vehicle Interface

Following from REQ-STK-08, a further compliance necessary states the following for the vibrational requirements for the spacecraft at the LV interface; frequencies must be $\geq$ 20 Hz longitudinally and $\geq$ 6 Hz laterally. In order to conduct this structural analysis, a study was made using ANSYS as a modelling software to conduct model analysis considering a variety of Ariane 6 compatible adapters as specified by [27]. This analysis used the geometric parametres of Figure 7.1b and Table 7.4. When considering the building of the composite, a ply

thickness of 125 μm[112] was considered with a layup orientation of $0°/-45°/45°/90°$ to ensure a symmetric layup. Furthermore, using the interior layout as described in Section 8.1.2, point masses were placed within the structure to represent the comprising interior subsystems. Furthermore, following the the description of vehicle adapters as described [27], a launch ring was placed as a fixed support located on the stowing structural face as described in Section 8.1.1. The result of this analysis is that lateral frequency compliance across the spectrum of adapters, but the best compliance of longitudinal frequency stems from the *PLA6 1666* adapter[27] which resulting in the following frequencies in Table 7.6.

Table 7.6: Launch Vehicle-Spacecraft Modal Analysis

Mode	1	2	3	4	5	6
Frequency [Hz]	7.217	13.571	14.232	17.36	19.224	23.517

Evaluating the direction deformation across all body axes, reveals that the first mode is mainly representative of lateral frequencies as an order-of-magnitude difference is seen between the lateral axes deformation and the longitudinal axis. At the second mode however, the order-of-magnitude of the deformation along the longitudinal axis increases by an order-of-magnitude, indicating the significance of this mode as the longitudinal constraint. This results are seen below in Table 7.7

Table 7.7: Deformations occurring from Modal Analysis

Mode	1	2
x [m]	$-6.08 \cdot 10^{-3}$	-0.11
y [m]	$-1.19 \cdot 10^{-2}$	-0.12
z [m]	0.168	0.356

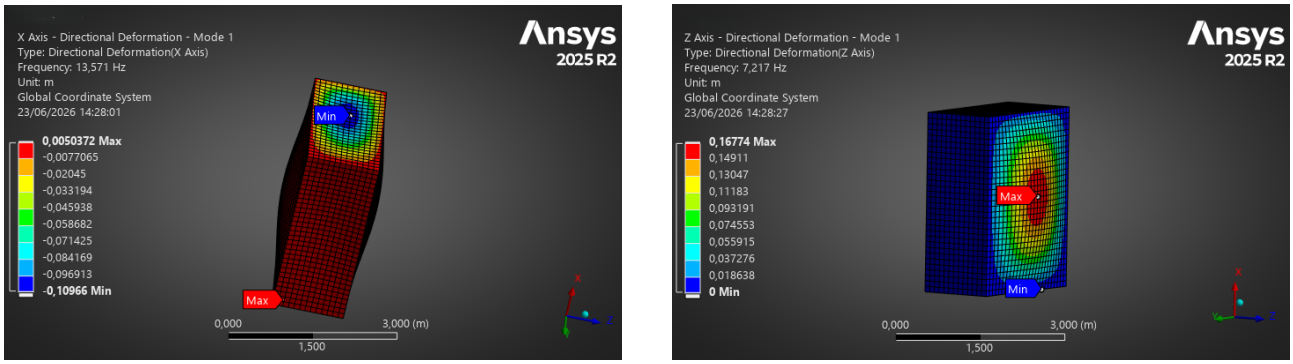

(a) Mode 2: X (Longitudinal Deformation)

(b) Mode 1: Z (Lateral) deformation

Figure 7.2: Visualisation of Model Deformation under Modal Loads

The longitudinal requirement is not met following this modal analysis. However this is to be expected as the model upon which modal analysis was performed did not include any physical internal structural elements such as structural frames as present in Hayabusa [2]. The only structure through which the vibrations can propagate are the large cross-sectional plates of the the external structure. Therefore it is expected that when these interior structural elements are added, the stiffness of the structure will improve considerably, resulting in a longitudinal natural frequency compliance.

7.1.4. Material Characteristics

Given the panel configuration in Table 7.4, Table 7.8 and Table 7.9 presents the overall material characteristics.

Table 7.8: Mechanical properties of honeycomb core materials.

Material Name	Density [kg/m^3]	Cell Size [mm]	Stabilized Comp. Strength [MPa]	Stabilized Comp. Modulus [MPa]	L Shear Strength [MPa]	L Shear Modulus [MPa]	W Shear Strength [MPa]	W Shear Modulus [MPa]
5052 Aluminium 37	37	6.0	1.35	310	0.96	220	0.58	112

Table 7.9: Material properties of CFRP skin

Material Name	Elastic Modulus [GPa]	Tensile / Compressive Strength [MPa]	Ply Thickness [mm]	Ply Weight [kg/m^2]
Epoxy UD Carbon Tape (0°)	130 / 115	2000 / 1300	0.125	0.19

7.1.5. Future Considerations

Overall, the system budgets are derived from Section 7.1.2. Cost is estimated using SMAD-based methodologies[113]. This results in the following budget:

Table 7.10: Structural Subsystem Budget

	Mass [kg]	Volume [L]	Power [W]	Cost [M€]
Structural Elements	59.95	190.32	N/A	3.0

There are several parametres that are not considered in this analysis. Firstly, the structural analysis is largely conducted without the inclusion of internal elements until the modal analysis. This results in an over-sizing of the structure as internal elements would provide alternate load-paths and increase the overall stiffness of the structure. Specifically, regarding stiffeners, no study is made with respect to internal bulkheads or stringer structures that would reinforce and stiffen the structure. Also, the specific connections not only between the CFRP skin panels and honeycomb core, but the connection between sandwich panels in addition to the connection between internal masses and the sandwich panels needs to be further studied. Additionally, there are further launch constrains that are not mentioned including the fairing separation event, the thermal shocks and the depressurisation of the fairing during launch. These are structural loads that must be considered in a later design stage. Furthermore, while the honeycomb panel design as been completed to obtain an optimised-for-mass combination of honeycomb core and skin panel, the thicknesses of the panel could pose an issue relating to handling and manufacturing. Finally regarding the space environment, due to the extreme range of temperatures experienced, analysis needs to be conducted regarding the thermal loads that the structure would subsequently experience. Ultimately, all of these considerations are elements of a structural analysis that must be studied further in the design phase.

7.2. Telemetry, Tracking, and Command (TT&C)

This section presents the detailed design of the Telemetry, Tracking, and Command (TT&C), responsible for receiving commands from ground networks, and sending science and housekeeping data back. It begins by consolidating mission-level link requirements, baseline assumptions Table 7.11, and derived TT&C constraints in Table 7.12. Section 7.2.3 establishes the RF front-end architecture, baseband processing chain, and spacecraft interfaces that define command routing and telemetry framing. Table 7.13 details the operational sequencing, pass planning, and ground network integration strategy. The section concludes with a master synthesis of baseline parameters (Section 7.2.4) and a forward-work roadmap in (Table 7.2.4).

7.2.1. Assumptions and Requirements

The design envelope is governed by a set of baseline assumptions that fix link budget parameters, hardware heritage, and orbital/pointing constraints. These are consolidated in Table 7.11. Mission-level operational requirements and derived TT&C subsystem targets are synthesized in Table 7.12, which also provides the rationale for each baseline decision.

Table 7.11: Design Assumptions for Telemetry, Tracking, and Command (TT&C).

Assumption ID	Description
RF & Link Budget	
ASS-TTC-01	Effective earth noise temperature is assumed to be $T_{sys} \sim 260\,K$ for all stations and only 1 station is used at time. [114]
ASS-TTC-02	Atmospheric, ionospheric, and weather-related attenuations are neglected; only free-space path loss (FSPL) is considered.
ASS-TTC-04	Signal bandwidth is assumed to be 400 MHz for Ka-band and 200 MHz for X-band.
ASS-TTC-05	Link capacity is modelled using the Shannon bit rate equation: $R_b = B \log_2(1 + \text{SNR})$.
ASS-TTC-06	The effects of error correction overhead and data compression are assumed to be equal and opposite (net zero effect on throughput).
ASS-TTC-07	Doppler shifts and ranging time delays are neglected in the link budget calculation.
Antenna & Hardware	
ASS-TTC-08	Ground-stations antenna diameters are assumed to be 20 m for X-band receivers and 30 m for Ka-band terminals.
ASS-TTC-9	The high-gain antenna (HGA) gain is assumed to be 35 dBi and 44 dBi for the X-band and Ka band antennas respectfully, based on Hayabusa heritage.[115]
ASS-TTC-10	Antenna aperture efficiency is considered perfect (ie: no losses from surface imperfections, spillover, or illumination taper).
ASS-TTC-11	Antenna degradation due to environmental exposure and ageing is not accounted for.
ASS-TTC-12	Effervescent of the antenna is assumed to be aprox 57% with the rest going into heat
ASS-TTC-13	The transmitter and reviver cable losses are assumed to be 5db.
Pointing & Orbital Dynamics	
ASS-TTC-14	Required pointing accuracy is assumed to be 0.1 times the Half Power Beamwidth (HPBW).
ASS-TTC-15	Antennas are assumed to maintain perfect boresight alignment with the Earth center.
ASS-TTC-16	Communication is restricted to direct-to-earth links, excluding signal hopping.
ASS-TTC-17	Link availability models exclude downtime caused by Sun/Moon interference or Visablity of the
ASS-TTC-18	Orbital mechanics are modelled using the J2000 epoch and follow Keplerian motion.

Table 7.12: Requirements on the TT&C subsystem

Requirement ID	Requirement	Requirement type
REQ-MIS-03	Mission progress shall be monitored continuously by ground operations.	Driving
REQ-MIS-05	Biomining telemetry shall be monitored in real time.	Key
REQ-MIS-17	The cell culture health shall be continuously monitored during bioprocessing operations.	Key
REQ-SYS-04	The system shall enable transmission and reception of data by the spacecraft from and to Earth.	Key
REQ-TTC-01	The mission shall have a minimum downlink data rate capability of ≥ 8 kbps) with the HGA throughout the mission.	Driving
REQ-TTC-02	The TT&C subsystem shall close the downlink with a link margin of at least +3 dB at the maximum Itokawa–Earth range.	Driving
REQ-TTC-03	The mission shall have an uplink data rate of 320 bps.	Key

7.2.2. Link budget calculations

To calculate the amount of link budget available, the distance of transmission must be known. Given that Itokawa is an Apollo group [1] Asteroid the range of distances between the Earth and Itokawa ranges from 0.1 – 2.6AU. As a worst case scenario, the upper bound of this distance will be used to size the antennas.

Using that along side the assumptions made in Table 7.11 a link budget can be made and summarised in Section 7.2.4

[1] Apollo NEAs have a semi-major axis $\geq$ 1.0AU and perihelion distance $\leq$ 1.017 AU, most notably, they cross the Semi-Major axis of Earth.

7.2.3. RF and Baseband Architecture

The TT&C architecture follows a switching signal path based on Hayabusa [115]. The spacecraft has a total of 6 antennas that can be divided into 3 main groups, high gain antennas (HGA), medium gain antennas (MGA) and low gain antennas (LGA).

The high gain antenna is based on the dual high gain antennas of Hayabusa 2 where the advantage of operating on 2 different communication bands is used. This allows for redundancy as well as taking advantage of the of the reliability of the X band and high data rate of the Ka band. HGA will be used when downstreaming a lot of data scientific data like in the global mapping stage Table 4.2.

Then there is the MGA that can turn independently of the spacecraft. This is done with a turret at the edge of the spacecraft which allows for a wide range of pointing area to keep a reliable downlink signal while the spacecraft is preforming manurers and keeping it's solar panel ornated at the sun. Then there are LGA which are extremely low bit rate antennas that make sure that there is still a passive way of communicating with the spacecraft when complications happen.

Table 7.13: Failure effect of X-band switches on mission mode availability (Signal Path Mapping).

	Safe	Phase 3	Phase 4	Phase 5	Phase 6
Ka-band HGA	-	-	O	-	-
X-band HGA	-	-	B	-	B
X-band MGA	B	O	-	B	O
X-band LGAs	O				

"O" Indicates the preferred antenna for operations "B" Indicates the antenna that still can carry out the functionality to a reduced degree

Signal routing is managed by an X-band and Ka-band switch network that isolates fault paths while maintaining operational continuity. Table 7.14 maps the switch topology to antenna availability, ensuring that a single switch failure only degrades one signal path without cascading loss across the suite. The communication flow between ground networks, TT&C hardware, and spacecraft payloads is illustrated in Figure 7.3.

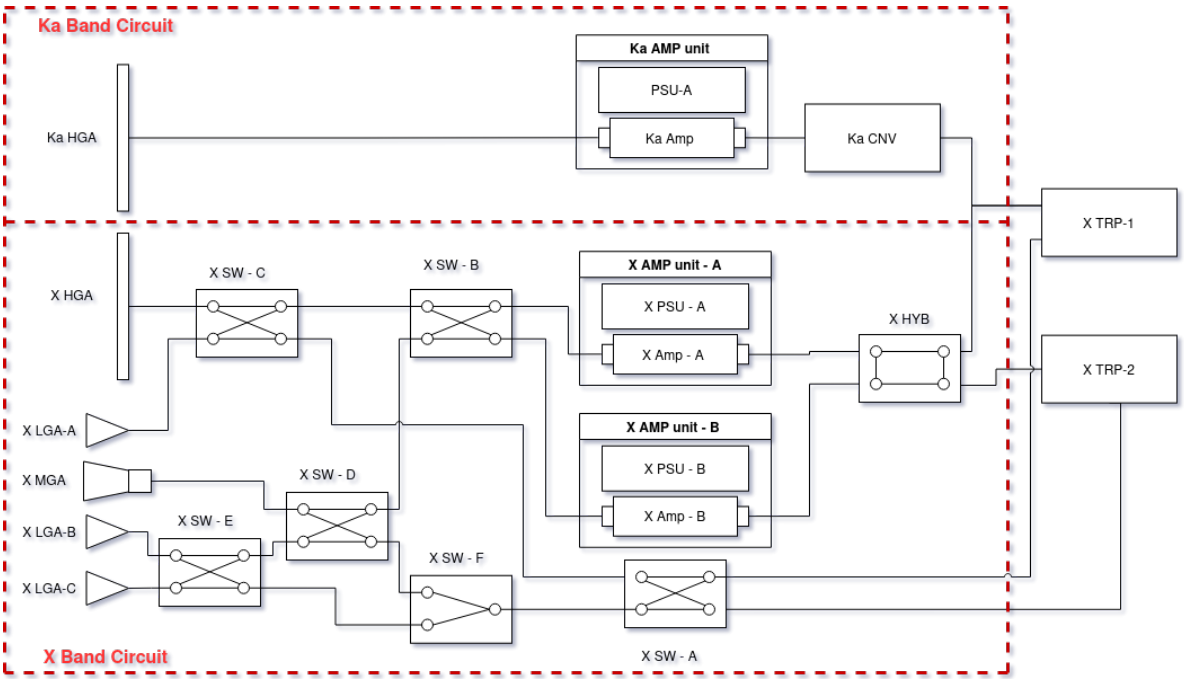

Figure 7.3: Communication flow diagram

7.2.4. TT&C Summary

Below is a table that outlines the specification and system specifications

Table 7.14: Failure effect of X-band switches on antenna availability (Signal Path Mapping).

	XHGA	XMGA	XLGA-A	XLGA-B	XLGA-C
X SW-A					
X SW-B	X				
X SW-C	X			X	
X SW-D		X		X	
X SW-E				X	X
X SW-F					

"x" indicates a switch that resides in the signal path of the antenna. Failure of this switch results in loss of availability for that antenna.

Table 7.15: TT&C Link budget and Specifications

Configuration	Gain (dBi)	Downlink rate in kbps 2.6 AU	Uplink rate in bps 2.6 AU	Half power angle	Power use (W)	Mass (per unit)	Volume (L)
Ka HGA	44	72	3046	0.45°	150	8.7	64
X HGA	35	9.1	385	1.3°	150	8.5	64
X MGA	14	0.07	3.0	14°	20	5	21
X LGA	0	0.003	0.12	71°	3	1	0.5
Total System	NA	NA	NA	NA	150	25.2	150.5

Forward Work
Because this design relies on static link budgets and heritage hardware profiles, several key assumptions that could be looked into further

1. **Doppler Compensation and Ranging Calibration:** The neglect of Doppler shifts (**ASS-TTC-07**) will be replaced with trajectory-derived frequency offset tables to refine modem PLL acquisition times and ranging accuracy.
2. **Degradation effects** The effect of heat cycles and radiation should be quantified over the life of the mission
3. **Antenna Pointing Accuracy Verification:** The 0.1 HPBW requirement (**ASS-TTC-14**) couples directly to ADCS fine-pointing performance and structural flexure; a combined TT&C-ADCS jitter analysis is required before CDR.
4. **Ground Network Availability Scheduling:** Link availability excludes Sun/Moon constraints (**ASS-TTC-17**). Phase B will generate a formal ground station visibility matrix to confirm pass durations meet science downlink windows.

7.3. Command and Data Handling (C&DH)

This section presents the detailed design of the Command and Data Handling (C&DH) subsystem, the central nervous system of spacecraft which handles, payload data routing, fault management, and autonomous decision-making. It begins by consolidating mission-level operational constraints, baseline assumptions, and derived C&DH requirements in Section 7.3.1. Section 7.3.2 establishes the bus topology and hardware/software architecture, defining how telecommand, telemetry, and payload data are managed. Table 7.3.2 details the fault detection, isolation, and recovery (FDIR) logic that enables survival across all payload chains. The section concludes with a master synthesis of baseline parameters (Table 7.19) and a forward-work roadmap (Table 7.3.3).

7.3.1. Assumptions and Requirements

The C&DH architecture is designed to satisfy Bioreactor monitoring latency requirements, support one-fault-tolerant (1-FT) redundancy , buffer high-volume science telemetry, and operate within strict mass/power/volume allocations. Table 7.16 consolidates the governing assumptions that fix the design envelope, while Table 7.17

synthesizes resolved mission requirements, derived subsystem constraints, and the rationale for each baseline decision.

Table 7.16: Consolidated Design Assumptions for the C&DH Subsystem.

Assumption ID	Description
ASS-CDH-01	Total C&DH mass is ≤ 10 kg Based Hayabusa 2 [115]
ASS-CDH-02	The processor chain maintains functional operation up to a total ionizing dose (TID) of ~ 5 krad(Si).
ASS-CDH-03	SpaceWire payload bus supports from the LMC_{OOL}, bioreactor controllers, HMS tiers, and RSS instruments without contention.
ASS-CDH-04	Hot/cold redundancy switching latency is bounded at ≤ 2 s, preserving continuous downlink during nominal operations.
ASS-CDH-05	FDIR logic operates autonomously for all Tier-1 and Tier-2 faults; Tier-3 events require ground-in-the-loop resolution.
ASS-CDH-06	Non-volatile memory (EDR/FDR) capacity is sized to retain ≥ 30 days
ASS-CDH-07	Platform power budget reserves a 25% margin above nominal C&DH draw to accommodate transient bus loading and fault modes.

The primary payload monitoring requirements and platform-level reliability constraints have been evaluated against heritage flight computers and radiation environment models. Table 7.17 resolves these conflicts, establishes the updated design baselines, and explicitly outlines derived requirements that must be adopted by the TT&C, ADCS, EPS, and payload subsystems.

Table 7.17: Synthesis of resolved mission/system requirements and derived C&DH baseline parameters.

Requirement ID	Subject / Target	Design Baseline	Rationale & Resolution
Part I: Driving requirements on C&DH gsubsystem design			
REQ-MIS-05	LMC_{OOL} health monitoring real-time.	≤ 500 ms telemetry cycle time.	LMC_{OOL} streaming rate exceeds the nominal downlink window; C&DH buffers and timestamps data for store-and-forward or burst transmission to satisfy local polling latency.
REQ-MIS-17	LoC health status monitoring.	Continuous polling at 1 Hz.	Review confirms ≤ 1 s latency requirement is met by local SpaceWire polling loop; external downlink latency does not affect closed-loop bioleaching control.
REQ-CDH-01	Science data buffering capacity.	16 Gbit solid-state storage allocation.	Accommodates the ~1.9 GB remote sensing campaign buffer plus HMS/LMC_{OOL} telemetry logs without downlink contention during proximity operations [25].
REQ-CDH-02	C&DH interfacing	C&DH always allows subsystem interaction and interfacing	CPU with sufficient data rate.
REQ-CDH-03	TT&C Interface framing rate.	$\geq 8kbps$ /s down directional link.	Supports downlink housekeeping telemetry compression at nominal pass durations.
Part II: Derived Subsystem Requirements (Platform Interfaces)			
REQ-SYS-07	Telecom & data handling enablement.	dual-core pair with SSR.	Provides fault-tolerant command execution, telemetry framing, and payload routing backbone across all instrument chains.
REQ-POW-DER-01	Power rail capability.	Programmable load switches per OBC GPIO.	Enables controlled power-up/down of payload chains, SSR fault isolation, and safe-mode heater prioritisation.
REQ-RAMS-04	1-FT redundancy on main processors.	Hot/cold OBC + redundant SSR/EDR.	Single processor or memory chain failure triggers automatic switchover; mission continuity is preserved without ground intervention.

7.3.2. C&DH Architecture Design

The C&DH subsystem employs a bus architecture optimized for fault isolation, and heritage reliability. The central processing chain consists of two redundant computers running in a hot/cold standby configuration. They are connected to a dedicated SSR/EDR unit containing the flight software image, configuration parameters,

and critical event records. Figure 7.4 illustrates the complete hardware/software partitioning and data flow pathways.

Data routing is split across two physically isolated buses to prevent payload contention from degrading platform stability:

- **Platform Bus (MIL-STD-1553B):** Carries time-critical housekeeping, TT&C telecommand/telemetry frames, ADCS pointing vectors, and EPS status loops. The bus topology uses a single central terminal.
- **Payload Bus (SpaceWire):** Connects the OBC directly to the LMC_{OOL} chamber, bioreactor control valves, all four HMS sensor tiers, remote sensing suite instruments, and the sampling arm.

The TT&C subsystem interfaces with the C&DH through a dedicated RF-to-baseband data bridge that parses telecommand frames and injects telemetry into the MIL-STD-1553B network during nominal downlink passes. EPS supplies regulated power rails to all OBC/SSR components, while ADCS provides fine-pointing vectors to the HGA mount for precise beam tracking. The complete data handling topology is visualized in Figure 7.4.

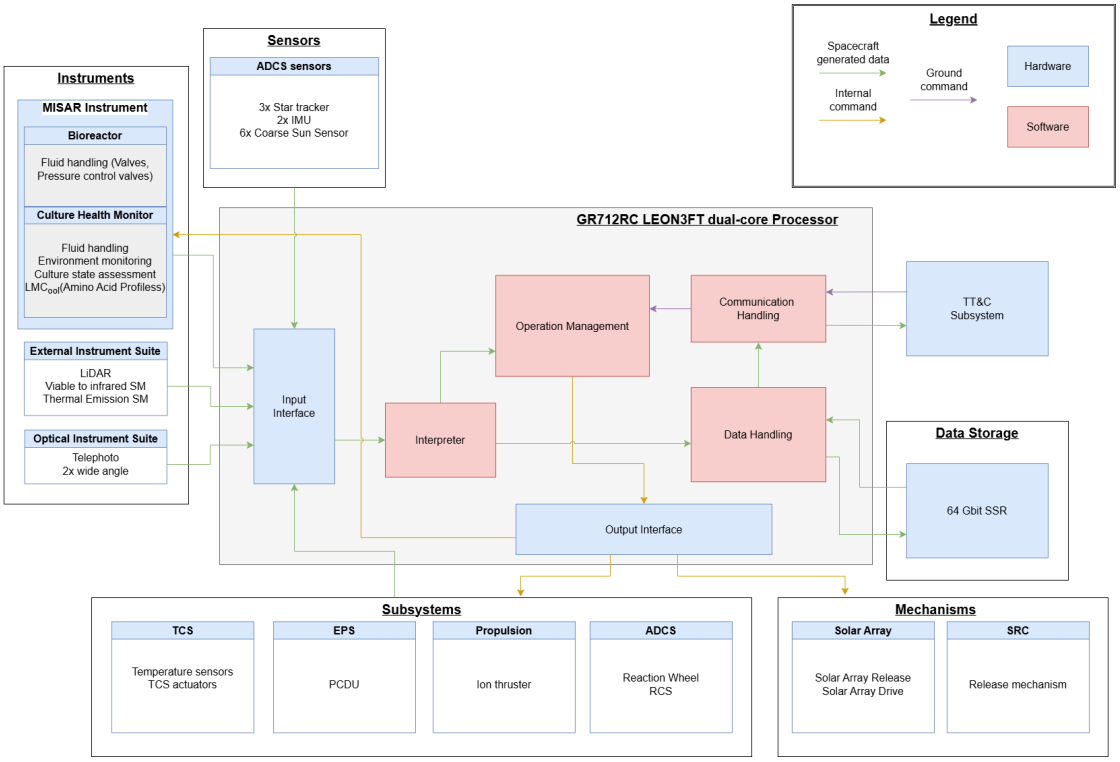

Figure 7.4: Hardware/Software architecture diagram showing OBC redundancy, bus isolation, and payload chain connections.

Radiation Environment, Sizing Logic & Data Management

The C&DH sizing baseline is driven by the integrated ionising radiation environment during the live-organism phase (outbound cruise plus asteroid stay, ~700–1000 d). Table 7.18 summarizes the dose budget behind a

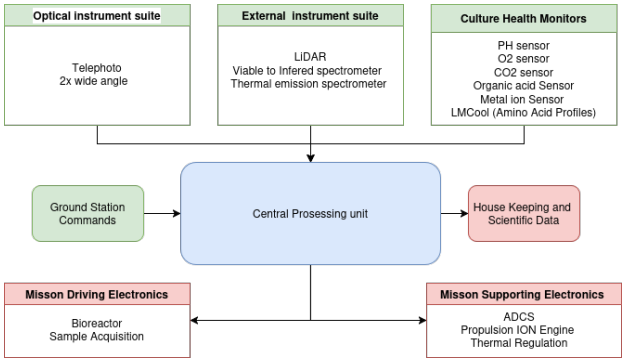

Figure 7.5: Data Handling Diagram

representative 1 g cm^{-2} aluminium-equivalent wall.

Table 7.18: Mission ionising-radiation dose budget by contributor, behind ~1 g cm^{-2} Al-eq. shielding.

Contributor	Characteristic rate / event	Integrated (phase)	Source
Galactic cosmic rays (GCR)	~0.46 mGy d^{-1} abs.	~0.32–0.46 Gy	[116]
Solar particle events (Oct-1989 class)	~20–100 mGy/event (×~0.5 at 1.376 AU); 1–2 events	~0.02–0.10 Gy	[**BadhwarAtwell1999**, 116]
Background SPE (solar max)	—	~0.05–0.20 Gy	[**ECSS_E_ST_10_04C_Rev1**]
Trapped (Ariane 62 Van Allen escape)	hours-scale traverse	< 0.05 Gy	[**AE9AP9**]
Total – phase	—	~0.5–0.7 Gy	

The LEON3FT (GR712RC) is a graded-silicon processor with a typical TID hardness of ~ 5–10 krad(Si), providing a margin against the conservative phase-integrated dose of 0.7 Gy (**ASS-CDH-02**). Single-event effects (SEE) are mitigated through triple-modularity duplication (TMR) on critical registers, watchdog timers that detect instruction lock-ups, and automatic memory scrubbing routines in the flight software. During time critical operations like the sampling operations the hot/cold configuration is changed to a hot/hot configuration to allow for a quick takeover in the event of a computer failure.

Mass, volume, and power are sized conservatively within platform allocations:

- **Mass:** ~ 10 kg total (OBC pair + SSR/EDR + cooling mounts)
- **Volume:** ≈ 9.1–10 L, accommodated within standard rack-mount form factors; clearance margins allow for thermal interface materials and vibration potting.
- **Power:** Nominal draw of 30 W under full processing load with one computer. This leaves a 25% margin above peak operational demand, satisfying **ASS-CDH-08** and ensuring EPS can support simultaneous fault-mode power surges without bus droop.

Fault Detection, Isolation, and Recovery (FDIR)

The FDIR is a hierarchical state-machine logic designed to preserve mission life while minimizing ground contact overhead. It operates across three tiers of autonomy, with explicit trigger conditions, recovery actions, and fallback states defined in the contingency action plan. The logic explicitly accounts for payload-specific fault modes across bioleaching, monitoring, and remote sensing chains:

- ***Tier 1: Component Level.*** Hardware watchdogs and voltage/current monitors track individual rails and instruments. If a single payload rail (e.g., LMC_{OOL} pump driver or bioreactor valve actuator) exceeds current limits or stops responding issues a controlled power-cycle via programmable load switches (**REQ-EPS-03**). Recovery time is bounded at ≤ 1 s.
- ***Tier 2: Subsystem Level.*** Bus arbitration logic monitors MIL-STD-1553B token rotation and SpaceWire link integrity. If a bus goes silent for > 500 ms or an ADCS error exceeds the safe-pointing threshold, FDIR executes pre-programmed "Safe Mode" sequences: HGA sun-pointing, payload power-down, heater prioritisation, and OBC switchover to the cold spare (**REQ-RAMS-04**). Switching latency is validated at ≤ 2 s (Section 7.3.2). SpaceWire flow-control buffers prevent $\mathrm{LMC}_{\mathrm{OOL}}$ data overflow during pump stalls.
- ***Tier 3: Mission Level.*** For unrecoverable faults (e.g., catastrophic OBC lockup, SSR flash corruption, bioreactor leak detection, or RSS cold-radiator failure), the C&DH enters "Deep Safe" state. All non-volatile memory is flushed, critical parameters are preserved in radiation-hardened EEPROM, and the system awaits ground telemetry handshake before resuming operations. This tier requires human-in-the-loop resolution but guarantees zero data loss for ≥ 30 days (**ASS-CDH-07**).

The FDR logic is verified through a fault injection test matrix that simulates > 95% of single-point failure modes across the bus and processor chains. Redundant trigger paths (hardware watchdogs *and* software state polling) ensure no single firmware bug disables recovery capability.

7.3.3. C&DH Design Summary

The preliminary C&DH design successfully closes through heritage-driven component selection, explicit redundancy posturing, and tiered FDR autonomy. By leveraging graded-silicon processing and isolated

bus topologies, the architecture satisfies real-time payload monitoring requirements while maintaining strict mass/power margins within the platform allocation.

Table 7.19 synthesizes the final baseline parameters, operational limits, and interface setpoints that define the C&DH architecture. wa

Table 7.19: Master synthesis of C&DH baseline parameters and operational setpoints.

Parameter	Baseline Value	Notes / Bounding Limits
Processing Core	dual-core pair	Hot/cold redundant; TMR on critical registers.
Memory/Storage	64 Gbit SSR + EDR/FDR banks	≥ 30 day store-and-forward capacity; handles ~1.9 GB RSS buffer.
Platform Bus	MIL-STD-1553B	Central terminal topology; ≤ 2 Mbit/s framing rate.
Payload Bus	SpaceWire	Direct OBC connection to LMC_{OOL}, HMS, bioreactor, RSS, arm; ≤ 500 ms sensor polling latency.
Fault Tolerance Posture	1-FT (Processor chain)	Automatic switchover; ≤ 2 s transition time.
TID Hardness Margin	≥ 7× design envelope	Nominal phase dose ~0.6 Gy; qualified to ~5 kGy.
Power Draw (Nominal)	30 W	Includes full payload polling + bus framing; 25% EPS margin reserved.
Mass / Volume	~ 12 kg / ~ 9.5 L	Fits within allocated rack space with potting clearance.
FDR Autonomy Level	Tier-1/2: Autonomous	Tier-3 requires ground intervention; zero data loss guaranteed.

Forward Work

Because this design relies on heritage radiation models and static bus profiling, several key assumptions must be explicitly investigated and retired in Phase B. The following open items establish the roadmap for detailed design maturation:

1. **Radiation Testing and SEE Cross-Section Characterization:** The baseline TID margin (**ASS-CDH-02**) assumes graded-silicon performance holds at the projected dose rate. Phase B must conduct single-event upset (SEU) cross-section testing on the GR712RC flight software image to validate TMR effectiveness and refine memory scrubbing intervals.
2. **SpaceWire Payload Contention & LMC_{OOL} Data Formatting:** The ≤ 500 ms polling latency (Table 7.17) must be verified under concurrent bioleaching valve sequencing and HMS tier-3 chip reads. Phase B will generate a formal SpaceWire routing matrix and data packet format specification for the LMC_{OOL} biomarker streams.
3. **FDR Fault Injection and Recovery Timing Validation:** The Tier-1/2 recovery bounds (≤ 1 s component cycle, ≤ 2 s OBC switchover) require hardware-in-the-loop (HIL) testing. Phase B must execute a full fault matrix to verify watchdog tripping times and cold spare boot sequences under worst-case thermal conditions.
4. **SSR Data Compression & Downlink Closure:** The ≥ 30 day telemetry retention assumption (**ASS-CDH-07**) must be verified against actual payload data rates. A lossless compression algorithm (e.g., CCSDS Housekeeping/SMS) must be developed and validated to ensure the 64 Gbit buffer comfortably contains the RSS campaign plus continuous HMS/LMC_{OOL} logs without overflow during communication blackouts.
5. **Power Rail Sequencing and Inrush Current Validation:** The 25% power margin (**ASS-CDH-07**) assumes controlled load switching. Phase B must model simultaneous SSR relay closures for the bioreactor heaters, HMS pumps, and RSS cold radiators to confirm EPS can handle transient inrush without bus droop or brownout triggering FDR Safe Mode.

7.4. Propulsion System

The propulsion subsystem consists of two main branches. The ion propulsion system provides the high-efficiency cruise capability required for the outbound, rendezvous and return trajectory phases. The Chemical/RCS

system provides high-thrust and reaction-control functions. This section first defines the common propulsion requirements, assumptions and interface logic. The ion propulsion system is then sized separately from the Chemical/RCS system, because both branches use different propellants, thrust levels, storage concepts and operational roles. The section concludes with a combined propulsion summary, derived subsystem requirements and forward work.

7.4.1. Propulsion Scope, Requirements and Assumptions

Design Assumptions

Table 7.20: Consolidated design assumptions for the propulsion subsystem.

Assumption ID	Description
ASS-PRP-01	Xenon propellant is stored strictly in a single-phase supercritical state at a continuous 20°C and 150 bar (MEOP) to ensure a static center of mass.
ASS-PRP-02	The xenon COPV utilizes a spherical geometry to minimize structural mass, assuming this shape fits within the volumetric packaging constraints of the rectangular spacecraft bus.
ASS-PRP-03	The xenon COPV dry mass scales at 15% of the loaded xenon propellant mass.
ASS-PRP-04	A 10% tank-volume allowance is applied to the xenon fluid volume to accommodate thermal expansion, residuals and packaging uncertainty.
ASS-PRP-05	The xenon mechanical feed system architecture is conservatively bounded at a dry mass of 5.0 kg, based on NEXT program single-string heritage.
ASS-PRP-06	The Electrical Power System (EPS) is assumed to provide up to 2.5 kW of continuous PPU power, and the broader mass budget guarantees an 80 kg dry mass allocation for the ion propulsion subsystem.
ASS-PRP-07	The Chemical/RCS propellant is LMP–103S and is sized using a representative specific impulse of 250 s.
ASS-PRP-08	The Chemical/RCS system uses the Bradford ECAPS 22 N HPGP thruster as reference hardware for both departure and RCS functions.
ASS-PRP-09	Chemical/RCS post-departure propellant calculations use the spacecraft mass after the Earth-departure burn.
ASS-PRP-10	Chemical/RCS propellant margins follow Section 8.3.1: the Earth-departure burn uses the astrodynamics design ΔV, analytically defined TCM and SRC-divert manoeuvres carry 5 % ΔV margin, and attitude-control, desaturation and proximity-control allowances carry 100 % margin. A 2 % residual propellant allowance is then added separately.
ASS-PRP-11	The ion propulsion propellant is sized after the Chemical/RCS Earth-departure burn, using the post-departure spacecraft mass as the initial mass for the heliocentric low-thrust phase.

The propulsion sizing follows the budget methodology and margin philosophy defined in Section 8.3.1. Equipment-level maturity margins are included in the dry hardware budgets, while the 20 % system-level dry-mass margin is only applied in the spacecraft roll-up. Propellant residuals are kept separate from usable propellant and are applied as a 2 % residual allowance. Tank volumes are sized for the margin-inclusive loaded propellant mass plus volume allowance.

Existing Propulsion Requirement Inputs

The propulsion subsystem is mainly driven by the mission-level requirement to enable transit from Earth to the target asteroid, while also remaining compatible with the Ariane 62 rideshare mass envelope and the ESA F-class cost constraint. The existing requirement inputs used by the propulsion design are summarised in Table 7.21.

Table 7.21: Existing requirement inputs retained for propulsion subsystem design.

Requirement ID	Requirement	Propulsion relevance
REQ-MIS-06	The mission propulsion shall enable transit from Earth to the target NEA.	Drives total propulsion architecture and trajectory closure.
REQ-STK-08	The mission shall be launched on Ariane 62 in compliance with the Ariane 62 User's Manual.	Drives wet-mass and stowed-volume compatibility.
REQ-SYS-01	The mission shall ensure wet mass compatibility with the Ariane 62 launcher including the required system margin.	Drives total propellant and hardware mass closure.
REQ-STK-07	The mission shall comply with the ESA F-class cost cap of 205 Me, excluding launch.	Drives use of COTS and heritage propulsion hardware where possible.
REQ-STK-10	The spacecraft shall comply with applicable space-debris mitigation requirements.	Drives propulsion passivation and end-of-life interfaces.

7.4.2. Ion Propulsion System

Architecture Justification

While Hall-Effect Thrusters (HET) offer higher thrust-to-power ratios and simpler power processing architectures, a Gridded Ion Thruster (GIT) is chosen for the Silicon Shepherd primary transit. HETs typically operate at a specific impulse (I_{sp}) of 1500–2000 seconds due to limitations in applied discharge voltage and plasma confinement [117, 118]. Utilizing a HET would require a propellant mass fraction that violates the strict Ariane 62 rideshare wet-mass limit. Conversely, the GIT architecture electrostatically accelerates ions through biased grids, allowing it to easily exceed an I_{sp} of 3000 seconds [117]. This makes it the only commercially mature technology capable of closing the mass budget for this F-class profile. Consequently, the trade-off is restricted to GIT working propellants and OTS hardware.

Ion Propellant Trade-Off Framework

Before selecting the specific off-the-shelf thruster, the propellant must be decided. The propellant drives the storage volume, the Power Processing Unit (PPU) electrical requirements, and the total system mass.

Evaluation Criteria and Weights To ensure alignment with the mass and cost constraints, the following criteria are defined:

- **Heritage & Compatibility (Weight: 0.35):** High Technology Readiness Level (TRL) and interaction with spacecraft materials.
- **Storage Density (Weight: 0.25):** Ability to store the propellant densely to meet the spacecraft volume limit.
- **Performance (Weight: 0.25):** Lower ionization energy relative to atomic mass maximizes the thrust-to-power ratio [119].
- **Cost & Availability (Weight: 0.15):** Attainable within the €205M F-class cap.

Table 7.22: Propellant Characteristics and Weighted Decision Matrix

Propellant	Xenon (Xe)	Krypton (Kr)	Argon (Ar)	Iodine (I_2)
Atomic Mass (amu) [119]	131.3	83.8	39.9	~253.8
1st Ionization Energy (eV) [119]	12.1	14.0	15.8	~10.45
Heritage & Comp. (0.35)	5	4	4	2
Storage Density (0.25)	3	2	1	5
Performance (0.25)	5	3	2	4
Cost & Avail. (0.15)	1	3	5	5
Total Weighted Score	**3.90**	**3.10**	**2.90**	**3.70**

Trade-Off Analysis Based on the weighted trade-off analysis, Xenon is selected as the baseline propellant for the primary transit. It remains the benchmark for space applications due to its low first ionization energy (12.1 eV), high atomic mass, and chemical inertness [120, 119], which collectively maximize the thrust-to-power ratio within the system power limit. While its high cost and requirement for high-pressure storage [121] negatively impact its volumetric and financial scoring, its unparalleled flight heritage secures its selection for a F-class mission. Iodine presents a strong theoretical alternative: it is stored at an ambient pressure as a solid and its volumetric capacity is substantially higher than Xenon [121], yielding the highest density score. Although, Iodine is highly reactive and creates a chemically aggressive environment that is incompatible with standard spacecraft metals and plastics [122, 121]. This severe material incompatibility drastically lowers its heritage score, ruling it out for this baseline. Finally, both Krypton and Argon are eliminated from consideration as they suffer from lower atomic masses and higher ionization potentials (e.g., 15.8 eV for Argon) [119], which draws excessive power away from beam acceleration. Furthermore, Krypton's lower density requires significantly larger, higher-pressure tanks [120].

Off-The-Shelf Thruster Selection

To further progress into a detailed design, a selection between relevant Off-The-Shelf (OTS) thrusters must be conducted. These will be selected based on heritage and origin of production, preferably leaning towards a more European orientated selection confining towards the F-class mission budget constraints. The preliminary selection of thrusters is hence provided following a comprehensive trade-off. Three distinct thruster profiles were evaluated:

- **The EU Baseline (ArianeGroup RIT-2X):** A European Radiofrequency Ion Thruster. Its published operational envelope demonstrates significant throttle-ability, allowing it to operate efficiently at multiple power input ranges [123].
- **The EU Heavy Alternative (QinetiQ T6):** A Kaufman-type Gridded Ion Thruster with extensive ESA heritage. While it offers an exceptional specific impulse of up to 4400 s [124], its nominal operating envelope requires between 2.4 kW and 4.5 kW [125].
- **The Benchmark (NASA/L3Harris NSTAR):** The American thruster flown on the *Deep Space 1* and *Dawn* missions. While ITAR restrictions and ESA's procurement preferences preclude its selection, it serves as the historical benchmark. Operating at a maximum of 2.3 kW with an 8.33 kg dry mass [126].

The specific physical and electrical characteristics of the candidate thrusters are detailed in Table 7.23.

Table 7.23: Characteristics of candidate COTS gridded ion thrusters.

Parameter	ArianeGroup RIT–2X	QinetiQ T6	NASA NSTAR
Technology	Radiofrequency GIT	Kaufman GIT	Kaufman GIT
Input power range	2.0–5.3 kW [123]	2.4–4.5 kW [125]	0.5–2.3 kW [126]
Nominal thrust	70–215 mN [123]	30–230 mN [124]	19–92 mN [126]
Specific impulse	2450–3500 s [123]	~4400 s [124]	1900–3100 s [126]
Thruster dry mass	< 10 kg [123]	8.3 kg [124]	8.33 kg [126]

Evaluation Criteria and Weights With the thrusters brought to three candidate profiles, a weighted trade-off is required to baseline the primary hardware. This trade-off must reconcile a critical subsystem tension: preliminary astrodynamic trajectory optimization demands a high low-thrust capability, while the Electrical Power System (EPS) restricts continuous PPU power draw to approximately 2.5 kW [ASS-PRP-06].

The criteria are weighted toward resolving this power/thrust conflict while strictly adhering to programmatic constraints:

- **Power/Thrust Synergy (Weight: 0.35):** The ability to approach the astrodynamic thrust requirement while remaining highly throttleable to avoid catastrophic EPS overruns.
- **EU Attainability (Weight: 0.30):** The hardware must be sourced within Europe to eliminate ITAR export restrictions, satisfying ESA F-class procurement preferences.
- **Heritage & Reliability (Weight: 0.20):** Demonstrated deep-space flight heritage and resistance to long-term degradation.
- **System Mass Impact (Weight: 0.15):** The dry mass of the thruster assembly must comfortably fit within the 80 kg subsystem allocation.

Table 7.24: COTS gridded ion thruster weighted decision matrix.

Criterion	Weight	ArianeGroup RIT–2X	QinetiQ T6	NASA NSTAR
Power/thrust synergy	0.35	4	3	1
EU attainability	0.30	5	5	1
Heritage and reliability	0.20	4	5	5
System mass impact	0.15	4	4	4
Total weighted score	**1.00**	**4.30**	**4.15**	**2.25**

Trade-Off Justification Based on the weighted analysis, the **ArianeGroup RIT-2X** is selected as the baseline primary thruster because it offers the optimal thermodynamic and programmatic compromise for the *Silicon Shepherd* architecture. It is critical to address the inverse relationship between propellant mass savings and electrical power, which fundamentally drives this selection. While the Tsiolkovsky rocket equation dictates that a higher specific impulse (I_{sp}) exponentially reduces propellant mass, the kinetic energy required to accelerate the plasma scales with the square of the exhaust velocity ($E_k \propto v^2$).

The RIT-2X navigates this bottleneck well. Its scalable radiofrequency architecture suggests compatibility with the required thrust range while allowing operation in lower-power throttle bands when EPS margin is limited [123]. This supports the strict PPU power constraint while maintaining an exhaust velocity high enough to close the wet-mass budget. Furthermore, its European origin ensures a maximum score in attainability, and its radiofrequency ionisation removes the discharge-cathode erosion mechanism, although neutraliser lifetime must still be verified.

The **QinetiQ T6** serves as a strong alternative with unparalleled ESA flight heritage [125]. However, its operational envelope is fundamentally designed for higher power regimes. Achieving its exceptional mass-saving I_{sp} (~4400 s) demands pushing the PPU to its absolute limits [124], introducing severe electrical margin risks and lowering its synergy score. Finally, the **NASA NSTAR** is eliminated. As an American asset, it introduces unacceptable ITAR procurement risks. More critically, its absolute maximum thrust output of 92 mN [126] makes it physically incapable of satisfying the highest astrodynamic thrust requirement regardless of available power.

Xenon Storage and Tank Sizing

The ion propellant is sized after the Chemical/RCS Earth-departure burn, using the post-departure (pd) spacecraft mass. This mass is calculated using the initial launch wet mass and the initial propellant mass.

$$m_{sc,wet} = 1300kg \tag{7.6}$$

$$m_{p,dep} = 180.3kg \tag{7.7}$$

$$m_{post-dep} = m_{sc,wet} - m_{p,dep} = 1119.7kg \tag{7.8}$$

Considering the ion propulsion ΔV is taken as 3.71 km/s. Following Section 8.3.1, a 5 % electric-propulsion cruise margin is applied, giving

$$\Delta V_{\text{ion,eff}} = 1.05 \times 3710 = 3860\,\text{m/s}.$$

Using the conservative lower-bound RIT–2X specific impulse of $I_{sp} = 2450$ s, the usable xenon propellant mass is

$$m_{\text{Xe,usable}} = 1119.7\left[1 - \exp\left(-\frac{2520}{3710 \cdot 9.80665}\right)\right] = 111.5\,\text{kg}.$$

A 2 % residual xenon allowance is added separately,

$$m_{\text{Xe,res}} = 0.02\, m_{\text{Xe,usable}} = 2.2\,\text{kg},$$

so the loaded xenon mass is

$$m_{\text{Xe,loaded}} = 113.7\,\text{kg}.$$

To satisfy the volume limit of the Ariane 62 rideshare, the xenon propellant must be stored at high density utilizing a Composite Overwrapped Pressure Vessel (COPV). In comparison to a traditional Type I all-titanium pressure vessel, which would impose an increased dry mass 35 to 40 kg to contain 150 bar of internal pressure

[113], the COPV architecture leverages a high-specific-strength carbon overwrap to reduce the storage mass by over 50% [117]. Consequently, the COPV was chosen to protect the subsystem's 80 kg dry mass allocation.

Using the same representative supercritical xenon density as before, $\rho_{Xe} = 1600\,\mathrm{kg/m^3}$, the required xenon fluid volume is

$$V_{Xe} = \frac{113.7}{1600} = 0.0711\,\mathrm{m^3} = 71.1\,\mathrm{L}.$$

Applying the 10 % tank-volume allowance from Section 8.3.1,

$$V_{\mathrm{tank,Xe}} = 1.10 \times 71.1 = 78.2\,\mathrm{L}.$$

Assuming a spherical geometry to optimize stress distribution and mass efficiency, this internal volume corresponds to a tank diameter of approximately

$$D_{Xe} = \left(\frac{6V_{\mathrm{tank,Xe}}}{\pi}\right)^{1/3} = 0.531\,\mathrm{m}.$$

Using the existing COPV mass heuristic of 15 % of loaded propellant mass, the xenon COPV dry mass is

$$m_{\mathrm{COPV,Xe}} = 0.15 \times 113.7 = 17.1\,\mathrm{kg}.$$

Geometry Selection and Heritage Justification While spacecraft buses typically favour cylindrical tank geometries to optimize volumetric packaging, a spherical geometry is selected for this preliminary architecture (ASS-PRP-02). In high-pressure applications, the uniform hoop stress of a sphere represents the minimum structural mass for a pressure vessel [113]. By assuming a 0.531 m sphere, the propulsion subsystem establishes a low dry-mass storage baseline, maximizing the available mass margin for the broader system.

This approach aligns with mass-constrained deep-space electric propulsion heritage, notably NASA's *Dawn* mission, which utilized a centrally mounted spherical COPV to minimize dry mass while storing 425 kg of supercritical Xenon [127]. However, it is acknowledged that as the mechanical layout matures in the next phase of design, volumetric packaging constraints within the rectangular bus may require trading this optimal spherical mass for a cylindrical tank geometry. Such a transition would require systems engineering to expend part of the propulsion dry-mass margin to accommodate the thicker composite overwrap required by cylindrical hoop stresses.

Thermodynamic Storage State Xenon possesses a critical temperature of 16.6°C. To prevent the propellant from dropping into a two-phase regime, standard aerospace practice dictates storing the fluid in a single-phase supercritical state [**sutton2016rocket**]. In this supercritical state, the fluid fills the pressure vessel uniformly, ensuring the local propellant Center of Mass (CoM) remains static at the geometric center of the tank, thereby simplifying ADCS momentum management.

Consequently, the nominal storage conditions are at a continuous temperature of 20°C and an MEOP of 150 bar (ASS-PRP-01, REQ-TCS-DER-01). While a two-phase Propellant Management Unit (PMU) architecture, similar to that used on JAXA's *Hayabusa2* [128], was considered to mitigate the continuous electrical heater power required by the TCS this method was ultimately shelved. The decision was made to a strictly supercritical storage architecture to prioritise ADCS stability and minimise feed system mechanical complexity.

Ion Propulsion Architecture Overview and Configuration

The Silicon Shepherd ion propulsion subsystem is designed to satisfy the heliocentric low-thrust transfer requirement while remaining compatible with the Ariane 62 wet-mass constraint. To achieve this, the architecture integrates high-pressure supercritical xenon storage with a regulated mechanical feed system, terminating at a fault-tolerant electrostatic thruster array.

Redundancy and Fault Tolerance Deep-space missions utilizing electric propulsion rely on extended, multi-year burn durations. Consequently, grid erosion, neutraliser degradation, and single-point electrical failures represent critical mission-ending risks [117]. To achieve the necessary single-fault tolerance, the architecture baselines a 1+1 cold redundancy configuration (REQ-RAMS-02). The system mounts two identical ArianeGroup RIT-2X thrusters on the aft thrust structure; one unit serves as the active primary thruster, while the second remains fully inactive but mechanically and electrically integrated as a backup.

This cold-redundant approach mirrors the high-reliability flight heritage of NASA's Dawn mission, which carried three ion engines but operated only one at a time to guarantee trajectory closure in the event of unforeseen component degradation [127].

System Integration and Flow As calculated in Table 7.4.2, the loaded xenon propellant mass is 113.7 kg, stored at 20°C and 150 bar within a 78.2 L COPV. The high-pressure feed section routes the fluid through a filter to protect downstream valve seats, followed by a normally closed pyrotechnic valve (REQ-RAMS-02). This pyrotechnic isolation is strictly required to prevent high-pressure xenon leakage through mechanical interfaces during extended ground operations and launch vehicle ascent [117]. Following orbital deployment and pyrotechnic actuation, a high-pressure latch valve provides a reusable mechanical shut-off capability. A mechanical pressure regulator then steps the variable upstream xenon pressure down to a constant 2.5 bar operational pressure, doing so without drawing continuous electrical power from the bus [117].

To accommodate the 1+1 redundant thruster configuration, the low-pressure plumbing splits into two parallel, fully isolatable branches immediately downstream of the mechanical regulator. This separation is similar to the flight-proven, fault-tolerant architecture of NASA's *Dawn* spacecraft [127]. Flow to the active Main Thruster is governed by Low-Pressure Isolation Valve A (LPIV-A), while the Redundant Thruster is sealed by LPIV-B. This ensures that a pneumatic failure in the active thruster can be isolated without compromising the backup system's ability to complete the mission [127].

Within each respective branch, the flow undergoes a final split into dedicated Proportional Flow Control Valves (PFCVs). These provide the independent milligram-per-second mass flow regulation required by the RIT-2X architecture to feed the main ionisation chamber and the neutraliser cathode separately [123]. The complete fluid routing is mapped in the preliminary flow diagram provided in Figure 7.6.

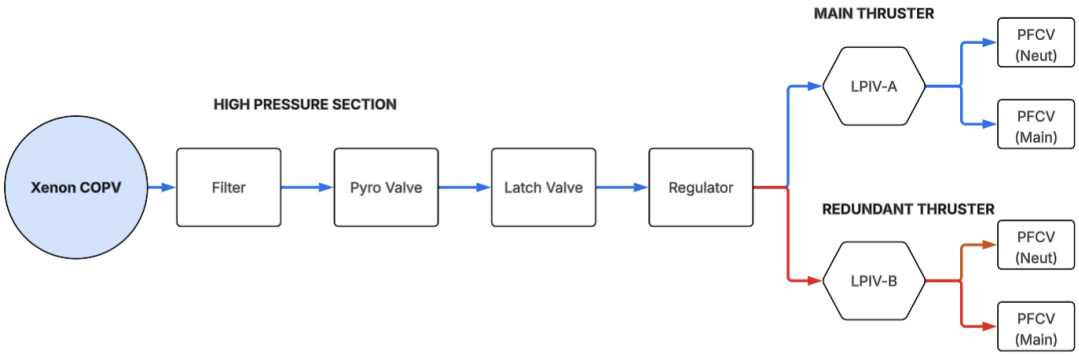

Figure 7.6: Piping and Instrumentation Diagram (P&ID) of the *Silicon Shepherd* ion propulsion architecture, detailing the 150 bar supercritical storage, mechanical regulation, and the low-pressure branch split servicing the 1+1 cold-redundant RIT-2X thrusters.

The feed system design is based on the single-string Propellant Management System (PMS) architecture developed for the NASA Evolutionary Xenon Thruster (NEXT) program. By adopting this flight-proven mechanical configuration, comprising high-pressure isolation, mechanical pressure regulation, and low-pressure metering, the feed system is bounded at a conservative nominal mass of 5.0 kg [129] (ASS-PRP-05).

7.4.3. Chemical Propulsion and Reaction Control System

The spacecraft uses a shared green-monopropellant chemical propulsion system for both high-thrust manoeuvres and reaction-control functions. In the remainder of this section, this dual-use subsystem is referred to as the Chemical/RCS system. Its main functions are the Earth-departure burn from the high-energy rideshare orbit, deterministic cruise trajectory-correction manoeuvres, Itokawa proximity manoeuvres, reaction-wheel desaturation, sampling-support and abort manoeuvres, and the post-SRC spacecraft divert.

This section closes the Chemical/RCS hardware and propellant sizing. The astrodynamics chapter provides the Earth-departure and cruise-TCM ΔV inputs, while the ADCS/stability-control section provides the disturbance, desaturation and proximity-control drivers. The spacecraft divert ΔV after Sample Return Capsule release is taken from the SRC section, since it is driven by the required Earth-miss distance and capsule separation timeline. Propellant masses are only computed here, after the propellant and thruster technology have been selected, to avoid double-counting between ADCS, astrodynamics, SRC and propulsion.

Propellant and Thruster Selection

The selected Chemical/RCS technology is a green monopropellant system using LMP–103S. This propellant is an ADN-based hydrazine replacement with European flight heritage through the Bradford ECAPS High Performance Green Propulsion (HPGP) family. A green monopropellant system was selected over classical

hydrazine and hydrazine-family bipropellant because it reduces handling toxicity and ground-processing burden, while still providing sufficient high-thrust capability for the spacecraft-side departure burn and RCS functions. Non-hydrazine bipropellant concepts were considered less suitable at this design stage because their flight maturity and supplier availability are lower for the required small-spacecraft reaction-control architecture.

The reference thruster is the Bradford ECAPS 22 N HPGP thruster, operated on LMP–103S. Its main properties are summarised in Table 7.25. For all preliminary propellant sizing in this section, a representative specific impulse of 250 s is used, which lies within the datasheet steady-state vacuum range.

Table 7.25: Reference properties of the Bradford ECAPS 22 N HPGP thruster used for the Chemical/RCS system [130].

Property	Value
Thruster type	HPGP monopropellant
Propellant	LMP–103S
Nominal thrust class	22 N
Thrust range	5.5–22 N
Inlet pressure range	5.5–24 bar
Steady-state vacuum I_{sp}	243–255 s
Representative I_{sp} used for sizing	250 s
Density impulse	2957–3108 Ns/L
Minimum impulse bit	$\leq$ 0.44 Ns
Thruster mass	1.1 kg
Overall length	260 mm
Reactor pre-heating power	25–50 W
Target propellant throughput	150 kg
Target longest continuous firing	45 min
Maturation level	TRL 5/6

Thruster Configuration

The baseline layout uses fourteen 22 N thrusters. Four axial thrusters are mounted on the aft face and provide the main Earth-departure burn. Two axial thrusters are mounted on the opposite face to provide direct reverse-axis translation without requiring a full spacecraft slew. The remaining eight thrusters are arranged as canted pairs on the four lateral faces. The cant angle means that the side thrusters are tilted away from the local face normal, allowing paired firings to generate lateral forces while differential firings generate attitude-control torques. These side thrusters therefore provide lateral translation, attitude torques, reaction-wheel desaturation, proximity manoeuvres and abort support.

The Earth-departure burn uses the four aft axial thrusters, giving

$$T_{\text{dep}} = 4 \times 22 = 88\,\text{N}.$$

The four departure thrusters are placed symmetrically around the spacecraft centreline so that the net torque during the long burn is as small as possible. The two opposite axial thrusters are not sized for the main burn, but they are included because the spacecraft still needs reverse-axis authority during proximity operations and possible abort cases. The resulting layout is less symmetric than a sixteen-thruster configuration, but it gives preliminary six-degree-of-freedom control while avoiding the mass and packaging penalty of four thrusters on both axial faces.

The final thruster cant angles and firing logic shall be verified using a control-allocation matrix once the centre-of-mass location, CAD geometry, plume keep-out zones and thruster locations are fixed. Plume impingement on the solar arrays, radiators, sampling arm, high-gain antenna and Sample Return Capsule must also be checked before the layout is frozen.

Chemical/RCS Manoeuvre Inputs

The Chemical/RCS propellant budget is split into two parts. The first part is the Earth-departure burn, which is driven by the astrodynamics interface. The selected practical trajectory baseline uses the astrodynamics design value

$$\Delta V_{\text{dep}} = 366\,\text{m/s}.$$

This value is treated as the departure design interface and is therefore not given an additional propulsion-side ΔV margin. The second part consists of post-departure Chemical/RCS usage. The inputs are taken from the astrodynamics, ADCS/stability-control, operations and SRC sections. Margins are applied according to Section 8.3.1: analytically defined manoeuvres receive 5 % ΔV margin, while attitude-control, desaturation and proximity-control allowances receive 100 % margin.

Table 7.26: Chemical/RCS sizing inputs imported from astrodynamics, ADCS/stability-control, operations and SRC analyses. Margins follow Section 8.3.1.

Category	Contribution	Base sizing input	Margin rule
Departure	Earth-departure burn from HEO reference	$\Delta V = 366\,\mathrm{m/s}$	Included in astrodynamics interface
Disturbances	Reaction-wheel desaturation over cruise, stay and return	$\Delta H = 3047\,\mathrm{Nms}$	100 %
Disturbances	SRP translational station-keeping during asteroid stay	$\Delta V = 5.45\,\mathrm{m/s}$	100 %
Navigation	Cruise trajectory correction, outbound and return	$\Delta V = 15.0\,\mathrm{m/s}$	5 %
Operations	Mapping manoeuvre at 6 km, six hops	$\Delta V = 0.12\,\mathrm{m/s}$	100 %
Operations	Close inspection at 500 m, gravity-hover estimate	$\Delta V = 5.06\,\mathrm{m/s}$	100 %
Operations	Touch-and-go sampling support, six attempts	$\Delta V = 4.08\,\mathrm{m/s}$	100 %
Special	Sample-return capsule release and bus divert	$\Delta V = 34.7\,\mathrm{m/s}$	5 %

Propellant Mass Sizing

The propellant mass for each ΔV contribution is estimated with the rocket equation,

$$m_p = m_0 \left[1 - \exp\left(-\frac{\Delta V}{I_{sp} g_0}\right)\right],$$

where m_0 is the spacecraft mass before the manoeuvre, $I_{sp} = 250\,\mathrm{s}$ and $g_0 = 9.806\,65\,\mathrm{m/s^2}$. The spacecraft wet mass before Chemical/RCS Earth departure is taken as

$$m_{\mathrm{SC,wet}} = 1300\,\mathrm{kg}.$$

For the Earth-departure burn, this gives

$$m_{p,\mathrm{dep}} = 1300 \left[1 - \exp\left(-\frac{366}{250 \cdot 9.80665}\right)\right] = 180.3\,\mathrm{kg}.$$

The post-departure spacecraft mass used for the following Chemical/RCS and ion-propulsion estimates is therefore

$$m_{\text{post-dep}} = 1300 - 180.3 = 1119.7\,\mathrm{kg}.$$

For the desaturation contribution, the required propellant mass is estimated from the angular impulse that must be removed from the reaction wheels. Assuming an effective RCS moment arm of $\ell_{\mathrm{eff}} = 0.5\,\mathrm{m}$ and applying the 100 % angular-momentum-management margin from Section 8.3.1,

$$m_{p,\mathrm{desat}} = 2\frac{\Delta H}{\ell_{\mathrm{eff}} I_{sp} g_0} = 4.97\,\mathrm{kg}.$$

The resulting Chemical/RCS propellant budget is shown in Table 7.27. The table separates usable propellant from residual propellant to remain consistent with Section 8.3.1.

The total loaded LMP–103S propellant mass carried forward to the spacecraft mass budget is therefore

$$m_{\mathrm{LMP,loaded}} = 227.0\,\mathrm{kg}.$$

Table 7.27: Chemical/RCS propellant budget using $m_{SC,wet}$ = 1300 kg. Margins follow Section 8.3.1.

Category	Contribution	Effective basis	Margin	m_p [kg]
Departure	Earth-departure burn	ΔV = 366 m/s	Included	180.28
Disturbances	Reaction-wheel desaturation	ΔH = 6094 Nms	100 %	4.97
Disturbances	SRP translational station-keeping	ΔV = 10.90 m/s	100 %	4.97
Navigation	Cruise trajectory correction	ΔV = 15.75 m/s	5 %	7.17
Operations	Mapping manoeuvre at 6 km	ΔV = 0.24 m/s	100 %	0.11
Operations	Close inspection at 500 m	ΔV = 10.12 m/s	100 %	4.61
Operations	Touch-and-go sampling, six attempts	ΔV = 8.16 m/s	100 %	3.72
Special	Sample-return capsule divert	ΔV = 36.44 m/s	5 %	16.52
Post-departure RCS usable subtotal				**42.07**
Total usable LMP–103S propellant				**222.35**
Residual propellant allowance, 2 %				4.45
Total loaded LMP–103S propellant				**226.80**

Tank and Pressurant Sizing

The tank is sized for the loaded LMP–103S propellant mass, including the 2 % residual propellant allowance. The liquid propellant volume is estimated using a representative LMP–103S density of

$$\rho_{LMP} = 1.24\,\text{kg/L}.$$

The required liquid volume is

$$V_{LMP} = \frac{m_{LMP,loaded}}{\rho_{LMP}} = \frac{226.98}{1.24} = 183.1\,\text{L}.$$

Using a maximum tank fill fraction of 90 %, which is slightly more conservative than the minimum 10 % tank-volume allowance in Section 8.3.1, the required internal tank volume is

$$V_{tank,min} = \frac{183.1}{0.90} = 203.4\,\text{L}.$$

A preliminary total LMP–103S tank allocation of 210 L is therefore retained. This provides volume margin for ullage, residuals, thermal expansion, line fill and packaging uncertainty. The final design may split this volume over multiple tanks to reduce centre-of-mass migration and improve packaging around the spacecraft structure.

The system is assumed to be pressure-fed using helium. A first-order pressurant storage volume is estimated from

$$V_{He,store} \approx \frac{p_{reg} V_{tank}}{p_{store} - p_{reg}},$$

with a representative regulated feed pressure of 16 bar, storage pressure of 200 bar and tank volume of 210 L. This gives

$$V_{He,store} \approx \frac{16 \cdot 210}{200 - 16} = 18.3\,\text{L}.$$

A 25 L helium COPV allocation is retained at this stage to include regulator volume, residuals, non-ideal gas behaviour, temperature effects and packaging uncertainty.

Earth-Departure Burn Duration

The Earth-departure burn is performed by the four aft axial thrusters. The total propellant mass flow rate during this burn is approximated as

$$\dot{m}_{dep} = \frac{T_{dep}}{I_{sp} g_0} = \frac{88}{250 \cdot 9.80665} = 0.0359\,\text{kg/s}.$$

Using the Earth-departure propellant mass from Table 7.27, the burn time is

$$t_{\text{dep}} = \frac{m_{p,\text{dep}}}{\dot{m}_{\text{dep}}} = \frac{180.3}{0.0359} = 5024\,\text{s} = 83.7\,\text{min}.$$

This burn is long compared with an impulsive manoeuvre and must therefore be treated as a finite-burn Earth-departure case in later astrodynamic refinement. The burn duration also exceeds the current target longest continuous firing value quoted for the reference thruster, so either segmented firing, thruster qualification extension, additional departure thrusters, or a revised departure implementation must be verified in later design phases.

7.4.4. Propulsion Subsystem Summary

The preliminary propulsion architecture combines a high-efficiency ion propulsion branch for heliocentric transfer with a dual-use Chemical/RCS branch. The Chemical/RCS system performs the high-thrust Earth-departure burn first, using the 1300 kg launch mass as its initial mass state. The resulting post-departure spacecraft mass of 1119.7 kg is then used as the initial mass state for the xenon propellant sizing of the ion propulsion system.

A master mass and cost budget for both branches is provided in Table 7.28. It should be heavily emphasized that the estimated costs—roughly €15.5 million for the ion branch and €5 million for the Chemical/RCS branch—are very rough order-of-magnitude (ROM) estimates. They are derived from historical subsystem integrations, preliminary vendor data, and analogous flight hardware. These figures carry high uncertainty and will fluctuate based on supply chain variables, final COTS component sourcing, and detailed Phase B definitions.

Table 7.28: Master propulsion subsystem budget and ROM cost estimates. Dry hardware values include equipment-level maturity margins only.

Item	Nom. [kg]	Margin	Mass [kg]	Vol. [L]	Est. Cost	Basis / note
Ion Propulsion Subsystem						
RIT–2X thrusters	20.0	10 %	22.0	–	–	Two thrusters (1+1 cold-redundant).
Xenon COPV	17.1	20 %	20.5	78.2	–	Custom tank (15 % of loaded Xe).
Xenon feed system	5.0	10 %	5.5	–	–	NEXT-based feed-system allowance.
PPU/RFG & thermal hardware	13.0	20 %	15.6	–	–	Electronics and local support hardware.
Dry Ion System	**55.1**	–	**63.6**	**78.2**	**~15.5 M**	**Excludes system-level dry margin.**
Loaded Xenon	113.7	–	113.7	–	–	111.5 kg usable + 2.2 kg residual.
Chemical/RCS Subsystem						
22 N HPGP thrusters	15.4	10 %	16.9	7	–	14 thrusters at 1.1 kg each.
LMP–103S tanks	28.0	20 %	33.6	210	–	210 L allocation.
He tank & regulator	8.0	20 %	9.6	25	–	25 L COPV and regulation.
Valves, filters, lines	12.0	10 %	13.2	12	–	First-order feed allowance.
Brackets & thermal hardware	8.0	20 %	9.6	8	–	Mounting, heaters, local harness.
Dry Chem/RCS System	**71.4**	–	**82.9**	**262**	**~5.0 M**	**Excludes system-level dry margin.**
Loaded LMP–103S	227.0	–	227.0	–	–	222.5 kg usable + 4.5 kg residual.
Combined Propulsion Totals						
Total Dry Mass	**126.5**	–	**146.5**	**340.2**	**~20.5 M**	**Total dry propulsion hardware.**
Total Wet Mass	–	–	**487.2**	**340.2**	–	**Hardware plus all loaded propellants.**

The loaded propellant masses in Table 7.28 include the 2 % residual propellant allowance from Section 8.3.1. The 20 % system-level dry-mass margin and the overarching spacecraft harness mass are applied separately in the system mass-budget roll-up.

Derived Requirements and Interfaces

The propulsion subsystem creates several interface requirements for the rest of the spacecraft. The derived requirements in Table 7.29 are restricted to interfaces that follow directly from the current propulsion analysis

and sizing. Broader verification items, such as detailed plume analysis and end-of-life passivation, are kept in the forward-work list rather than included as formal derived requirements at this stage.

Table 7.29: Derived spacecraft subsystem requirements from the propulsion subsystem.

Requirement ID	Subject / target	Design baseline	Rationale
REQ-RAMS-02	Ion architecture	1+1 cold redundancy	Electric propulsion is vulnerable to long-duration degradation and single-string electrical failures.
REQ-TCS-DER-01	Thermal Control	Continuous 20°C xenon tank conditioning	Xenon must remain supercritical at 150 bar to avoid two-phase slosh and CoM variation.
REQ-RAMS-03	Mechanisms	Pyrotechnic xenon isolation valves	Normally closed isolation is required to prevent high-pressure xenon leakage during ground, launch and early mission phases.
REQ-EPS-DER-01	Power / EPS	RIT–2X throttle compatibility with lower-power operating points	The ion propulsion operating point must remain compatible with the available cruise/thrust-mode PPU power.
REQ-PROP-DER-02	Chemical/RCS architecture	Fourteen 22 N HPGP thrusters	The Chemical/RCS system must cover both the Earth-departure cluster and post-departure RCS functions.
REQ-DER-ADCS-01	ADCS interface	Chemical/RCS control authority for ADCS-driven manoeuvres	ADCS passes wheel desaturation, SRP station-keeping and proximity-control drivers to Chemical/RCS.
REQ-DER-TCS-02	Thermal Control	HPGP reactor pre-heating and feed-line thermal accommodation	HPGP thrusters require pre-heating and temperature-compatible propellant/feed-line operation.
REQ-DER-EPS-02	Power / EPS	RCS-active state includes HPGP pre-heating power	Manoeuvre and sampling modes must reserve short-duration thruster pre-heating power.
REQ-RAMS-02	Mechanisms / storage	Pressure-fed LMP–103S storage and helium pressurisation	The mechanical layout must accommodate the 210 L LMP–103S allocation and 25 L helium allocation.

Forward Work

Because the propulsion subsystem combines a low-thrust ion branch with a dual-use Chemical/RCS branch, several assumptions must be refined in the next design phase. The current design closes the preliminary resource allocations but relies on empirical estimates that must be validated:

1. **Volumetric Packaging and CoM Shift:** The spherical xenon COPV, LMP–103S tanks, and helium storage must be closed in detailed 3D CAD. The layout must minimize centre-of-mass (CoM) migration during propellant depletion and verify whether the 0.531 m xenon sphere fits the structural bus without forcing a transition to a cylindrical tank that would consume mass margin.
2. **Detailed EPS and Thermal Coupling:** The RIT–2X throttle band requires a transient power balance analysis against solar array degradation and potential eclipse shadowing. Additionally, maintaining supercritical xenon at 20°C and pre-heating HPGP reactors requires detailed thermal modelling to size the respective heaters and MLI.
3. **Plume Impingement and Control Allocation:** Plume clearances for the solar arrays, radiators, high-gain antenna, and SRC must be verified for both the ion and chemical thrusters. A six-degree-of-freedom control-allocation matrix must validate the 14-thruster RCS layout for all manoeuvres, including ADCS desaturation against continuous parasitic torques generated by ion thrust misalignments.
4. **Finite-Burn and Firing Duration Checks:** The hour-long Earth-departure burn must be verified for finite-burn losses, steering losses, and outgoing asymptote targeting. The continuous firing duration of the aft 22 N HPGP thrusters must also be checked against qualification limits.
5. **Feed-System Component Sourcing:** The empirical mass allowances (5.0 kg for ion, 12.0 kg for chemical) must be replaced with a bottom-up mass and cost budget using specific European COTS high-pressure latch valves, mechanical regulators, and sensors to solidify the Phase B definitions.

7.5. Thermal Control System (TCS)

The Thermal Control System (TCS) holds every flight element inside its qualified temperature range across mission phases. It starts by consolidating the design assumptions together with the payload, power, and newly derived subsystem requirements. Section 7.5.1 then establishes the thermal environment and the hot and cold case definitions across the 0.953-1.695 AU heliocentric range, followed by Section 7.5.2, which defines the nodal thermal mathematical model and solves the case matrix, Section 7.5.4, which sizes the architecture against the cold-case heater budget, and Section 7.5.5 closes with the resource budget, verification plan, and forward-work roadmap.

7.5.1. Assumptions and Requirements

Table 7.30: Consolidated Design Assumptions for the TCS.

Assumption ID	Description
ASS-THER-01	The bioleaching setpoint of 25 ± 5 °C is a payload-performance requirement set above the 19.5–20.2 °C flight heritage.
ASS-THER-02	The aqueous growth medium freezes at 0 °C, hence, freeze prevention is treated as a hard biological survival limit.
ASS-THER-03	The health monitoring 0–40 °C window is held by a dedicated chip-scale Peltier element.
ASS-THER-04	The MLI outer surface is effectively grey ($\alpha_s/\varepsilon \approx 1.0$) for the bus-equilibrium envelope.
ASS-THER-05	Installed MLI effective emittance is $\varepsilon^* = 0.01$–0.05 (15–20 layers).
ASS-THER-06	Asteroid albedo and IR are < 1% of direct solar at ≥ 1 km station-keeping and are neglected.
ASS-THER-07	The ammonia VCHP cold-lockout is modelled as near-zero conductance below the working-fluid saturation temperature and full conductance above.

The payload, power, and mission requirements have been evaluated against the baseline design, flight heritage, and as-flown setpoints. Furthermore, the detailed thermal design imposes new derived constraints on the spacecraft bus and payload to hold every element within its qualified band. Table 7.31 synthesizes these, establishes the updated design baselines, and outlines the derived requirements that must be adopted by the respective spacecraft subsystems.

Table 7.31: Synthesis of resolved thermal requirements and derived spacecraft subsystem requirements.

Requirement ID	Subject / Target	Design Baseline	Rationale & Resolution
Part I: Thermal Limit Resolutions (Payload & Bus Setpoints)			
REQ-TCS-01	Original: The TCS shall keep the bioreactor within specified temperature bounds.	25 ± 5 °C.	Parent `REQ-TCS-DER-07` (bioleaching yield). The band is set above the 19.5–20.2 °C flight heritage. Additionally, lyophilised conidia are to be held in the heritage cold-storage band during the dormant cruise.
REQ-TCS-02	Original: The TCS shall keep instruments within specified temperature bounds.	Per-unit bands (Table 7.32).	Each unit is traced to a vendor or heritage datasheet.
REQ-TCS-03	The growth medium shall remain within specified temperature bounds in all phases.	> 0 °C (all phases).	The aqueous medium's freezing point is a hard biological survival limit, since freeze damage is irreversible.
REQ-TCS-04	The battery shall be charged and kept within specified temperature bounds.	+10 to +30 °C, and floor 0 °C.	The Midterm 0–10 °C figure confused the lower charge limit with the optimal; corrected to the full charge band with the lithium-plating do-not-charge floor.

Continued on next page...

Table 7.31 Continued from previous page

Requirement ID	Subject / Target	Design Baseline	Rationale & Resolution
Part II: Derived Subsystem Requirements (Bus & Payload Interfaces)			
REQ-EPS-DER-02	EPS/heater power	~120 W cold case (VCHP).	EPS shall allocate operational and survival heater power across all modes, including eclipse and safe-mode. The ~220 W passive case bounds the worst case if the VCHP cold-lockout degrades.
REQ-STRUC-DER-03	Structure/config	Radiator, MLI & VCHP placement	Structure shall close the bus envelope and freeze the MLI area at ~31.2 m^2.
REQ-PAY-01	Payload / reactor	Reactor wall, heat load & Peltier duty.	Payload shall provide 76W of internal heat load.

Changes from the Midterm. Five key requirement-level changes are applied for the Final Report.

1. The battery charge window moves from 0-10 °C to a life-optimised 10-30 °C with a 0 °C absolute floor, following the SAFT space cell life data [131, 132].
2. The transit-cruise temperature constraint for the payload has been set to 4-10 °C(Section 6.1).
3. The return-cruise payload constraint of 1.5-11.5 °C is removed. This is because the SRC returns processed and unprocessed regolith only, with no biological material across the Category V containment boundary(Section 6.1).
4. The health monitoring system acceptance band is stated as 0-40 °C for the full monitoring chain.
5. The MLI blanket area moves from a 25 m^2 OSIRIS-REx proxy to 31.2 m^2, derived from the locked bus envelope $3.2 \times 2.6 \times 1.3$ m.

Per-subsystem limits. Finally, Table 7.32 lists, for each subsystem, the thermally most-driving element and its operating thermal envelope.

Table 7.32: Silicon Shepherd subsystem temperature requirements, showing only the most thermally driving element(s) per subsystem. Phases: P1 launch, P2 outbound cruise, P3 proximity/mapping, P4 sampling, P5 bioleaching, P6 return cruise, P7 SRC EDL, and All = all phases.

Subsystem	Element	Operating range	Phase
Payload: bioreactor	Microbial culture, bioleaching[8, 3]	25 ± 5 °C (team req.)	P5
	Microbial culture, transit storage[3]	4–10 °C	P1–P4
	Growth medium	> 0 °C (no freeze)	P1–P5
Payload: health monitoring	LMCOOL + full monitoring suite	0–40 °C	P5
Remote sensing	VNIRS detector (NIRS3-class)[87]	−85 °C (188 K)	P3
	TIRS (μ-bolometer-class)	thermal stability only	P3
	Cameras (ONC-class CCD)[133, 134]	−30 °C nominal; +20 °C worst case	P3, P4
C&DH	On-board computer (GR712RC)[135]	−55 to +125 °C	All
EPS	Battery (space Li-ion), *charge*[132, 131]	+10 to +30 °C, 0 °C abs. floor	Safe
	Battery (space Li-ion), *discharge* [131]	−50 to +60 °C	Safe
Propulsion	Xe tank (supercritical COPV)[136, 137, 138]	~16.6–30 °C, > 16.6 °C abs. floor	P2, P3, P6
	RCS fuel (LMP–103S)	> freeze for LMP–103S −7 °C	P3, P4, P6, P7
ADCS	Star trackers (ASTRO APS-class)[139]	−30 to +60 °C	Safe

7.5.2. Thermal Mathematical Model

The thermal design is closed against a lumped-parameter nodal model, the standard method for preliminary spacecraft thermal analysis [140, 141], in which the spacecraft is discretised into a set of isothermal nodes, each carrying a capacitance $C_i = m_i c_{p,i}$ and exchanging heat conductively and radiatively with its neighbours and with a deep-space boundary held at $T_\infty = 4\,\mathrm{K}$ [141]. This fidelity is deliberate rather than a limitation. At the present design stage the dominant uncertainties are boundary conditions, the reactor wet mass, the installed MLI quality, and the attitude-dependent view factors, none of which are yet frozen. Hence, a node network that resolves every binding temperature requirement is therefore both sufficient and fully auditable. The node resolution is set by the requirement table rather than by geometry: one node per element with an independent temperature limit, with sub-nodes added only where an intra-component gradient is itself a requirement.

Node decomposition

The model carries fifteen state nodes, grouped by the requirement each resolves. The bus is split into sunlit and shaded panels: the cold case is set by the shaded-side equilibrium, the hot case by solar load on the sunlit side. The reactor is resolved into three sub-nodes—core, jacket, and endcap—because the spatial-uniformity limit and the safe-mode coast-down time (Case 6) are intra-reactor phenomena a single lumped node cannot express; the aqueous medium and culture are lumped into the core, where they dominate the reactor capacitance. The remaining nodes each map to one killer constraint or distinct heat path: the Li-ion battery (charge floor), the avionics/SSR box (quiescent dissipation, warmest internal source), the OSR radiator panel, the LMCOOL/Peltier assembly, the RCS lines and Xe COPV (freeze/critical-point floors), and the VNIRS detector. For powered cruise (Case 8) two further nodes—the EP power electronics (PPU/RFG) and the thruster head—are appended; in every other case these are inactive and the core thirteen-node set applies. The VNIRS detector sits at 188 K (−85 °C) [87], the −80 °C-class cold point of the spacecraft and the reason it is carried on a dedicated cold radiator rather than coupled to any warm node.

Conductive couplings

Conductive links use $K_{ij} = kA/L$, each derived from its interface geometry and material. Three of these couplings are design choices rather than as-built facts, and each encodes a thermal-control intent. The reactor mounts to the bus via Ti-6Al-4V standoffs, selected for their low thermal conductivity ($k = 7\,\mathrm{W\,m^{-1}\,K^{-1}}$) to thermally decouple the reactor from bus transients. This keeps the reactor heater authority focused on the payload rather than leaking into the bus, and is the reason the reactor can be held at setpoint independently of the cold bus. The reactor-to-PCM link is a bonded aluminium doubler, but its effective conductance is deliberately bottlenecked by the PCM's own internal conductivity ($k_{\mathrm{PCM}} = 0.21\,\mathrm{W\,m^{-1}\,K^{-1}}$), so the buffer charges and discharges on the PCM time constant rather than instantaneously. The bus-to-radiator link is the ammonia VCHP, modelled as a binary switch: $K_{\mathrm{VCHP}} \approx 0$ below the working-fluid saturation temperature and at full conductance above it (ASS-THER-08). This binary idealisation is a conservative simplification of the true behaviour, because it credits zero parasitic radiator loss when the pipe is locked out, which over-states the cold-case heater duty rather than under-stating it. The LMCOOL couples to the bus through the Peltier baseplate (ASS-THER-04).

Radiative couplings

The blanket is collapsed to a single effective radiative resistance,

$$Q_{\mathrm{MLI}} = \varepsilon^* \,\sigma\, A_{\mathrm{MLI}} \left(T_{\mathrm{inner}}^4 - T_\infty^4\right), \qquad \varepsilon^* = 0.0168,\ A_{\mathrm{MLI}} = 9.46\,\mathrm{m^2}, \tag{7.9}$$

with ε^* taken at the midpoint of the 0.01–0.05 range reported for a 15–20 layer blanket [141, 140]. Treating the blanket as one resistance is justified because, at $\varepsilon^* \sim 0.017$, the blanket is by design the least-conductive path in the model, so its internal layer-by-layer detail does not change the system heat balance. The radiator patch uses an OSR finish ($\varepsilon_{\mathrm{OSR}} = 0.80$, $\alpha_s = 0.10$) [141], chosen for its low solar absorptance so that the panel rejects internal dissipation without being overwhelmed by absorbed sunlight when sun-exposed:

$$Q_{\mathrm{rad}} = \varepsilon_{\mathrm{OSR}}\,\sigma\, A_{\mathrm{rad}} \left(T_{\mathrm{bus}}^4 - T_\infty^4\right). \tag{7.10}$$

The external environment is the solar flux at heliocentric distance r, $S(r) = 1361\,(1\,\mathrm{AU}/r)^2\,\mathrm{W\,m^{-2}}$, swept over the Itokawa transfer range $r = 0.953$–$1.695\,\mathrm{AU}$. Asteroid albedo and IR are neglected (**ASS-THER-07**): at the $\geq 1\,\mathrm{km}$ station-keeping distance they contribute under 1 % of the direct solar term, so the environment is fully described by the solar flux and the 4 K sink.

Governing equation, solution, and local conditioning
Each node obeys the energy balance

$$C_i \frac{\mathrm{d}T_i}{\mathrm{d}t} = Q_{\mathrm{env},i} + Q_{\mathrm{diss},i} + Q_{\mathrm{heater},i} + \sum_j K_{ij}\,(T_j - T_i) + \sum_j \sigma R_{ij}\,(T_j^4 - T_i^4), \tag{7.11}$$

which is the lumped-network form of [140]. Steady-state cases set the left side to zero and are solved by Newton–Raphson iteration on the nonlinear radiative terms, transients use `scipy.integrate.solve_ivp` with the RK45 integrator. The LMCOOL chip is trimmed by a thermoelectric cooler modelled as a controlled heat pump that lifts Q_{cold} from the chip at an electrical cost $W_{\mathrm{in}} = Q_{\mathrm{cold}}/\mathrm{COP}$, with COP $\approx$ 0.3–0.5 at ΔT = 5–15 K for a chip-scale device, so the full deposit to the bus is $Q_{\mathrm{bus}} = Q_{\mathrm{cold}} + W_{\mathrm{in}}$. The Peltier carries only the chip-local ±1 °C trim, hence, the bus-level balance is held by the VCHP and the Kapton heaters.

7.5.3. Mission Thermal Cases and Results

The case matrix brackets the worst conditions the TCS must survive and isolates each requirement-specific transient. Two opposing bounds size the architecture: the *hot case* (peak solar plus peak internal dissipation) fixes the radiator area, and the *cold case* (minimum solar, quiescent operation) fixes the heater duty. Because the entire Itokawa transfer environment is colder than every payload setpoint, the mission is fundamentally *cold-biased*: the design problem is heat retention and trim heating, with external rejection needed only at perihelion with the radiator sun-exposed. Two internal heat terms recur: the reactor's 76.5 W during bioleaching (Section 6.1, including pump, sensor, and mixing dissipation) and the ~100 W bus quiescent load—the always-on waste heat of avionics, transponder, and PCDU present in every powered mode, acting as free internal heating. The operational cold case credits this quiescent load; it vanishes only on total power loss, i.e. the safe-mode coast-down of Case 6, where the heaters are unpowered regardless.

Table 7.33: Thermal case matrix. Each case isolates one driver; the hot and cold cases bound the architecture and the remainder verify individual requirements.

Case	Phase	Drives	Setup	Heaters
1	Sweep 0.953–1.695 AU	Need for heating	Bus floats freely: only the always-on 100 W quiescent electronics load plus minimum solar, no heaters	off
2	Perihelion 0.953 AU	Radiator area	Peak 220 W dissipation, bioleaching active, largest (8.32 m^2) face to the Sun, OSR radiator sun-exposed	off
3	Aphelion 1.695 AU	Heater duty	Hold 25 °C, VCHP in cold-lockout (radiator decoupled), 100 W quiescent credited, smallest (3.38 m^2) sunlit face	on
4	Outbound P1–P4 / return P6	Storage hold	Culture held 4–10 °C (mid 7 °C), pumps off, VCHP locked	trim
5	Aphelion, safe mode	Survival time	Total power loss: radiative coast-down to the 0 °C floor	none
6	Bioleaching P5	PCM buffer adequacy	Time-domain absorption of the LMCOOL TEC duty-cycle heat spike	—
7	Cruise P1–P4 / P6	EP waste heat	EP firing on/off: PPU/RFG on a dedicated radiator, head self-radiating, parasitic head leak to the bus	trim

Case 1 – heliocentric sweep, free-float. With heaters off and only the quiescent dissipation (Q_{diss} = 100 W) plus minimum solar input, the bus free-floats to −19.7 °C at 1.695 AU, from the balance $Q_{\mathrm{diss}} + Q_{\mathrm{solar}}$ = 130.8 W against $(\varepsilon A)_{\mathrm{eff}}\,\sigma\,T^4$. This is the key structural result: the quiescent load alone holds the bus ~ 55 K warmer than the bare-environment equilibrium (~ −75 °C, no internal heat), but it still sits 45 K below the bioleaching setpoint and 20 K below the battery charge floor. Active heating is therefore mandatory in every operational mode, which is the quantitative argument that eliminates any all-passive architecture and forces the hybrid class.

Case 2 – hot case, 0.953 AU. At peak dissipation (Q_{diss} = 280 W, bioleaching active) and S = 1498.6 W m^{-2}, with the OSR radiator sun-exposed, the bus would free-float to 68.3 °C, well above the 30 °C upper bioleaching limit, so the radiator must be enlarged to reject the internal load. The net load the radiator must carry to

hold $T_{\text{bus}} = 30\,^{\circ}\text{C}$ is the peak dissipation plus the absorbed solar on the worst-case sunlit face (the largest, $A_{\max} = 3.2 \times 2.6 = 8.32\,\text{m}^2$), less what the blanket re-emits at 30 °C,

$$Q_{\text{reject}} = Q_{\text{diss}} + \alpha_{\text{bus}}\, S(0.953)\, A_{\max} - \varepsilon^{*}\sigma A_{\text{MLI}}\left(T_{\text{bus}}^4 - T_{\infty}^4\right) = 200 + 155.9 - 76.1 = 279.7 \approx 280\ \text{W}, \tag{7.12}$$

where using the largest face is the hot-case-worst attitude, in contrast to the smallest face used for the cold case of Eq. (7.16). That asymmetry is why the two solar terms differ. The required area follows from the OSR balance, the emitted flux less the absorbed solar at exposure fraction f,

$$A_{\text{rad}}(f) = \frac{Q_{\text{reject}}}{\varepsilon_{\text{OSR}}\,\sigma\left(T_{\text{rad}}^4 - T_{\infty}^4\right) - \alpha_{s,\text{OSR}}\, S(0.953)\, f}, \qquad T_{\text{rad}} = 303.15\ \text{K}, \tag{7.13}$$

in which the OSR emits $\varepsilon_{\text{OSR}}\sigma(T_{\text{rad}}^4 - T_{\infty}^4) = 383\,\text{W m}^{-2}$ and absorbs at most $\alpha_{s,\text{OSR}} S = 150\,\text{W m}^{-2}$ when fully sun-lit [141]. The area is therefore dominated by the radiator's own solar exposure, not by the heat to be rejected: a fully sun-exposed OSR ($f = 1$) needs $A_{\text{rad}} = 280/(383 - 150) = 1.20\,\text{m}^2$, whereas an edge-on or shaded OSR ($f = 0$) needs only $280/383 = 0.73\,\text{m}^2$. The adopted nominal is $\approx 0.9\,\text{m}^2$, consistent with partial exposure. This is the single largest open thermal-sizing parameter, and it is not locked because it depends on the attitude profile.

Case 3 – cold case, 1.695 AU, VCHP locked. This case sets the survival heater budget and is derived below. The effective radiative loss coefficient combines the blanket and the OSR patch,

$$(\varepsilon A)_{\text{eff}} = \varepsilon^{*} A_{\text{MLI}} + \varepsilon_{\text{OSR}} A_{\text{rad}} = 0.0168 \times 31.2 + 0.80 \times 0.50 = 0.159 + 0.400 = 0.924\ \text{m}^2, \tag{7.14}$$

where the result is dominated not by the $31.2\,\text{m}^2$ blanket but by the small OSR patch: at $\varepsilon_{\text{OSR}} = 0.80$ a $0.5\,\text{m}^2$ radiator contributes $0.40\,\text{m}^2$ of εA, compared to $0.52\,\text{m}^2$ of the entire blanket. The cold-case loss at the 25 °C setpoint and the cold-case solar input on the smallest sun-facing area are

$$Q_{\text{out}}(25\,^{\circ}\text{C}) = (\varepsilon A)_{\text{eff}}\,\sigma\left(T_{\text{set}}^4 - T_{\infty}^4\right) = 0.559 \times 5.6704 \times 10^{-8} \times \left(298.15^4 - 4^4\right) = 250.4\ \text{W}, \tag{7.15}$$

$$Q_{\text{solar}} = \alpha_s\, \tfrac{1361}{1.695^2}\, A_{\text{proj}} = 0.05 \times 473.7 \times 1.3 = 30.8\ \text{W}. \tag{7.16}$$

The cold-case heater duty to hold the setpoint then credits the always-present quiescent dissipation,

$$Q_{\text{heater}} = Q_{\text{out}} - Q_{\text{diss}} - Q_{\text{solar}} = 250.4 - 100 - 30.8 = 119.7 \approx 120\ \text{W}, \tag{7.17}$$

where the solar input of Eq. (7.16) is evaluated on the smallest sun-facing area (the $1.3 \times 2.6\,\text{m}$ face), the cold-case-worst attitude. The lumped network solved at steady state returns 119.65 W, agreeing with Eq. (7.17) to within 0.01 %, which confirms the implementation reproduces the single-resistance physics. The 120 W duty is the value carried into the EPS heater allocation. This supersedes the Midterm 75 W.

Case 4 – transit and return storage. On the outbound leg (P1–P4) the lyophilised conidia are held in the 4–10 °C heritage cold-storage band [3]. With the VCHP in cold-lockout, the wrap and the isolating standoffs keep the reactor cold-coupled to the floating bus, so holding the culture at the 7 °C midpoint needs only between +5.0 W (perihelion) and +8.5 W (aphelion) of trim heat across the whole transfer, with no active cooling required at any point. On the return cruise (P6) no biological material crosses the Category V containment boundary, so the only payload-side limit is the 0 °C battery charge floor. Because that floor is already enclosed by the 4–10 °C outbound hold already demonstrated above, the return leg is non-binding and requires no separate analysis.

Case 5 – safe-mode survival. With heater authority lost at aphelion, the reactor coasts down radiatively with linearised time constant $\tau = C_{\text{reactor}}/\left(4\,\varepsilon\, A_{\text{wrap}}\,\sigma\, T_{\text{set}}^3 + K_{\text{mount}}\right)$. The capacitance is set by the reactor wet mass, carried as a 40 kg nominal / 100 kg pessimistic bracket ($C_{\text{reactor}} = 173$–$424\,\text{kJ K}^{-1}$, dominated by the aqueous medium), giving $\tau = 165$–$405\,\text{h}$. The fall from the 25 °C setpoint to the 0 °C no-freeze floor then takes $\approx 48\,\text{h}$ (40 kg) to $\approx 117\,\text{h}$ (100 kg), scaling linearly with wet mass, which is the ground-recovery window before the freeze limit is threatened.

Case 6 – PCM transient buffer. Distinct from the steady spatial-uniformity check of Case 5, this case is a time-domain one. The 0.3 kg n-heptadecane charge ($T_m = 22.3\,^{\circ}\text{C}$, $L_f = 213\,\text{kJ kg}^{-1}$ [142]) stores $Q_{\text{buffer}} = 63.9\,\text{kJ} \approx 17.8\,\text{Wh}$ of latent capacity. Against the peak LMCOOL TEC duty-cycle mismatch of $\sim 36\,\text{W}$ it buffers for $63\,900/36 = 1775\,\text{s} \approx 30\,\text{min}$, which comfortably exceeds the proportional heater control-loop response time. The PCM therefore absorbs short metabolic and TEC transients at the 22 °C melt point without the heaters chattering, rather than carrying any steady-state load.

Case 7 – powered cruise, EP firing. On the cruise legs (P1–P4 outbound, P6 return) the RIT 2X fires intermittently, so the TCS must be robust to the engine being both on and off. At the 4 kW operating point the thruster assembly is ≈ 65 % efficient, meaning: ≈ 2.6 kW leaves as beam power, the hot grid/head (~ 275 °C) radiates its ~ 1.3 kW directly to space from its own external surface, and the PPU and RFG dissipate ≈ 471 W of bus-side electrical waste heat (the $\eta_{\mathrm{PPU}}/\eta_{\mathrm{RFG}}$ split is an engineering assumption pending vendor data). This 471 W is rejected by a dedicated OSR radiator, decoupled from the reactor zone, sized from Eq. (7.13) at $A_{\mathrm{EP}} = 1.08\,\mathrm{m}^2$ for a 45 °C baseplate at perihelion. With the PPU/RFG decoupled and the head self-radiating, the only EP-to-reactor coupling is the parasitic conduction down the head's isolating mount, ≈ 46–55 W. During the cruise storage state, the VCHP is in cold-lockout, so this leak warms the bus enough to flip the reactor from needing +5 to +8.5 W of trim heat (engine off) to needing active cooling (engine on). The VCHP must therefore modulate open while the engine fires, or the head-mount conductance must be tightened. Outside this parasitic term the reactor setpoint is insensitive to engine state, which is the reason the PPU/RFG are carried on their own panel.

7.5.4. Thermal Architecture Layout

The physical layout follows three placement rules: isolate the reactor from both the cold bus and every internal heat source, keep the two warm radiators and the single cold radiator on independent, non-sun-facing surfaces so none cross-couples, and cluster the warm dissipators so their quiescent waste heat is banked rather than lost. The resulting guidelines for the architecture are as follows.

- **Reactor (centre, isolated).** The reactor is mounted on the shaded interior panel via four low-conductivity Ti-6Al-4V standoffs and is fully MLI-wrapped, so its heater authority stays focused on the payload rather than leaking into the bus. The 0.3 kg PCM doubler is bonded directly to the reactor wall, and the ≥ 3 Kapton heater zones are distributed over the reactor exterior.
- **Reactor OSR radiator (anti-Sun face, short VCHP run).** The reactor radiator sits on an external anti-Sun face and is connected to the reactor zone by the ammonia VCHP over the shortest practical line length. This is the only reactor-to-space path when the VCHP is open, and it is cold-locked for storage and cold cruise.
- **EP electronics and their radiator (separate face).** The PPU and RFG are co-located on a different face with their own dedicated 1.08 m^2 OSR radiator, sharing no heat-pipe with the reactor zone, so the reactor never sees the ~ 471 W EP bus load.
- **EP thruster head (external).** The head is gimballed externally and radiates its ~ 1.3 kW to space on its own high-emittance surface, mounted on a deliberately low-conductance standoff so the ~ 275 °C head barely touches the bus. Furthermore, it is placed away from both the reactor zone and the VNIRS radiator.
- **VNIRS cold radiator (anti-Sun, external, decoupled).** The 188 K detector is carried on its own 176 cm^2 radiator on an anti-Sun face with a clear deep-space view, thermally decoupled from every warm node because it operates in the opposite regime.
- **Warm cluster (battery + avionics).** The battery and the avionics/SSR box are grouped on the warm interior, off the cold walls, so the quiescent dissipation that holds the bus ~ 55 K above the environment equilibrium is deposited where it is needed. Moreover, the battery sits next to the avionics to employ its waste heat against the 0 °C charge floor.
- **HMS (local).** The HMS chip-scale TEC and its cold plate are mounted locally and couple to the bus only through the Peltier baseplate, carrying the chip ±1 °C trim without adding to the bus balance.

The two warm radiators (reactor OSR, EP OSR) are on different faces, and the cold VNIRS radiator on a third, all anti-Sun, so radiator exposure is set by attitude alone. Finally, the MLI blanket is continuous around the whole bus with cut-outs only for the three radiators and the head mount.

7.5.5. TCS Design Summary

The architecture and its primary parameters are locked: the T-2 VCHP-hybrid configuration, the bus envelope, $A_{\mathrm{MLI}} = 9.46\,\mathrm{m}^2$, the cold-case heater duty, the radiator-sizing method, and the 0.3 kg PCM charge. Table 7.34 summarises the as-sized TCS. The cold-case duty is verified by the closed-form energy balance and the steady-state node agreeing to 0.01 %; this is a consistency check on the implementation rather than independent validation, because both apply the same single-resistance physics. Genuine independent verification requires the transient run with modulating VCHP conductance and resolved reactor capacitances, which is the principal open analysis.

Table 7.34: TCS final sizing summary.

Parameter	Value	Tag	Basis
MLI blanket area	31.2 m^2	bus $3.2 \times 2.6 \times 1.3$ m	
Kapton heater zones	≥ 3	Reactor zoning, Case 5	
MLI blanket mass	$\approx$9.4 kg	0.3 kg $m^{-2} \times 31.2$ m^2	
TCS total mass	25.6 kg	Per component sum	
Max heater duty	120 W	Case 3	
TCS total volume	30 L	Per component sum	
Cost	2.0–3.0 M€	Heritage-bracketed	

Forward work for CDR. The following must close before the design is frozen, in rough order of impact:

- **Hot-case worst stack.** Confirm whether the TWTA transmit window coincides with proximity operations, which sets the peak dissipation feeding Case 2.
- **Independent verification.** Run the transient TMM with modulating VCHP conductance and the resolved reactor capacitances; report the cold-case duty and hot-case area, and state the discrepancy.
- **EP head isolation.** The head-to-bus mount conductance $K_{\text{thr,bus}}$ sets the 46–55 W parasitic leak that drives the Case 8 powered-cruise behaviour; it is the dominant powered-cruise configuration uncertainty and decides whether the VCHP must modulate during firing.

7.6. Attitude Determination and Control System (ADCS)

The ADCS subsystem is treated at spacecraft level, covering attitude determination, three-axis attitude control, and the Guidance, Navigation and Control (GNC) sensing required for asteroid-relative proximity operations. The Chemical/RCS thrusters are treated as a shared control-actuator interface rather than as ADCS-owned hardware: the ADCS defines the disturbance-rejection, wheel-desaturation, proximity-control and sampling-support functions that the thrusters must provide, while their hardware, propellant and feed system are sized in Section 7.4.3.

The section is organised as follows. Table 7.35 and Table 7.36 first set out the governing assumptions and the top-level and derived requirements. The attitude-determination and relative-navigation suite is then selected to meet the pointing-knowledge, ranging and proximity-navigation requirements, followed by the reaction-wheel configuration sized for nominal three-axis control with single-wheel-failure tolerance. The disturbance environment and proximity-control drivers are derived next and passed to the Chemical/RCS propellant sizing in Section 7.4.3. The pointing budget then closes the proximity pointing-control requirement, after which the stability and control characteristics are consolidated. The section ends with the ADCS power-state interface to the system-level power budget and a summary of the ADCS hardware budget including forward work.

7.6.1. Assumptions and Requirements

The assumptions driving the design of the ADCS subsystem are gathered in Table 7.35:

Table 7.35: Consolidated Design Assumptions for the ADCS Subsystem.

Assumption ID	Description
ASS-ADCS-01	The Solar Radiation Pressure (SRP) is assumed to act on the spacecraft at a distance of 1 AU during cruise as a conservative assumption.
ASS-ADCS-02	During the stay at the asteroid, SRP is assumed to act at 0.95 AU, consistent with the worst-case perihelion distance of the Itokawa orbit.
ASS-ADCS-03	A representative post-departure spacecraft mass of 1119.7 kg (Section 7.4.3) is used for disturbance-acceleration and proximity-control estimates. Propellant masses are computed in the Chemical/RCS section.
ASS-ADCS-04	The control modes Orbit Insertion, Acquisition and Safe Mode are not considered in this analysis.
ASS-ADCS-05	The largest face of the spacecraft is assumed to be constantly facing the Sun.
ASS-ADCS-06	An effective CoP–CoM offset of 0.2 m is assumed for the SRP torque calculation.
ASS-ADCS-07	The gravitational disturbance is neglected for station-keeping at $r \geq 6$ km, where SRP dominates and partially opposes it; it is retained for close inspection at $r = 500$ m.

Continued on next page...

Table 7.35 Continued from previous page

Assumption ID	Description
ASS-ADCS-08	The Earth-departure burn is not analysed in the ADCS section. Its thrust-vector alignment is treated only as an ADCS/Chemical-RCS interface constraint, while burn sizing is closed in the Chemical/RCS and astrodynamics sections.
ASS-ADCS-09	The PALT and TRIS/LRF-type LiDAR ranging sensors are treated as ADCS/GNC hardware. PALT provides kilometre-scale approach and proximity altimetry, while TRIS/LRF provides short-range terminal descent and TAG altitude information. Their mass, power and volume are therefore included in the ADCS budget rather than in the remote sensing suite.

The requirements driving the ADCS design are stated in Table 7.36; combining both top-level requirements and derived requirements from other subsystems.

Table 7.36: Synthesis of Top-Level and Derived ADCS Requirements.

Requirement ID	Requirement	Rationale & Verification
Part I: Top-Level ADCS Requirements		
REQ-ADCS-01	The ADCS shall provide an RCS ΔV capability of at least **600** m/s.	Bounds the total RCS velocity budget for proximity operations and mission manoeuvres; closed against the propellant budget in §7.6.
REQ-ADCS-02	The ADCS shall provide **three-axis** attitude control.	Met by four W18 reaction wheels in a skewed pyramid, providing three-axis authority with single-wheel-failure tolerance.
REQ-ADCS-03	The ADCS shall maintain the main-engine thrust vector **through the spacecraft centre of mass** during the main chemical burn.	RCS thruster layout positioned so the main chemical burn produces no net disturbance torque about the centre of mass.
Part II: Derived ADCS Requirements		
REQ-ADCS-DER-01	During Phase 4 (proximity operations), the ADCS shall provide a pointing control accuracy of $\leq$ **0.008**° per axis.	Proximity-operations control accuracy; closed via GN&C loop simulation in the proximity environment.
REQ-ADCS-DER-02	During Phase 4, the ADCS shall reconstruct the spacecraft attitude (pointing knowledge) to within $\leq$ **0.005**°.	Bus attitude reconstruction; met by three ASTRO APS star trackers ($\leq 9.4''$ RSS) with IMU bridging.
REQ-ADCS-DER-03	During Phase 4, the ADCS shall limit pointing jitter to $\leq$ **0.004**°/s.	Remote-sensing pointing stability under proximity disturbances; verified by control-jitter simulation.
REQ-ADCS-DER-04	The ADCS shall spin up the SRC to **15** RPM prior to atmospheric entry.	Provides gyroscopic stiffness to the SRC during the rarefied-flow entry transit; verified by analysis and test (§6.5).
REQ-ADCS-DER-05	The ADCS shall maintain solar-array pointing within **10**° of the Sun line during all cruise and thrust modes.	Maintains array power generation during all cruise and thrust modes.

7.6.2. Attitude Determination Configuration

REQ-ADCS-DER-02 requires bus pointing knowledge within 0.005° ($\approx$ 18 arcsec). To satisfy this, attitude determination instruments must be selected that hold this knowledge under the operational conditions near the asteroid and provide redundancy in the case one sensor fails.

Sensor roles

An 18 arcsec floor cannot be met by coarse Sun sensors ($\sim$ 0.1–1°) or by IMU propagation alone, so star trackers are retained as the primary absolute reference. The ASTRO APS [139] delivers $<$ 1 arcsec random error cross-boresight and $<$ 8 arcsec about the boresight, with $<$ 5 arcsec bias on all axes; a single head therefore meets 18 arcsec on every axis, with the worst-case roll axis at $\sqrt{8^2 + 5^2} \approx 9.4$ arcsec (1σ RSS), leaving healthy margin. The IMU (Astrix NS fibre-optic gyro [143]) provides high-rate attitude propagation between star-tracker updates and through slews and short occultations; with bias stability of 0.005°/h and ARW $< 0.0025°/\sqrt{\text{h}}$, its drift over a $\sim$ 60 s bridging interval is of order 1 arcsec, small against the budget. The six coarse Sun sensors

[144] are retained for Sun acquisition, coarse attitude, and safe-mode recovery, outside the precision chain. The PALT and TRIS LiDAR/ranging sensors are added to the ADCS/GNC sensor suite to provide asteroid-relative range and altitude information during approach, proximity operations and terminal sampling.

Head count
Two requirements drive the star-tracker count from two to three. First, REQ-ADCS-DER-02 must hold after a single sensor failure (selected redundancy philosophy): a third head ensures at least two compliant star trackers remain after any single failure. Second, the ASTRO APS Sun exclusion (26° half-cone) and Earth exclusion (~ 20°) mean individual heads are intermittently blinded during proximity operations, as Itokawa and the Sun intrude on individual fields of view; three mutually separated boresights ensure at least two unobstructed heads at all proximity attitudes. A single three-head configuration therefore satisfies both the single-fault-tolerance and the occultation-clearance requirements. When fewer than two heads have a valid solution, the IMU bridges the gap, while the remote-sensing cameras and the ADCS/GNC LiDAR sensors provide asteroid-relative navigation support through landmark tracking and direct ranging.

Compliance and budget impact
The selected suite — three ASTRO APS star trackers in a separated-boresight triad, two Astrix NS fibre-optic IMUs, six Bradford coarse Sun sensors, and a PALT/TRIS LiDAR ranging set, augmented by remote-sensing camera products during proximity operations — meets **REQ-ADCS-DER-02** with single-fault tolerance and is robust to asteroid/Sun occultation. The worst-case roll axis holds $\leq 9.4''$ ($\approx 0.0026°$) RSS knowledge against the 0.005° (18″) requirement, leaving ~1.9× margin. Summing the unit budgets (Table 7.37) gives an attitude-determination and relative-navigation-suite total of ~ 13.7 kg, ~ 60 W, and ~ 24.9 L. Relative to the previous ADCS-only sensing baseline, the transfer of the PALT/TRIS LiDAR ranging set from the remote sensing suite accounts for +2.5 kg, +18 W, and +1.8 L. These values propagate into the ADCS subsystem totals.

Table 7.37: Final ADCS attitude determination and relative-navigation suite and unit budget totals.

Component	Qty	M [kg]	P [W]	V [L]	Selection / key spec
Star tracker (ASTRO APS) [139]	3	6.0	18.0	16.9	$< 9.4''$ (1σ RSS) all axes; 26° Sun, ~ 20° Earth exclusion
IMU (Astrix NS) [143]	2	3.9	24.0	4.0	FOG; bias 0.005°/h, ARW $< 0.0025°/\sqrt{\text{h}}$
Coarse Sun sensor (Bradford) [144]	6	1.3	0.0	2.2	±1.5° (3σ) boresight; passive, self-redundant
LiDAR ranging set (PALT + TRIS/LRF)	2	2.5	18.0	1.8	PALT for approach/proximity altimetry; TRIS/LRF for terminal TAG ranging.
Optical navigation imaging interface	–	–	–	–	Remote-sensing cameras provide image products for landmark tracking by interface
Total		**13.7**	**60.0**	**24.9**	

LiDAR Relative-Navigation Sensors

The PALT and TRIS LiDAR/ranging sensors are included in the ADCS/GNC sensor suite rather than in the remote sensing suite, because their primary function is navigation and control rather than science characterisation. The remote sensing suite may use the resulting range and altimetry products for topographic scaling and shape-model support, but the sensors themselves are operated as part of the asteroid-relative navigation loop.

The baseline is a two-range-band architecture. The PALT unit acts as the approach and proximity altimeter. It is used during the approach from the Home Position, during the global characterisation phase around 6 km, and during descent toward the siting altitude around 500 m. Its role is to provide direct line-of-sight range measurements to the asteroid surface, supporting station-keeping, altitude knowledge and topographic scale calibration. This is consistent with the Hera Planetary Altimeter concept, where PALT is described as a compact LiDAR used for surface altimetry and close-range asteroid operations [86].

At lower altitude, the terminal TRIS/LRF-type sensor provides short-range altitude information for close inspection and TAG. It is therefore active during the 500 m inspection phase, descent below the main altimeter operating envelope, and the final sampling sequence. This follows the Hayabusa2 guidance approach, where LiDAR and laser range finder altitude information are used during autonomous descent and touchdown operations [145, 13]. The exact hand-over altitude between PALT and TRIS is left to later GNC design, but the preliminary architecture assumes PALT covers kilometre-scale approach and proximity operations, while TRIS/LRF covers terminal descent and sampling.

The LiDAR sensors therefore provide range and altitude observables to the GNC filter, while the remote-sensing cameras provide image products for landmark tracking and surface-feature navigation. The two data

types are complementary: camera images constrain lateral position and surface feature motion, while LiDAR directly constrains range-to-surface.

7.6.3. Reaction Wheels

The Bradford W18-class reaction wheel [146] has been selected for the ADCS subsystem. Three wheels provide full three-axis control, satisfying **REQ-ADCS-02**; a fourth is added in a skewed pyramid configuration to provide single-wheel-failure redundancy. Each reaction wheel assembly (RWA) is driven by a wheel-drive electronics (WDE) channel; since the WDE is a two-channel unit, the four wheels are served by two WDE boxes. This gives a total reaction-wheel-set mass of 30.14 kg. The primary specifications of the W18 are listed in Table 7.38.

Table 7.38: Bradford W18 reaction wheel unit

Characteristic	W18
Momentum storage	18 Nms
Max. operational speed	4000 RPM
Max. gross torque	0.265 Nm
Torque loss at max. speed	0.037 Nm
Torque rise/fall time	80 ms
RWA mass (per wheel)	5.20 kg
2-channel WDE mass (per box)	4.67 kg
RWA dimensions	∅295 × 125 mm
WDE dimensions	258 × 181 × 143 mm
Peak power (max. torque & speed)	168 W
Steady-state power (max. speed)	29 W
Quiescent power	7.6 W
Data interface	MIL-STD-1553B / analogue

7.6.4. Disturbance and RCS Control Drivers

This section summarises the stability and control drivers relevant to the ADCS and Chemical/RCS interface. The disturbance, desaturation and proximity-control quantities derived in this section are passed to the Chemical/RCS sizing in Section 7.4.3.

Disturbance Environment

The main disturbances acting on the spacecraft are Solar Radiation Pressure (SRP) and, during close proximity operations, the asteroid gravity field. These disturbances induce unwanted rotations when their line of action is not aligned with the spacecraft centre of mass, and they also create translational station-keeping demands during asteroid operations.

The SRP force is calculated as [147]:

$$F_s = (1 + \rho)P_s S. \tag{7.18}$$

Here ρ is the reflectivity, P_s is the solar radiation pressure, and S is the exposed surface area. The bus reflectivity is taken as $\rho_{\text{bus}} = 0.88$, the solar array reflectivity as $\rho_{\text{SA}} = 0.3$, the largest bus face as $S_{\text{bus}} = 1.6\,\text{m}^2$, and the solar array area as $S_{\text{SA}} = 22.7\,\text{m}^2$. At 1 AU,

$$P_s = \frac{\Phi_0}{c} = \frac{1361}{2.998 \times 10^8} \approx 4.54 \times 10^{-6}\ \text{N/m}^2.$$

The resulting SRP disturbance force at 1 AU is

$$F_s = (1 + 0.88)(4.54 \times 10^{-6})(1.6) + (1 + 0.3)(4.54 \times 10^{-6})(22.7) \approx 1.48 \times 10^{-4}\ \text{N}.$$

Using an effective CoP–CoM offset of 0.2 m gives the conservative SRP torque

$$T_{\text{SRP,1 AU}} = 0.2 \cdot 1.476 \times 10^{-4} \approx 2.95 \times 10^{-5}\ \text{Nm}.$$

During the asteroid stay, the spacecraft is assumed to operate near Itokawa's perihelion distance of 0.95 AU, giving

$$T_{\mathrm{SRP},0.95\,\mathrm{AU}} \approx 3.25 \times 10^{-5}\ \mathrm{Nm}.$$

The accumulated wheel momentum follows from $\Delta H = Tt$:

$$\Delta H_{\mathrm{out}} = 2.95 \times 10^{-5} \cdot (350 \cdot 86400) \approx 892\,\mathrm{Nms}, \tag{7.19}$$

$$\Delta H_{\mathrm{stay}} = 3.25 \times 10^{-5} \cdot (436 \cdot 86400) \approx 1224\,\mathrm{Nms}, \tag{7.20}$$

$$\Delta H_{\mathrm{ret}} = 2.95 \times 10^{-5} \cdot (365 \cdot 86400) \approx 930\,\mathrm{Nms}. \tag{7.21}$$

The total momentum that must be unloaded over the mission is therefore

$$\Delta H_{\mathrm{tot}} = \Delta H_{\mathrm{out}} + \Delta H_{\mathrm{stay}} + \Delta H_{\mathrm{ret}} \approx 3047\,\mathrm{Nms}. \tag{7.22}$$

The same SRP environment also creates a translational station-keeping driver during the asteroid stay. At 0.95 AU, the SRP force is approximately $F_{\mathrm{SRP}} = 1.62 \times 10^{-4}$ N, giving

$$a_{\mathrm{SRP}} = \frac{F_{\mathrm{SRP}}}{m_0} = \frac{1.62 \times 10^{-4}}{1119.7} \approx 1.45 \times 10^{-7}\ \mathrm{m/s^2}.$$

Over the asteroid stay of $t_{\mathrm{stay}} = 436\,\mathrm{d}$, this corresponds to

$$\Delta V_{\mathrm{SRP}} = a_{\mathrm{SRP}} t_{\mathrm{stay}} \approx 5.45\,\mathrm{m/s}. \tag{7.23}$$

The gravity-gradient torque about a principal axis is estimated as [113]

$$T_g = \frac{3\mu}{2R^3} \left| I_{zz} - I_{yy} \right| \sin(2\theta). \tag{7.24}$$

The worst case occurs at $\theta = 45°$. With $\mu_{\mathrm{Itokawa}} \approx 2.34\,\mathrm{m^3/s^2}$ and $|I_{\max} - I_{\min}| = 2646\,\mathrm{kg\,m^2}$ Table 8.1, the gravity-gradient torque at $R = 6000\,\mathrm{m}$ becomes

$$T_{g,\max} = \frac{3 \cdot 2.34}{2 \cdot 6000^3} \cdot 2621 \approx 4.3 \times 10^{-8}\ \mathrm{Nm}.$$

This is roughly 0.1% of the SRP disturbance torque during proximity operations and is therefore neglected for the 6 km mapping campaign. At the 500 m inspection range it rises to approximately 7.4×10^{-5} Nm, comparable to and locally exceeding the SRP torque; however, over the short 150 h inspection the accumulated momentum (~40 Nms) remains bounded and is absorbed within the wheel and desaturation budget.

Proximity-Control Drivers

Several proximity-operation activities require translational Chemical/RCS capability. These values are reported here as control drivers only; the corresponding propellant mass is computed in Section 7.4.3.

During global mapping at $r = 6\,\mathrm{km}$, the spacecraft translates between latitude stations as described in Section 4.4.4. The chord length between two consecutive stations is

$$d = 2r \sin\left(\frac{\theta}{2}\right) = 2 \cdot 6000 \sin(15°) \approx 3106\,\mathrm{m}.$$

The total transfer time allocated to the six hops is 504 h, giving $t_{\mathrm{hop}} = 84\,\mathrm{h}$ per transfer. Since each hop is modelled as an accelerate–coast–decelerate transfer, the cruise speed is

$$v_{\mathrm{hop}} = \frac{d}{t_{\mathrm{hop}}} \approx 1.03\,\mathrm{cm/s}.$$

Each hop therefore costs $\Delta V_{\mathrm{hop}} = 2v_{\mathrm{hop}}$, and the total mapping manoeuvre driver is

$$\Delta V_{\mathrm{map}} = 2N_{\mathrm{hop}} v_{\mathrm{hop}} \approx 0.12\,\mathrm{m/s}. \tag{7.25}$$

A closer inspection phase is performed at $r = 500\,\mathrm{m}$ for a total of $t = 150\,\mathrm{h}$. At this range, the local gravitational acceleration is

$$a_{\mathrm{grav}} = \frac{\mu}{r^2} \approx 9.37 \times 10^{-6}\ \mathrm{m/s^2}.$$

For a conservative body-fixed hover estimate, this gives

$$\Delta V_{\text{inspect}} = a_{\text{grav}} t \approx 5.06\,\text{m/s}. \tag{7.26}$$

For the touch-and-go sampling manoeuvre, each acquisition is assumed to cost $\Delta V \approx 0.68\,\text{m/s}$ [115]. With six acquisition attempts sized for the campaign, the sampling driver is

$$\Delta V_{\text{TAG}} = N_{\text{TAG}} \Delta V = 6 \times 0.68 = 4.08\,\text{m/s}. \tag{7.27}$$

ADCS and GNC Inputs to Chemical/RCS Sizing

The resulting ADCS and GNC drivers imported by the Chemical/RCS propulsion section are summarised in Table 7.39.

Table 7.39: ADCS and GNC drivers imported by the Chemical/RCS propellant sizing. Propellant masses are computed in Section 7.4.3.

Category	Contribution	Sizing basis
Disturbances	Reaction-wheel desaturation over cruise, stay and return	$\Delta H = 3047\,\text{Nms}$
	SRP translational station-keeping during asteroid stay	$\Delta V = 5.45\,\text{m/s}$
Operations	Mapping manoeuvre at 6 km, six hops	$\Delta V = 0.12\,\text{m/s}$
	Close inspection at 500 m, gravity-hover estimate	$\Delta V = 5.06\,\text{m/s}$
	Touch-and-go sampling support, six attempts	$\Delta V = 4.08\,\text{m/s}$

Chemical/RCS Interface Compliance

The quantities in Table 7.39 form the ADCS and GNC input to the Chemical/RCS propulsion design. They define the disturbance rejection, wheel unloading and proximity-control functions that the Chemical/RCS system must support, while the corresponding thruster hardware, propellant mass, tank volume and feed system are closed in Section 7.4.3. The total RCS velocity budget (**REQ-ADCS-01**, $\Delta V \geq 600\,\text{m/s}$) is likewise closed there, dominated by the 366 m/s Earth-departure burn and supplemented by trajectory-correction manoeuvres, the post-SRC deflection manoeuvre, and the proximity and desaturation drivers in Table 7.39.

The selected Chemical/RCS configuration satisfies these ADCS-driven functions through the fourteen-thruster layout described in Section 7.4.3. The two opposite axial thrusters and eight canted lateral thrusters provide the translational and rotational authority required for proximity operations, reaction-wheel desaturation, sampling support and contingency manoeuvres. In particular, the lateral canted pairs allow paired firings for mainly translational control and differential firings for attitude-control torques.

From the ADCS perspective, the Chemical/RCS subsystem is therefore treated as a control-actuator interface rather than as ADCS-owned hardware.

7.6.5. Pointing Budget

REQ-ADCS-DER-01 asks for pointing control within 0.008° (28.8″) about each axis during proximity operations (Phase 4) 4.1. Where the spacecraft actually points is the sum of three things: how well it knows its own attitude (the star-tracker solution), how much that estimate drifts while the gyros propagate between star-tracker updates, and how tightly the control loop holds the body on the commanded attitude against disturbances. The first two are the determination performance; the third is the control loop.

The term that has to be derived is the control-loop tracking error: how far the body sags off the commanded attitude under a steady disturbance torque. The reaction-wheel loop can be modelled as a torsional spring. A proportional controller pushes back with a restoring torque proportional to the pointing error, so under a constant disturbance the body settles at a small fixed offset, just as a spring stretches to a fixed length under a constant load. The stiffness of that spring is $K_p = I\,\omega_c^2$, with I the axis inertia and ω_c the control bandwidth, and the steady-state offset is simply the disturbance torque divided by that stiffness:

$$\theta_c = \frac{T_d}{K_p} = \frac{T_d}{I\,\omega_c^2}.$$

Every input is taken at its worst case. The inertia is the smallest principal value, $I_{\min} = 1444\,\text{kg m}^2$ Table 8.1, because the softest axis sags the most. The disturbance is the worst sustained proximity torque, the SRP torque $T_d = 3.25 \times 10^{-5}\,\text{Nm}$. The bandwidth is a deliberately low $\omega_c = 0.05\,\text{Hz}$. This gives

$$\theta_c = \frac{3.25 \times 10^{-5}}{1444\,(2\pi \cdot 0.05)^2} \approx 2.3 \times 10^{-7}\ \text{rad} \approx 0.05''.$$

The bandwidth is kept low on purpose: it must stay below the lowest structural mode of the deployed solar array so the controller does not excite the flexible structure, and it sits comfortably within what the W18 wheels can deliver given their 80 ms torque rise/fall time stated in Table 7.38.

The practical consequence is that the pointing error is set almost entirely by how well the star trackers know the attitude, not by the control loop. Combining the three independent terms as a root-sum-square gives the budget in Table 7.40.

Table 7.40: Phase 4 absolute pointing-control budget (per axis, worst case, 1σ).

Contributor	1σ [″]	Basis
Attitude knowledge (star-tracker triad)	9.4	RSS of 8″ about-boresight and 5″ bias [139].
Inertial propagation between updates	1.0	Astrix NS ARW over a ~ 60 s bridging interval [143].
Control-loop tracking error	0.05	$T_{\mathrm{SRP}}/(I_{\min}\omega_c^2)$; Table 8.1 inertia.
RSS total (1σ)	**9.5**	$\approx 0.0026°$
Requirement (REQ-ADCS-DER-01)	**28.8**	$0.008°$ per axis
Margin	**3.0×**	Compliant.

The total comes to $\approx 9.5''$ ($0.0026°$), meeting REQ-ADCS-DER-01 with about 3× margin. The driver is the star-tracker knowledge term; the control loop and gyro propagation are small by comparison. The fast, time-varying part of the wheel-induced error is a rate rather than a static offset, so it is handled separately as control jitter against REQ-ADCS-DER-03.

7.6.6. Stability and Control Characteristics

The final stability and control characteristics of the spacecraft are summarised in Table 7.41. These values combine the selected ADCS hardware with the Chemical/RCS actuator interface and the disturbance analysis above.

Table 7.41: Preliminary stability and control characteristics of the spacecraft.

Characteristic	Current value / treatment	Design implication
Attitude knowledge	$0.005°$ requirement; met by three star trackers with IMU bridging	Supports remote sensing and proximity navigation.
Asteroid-relative ranging	PALT for approach/proximity altimetry; TRIS/LRF for terminal descent and TAG	Provides range observables for GNC and may support topographic scaling by interface to the remote sensing suite.
Nominal attitude control	Four W18 reaction wheels in skewed pyramid	Provides three-axis control with single-wheel-failure tolerance.
Wheel torque	0.265 Nm gross torque per W18 wheel	Sufficient margin over environmental disturbance torques.
Momentum storage	18 Nms per wheel	Requires periodic unloading over long cruise and asteroid-stay phases.
Dominant disturbance torque	SRP torque of order 3×10^{-5} Nm	Drives wheel desaturation requirement.
Gravity-gradient torque	Negligible at 6 km; small at 500 m	Not a dominant sizing driver compared with SRP.
RCS control force / torque	22 N per thruster; couple ≈ 22 Nm at $\ell_{\mathrm{eff}} = 0.5$ m	Far exceeds the 0.265 Nm wheel torque and $\sim 3 \times 10^{-5}$ Nm disturbance; provides wheel unloading, proximity control, sampling support and abort authority.
Control allocation	Not yet closed	Requires full 6-DOF allocation matrix with final CoM and thruster geometry.

Continued on next page...

Table 7.41 Continued from previous page

Characteristic	Current value / treatment	Design implication
CoM / thrust-vector limit	CoG offset ≤ 57 mm Table 8.1; residual main-burn torque trimmed by RCS	Bounded offset within RCS trim authority; closes **REQ-ADCS-03**.

7.6.7. ADCS Power-State Budget Interface

For the system-level power budget, the detailed ADCS hardware is reduced to four representative power states. The Chemical/RCS thruster hardware is sized in Section 7.4.3, but one RCS-ready power state is retained here because ADCS-controlled manoeuvres require thruster thermal readiness. The PALT/TRIS LiDAR ranging set is included only in proximity-navigation and RCS-active states.

Table 7.42: ADCS power states.

ADCS power state	Power build-up	Power [W]	Used in global modes
Safe pointing	24.0 W IMUs + 4 × 7.6 W reaction wheels in quiescent mode	54.4	Safe
Nominal pointing	42.0 W attitude-determination suite excluding LiDAR + 4 × 29.0 W reaction wheels in steady-state operation.	158.0	Cruise/Thrust, Standby, Sensing, Comms, Bioprocessing
Proximity navigation and ranging	158.0 W nominal pointing + 18.0 W PALT/TRIS LiDAR ranging set.	176.0	Sensing, Sampling, Manoeuvre
RCS-active control	158.0 W nominal pointing + 18.0 W PALT/TRIS LiDAR ranging set + 4×50.0 W RCS thruster reactor pre-heating.	376.0	Sampling, Manoeuvre

The values in Table 7.42 are direct sums of listed component powers plus one explicit RCS thermal-readiness assumption. If the propulsion design later confirms that fewer or more thrusters must be pre-heated simultaneously, only the RCS-active state should be updated.

7.6.8. ADCS Summary

The selected ADCS architecture combines three star trackers, two inertial measurement units, six coarse Sun sensors, a PALT/TRIS-LRF LiDAR ranging set, and four W18 reaction wheels in a skewed pyramid configuration. This provides the required attitude knowledge for remote-sensing operations, kilometre-scale PALT ranging for approach and proximity operations, terminal TRIS/LRF ranging for TAG, safe-mode Sun acquisition, and nominal three-axis attitude control without continuous use of the Chemical/RCS thrusters.

The RCS is not included in the ADCS hardware budget. Instead, the ADCS defines the control functions that require Chemical/RCS support: reaction-wheel desaturation, proximity manoeuvres, sampling support and contingency aborts. The corresponding disturbance and control drivers are summarised in Table 7.39, while the propellant mass, tank volume, thruster hardware and feed system are closed in Section 7.4.3.

Table 7.43: Preliminary ADCS hardware budget excluding Chemical/RCS propulsion hardware.

Element	Qty.	Mass [kg]	Dimensions [mm]	Sizing note
Star trackers (ASTRO APS)	3	6.0	154 x 154 x 237	Primary precision attitude reference.
IMUs (Astrix NS)	2	3.9	130 x 130 x 117	High-rate attitude propagation and bridging.
Coarse Sun sensors (Bradford)	6	1.3	110 x 110 x 30	Sun acquisition and safe-mode recovery.
LiDAR ranging set (PALT + TRIS)	2	2.5	120 x 150 x 100	Approach, descent and terminal TAG ranging.
Reaction wheels (W18)	4	30.1	Ø295 × 125 and 258 × 181 × 143	Four RWA plus two two-channel WDE boxes.
Total ADCS hardware	–	**43.8**	**72.9**	Excludes Chemical/RCS hardware and propellant.

The main remaining ADCS design uncertainty is the coupling between the reaction wheels, the fourteen-thruster Chemical/RCS layout, the PALT/TRIS-LRF ranging geometry and the final spacecraft centre-of-mass

envelope. In later design phases, a six-degree-of-freedom control-allocation matrix shall be built to verify wheel unloading, proximity-control authority, LiDAR line-of-sight coverage, PALT–TRIS/LRF hand-over altitude, plume keep-out constraints and single-failure cases.

Forward work for ADCS The following must close before the design is frozen, in rough order of impact

- Build the 6-DOF control-allocation matrix once the thruster geometry and CoM envelope are fixed, verifying wheel desaturation, proximity-control authority and single-failure cases (closes **REQ-ADCS-03**).
- Run an end-to-end GNC closed-loop simulation to confirm pointing control and knowledge (**REQ-ADCS-DER-01**, **REQ-ADCS-DER-02**) beyond the present budget-level analysis.
- Perform a control-jitter / micro-vibration analysis to verify **REQ-ADCS-DER-03** ($\leq 0.004\,^\circ\,\mathrm{s}^{-1}$).
- Confirm the 0.05 Hz control bandwidth sits below the deployed solar array's first flexible mode, using the structural modal survey.
- Close the SADA Sun-tracking loop and verify the $\leq 10^\circ$ solar-array pointing requirement (**REQ-ADCS-DER-05**).

7.7. Electrical Power System (EPS)

In the following section the design of the Electric Power System (EPS) is outlined. The section is structured as follows. Section 7.7.1 underlines the assumptions and the driving requirements for the EPS, establishing the design constraints that drive all subsequent system design decisions. Section 7.7.2 delves into the EPS architecture and shows a block diagram of the EPS with all relevant components used. Section 7.7.3 details the solar environment experienced during the mission and the design drivers. Section 7.7.4 defines the overall power budget for the different operational modes. Section 7.7.5 details the sizing methodology behind the solar arrays and the batteries. Section 7.7.6 considers the power management strategy based on throttling the propulsion power according to heliocentric distance. Section 7.7.7 summarises the preliminary EPS characteristics and first-order mass estimates. Lastly, Section 7.7.8 summarizes all findings and proposes the work necessary for the next phases of mission design.

7.7.1. Assumptions & Requirements

The assumptions used in the EPS design are gathered and displayed in Table 7.44:

Table 7.44: Assumptions for the Electrical Power System (EPS).

Requirement ID	Description
ASS-EPS-01	Battery charged at launch can power spacecraft for safe mode operations t_{safe} of 2 hours, until solar arrays are fully deployed and can start generating power to sustain more demanding operational modes.
ASS-EPS-02	Li-ion batteries are used with a depth of discharge (DoD) limited to 30% to preserve cell cycle life.
ASS-EPS-03	Mission lifetime is ~4 years. Radiation-induced degradation of solar cells is applied at a rate of 0.92%/year for triple-junction GaAs cells in the inner asteroid belt environment, consistent with values reported in [113]. Over the 4-year mission, this yields an EOL degradation factor of $\eta_{\mathrm{deg}} = (1 - 0.0092)^4 \approx 0.964$.
ASS-EPS-04	The primary power bus is regulated at 28 V, consistent with deep-space mission heritage.
ASS-EPS-05	A 20% margin is applied at the final level of calculations to account for uncertainties not yet captured in the preliminary sizing.
ASS-EPS-06	Duty cycle values, when implemented, are first-order estimates and have to be improved upon in subsequent design phases.
ASS-EPS-07	Component costs are preliminary Phase 0 order-of-magnitude (ROM) estimates in FY26 €, derived from representative \$/W and \$/Wh figures for flight-qualified hardware.
ASS-EPS-08	The 2 h safe-mode duration t_{safe} (ASS-EPS-01) is adopted as the primary battery-sizing driver, rather than eclipse survival, since no significant eclipse periods are encountered at Itokawa.

Continued on next page...

Table 7.44 Continued from previous page

Requirement ID	Description
ASS-EPS-09	Component volumes are preliminary rough order-of-magnitude estimates based on representative specific-volume and packaging-density values from comparable flight hardware. Detailed dimensions are to be defined once vendor-specific hardware is selected.

The requirements driving the EPS design have been consolidated and gathered in Table 7.45

Table 7.45: Consolidated Requirements for the Electrical Power System (EPS).

Requirement ID	Description
REQ-EPS-01	The EPS shall provide continuous, uninterrupted power to all spacecraft subsystems throughout all operational modes for the full mission lifetime.
REQ-EPS-02	The solar arrays shall deliver sufficient power at 1.7 AU EOL to sustain simultaneous ion propulsion and spacecraft housekeeping operations with a 20% system margin.
REQ-EPS-03	The battery shall sustain safe mode operations for a minimum of 2 h following launch, prior to solar array deployment and power generation.
REQ-EPS-04	Battery depth of discharge shall not exceed 30% in any operational scenario to preserve cycle life and maintain adequate contingency capacity.
REQ-EPS-05	The EPS shall accommodate the full throttle range of the ion propulsion system, from minimum reliable PPU input power to maximum available array surplus.
REQ-EPS-06	The main power bus shall be regulated at 28 V, while a dedicated high-voltage bus shall be provided to the PPU to support propulsion requirements.

7.7.2. EPS architecture

The EPS is structured around four primary elements, each with a defined role: the solar arrays, the battery, the Power Conditioning and Distribution Unit (PCDU), and the Power Processing Unit (PPU). Figure 7.7 shows the overall architecture of the EPS and how the different subsystems are connected.

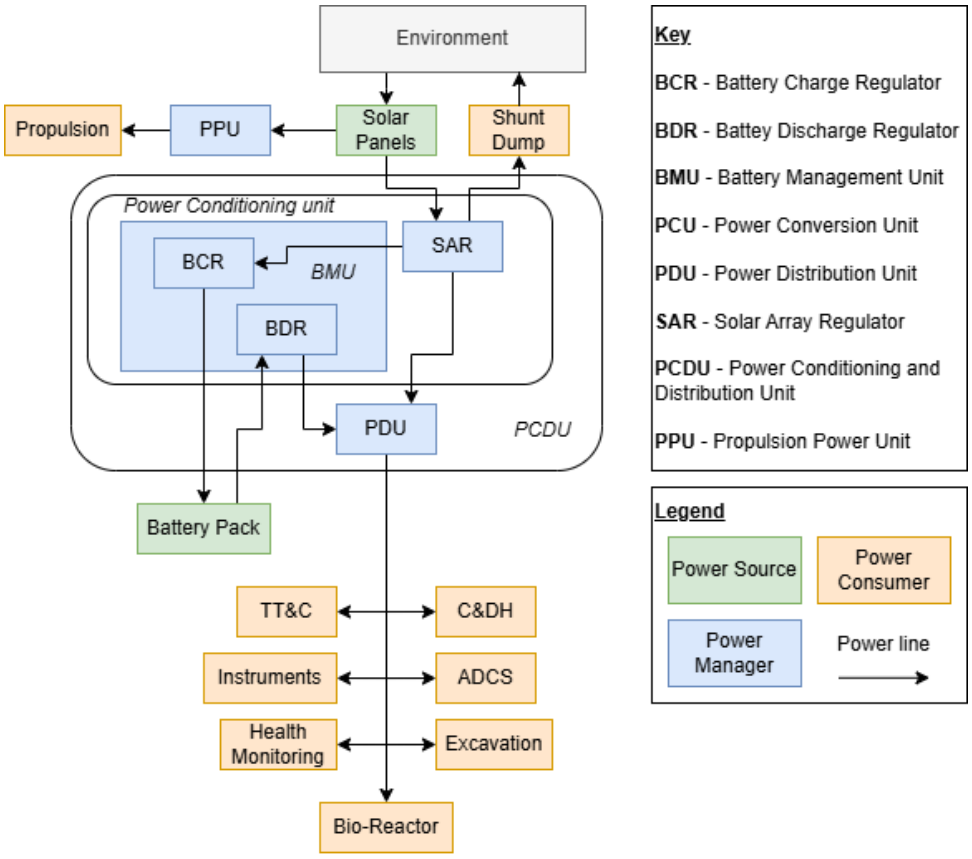

Figure 7.7: EPS Architecture

- **Solar arrays** are the main power source for the spacecraft throughout all mission phases beyond LEOP. Deployable rigid panels of triple-junction GaAs cells (InGaP/InGaAs/Ge) are selected, consistent with the heritage of comparable deep-space solar electric propulsion missions including Dawn, Hayabusa2 and BepiColombo [148, 149, 150]. Single-axis articulation is assumed to maintain continuous sun-pointing. Array sizing is driven by the worst-case operating condition at 1.7 AU EOL, as detailed in Section 7.7.3.
- **The battery** is included to handle transient and contingency loads and is not designed to sustain any ion propulsion operation requirements. Propulsion power is supplied entirely and directly through the solar arrays via the PPU. The battery serves three specific roles: powering all spacecraft systems during the launch and early operations phase (LEOP) and commissioning windows prior to solar array deployment, sustaining safe mode operations in the event of unforeseen circumstances, and counteracting short-duration peak transient loads arising from the simultaneous activation of C&DH, TT&C, ADCS, and thermal control subsystems. Lithium-ion batteries are chosen with a maximum DoD of 30% per ASS-EPS-03.
- **The PCDU** is responsible for bus voltage regulation, power distribution to all spacecraft subsystem loads, load switching, and fault protection. Maximum Power Point Tracking (MPPT) regulators are included on the array inputs to ensure full power extraction across the varying solar flux levels encountered between 1.0 and 1.7 AU.
- **The PPU** is a dedicated high-voltage converter (~150 V) serving the ion propulsion system exclusively. It is isolated from the spacecraft housekeeping bus, which is regulated at 28 V by the PCDU. Under the throttling strategy described in Section 7.7.6, the PPU power inputs vary with heliocentric distance and available array power. The PPU must therefore be specified to handle a wide range of input powers, as further discussed in Section 7.7.7.

7.7.3. Solar environment and design drivers

The solar flux available to the spacecraft varies continuously as a function of heliocentric distance, governed by the inverse square law:

$$G(r) = \frac{G_0}{r^2} \tag{7.28}$$

where $G_0 = 1361$ W/m^2 is the solar constant at 1 AU and r is the heliocentric distance in AU. At the mission operational distance of 1.7 AU:

$$G(1.7) = \frac{1361}{1.7^2} \approx 471 \text{ W/m}^2 \tag{7.29}$$

The total electrical output of the array at any heliocentric distance is:

$$P_{\text{array}}(r) = A \cdot G(r) \cdot \eta_{\text{cell}} \cdot \eta_{\text{packing}} \cdot \eta_{\text{deg}} \cdot \eta_{\text{point}} \tag{7.30}$$

where A is the total deployed solar-array area, η_{cell} is the solar-cell conversion efficiency, η_{packing} is the packing factor accounting for inactive panel area such as inter-cell gaps, wiring, hinges and structural elements, η_{deg} captures cumulative radiation and UV-induced degradation over the mission lifetime, and η_{point} accounts for power loss due to a conservative 10° solar-array pointing error. The numerical values adopted for each parameter are stated in Table 7.47.

The design point considered is the worst combination of two effects: maximum distance from the Sun and maximum accumulated cell degradation, both occurring simultaneously at mission end. For this mission, that condition is $r = 1.7$ AU with $\eta_{\text{deg}} = 0.964$ applied (ASS-EPS-03).

7.7.4. Power Demand Summary

The spacecraft load budget across all defined operational modes is presented in Table 7.46. Values are unmargined representative operating powers in watts.

Table 7.46: Mode-based spacecraft power budget (W).

Subsystem	Safe	Cruise	Standby	Sensing	Comms	Sampling	Bioprocessing	Manoeuvre
C&DH	30	30	30	30	30	30	30	30
TT&C	20	20	20	20	150	20	150	20
ADCS	54.4	158	158	158	158	358	158	358
TCS	120	120	120	120	120	120	120	120
Ion propulsion	–	–	–	–	–	–	–	–
Remote sensing	–	–	–	48	–	28	–	28
Sampling mechanism	–	–	–	–	–	12	–	–
MISAR	–	–	–	–	–	–	76.5	–
HMS	–	–	–	–	–	–	10	–
Total	224.4	328	328	396	458	588	544.5	576

First, the **ion propulsion** load is deliberately excluded from the spacecraft load table. The ion engine and its PPU represent a variable load whose magnitude is governed by the throttling strategy and the available surplus array power at each heliocentric distance, rather than a fixed demand imposed on the EPS, as further discussed in Section 7.7.6. Treating it as a fixed entry would overstate the design requirement at distances closer than 1.7 AU and misrepresent the system's operational philosophy.

Second, at this stage of the design, the PPU conversion losses and ion engine complementary loads are conservatively absorbed within the 20% system design margin (ASS-EPS-05). A dedicated propulsion power budget will be developed in the next design stages once thruster selection, throttling strategies and PPU specifications are defined.

The non-propulsion design-driving mode is **Sampling mode** at an unmargined total of 588 W, driven by simultaneous ADCS pointing sensor activation (358 W) and sampling mechanism engagement (12 W).

7.7.5. Sizing methodology

The total power the arrays must deliver at 1.7 AU EOL is the sum of spacecraft housekeeping loads during cruise and the ion propulsion demand:

$$P_{\text{req}} = (P_{\text{HK}} + P_{\text{thruster}}) \times \left(1 + M_{\text{sys}}\right) \tag{7.31}$$

where $P_{\text{HK}} = 328$ W (cruise mode housekeeping, from Table 7.46), $P_{\text{thruster}} = 3000$ W (ion propulsion demand at design point), and $M_{\text{sys}} = 0.20$ is the system margin per ASS-EPS-05:

$$P_{\text{req}} = (328 + 3000) \times 1.20 = 3368 \times 1.20 = 3993.6 \text{ W} \tag{7.32}$$

The required total deployed solar-array area is obtained by inverting Equation 7.30:

$$A_{\text{req}} = \frac{P_{\text{req}}}{G(1.7) \cdot \eta_{\text{cell}} \cdot \eta_{\text{packing}} \cdot \eta_{\text{point}} \cdot \eta_{\text{deg}}} \tag{7.33}$$

Substituting the values from Table 7.47:

$$A_{\text{req}} = \frac{3993.6}{471 \times 0.28 \times 0.85 \times 0.985 \times 0.964} \approx 37.5 \text{ m}^2 \tag{7.34}$$

A total deployed solar-array area of **38 m**^{2} is chosen, split across two rigid deployable panels of 19 m^2 each.

Table 7.47: Solar array sizing parameters and technology assumptions.

Parameter	Symbol	Value	Basis
Solar constant at 1 AU	G_0	1361 W/m^2	Standard
Solar flux at 1.7 AU	$G(1.7)$	471 W/m^2	Eq. 7.29
Cell type	–	TJ GaAs	Heritage [148, 149]
Cell efficiency (BOL)	η_{cell}	28%	Heritage
Panel packing factor	η_{packing}	0.85	Rigid deployable panel
Pointing loss (10° off-axis)	η_{point}	0.985	cos(10°) = 0.985, conservative for single-axis pointing
EOL degradation (4 yr, 0.92%/yr)	η_{deg}	0.964	ASS-EPS-03: $(1 - 0.0092)^4$
System margin	M_{sys}	20%	ASS-EPS-05

With the array area established, the BOL output at 1 AU can be recovered by scaling back to G_0 and removing the degradation factor:

$$P_{\text{BOL,1AU}} = A_{\text{req}} \cdot G_0 \cdot \eta_{\text{cell}} \cdot \eta_{\text{packing}} \cdot \eta_{\text{point}} \tag{7.35}$$

$$P_{\text{BOL,1AU}} = 38 \times 1361 \times 0.28 \times 0.85 \times 0.985 \approx 12124.3 \text{ W} \tag{7.36}$$

The battery is sized to the safe mode scenario (ASS-EPS-01): sustaining 224.4 W for 2 h at a maximum DoD of 30%. The required battery energy capacity is defined as:

$$E_{\text{batt,raw}} = \frac{P_{\text{safe}} \times t_{\text{safe}}}{\text{DoD} \times \eta_{\text{discharge}}} \tag{7.37}$$

where $\eta_{\text{discharge}} = 0.95$ is the Li-ion discharge efficiency.

$$E_{\text{batt,raw}} = \frac{224.4 \times 2}{0.30 \times 0.95} \approx 1575 \text{ Wh} \tag{7.38}$$

A battery capacity of approximately 1.6 kWh is therefore required before any additional design margin. Applying the 20% system margin from ASS-EPS-05 gives:

$$E_{\text{batt,sel}} = 1575 \times 1.20 \approx 1890 \text{ Wh} \tag{7.39}$$

For a conservative Li-ion specific energy of 150 Wh/kg, this gives a first-order battery mass of:

$$m_{\text{batt}} = \frac{1890}{150} \approx 12.6 \text{ kg} \tag{7.40}$$

7.7.6. Propulsion Power Management Strategy

Early EPS iterations treated ion propulsion as a constant 3000 W load independent of heliocentric distance, which is physically unrealistic: an array sized for 3000 W at 1.7 AU EOL produces approximately 12.1 kW at 1 AU BOL—over three times the propulsive design-point demand. Capping thruster input at 3000 W regardless of distance would leave a large fraction of array power unused near 1 AU. To exploit this surplus, the propulsion system is designed for throttling and parallel operation of multiple ion thrusters, with active-unit count and throttle level scaled to available array power at each heliocentric distance. This maximises ΔV accumulation during early cruise, when solar flux and available power are highest.

The adopted **throttling strategy** follows the heritage of solar-electric-propulsion missions such as Dawn and BepiColombo [148, 150]. The PPU input power available for propulsion is bounded by both the available array power and the hardware limits of the selected PPU/thruster configuration:

$$P_{\text{PPU,in}}(r) = \min\left[P_{\text{PPU,max}}, P_{\text{array}}(r) - P_{\text{HK}} - P_{\text{reserve}}\right] \tag{7.41}$$

where $P_{\text{PPU,max}}$ is the maximum allowable PPU input power, P_{HK} is the spacecraft housekeeping power, and P_{reserve} accounts for operational contingency, EPS losses, thermal loads, and power margin not explicitly allocated to propulsion.

Since $P_{\text{array}}(r) \propto 1/r^2$, the power available to the propulsion system decreases as the spacecraft moves further away from the Sun. The thruster therefore operates at its highest power during the early cruise phase near 1 AU, where there is an excess of power available, and is throttled down as the spacecraft approaches the target at 1.7 AU. The final throttle profile must be defined together with the selected ion thruster, PPU, thermal design, and trajectory thrust schedule.

Power to the ion engine is supplied directly and continuously through the solar arrays, passing through the PPU. The battery serves as a contingency buffer for safe mode, LEOP, and other transient housekeeping peaks as described in Section 7.7.2. This is consistent with the architecture adopted by SEP transfer modules such as BepiColombo's MTM, where the cruise power system is sized around the solar array and the solar electric propulsion system [150].

7.7.7. Preliminary EPS characteristics

Table 7.48 summarises the first-order EPS sizing results. All values are preliminary Phase 0 estimates and are subject to change as the design matures. Technology assumptions are as stated in Table 7.47; mass and volume estimates adopt conservative values consistent with current deep-space heritage hardware.

Table 7.48: Preliminary EPS first-order sizing characteristics.

Parameter	Value	Basis / Assumption
Solar Arrays		
Required power at 1.7 AU EOL	3993.6 W	Eq. 7.32
Total deployed array area	38 m^2	Eq. 7.34, 2 deployable panels
BOL power at 1 AU	~12.1 kW	Eq. 7.36
Surplus power at 1 AU	~8.1 kW	Above 1.7 AU EOL design-point demand
Array specific mass	3 kg/m^2	Conservative for rigid triple-junction GaAs panel
Array mass	**114 kg**	
Array specific volume	~0.015 m^3/m^2	ROM rigid folding panel (ASS-EPS-07)
Array volume	**~0.57 m^3**	38 m^2 × specific volume
Array specific cost	~€690/W_{BOL}	ROM, flight-qualified TJ GaAs array, FY26€ (ASS-EPS-07)
Array cost	**~€8.3M**	12.1 $kW_{BOL,1AU}$ × specific cost
Battery		
Required energy capacity, before margin	1575 Wh	Eq. 7.38
Required energy capacity, with margin	1890 Wh	Eq. 7.39
Battery specific energy	150 Wh/kg	Li-ion, conservative deep-space value
Battery mass	**12.6 kg**	Eq. 7.40
Battery specific volume	~200 Wh/L	ROM pack-level volumetric energy density (ASS-EPS-09)
Battery volume	**~9.5 L**	1890 Wh / specific volume
Battery specific cost	~€1,290/Wh	ROM, qualified Li-ion space battery pack, FY26€ (ASS-EPS-07)
Battery cost	**~€2.4M**	1890 Wh × specific cost
PCDU & PPU		
PCDU mass	**10 kg**	First-order estimate
PCDU volume	**~16.7 L**	ROM packaging density ~600 kg/m^3, power electronics chassis (ASS-EPS-07)
PCDU cost	**~€2.6M**	ROM, deep-space PCDU w/ MPPT & fault protection
PPU input power range	~500 to 9000 W	Preliminary throttle range, bounded by Eq. 7.41 and PPU limits
PPU mass	**15 kg**	First-order estimate based on high-voltage PPU

Continued on next page

Table 7.48 – continued from previous page

Parameter	Value	Basis / Assumption
PPU volume	**~30 L**	ROM packaging density ~500 kg/m^3, accounts for HV insulation/thermal spacing (ASS-EPS-09)
PPU cost	**~€3.9M**	ROM, informed by NEXT/NEXT-C-class PPU heritage
EPS Total		
Total EPS mass	**~152 kg**	
Total EPS volume	**~630 L**	Sum of array stowed, battery, PCDU and PPU volumes
Hardware cost subtotal	~€17.2M	Sum of array, battery, PCDU and PPU ROM costs
Total EPS cost (incl. margin)	**~€20.6M**	Subtotal × 1.20 system margin (ASS-EPS-05)

- **Required power at 1.7 AU EOL:** The arrays must deliver 3993.6 W at 1.7 AU EOL to sustain simultaneous ion propulsion and spacecraft housekeeping during combined thrust and cruise windows.

- **Available power at 1 AU BOL:** The sized 38 m^2 array delivers approximately 12.1 kW at 1 AU BOL. This represents a power surplus of approximately 8.1 kW above the margined cruise/thrust design-point demand. Under the throttling strategy of Section 7.7.6, this surplus can in principle be used by the ion propulsion system during the early mission phase, subject to the selected thruster/PPU configuration, thermal rejection capacity, xenon feed system, and trajectory thrust schedule. Conveniently, this is also when the wet mass is highest near launch, so higher early thrust can directly benefit the ΔV budget.

The Dawn mission used two deployable solar-array wings with a total area of 36.4 m^2 and projected EOL power between 10.3 kW at 1 AU and 1.3 kW at 3 AU [148]. BepiColombo's Mercury Transfer Module uses two solar-array wings totalling approximately 42 m^2, with a peak output of about 13 kW and a solar electric propulsion demand of 10.3 kW during cruise thrust mode [150]. The preliminary deployed array area of 38 m^2 is therefore considered valid for a Phase 0 estimate.

7.7.8. EPS Design Summary

The EPS architecture for this asteroid mission adopts solar arrays as its primary power source, a supplementary battery, and a dedicated ion propulsion PPU. The worst-case design driver is the delivery of 3993.6 W at 1.7 AU EOL during cruise and thrust windows, combining 3000 W ion propulsion demand, 328 W spacecraft housekeeping, and a 20% design margin. A throttling strategy avoids the impracticality of fixed propulsion-load assumptions, instead using the elevated solar flux available during early cruise where possible, before throttling down as the spacecraft approaches 1.7 AU.

Preliminary sizing gives a total deployed array area of 38 m^2, which delivers ~12.1 kW at 1 AU BOL, a selected battery capacity of ~1890 Wh for a 2 h safe-mode survival case including margin, and a total EPS mass estimate of approximately 152 kg, including preliminary estimates for PPU and PCDU masses. These values are consistent with the Dawn and BepiColombo deep-space SEP heritage [148, 150].

Forward Work

The following items require development in subsequent design phases:

- Confirmation of PPU selection and detailed ion thruster configuration, enabling a detailed throttle table across the full mission trajectory to design the EPS
- Detailed radiation environment characterisation at the target asteroid orbit to refine the EOL degradation factor η_{deg}
- Battery sizing refinement based on confirmed LEOP duration, proximity, science and sampling operations, and detailed safe mode analysis
- Harness mass and resistive loss, which are currently excluded from the EPS mass estimate
- Trade study between rigid and flexible/rollable array panel technologies to deal with the mass and stowage volume at the currently required 38 m^2 solar array area

- Develope a proper substantiated EPS cost estimate using the SMAD/SSCM (Small Spacecraft Cost Model) mass-based cost-estimating relationships [113], rather than the informal $/W and $/Wh placeholder values used in this Phase 0 iteration

Derived Requirements

Finally, the EPS design imposes a set of derived requirements on other spacecraft subsystems. These capture the interface constraints and physical demands that the EPS places on the rest of the spacecraft subsystems to function as designed. Key among these are the structural accommodation of two 19 m^2 deployable array wings, the ADCS sun-pointing accuracy requirement that underpins the η_{point} sizing assumption, and the thermal rejection capacity required to handle PPU waste heat across the full throttle range. These derived requirements are summarised in Table 7.49.

Table 7.49: Derived requirements from the EPS to other subsystems.

Req. ID	Target Subsystem	Requirement	Rationale
REQ-STRUC-DER-01	Structures	The primary structure shall provide mounting interfaces for two deployable solar array wings, each with a deployed area of 19 m^2 and a stowed mass of no more than ~ 57 kg per wing.	Array sizing drives panel dimensions and mass loading on the structural interface.
REQ-STRUC-DER-02	Structures	The spacecraft structure shall accommodate the stowed solar array envelope within the available launch vehicle fairing volume.	A total deployed area of 38 m^2 implies significant stowed volume requiring early structural coordination.
REQ-ADCS-DER-05	ADCS	The ADCS shall maintain solar array pointing to within 10° of the sun vector during all cruise and thrust modes.	EPS sizing assumes a pointing accuracy of atleast 10°, from $\eta_{\text{point}} = \cos(10°) = 0.985$ at this stage.
REQ-TCS-DER-06	Thermal	The TCS shall provide heat rejection capacity sufficient to dissipate PPU waste heat across the full throttle input power range of 500–9000 W.	PPU losses scale accordingly with input power; insufficient thermal rejection capabilities risks damage to the PPU hardware and the subsystems on board.
REQ-PROP-DER-01	Propulsion	The ion propulsion PPU shall accept a variable input across the range 500–9000 W and shall not demand more than 3000 W for the ion propulsions.	The throttling strategy bounds propulsion draw to available array surplus per Eq. 7.41.
REQ-PROP-DER-02	Propulsion	The propulsion subsystem shall be capable of operating across a throttle range consistent with array power varying between ~4000 W at 1.7 AU EOL and ~12.1 kW at 1 AU BOL.	Array output varies by a factor of approximately three over the mission duration the propulsion system must accommodate this without requiring fixed-power operation.
REQ-CDH-DER-01	C&DH	The C&DH subsystem shall provide command and telemetry interfaces to the PCDU for load switching, fault protection triggers, and propulsion throttle level management.	MPPT regulation and power throttling require active commanding from the onboard computer.

8
System Overview

With the payload and bus subsystems defined, this chapter takes a macro perspective of the spacecraft, *Alicanto*, and designs so that the pieces close as a system. Section 8.1 presents the external and internal configuration. Section 8.2 then tests the mission against its €205 M cost cap, Section 8.3 consolidates the mass, volume, and power budgets with their margins, and Section 8.4 gathers the resulting system characteristics in one place. Section 8.5 closes the chapter by framing the return on a mission that, by design, sells nothing and is funded for the capability it proves.

8.1. Layout/Configuration

The overall layout and configuration are presented below to provide a visualisation of the created system and additionally to demonstrate general the general system compliance to REQ-STK-8. Section 8.1.1 presents the overall visualisation of the entire *Alicanto* spacecraft in addition to a reference view presenting the spacecraft in combination with the Ariane 62 launch vehicle. Finally, Section 8.1.2 will present a detailed internal view with the major subsystems indicated.

8.1.1. External Views

Presented are several figures which depict the external views of *Alicanto* in which the placement of external subsystems as described by Chapter 6 and Chapter 7 are shown. Firstly, Figure 8.1 details the external view of the spacecraft in a cruise configuration. Additionally a further view is provided that details the stowed configuration of the spacecraft. The overall coordinate system that follows is derived from Figure 7.1b and is indicated in both figures. When stowed in the Ariane 62 launch vehicle, the z-axis will be aligned with the launch vehicles longitudinal axis of thrust.

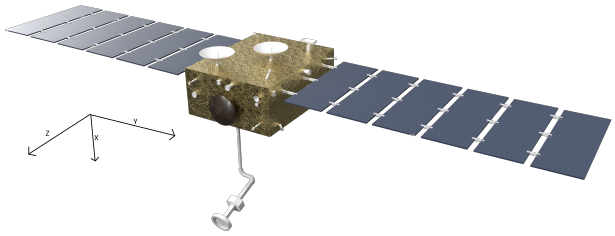

Figure 8.1: External View of Cruise Configuration of *Alicanto* Spacecraft

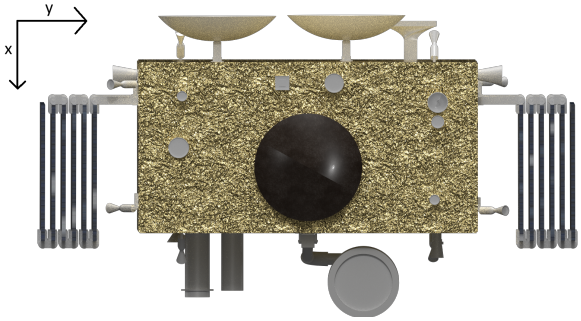

Figure 8.2: External View of Stowed Configuration of *Alicanto* Spacecraft

8.1.2. Internal Layout

Presented in Figure 8.3 is an internal view of the *Alicanto* spacecraft in which the placement of internal subsystems as specified in Chapter 6 and Chapter 7 are presented. This view provides visual verification of the volume compliance of the spacecraft structure with respect to internal subsystems and enables the centre of mass and mass moments of inertia calculations.

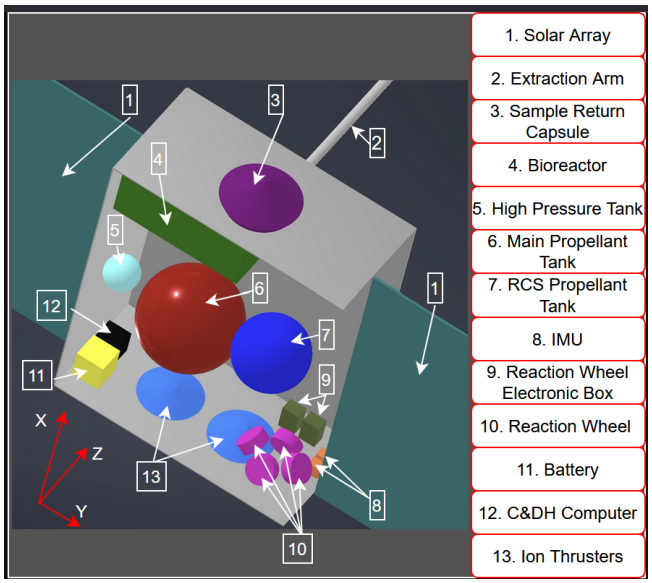

Figure 8.3: Detailed Internal Configuration Plot

Figure 8.3 provides a simplified viewing of the interior of the spacecraft, where the comprising subsystem elements are represented as to-scale volumes with appropriate geometries. The main exclusions from Figure 8.3 are thermal elements that are not comprised within the volume of a subsystem, in addition to system electrical wiring. In combination with external system elements as depicted in Section 8.1.1, the overall system geometric properties are defined below in Table 8.1. The centre of gravity (CoG) is calculated to have a negligible off-set from the desired centroidal position of the primary external structure as desired for propulsion and Ariane 62 compliance [27].

Table 8.1: System Geometric Properties

Mass Moments of Inertia [kg · m^2]		
Ixx	**Iyy**	**Izz**
3541.449	1437.766	4083.509

With respect to Table 8.1, the system is expected to have asymmetries with respect to the primary structure as modelling has been conducted with all internal subsystem as described above. As a further case study, the system is investigated for CoG shift when all propellant tanks are empty resulting in the following geometric properties and CoG deviation.

Table 8.2: System Geometric Properties

CoG Shifts & Mass Moments of Inertia [kg · m^2]								
x [m]	**y [m]**	**z [m]**	**Ixx**	**Iyy**	**Izz**	**Ixy**	**Ixz**	**Iyz**
0.034	0.074	0.076	3482.398	1400.32	3955.330	-92.968	130.962	-85.826

With respect to this case study and the resulting geometric properties as described in Table 8.2, the resulting shift does not result in a system deviation. In Section 7.6, following ASS-ADCS-06 the ADCS subsystem is sized conservatively considering a 0.2 m CoG offset. As the maximal CoG offset resulting from this case study is 0.076 m, this offset is covered by ASS-ADCS-06.

8.2. Cost Breakdown Structure

The Cost Breakdown Structure (CBS) answers the question: does the mission close inside its cost cap? The mission's Cost at Completion (CaC) ceiling of 205 M€ (2025 economic conditions) is a top-level requirement set by the F-class call as stated in the project description [151], not a project-chosen figure; it excludes launch services and the in-kind scientific payload (not counting the SRC), consistent with the ESA F-class accounting convention [152]. That envelope follows the ESA F-class accounting convention, under which the cap covers

all ESA-funded elements but explicitly omits the launcher and any Member State or international-partner contributions [152]. All values are reported in millions of euros at FY2025 economic conditions unless noted otherwise. United States dollar figures are converted at 0.92 €/$ and historical figures are escalated at the rate stated in each case, with escalation to the FY2036 launch year is treated as an open item (**CBS-01**) rather than applied speculatively here.

8.2.1. Cost Element Tree

The cost element tree in Figure 8.4 is an AND tree decomposition of every element that contributes to the development and production cost of the flight system [151]. Each leaf is a cost element, and the methods in Section 8.2.2 populate those leaves either directly (the bottom-up sum) or in aggregate (the top-down, analogue and parametric methods). The tree follows the standard space-segment, ground-segment, and launch-segment split. The project-level functions (systems engineering, project management, and product assurance) and assembly and integration are drawn as their own branches because they carry cost that no single subsystem owns. The payload and launch branches are shown for completeness but sit outside the ESA Cost at Completion: the payload is partner-provided, and the launcher is funded separately.

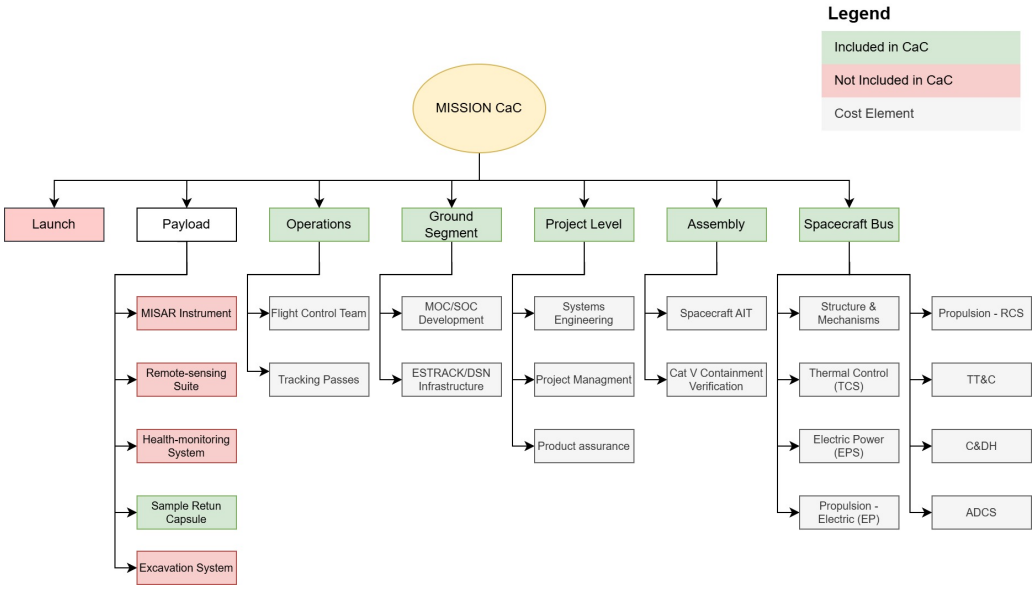

Figure 8.4: Silicon Shepherd cost element tree. The leaves are the cost elements summed in the bottom-up estimate (Method 4). The payload and launch branches lie outside the ESA Cost at Completion.

8.2.2. Estimation Methodology

At the current maturity the project has locked subsystem selections and mass budgets but does not yet have component-level vendor quotations for the full bus. A purely component-level bottom-up estimate is therefore premature, a point the NASA Cost Estimating methodology makes directly. Detailed bottom-up costing is not suitable for conceptual design because the data do not exist until detailed design [153]. The CBS instead estimates the spacecraft cost through four largely independent methods, from a top-down allocation to a subsystem-level bottom-up sum.

1. **Top-down ESA F-class envelope.** The published F-class cost decomposition, scaled to the adopted 205 M€ cap. This is the method the cap itself was written for.
2. **Analogue cross-check.** Recent flown asteroid-rendezvous missions, principally ESA's Hera, with NEAR Shoemaker as a deep-space planetary anchor.
3. **Parametric reality check.** The NASA uncrewed-planetary spacecraft Cost Estimating Relationship (CER) applied to dry mass, used as a from-scratch upper bound.
4. **Bottom-up subsystem sum.** The cost of each spacecraft subsystem, re-estimated at the final-design level and summed, with system-level wraps added. This is the most design-specific estimate and the one most sensitive to what each subsystem contains.

Table 8.3 summarises the approach, applicability, and base year of each.

Table 8.3: Cost estimation methods, scope and reference data.

Method	Basis and scope	Base year
F-class top-down	ESA F-class CaC decomposition (spacecraft, ESA project, operations), excluding launch and payload [152]	2018 e.c.
Analogue	Hera prime contract and total mission cost [154, 155], and NEAR spacecraft development [156, 157]	2020 / 1996
Parametric CER	Uncrewed-planetary CER, DDT&E = 11.279 $W^{0.5}$, W in lb, valid 191–2755 lb [153]	early-1990s $
Bottom-up subsystem sum	Per-subsystem cost at final design, summed, plus AIT, SE/PM, and product-assurance wraps [153, 113]	Final design

8.2.3. Spacecraft Cost Estimate

Method 1 – Top-down F-class envelope. ESA's response to the 2018 Fast-mission call caps the F-class contribution to ESA at 150 M€, excluding launch, Member State and partner contributions, with an internal split of 95–105 M€ for the spacecraft, 20–25 M€ for ESA project costs and 15–30 M€ for operations [152]. Comet Interceptor, the first F-class mission, fits this envelope as a sub-1000 kg Ariane 62 co-passenger with member-state instruments [158].

The 150 M€ figure is the 2018-conditions to-ESA envelope and is used here only as a top-down method input; the binding requirement is the later 205 M€ (2025 conditions) cap. The gap is consistent with both escalation (150 M€ at 2018 e.c. is roughly 169–179 M€ at 2024 e.c. for 2–3%/yr) and the added scope, electric primary propulsion, sample return, and Category V restricted verification, that distinguishes Silicon Shepherd from a flyby such as Comet Interceptor.

Method 2 – Analogue cross-check. The closest flown analogue is ESA's Hera, an asteroid-rendezvous mission with autonomous proximity operations around a small body. Hera cost 363 M€ total [155], including a 129.4 M€ OHB prime contract for detailed design, manufacturing and testing awarded in 2020 [154], approximately 150 M€ escalated to FY2025 at 3%/yr. Hera carries no SRC, electric main propulsion or biological payload, but includes twelve instruments that Silicon Shepherd treats as in-kind.

NEAR Shoemaker provides a deep-space, lower-heritage anchor: developed for slightly over $122M, against $479M for Mars Observer and roughly $1.4B for Cassini in the same era [156]. Normalised to present-day terms NEAR sits near 210–230 M€, above the F-class spacecraft line because it was closer to a from-scratch build with all SE&M charged to it [157], a useful upper analogue for checking Silicon Shepherd's heritage assumptions.

Method 3 – Parametric reality check. The NASA uncrewed-planetary DDT&E CER is

$$\text{DDT\&E} = 11.279\, W^{0.5},$$

with W the dry mass in pounds, valid over 191–2755 lb on sixteen data points [153]. For 721 kg dry mass it returns about $450M in early-1990s dollars, roughly twice the full 205 M€ cap before escalation, and several times the cap once escalated to FY2025.

This is expected: the CER represents a low-reuse spacecraft, whereas Discovery and F-class missions rely on heritage, reuse and lean management. Reconciling it with Table 8.5 implies an effective reuse factor of about 0.3, between off-the-shelf hardware with minor modification (0.2) and a largely existing design with limited new development (0.4) [153]. The mission therefore closes only if a substantial fraction of the platform is reused rather than newly qualified.

Method 4 – Bottom-up subsystem sum. The fourth estimate is the most design-specific: a subsystem-level sum excluding the in-kind payload, corresponding to the bus leaves of Figure 8.4, with a hardware-only floor of approximately 139.3 M€. To become a true spacecraft estimate rather than a floor, subsystem costs must include design, qualification and test labour, and system-level items—AIT, systems engineering, project management and product assurance—must be added separately. The NASA methodology captures these through subsystem and programme-level wraps [153], typically of order 30–40% [113]. The current build-up is given in Table 8.4.

8.2.4. Programmatic and Mission-Level Elements

Assembly, integration and test (AIT). Under the F-class accounting convention, AIT is not a free-standing element: prime-contractor AIT sits within the spacecraft cost, and ESA-side integration, product assurance, and oversight sit within the ESA project cost. This aligns with phase D2 in Section 3.1. Standard parametric practice

Table 8.4: Method 4 bottom-up subsystem cost build-up (FY2025 M€, ESA CaC scope, payload excluded). Open item **CBS-06**.

Element	Cost [M€]
Structure & mechanisms	3.0
Thermal control (TCS)	3.0
Electrical power (EPS)	20.7
ADCS	10.0
Propulsion – electric (EP)	15.5
Propulsion – RCS	5.0
TT&C	9.0
C&DH	5.0
Harness & integration h/w	2.0
Sample Return Capsule	20.0
Subsystem subtotal	**93.2**
+ AIT wrap (~15%) [113]	14.0
+ Programme wrap (SE/PM/PA 30%) [113]	28.0
Spacecraft estimate (Method 4)	**139.3**

Table 8.5: Spacecraft cost triangulation (FY2025 M€, ESA CaC scope). The anchors deliberately differ; the spread quantifies the dependence on heritage reuse.

Anchor	Spacecraft [M€]	Role
F-class top-down allocation (Method 1)	95–110	**Estimate**
Hera's prime contract, escalated (Method 2)	~150	Modern analogue
NEAR spacecraft, normalised (Method 2)	210–230	From-scratch marker
Uncrewed-planetary CER (Method 3)	>800	Upper bound, no heritage
Bottom-up subsystem sum + wraps (Method 4)	139.3	Most design-specific

places AIT at roughly 10-15% of spacecraft hardware as a wrap factor [113], which is already embedded in the Method 1 spacecraft line. What Silicon Shepherd adds, and what has no clean heritage anchor, is Category V verification, the biological containment qualification testing required. This is carried as an explicit uplift inside the ESA project line and flagged as a cost driver (**CBS-03**).

Ground segment and operations. This section aligns with Phase E outlined in Section 3.1. The F-class operations line runs from about 15 M€ for a short mission to 30 M€ for a year of operations [152]. Silicon Shepherd operates over a 1151-day arc with deep-space tracking through ESTRACK and DSN apertures [1]. Operations cost does not scale linearly with duration because the long cruise is low-tempo, but the deep-space tracking and the multi-year staffing push this up. The estimate is 20-30 M€ at base, with the tracking-pass cost as the dominant uncertainty (**CBS-04**).

Launch services. Launch is provided by Ariane 62 and, following the F-class convention and the Comet Interceptor precedent of an Ariane 62 co-passenger arrangement, is excluded from the 205 M€ CaC [152, 158]. For life-cycle completeness it is reported as a memo line. The declared Ariane 62 total launch price is about 75-90 M€ [159], and the most recent disclosed ESA dedicated booking, Sentinel-1D in late 2025, came to 82 M€ [160]. Flying as a co-passenger affects the cost share borne but not CaC compliance, since launch sits outside the cap either way (**CBS-05**).

Payload. The MISAR instrument, health-monitoring system, sample return capsule, and remote-sensing suite are partner-provided and funded outside the ESA CaC [1]. No payload procurement cost is therefore charged against the cap. The ESA-side obligations that do fall inside the cap, payload accommodation, and the Category V verification noted above, are captured in the spacecraft and ESA project lines.

8.2.5. Cost Summary and Cap Compliance

Table 8.6 assembles the base estimate and builds up to the Cost at Completion (CaC) through the project margin philosophy: 20% contingency on the base estimate, then a 10% management reserve on the contingency-loaded total, consistent with the 155 M€ executable target carried from the Baseline [1]. The CaC scope excludes launch and payload. Additionally, within Table 8.6 memo lines are shown for completeness and are not counted against the cap.

Table 8.6: Cost Breakdown Structure summary (FY2025 M€)

Element	Base estimate [M€]
Spacecraft (incl. AIT)	95–110
ESA project (SE/PM/PA + Category V verification)	20–30
Ground segment and operations (1140 d)	20–30
Base subtotal (executable level)	**135–170**
+ Contingency (20%)	27–34
+ Management reserve (10%)	16–20
Cost at Completion	**178–224**
Best estimate (most likely, base 150)	**198**
CaC cap (requirement)	**205**
Memo lines (outside CaC):	
Launch services (Ariane 62)	75–100
Payload (partner-provided, in-kind)	not charged

Taking the most-likely value of each line, spacecraft at the F-class allocation (cross-checked against the Method 4 bottom-up) and the ESA-project and operations lines at their midpoints, gives a base estimate near 150 M€. Through the 20% contingency and 10% reserve this yields a best-estimate CaC of 198 M€, inside the 205 M€ cap by roughly 7 M€. The 178–224 M€ figure is the uncertainty band around this point, not a competing estimate: the lower bound clears the cap by about 27 M€, the upper breaches it by about 19 M€. Method 4 corroborates the central value, adding its omitted operations line and the same reserve also lands it near 200 M€, so the point estimate is robust even though the band is wide. Cost is thus not closed: the point estimate complies, but compliance is conditional on holding the base at the 155 M€ target.

Within the ESA cap the cost risk concentrates in three TRL 4 items lacking a clean heritage anchor: Category V containment and re-entry verification (ESA project line), electric propulsion, and the sample return capsule. The parametric check frames the residual exposure: without heritage, this is a several-hundred-million-euro spacecraft, and the F-class accounting closes only because launch is funded separately, the payload (excluding the SRC) is in-kind, and substantial reuse is assumed.

The recommendation is to treat the 205 M€ cap as binding and to manage to the 155 M€ executable target, holding the three high-risk items under active cost-watch.

Table 8.7: Open items for the cost estimate.

ID	Item
CBS-01	Escalate all figures to the FY2036 launch year using a single stated index; fix the reference year.
CBS-02	Quantify Category V verification cost. No heritage anchor currently exists.
CBS-03	Confirm ESTRACK/DSN tracking-pass cost over the 1140-day arc.
CBS-04	Confirm dedicated vs. co-passenger Ariane 62 arrangement and launch-cost share.

8.3. Budget Breakdown

This section consolidates the current system-level resource budgets for the selected Silicon Shepherd architecture. The mass budget is closed using the adopted 20 % system-level margin and the updated 1300 kg spacecraft mass allocation. The volume and power budgets are retained as system-level budget interfaces: volume values are listed where subsystem returns are available, while missing entries remain open pending CAD and subsystem closure.

8.3.1. Budget Methodology and Margin Philosophy

The resource budgets are treated as Phase 0/A assessment-level budgets. The margin philosophy follows the ESA science-assessment margin approach [161]. At the current design iteration, subsystem owners have applied margins according to their own estimate maturity and subsystem-specific assumptions. The rules in Table 8.8 are therefore used as the system-level guideline for interpreting, reconciling and updating the budget returns, rather than as a claim that all subsystem tables have already used identical margin rules.

Three allowance types are distinguished:

- **Equipment-level maturity margins**, applied by subsystem owners according to the maturity of each equipment estimate.

- **System-level margins**, applied at spacecraft roll-up level to cover integration growth and remaining design uncertainty.
- **Operational contingency**, reserved for off-nominal operations and not used to close nominal subsystem budgets.

Table 8.8: Preliminary margin philosophy used for system-level budget reconciliation.

Budget item	Guideline margin rule
Equipment mass and power	5 % for off-the-shelf items, 10 % for minor modifications, and 20 % for new or strongly modified items.
System mass	A 20 % system-level margin is applied to the nominal spacecraft wet mass for the formal mass-closure case.
Harness	Harness is kept as a separate system-level item and estimated as approximately 5 % of the nominal dry mass.
Propellant and tanks	Propellant is carried separately from dry hardware. Tank volumes are sized for the margin-inclusive propellant load plus at least 10 % volume allowance.
Spacecraft power	A 20 % system-level margin is applied to nominal mode power. Solar arrays and batteries are sized at end-of-life using the margin-inclusive load.
ΔV	Analytically computed manoeuvres carry 5 % margin. Poorly defined manoeuvre allowances carry larger contingency depending on maturity.
Cost	Cost margins are handled in the Cost Breakdown Structure, with the ESA cost cap treated as the external constraint.

All subsystem budget tables shall state whether their listed values are raw estimates, equipment-level-margined estimates, or supplier values with implicit margin. The system roll-up then shows the nominal value, applied system margin, and margin-inclusive value as separate lines.

8.3.2. Budget Traceability Summary

Table 8.9: System budget traceability summary. Page numbers are generated automatically from the referenced section labels.

Budget	Primary location	Current status
Mass budget	Section 8.3.3, p. 112	Closed against 1300 kg allocation.
Volume budget	Section 8.3.4, p. 113	Closed against 55.7 m^3 allocation.
Power budget	Section 8.3.5, p. 114	Mode-based budget populated with current subsystem power states.
Cost budget	Section 8.2, p. 107	Covered by the Cost Breakdown Structure.
ΔV budget	Section 5.4, p. 31	Split between trajectory interfaces and propulsion sizing.
Link budget	Section 7.2, p. 65	Covered in TT&C subsystem sizing.
Thermal budget	Section 7.5, p. 84	Covered by thermal-control subsystem sizing.

8.3.3. Mass Budget

The current mass budget is built from the latest subsystem budget values, summarised in Table 8.10. Propellant masses are listed separately because they are added to the dry spacecraft mass to obtain the nominal wet mass. Harness is added at system level rather than assigned to individual subsystems.

The updated spacecraft mass allocation is 1300 kg. The design therefore closes against the current mass requirement with $\Delta m = 26.19$ kg.

This corresponds to approximately 2.0 % of the allocated launch mass. Mass therefore closes, but remains a critical system-level budget because the remaining margin is small compared with the current Phase 0/A design uncertainty.

Table 8.11: Mass-budget closure against the updated spacecraft mass allocation.

Metric	Nominal	Margin [%]	Incl. margin	Limit	Status
Mass [kg]	1061.51	20	1273.81	1300.00	Closes with 26.19 kg remaining.

The dominant mass contributors are the chemical/RCS propellant, EPS, the bioreactor, ion-main propellant, chemical/RCS dry hardware, ion-main dry hardware and structures. The mass budget is therefore mainly driven by the propulsion architecture, power subsystem and biological payload accommodation.

Table 8.10: Current system mass budget. Mass allocations are expressed relative to the nominal wet mass of 1061.51 kg.

Budget item	Mass [kg]	Wet-mass share [%]
Spacecraft bus		
ADCS	43.80	4.13
C&DH	12.00	1.13
EPS	152.00	14.32
Structures	59.95	5.65
Thermal Control	25.60	2.41
TT&C	25.20	2.37
Bus subtotal	**318.55**	**30.01**
Propulsion and consumables		
Propulsion – Chemical/RCS dry	82.90	7.81
Propulsion – Chemical/RCS propellant	226.98	21.38
Propulsion – Ion dry	63.60	5.99
Propulsion – Ion propellant	113.70	10.71
Propulsion subtotal	**487.18**	**45.89**
Payload and mission hardware		
Payload – Bioreactor	115.94	10.92
Payload – Health Monitoring / LMCOOL	5.23	0.49
Payload – Remote Sensing Suite	8.30	0.78
Sampling Mechanism	44.00	4.15
Sample Return Capsule (SRC)	46.00	4.33
Payload and mission subtotal	**219.47**	**20.68**
Subtotal before harness	**1025.20**	**96.58**
Harness	36.31	3.42
Dry mass incl. harness	**720.83**	**67.91**
Propellant mass	**340.68**	**32.09**
Nominal wet mass	**1061.51**	**100.00**
System-level margin, 20 %	212.30	20.00
Wet mass incl. 20 % **margin**	**1273.81**	**120.00**

8.3.4. Volume Budget

The volume budget distinguishes between the scalar sum of subsystem volume allocations and the spacecraft stowed volume. The subsystem values in Table 8.12 provide traceability to individual subsystem returns, while formal volume closure is performed on the CAD stowed volume against the launcher allocation.

Table 8.12: Current system volume budget. Values are listed where subsystem volume returns are available.

Budget item	Volume [L]	Treatment
Spacecraft bus		
ADCS	72.90	ADCS hardware only; excludes Chemical/RCS hardware and propellant.
C&DH	9.50	OBC, SSR and associated data-handling electronics.
EPS	630.00	Solar arrays, battery and PCDU accommodation.
Structures	190.32	Current structural volume allocation.
Thermal Control	30.00	Current thermal-control hardware allocation.
TT&C	150.50	Antenna and RF-chain accommodation.
Bus subtotal	**1083.22**	
Propulsion		
Propulsion – Chemical/RCS	262.00	Chemical/RCS hardware, tankage and propellant accommodation.
Propulsion – Ion	78.20	Xenon tank internal volume.
Propulsion subtotal	**340.20**	

Continued on next page...

Table 8.12 Continued from previous page

Budget item	Volume [L]	Treatment
Payload and mission hardware		
Payload – Bioreactor	142.69	MISAR instrument volume with margin.
Payload – Health Monitoring / LMCOOL	0.48	HMS estimate converted from 480.6 cm^3.
Payload – Remote Sensing Suite	9.60	Remote sensing instrument suite.
Sampling Mechanism	315.00	Stowed sampling mechanism envelope.
Sample Return Capsule (SRC)	170.00	Current stowed SRC accommodation allocation.
Payload and mission subtotal	**637.77**	
Total scalar component volume	**2061.19**	Subsystem-return sum; not a CAD accommodation proof.

The scalar component volume is therefore used only as a traceability check. The actual accommodation constraint is the spacecraft stowed volume from CAD, including packaging, clearances and configuration effects.

Table 8.13: Stowed-volume closure against the launcher volume allocation.

Metric	Nominal [m^3]	Margin [%]	Incl. margin [m^3]	Limit [m^3]	Status
CAD stowed volume	33.30	20	39.96	55.70	Closes with 15.74 m^3 remaining.

8.3.5. Power Budget

The power budget is closed by operational mode rather than by summing all subsystem peak powers. This avoids an unrealistic sizing case in which ion thrusting, full science sensing, high-rate downlink, sampling and bioprocessing are all assumed to occur simultaneously. The mode-based power budget is shown in Table 8.14.

Table 8.14: Mode-based spacecraft power budget. Values are representative operating powers in W. Harness, structures, EPS and the passive SRC are excluded as direct electrical loads.

Subsystem / total	Safe	Cruise	Standby	Sensing	Comms	Sampling	Bioprocessing	Manoeuvre
C&DH	30	30	30	30	30	60	30	30
TT&C	20	20	20	20	150	20	20	20
ADCS	54.4	158	158	176	158	376	158	376
TCS	120	120	120	120	120	120	120	120
Ion propulsion	–	3000	–	–	–	–	–	–
Remote sensing suite	–	–	–	48	–	28	–	28
Sampling mechanism	–	–	–	–	–	12	–	–
MISAR	–	–	–	–	–	–	76.5	–
HMS / LMCOOL	–	–	–	–	–	–	4.2	–
Total	**224.4**	**3328**	**328**	**394**	**458**	**616**	**408.7**	**574**
Total +20%	**269.3**	**3993.6**	**393.6**	**472.8**	**549.6**	**739.2**	**490.4**	**688.8**

Note: TT&C housekeeping and full-downlink powers are taken as 20 W and 150 W. The full-downlink state is only applied in Comms mode; Bioprocessing uses the housekeeping TT&C state unless a dedicated downlink pass is commanded. C&DH is doubled to 60 W during Sampling because the redundant cold computer is activated for this critical operation. The ion-propulsion entry represents the 3000 W cruise design-point load.

The EPS sizing case is selected from the maximum margin-inclusive operating mode. In the current mode table, Cruise is the driving mode because it includes the ion-propulsion load. The maximum margin-inclusive spacecraft load is therefore 3993.6 W. This value is passed to the EPS sizing together with the end-of-life solar-array assumptions and battery operating constraints.

Table 8.15: Power-budget closure against the current EPS sizing case.

Metric	Nominal	Margin [%]	Incl. margin	Limit / driver	Status
Maximum mode power [W]	3328.0	20	3993.6	EPS sizing case	Cruise mode drives the current power budget.

8.3.6. Cost Budget

The cost budget is handled in the Cost Breakdown Structure. The cost cap is therefore not repeated as a subsystem-by-subsystem resource table in this section. Instead, this section only records the traceability to the CBS through Table 8.9.

8.4. System Performance Analysis

Table 8.16 consolidates the performance and the full set of spacecraft system characteristics for the selected design choices.

Table 8.16: Consolidated performance and spacecraft system characteristics for the selected Silicon Shepherd baseline.

Characteristic	Value	Source / status
Mission profile and duration		
Mission architecture	Ariane 62 rideshare launch, chemical C_3-setting burn, low-thrust heliocentric cruise to (25143) Itokawa, proximity ops and TAG sampling, in-situ bioleaching, low-thrust return, SRC atmospheric entry and bus heliocentric disposal	Section 4.1, Table 5.6
LEOP duration	~6 h	Table 4.3
Outbound cruise	350 days (post-escape departure 2036-05-06 → Itokawa arrival ≈2037-04-21)	Table 4.3, Table 5.8
Asteroid residence (total)	≈436 days	Table 5.12
Asteroid observation & recon	157 days	Table 4.3
Sampling operations	7 days (TAG contact <1 min, up to 6 attempts)	Table 4.3
In-situ bioleaching	120 days	Table 4.3
Earth-return cruise	365 days (364.763 d; Itokawa departure 2038-07-01 → Earth encounter 2039-07-01)	Table 5.9
SRC deployment & re-entry	~24 h	Table 4.3
End-of-life passivation	~7 days	Table 4.3
Total mission duration	~3.2 years post-escape (~1151-day operations arc)	Table 5.9, Section 8.2
Mass budget		
Nominal (unmargined) wet mass	1061.51 kg	Table 8.11 (Table 8.8/8.10)
Wet mass incl. 20 % margin	1273.8 kg	Table 8.10/8.11
Launch / rideshare mass allocation	1300 kg	Table 8.9, Section 8.3.3 (updated)
Closure vs allocation	+26.19 kg (~2.0 % margin under 1300 kg)	Table 8.11
Mass-driving lines	Chemical/RCS propellant 226.98 kg, EPS 152.00 kg, bioreactor 115.94 kg, ion propellant 113.70 kg, chemical/RCS dry 82.90 kg	Table 8.11
Volume budget		
Unmargined stowed volume	33.3 m^3	Table 8.13
Volume at +10 %	39.96 m^3	Table 8.13
Stowed-volume allocation	55.70 m^3)	Table 8.13
Power budget		
Peak power (cruise thrusting), unmargined	3328 W (3000 W ion + 328 W bus)	Table 7.46 (Table 8.13)
Peak power incl. 20 % margin	3993.6 W (EPS sizing case)	Table 8.13
Eclipse / battery-sizing load	389 W	battery sizing, Section 7.7
Max non-propulsive mode power	616 W (Sampling), 739.2 W at +20 %	Table 8.13
Propulsion and propellant		
Primary EP thruster	ArianeGroup RIT-2X (RF ion), 1+1 cold-redundant	Table 7.4.2
Thrust	120 mN preliminary, T_{80} = 125.0 mN trade metric, ~80 mN at 2.0 kW	Table 7.4.2; Note (e)
PPU input limit	2.5 kW	Table 7.4.2
Specific impulse	3000 s capability; 2450 s (lower bound) used for xenon mass sizing	Section 7.4
Xenon propellant mass	113.7 kg (supercritical, 20°C / 150 bar, spherical COPV D ≈0.531 m, 10 % ullage, 17.1 kg COPV dry, with 80 kg EP dry allocation)	Table 7.4.2
RCS propellant	LMP–103S green monopropellant; 226.98 kg loaded (Chemical/RCS line), 82.90 kg dry hardware	Section 8.3.3, Section 7.4

continued on next page

Table 8.16: (continued)

Characteristic	Value	Source / status
Chemical Earth-departure burn	≈0.293 km/s nominal / ≈0.366 km/s design	Table 5.8, Section 7.4
Astrodynamic characteristics		
Target body	NEA (25143) Itokawa, S-type	Table 5.9
Dynamical model	Heliocentric, ECLIPJ2000 (Sun, Earth, Itokawa)	Table 5.9
Post-escape characteristic energy	C_3 = 6 km^2/s^2 ($v_{\infty,\oplus}$ = 2.45 km/s); 5 km^2/s^2 low-energy alt. (v_∞ = 2.24 km/s)	Table 5.8, Table 5.15
Outbound ion ΔV	≈3.10 km/s (incl. Itokawa rendezvous, $v_\infty \approx 0$)	Table 5.8
Return ion ΔV	0.608 km/s nominal / 0.760 km/s (+25 % margin)	Table 5.9
Main ion ΔV total	3.71 km/s nominal / 3.86 km/s design	Section 5.7
Cruise TCM allocation	15 m/s (Monte Carlo p95, outbound + return)	Table 5.7
Earth-arrival condition	$v_{\infty,\oplus}$ = 6.566 km/s, entry speed ≈12.878 km/s at **125** km	Table 5.9
Bus Earth-avoidance divert	≈34.7 m/s (500 km miss distance)	SRC Section 6
Attitude and pointing		
Pointing control accuracy	0.008° per axis	REQ-ADCS-DER-01
Pointing knowledge accuracy	0.005° (≈18 arcsec) required, ∼9.4 arcsec worst-case (1σ RSS) achieved	Section 7.6.2
Determination suite	3× ASTRO APS star trackers (triad) + 2× Astrix NS FOG IMU + 6× Bradford coarse Sun sensors + payload-in-the-loop optical nav	Table 7.35
Actuators	4× Bradford W18-class reaction wheels (skewed pyramid) + RCS desaturation	Section 7.6.3
TT&C, data and memory		
Frequency band / antennas	X-band, HGA / MGA / LGA-A / LGA-B; HGA gain 36 dBi (Hayabusa heritage)	Section 7.2
Downlink data rate	≥8 kbps (requirement), 32 kbps achieved in proximity Comms Mode (HGA)	REQ-TELE-01, Section 4.4
Uplink data rate	320 bps	REQ-TELE-03
Link margin requirement	≥+3 dB at max Itokawa-Earth range, closed margin +3 dB	REQ-TELE-02
System noise temperature	T_{sys} = 260 K, FSPL-only model	ASS-TTC-01, ASS-TTC-02
On-board computer	Hot/cold-redundant GR712RC (LEON3FT) pair, 1-FT; MIL-STD-1553B platform bus, SpaceWire payload bus	Figure 7.3.2
Solid-state recorder capacity	64 Gbit	Figure 7.3.2
Observation campaign data volume	∼15 Gbit (∼1.9 GB), store-and-forward	Chapter 6, REQ-CDH-01
C & DH mass / power / volume	9.00 kg / 30 W / 8.10 L	8.13
Electrical power system		
Solar array	GaAs triple-junction, BOL η = 28 %; total deployed area 38 m^2, two rigid panels 19 m^2 each	Section 7.7 (Eq. 7.31)
Array sizing distance	2.0 AU worst case	Section 7.7
Battery	Li-ion, 28 V bus, 30 % DoD; eclipse 389 W × 8 h; C_{batt} ≈487.5 Ah	Table 7.48
EPS hardware mass	≈152 kg	Table 8.10, Section 7.7
Design life	∼4 years	ASS-EPS-05
Coverage and visiting frequency (proximity ops)		
Proximity stations	Home 20 km / Mapping 6 km / Siting 500 m / Sampling 0 m	Section 4.4
Global surface coverage	7 sub-spacecraft latitude stations (equator, ±30°, ±60°, both poles); SPC shape model + multispectral + thermal-inertia map	Section 4.4
Observation cadence / visiting frequency	Itokawa rotation ∼12.1 h sweeps surface; ≥42 rotation periods in Sensing Mode (≈508 h, ∼21 d); mapping stage 48 d total	Section 4.4
Detailed reconnaissance	10 candidate sites (≈392 h, ∼16 d total)	Section 4.4
Final sampling sites	6 sites selected	Section 4.4
Ground segment and launcher		
Mission Operations Centre	ESA ESOC, Darmstadt (DE)	Section 4.4.5
Science Operations Centre	ESA ESAC, Madrid (ES)	Section 4.4.5
Tracking network	ESA ESTRACK (20 m X-band dishes) + DSN augmentation over 1140-d arc	Section 4.3, Section 8.2
Sample recovery site	Woomera Test Range (WPA), South Australia, Category V containment	Section 4.4.5

continued on next page

Table 8.16: (continued)

Characteristic	Value	Source / status
Launcher	Ariane 62, rideshare-compatible, allocation 1300 kg / 8.8 m^3, launch readiness 17/06/2036	REQ-STK-08/09, Section 8.3.3
Decommissioning, disposal and SRC		
End-of-life disposal	Heliocentric, non-Earth-intersecting disposal trajectory, full passivation (vent propellant lines, drain batteries, RF off), ~7 d	Phase 9, Table 5.9
Debris compliance	ESA SDMR (ESSB-ST-U-007), no LEO phase, conventional decay not a driver	REQ-STK-10
Sample Return Capsule	46.0 kg, 0.811 m, 60° sphere-cone, PICA TPS, spin-stabilised release 15 rpm, recovered at Woomera	SRC Section 6, ASS-SRC-01
SRC design entry velocity	12.878 km/s (C_D = 1.5) at 120 km interface, FPA −7.6° (corridor $\|\gamma_E\|$ = 7.4–7.8°), peak flux 854–899 W/cm^2 (nominal ~877)	Table 6.26

8.5. Return on Investment

Silicon Shepherd carries an ESA Cost at Completion (CaC) cap of 205 M€, excluding the Ariane 62 launch and the partner-provided payload (Section 8.2). Stripping the 20% contingency and 10% management reserve appropriate to this design maturity gives an executable budget $C_{\text{exec}} \approx 205/(1.20 \cdot 1.10) \approx 155$ M€, dominated by the spacecraft bus (~55–70% of C_{exec}). The direct operational cost (cruise, proximity operations, and return-and-recovery across the ~1,140-day post-escape phase) is a smaller, explicitly retained CBS line (Section 8.2). As a single-flight demonstrator with no series production, the production cost reduces to the one flight unit already inside the CaC. For such a mission the conventional definition

$$\text{RoI} = \frac{\text{Revenue} - \text{Cost}}{\text{Cost}} \tag{8.1}$$

only makes sense if "Revenue" is read as value delivered rather than income: the mission sells nothing and returns a science-sized sample. Two value channels are therefore analysed here: the direct financial return from the returned material (Section 8.5.1), and the strategic return from advancing autonomous space biomining from the laboratory to a flight-qualified capability (Section 8.5.2).

8.5.1. Direct Financial Return

The ≥ 5 g reference-regolith return is valued at CI-chondrite grade, $c_{\text{REE}} \approx 2.51$ ppm summed over the lanthanides, with the inter-element split also taken from CI-chondrite abundances [162]. Itokawa is an LL-chondrite, for which CI abundances are the standard first-order proxy [16]. The contained REE mass is

$$m_{\text{REE}} = 5\,\text{g} \times 2.51 \times 10^{-6} = 1.26 \times 10^{-5}\,\text{g}. \tag{8.2}$$

This mass is apportioned to the individual species by their CI fractions, then valued. However, REE commodity prices are quoted per kilogram of the traded *oxide* (Nd_2O_3, Pr_6O_{11}, and so on), not per kilogram of the pure metal. Each element mass is therefore converted to its oxide mass through the stoichiometric factor k (oxide molar mass divided by the contained element mass) before the price is applied. Table 8.17 carries this out for the six priced species the mission returns, one more than the REQ-MIS-13 minimum of five, at 2024-average prices from the USGS Mineral Commodity Summaries [4, 163].

Table 8.17: Commodity value of the six priced REE species in the 5 g reference return, at CI-chondrite grade [162] and 2024-average oxide prices [4, 163]. Element mass is converted to the traded oxide form via the stoichiometric factor k; prices are per kg of oxide. Praseodymium is the only price not listed by USGS and is taken from Argus.

Species	CI [ppm]	k	Element [g]	Oxide [g]	Price [US$/kg]	Value [US$]
Nd	0.457	1.166	2.28×10^{-6}	2.67×10^{-6}	56	1.49×10^{-7}
Pr	0.0928	1.208	4.64×10^{-7}	5.61×10^{-7}	56	3.14×10^{-8}
Dy	0.246	1.148	1.23×10^{-6}	1.41×10^{-6}	260	3.67×10^{-7}
Tb	0.0361	1.176	1.81×10^{-7}	2.12×10^{-7}	810	1.72×10^{-7}
Eu	0.0563	1.158	2.82×10^{-7}	3.26×10^{-7}	27	8.80×10^{-9}
Ce	0.613	1.228	3.07×10^{-6}	3.77×10^{-6}	1	3.77×10^{-9}
Total						7.3×10^{-7}

The summed value is $\sim 7.3\times10^{-7}$ USD, or $\sim 6\times10^{-7}$ € at the June 2026 rate of ~ 1.15 USD/€. The remaining low-value lanthanides (La, Sm, Y) sell at comparable single-dollar oxide prices and do not change the order of magnitude. Following that, treating the entire 5 g as 50×-enriched product (Section 6.1), reaches only $\sim 3\times10^{-5}$ €. The return is worth at most a few tens of microeuros. With no units sold, Equation 8.1 collapses to

$$\mathrm{RoI}_{\mathrm{financial}} = \frac{V_{\mathrm{REE}} - C_{\mathrm{CaC}}}{C_{\mathrm{CaC}}} = \frac{\sim 1\times10^{-5}\,€ - 205\,\mathrm{M}€}{205\,\mathrm{M}€} \approx -100\%. \tag{8.3}$$

This is the expected result for the sample-return class, not a flaw in the design. OSIRIS-REx returned ~ 120 g of Bennu regolith and Stardust ~ 1 mg of cometary dust, each against costs of order 10^8-10^9 US$, and the commodity value of either is indistinguishable from zero against its cost [164, 32]. The value of these missions has never been the mass they bring home. Silicon Shepherd's real return is the first in-situ bioleaching dataset from real asteroidal regolith in deep space, which has no commercial comparator and is the subject of the next section.

8.5.2. Strategic and Technology-Lineage Return

Market context. The global REE market was about 4 bn US$ in 2024 and is projected to reach 6-10 bn US$ by 2030-2035 at roughly 8.6-8.7% CAGR [165, 166]. The asteroid-mining market is far less settled: forecasts run from about 2 bn US$ today to 5-11 bn US$ by the mid-2030s, at CAGRs anywhere from 16-23% [167, 168]. That spread is the informative part: the demand is there, and what limits the sector is capability.

The deliverable is TRL advance. Silicon Shepherd moves the biomining and LMCOOL chain from TRL 4-5 at launch toward TRL 6-7. TRL 6, a model demonstrated in a relevant environment [169], is the maturity ESA generally expects before committing a concept to implementation. Its value is risk retirement: GAO assessments identify technology immaturity at programme inception as among the strongest predictors of cost growth and schedule slip [170]. The capability matures along a clear lineage:

Figure 8.5: Technology lineage. Each step scoped its successor; Silicon Shepherd extends the chain from crew-tended LEO to autonomous deep space [8, 3].

ESA strategic fit. ESA's Space Resources Strategy prioritises in-situ resource utilisation and early European positions [171]. Silicon Shepherd would be the first mission to carry biomining hardware into deep space, and its COSPAR Category V containment architecture (Section 12.6.4) demonstrates the planetary-protection readiness that any biological resource-return programme must inherit. This places it alongside ESA's existing demonstrators: neither Hera (~363 M€) [155] nor the F-class Comet Interceptor [31] generates revenue, and both are funded for the capability they prove rather than the product they sell.

The strategic return, therefore, relies on whether a follow-up mission actually flies. Silicon Shepherd does not approach break-even and is not meant to. The economics of any successor depend on feedstock grade and tonne-scale throughput, both of which sit outside this mission's scope and are flagged TBD, together with the launch learning curve and the follow-on unit cost. What this mission removes from that future ledger is process risk.

9
Verification, Validation & Compliance

Verification and validation (V&V) together ensure that the system is designed, built, and integrated such that it both meets its requirements and fulfils the Silicon Shepherd mission objectives. Verification confirms conformance to the formulated requirements, whereas validation confirms that the integrated system performs the mission and satisfies the stakeholder needs. This chapter defines the V&V approach, the resulting system verification plan, and consolidates the outcome in the compliance assessment of Section 9.2 against the current Phase 0 baseline.

9.1. Verification & Validation

Verification and Validation (V&V) ensures the system is designed, manufactured, and assembled correctly and adheres to specifications such that it fulfils the Silicon Shepherd mission objectives. Verification checks system compliance with formulated requirements during design and testing, while validation confirms the system's ability to successfully perform the mission and fulfil stakeholder requirements as intended.

In this chapter, V&V procedures to be followed throughout the design of the system are defined and preliminarily quantified, with the V&V approach and outline first defined in Section 9.1.1. The core methodology for V&V is then given in subsections 9.1.2 and 9.1.3. As simulation will be heavily employed for the dynamic and autonomous parts of the mission, it is treated within the broader Analysis category rather than as a stand-alone method.

9.1.1. V&V Approach

The V&V approach follows the systems engineering V-model. The main verification methods are **Analysis (Ana)**, **Review of Design (RoD)**, **Inspection (Insp)**, and **Test**. Analysis is used for budgets and models such as the ΔV budget, power budget, mass budget, thermal modelling, link-budget calculations, and structural load estimates. RoD is used when compliance can be demonstrated by checking design documentation, such as when a system-level requirement is met by the selected subsystem architecture. Inspection is used for physical system checks and compliance checks against external constraints, such as launcher compatibility, cost limits, planetary protection, and biosafety requirements. Testing is planned for later design and MAI stages, once representative hardware exists, and includes activities such as functional testing, vibration testing, thermal-vacuum testing, and biological containment testing. Although simulation is listed separately as **Sim** in the tables, it is considered part of the broader Analysis category because it is used to evaluate dynamic behaviour, such as autonomous operations, proximity navigation, attitude control, and collision avoidance. In the validation plan, **Demo** refers to post-mission demonstration using flight results or returned-sample analysis. This distinction is important because most spacecraft functions can be verified before launch, while the actual biomining performance and returned-sample science objectives can only be validated after mission completion.

At the current stage of design, V&V procedures have primarily been performed on the requirements derived from stakeholder needs, with the resulting per-requirement methods and Phase 0 compliance status consolidated in Table 9.1.

9.1.2. System Verification

Software V&V Plan

Mission software will be verified through unit tests of custom code modules. Third-party tools are not verified directly, but mission-script outputs will be checked against analytical or literature reference cases. No mission-critical software has been completed yet, so testing is deferred to the next design phase.

Unit tests results Verification testing of the code so far has combined white-box and black-box testing. In the white-box stage, an AI coding assistant (Qwen3-coder:30b [172]) was used to inspect the code's logic, where identified errors were then corrected and the outputs rechecked. In the black-box stage, unit tests exercise

each function against a known reference, typically handwritten calculations, worked examples from the lecture material, or cases confirmed with external experts.

9.1.3. Requirement Verification

Table 9.1 sets out the requirement verification plan: for each requirement it states the verification method and the planned activity. The methods are Analysis (Ana), Simulation (Sim), Review of Design (RoD), Inspection (Insp) and Test, assigned according to the nature of the requirement. The table additionally carries a per-requirement compliance **Check** against the current Phase 0 baseline, so that the verification plan and the compliance matrix are consolidated into a single listing rather than duplicating the requirement set across two tables. The grading scheme behind the Check column, and the resulting compliance assessment, are presented in Section 9.2.

Table 9.1: Combined verification plan and compliance matrix for the Silicon Shepherd mission, assessed against the Phase 0 baseline. Section reference locates the supporting analysis.

Req ID	Requirement	Method	Description	Check
Stakeholder				
REQ-STK-01	The mission shall demonstrate space-based microbial biomining of REEs and/or PGEs.	Ana + Test	Demonstrate end-to-end bioleaching of REEs/PGEs from regolith simulant under representative conditions.	C (§6.1)
REQ-STK-02	The mission shall operate autonomously.	Sim + Test	Test nominal and contingency autonomy cases, including safe mode, comms loss, and proximity ops.	C (§12.5)
REQ-STK-03	The mission shall operate on a NEA.	RoD	Review mission and trajectory design confirming operations at the target NEA.	C (§5)
REQ-STK-04	The mission shall return processed and unprocessed asteroidal material to Earth.	Ana + Test	Trace the return chain; test capture, transfer, and sealing of processed and unprocessed material.	C (§6.5)
REQ-STK-05	The mission shall characterise the target asteroid's surface morphology and composition.	Ana + RoD	Review the remote sensing suite against the morphology and composition objectives.	C (§6.4)
REQ-STK-06	The mission shall enable a comparative analysis of the energetic cost of extracted elements to terrestrial extraction methods.	Analysis	Analyse the energetic cost of the demonstrated extraction against representative terrestrial methods.	C (§11.3)
REQ-STK-07	The mission shall comply with the ESA F-class cost cap of €205 M, excluding launch.	Insp	Review bottom-up cost sum against ESA F-class constraints.	PC (§8.2)
REQ-STK-08	The mission shall be launched on Ariane 62 in compliance with the Ariane 62 User's Manual.	Insp	Review mechanical & electrical interfaces.	C (§5.2)
REQ-STK-09	The mission shall comply with the ESA F-class development schedule, with a launch readiness date by **17/06/2036**.	Insp	Review schedule against ESA milestones.	C (§3.2)
REQ-STK-10	The spacecraft shall comply with the ESA Space Debris Mitigation Requirements (ESSB-ST-U-007).	Insp + Test	Perform compliance assessment against the ESA-SDMR.	C (§11.2)
REQ-STK-11	The mission shall comply with COSPAR planetary protection requirements applicable to Category V restricted Earth-return missions.	Insp + Test	Review planetary protection docs and validate sterilisation.	C (§6.5)
REQ-STK-12	The mission shall integrate the TU Delft LMC_{OOL} as one of the primary sensor elements of the culture HMS.	Insp + Test	Integrate LMC_{OOL} and perform functional system tests.	C (§6.2)
REQ-STK-13	The selected microbial culture shall pose no biological risk to ground operators during integration, testing, and launch operations.	Test	Validate biological containment and perform hazard assessment for ground ops.	C (§6.1)
REQ-STK-14	The architecture shall demonstrate a credible scalability pathway to higher-throughput implementation.	Analysis	Analyse how bioreactor throughput, power, and mass scale to a higher capacity.	C (§11.3)
Mission				

Continued on next page

Table 9.1 – *Continued from previous page*

Req ID	Requirement	Method	Description	Check
REQ-MIS-01	The mission shall conduct REE/PGE extraction from asteroidal regolith in microgravity conditions.	Ana + Test	Analyse and test bioleaching under simulated microgravity.	C (§6.1)
REQ-MIS-02	The mission shall enable scientific activities on Itokawa.	Insp + RoD	Review integrated science instruments against objectives and perform tests during ORR, FRR.	C (§6.4)
REQ-MIS-03	Mission progress shall be monitored continuously by ground operations.	Insp + RoD	Inspect telemetry system and housekeeping data.	C (§7.2)
REQ-MIS-04	The mission shall enable autonomous operations.	Sim + Test	Test autonomous control under nominal/contingency scenarios.	C (§7.3)
REQ-MIS-05	Biomining telemetry shall be monitored in real time.	Insp + RoD	Review bioreactor health monitoring interface.	C (§6.2)
REQ-MIS-06	The mission propulsion shall enable the outbound and inbound cruise from Earth to Itokawa.	Analysis	Design full trajectory; compute ΔV budget with margins.	C (§5.8)
REQ-MIS-07	The spacecraft shall be navigated throughout the course of the mission.	Ana + RoD	Review navigation concepts/accuracies against trajectory targets.	C (§7.6)
REQ-MIS-08	The spacecraft shall demonstrate structural and functional reliability in the asteroid proximity environment.	Ana + Test	Conduct subsystem environmental tests; analyse structural/functional performance. Environmental test campaign per the MAIP (Section 3.3).	C (§7.1)
REQ-MIS-09	The mission shall ensure spacecraft protection against micro-ejecta and electrostatic dust.	Ana + RoD	Analyse Itokawa dust data; review shielding and mitigation strategies.	C (§7.1)
REQ-MIS-10	The mission shall operate safely in the near-surface environment of Itokawa.	Ana + Sim	Model near-surface gravity; simulate proximity ops and collision avoidance.	C (§6.3)
REQ-MIS-11	The mission shall perform pre-sampling characterisation of the surface of Itokawa.	RoD	Review the AFC/SMC cameras, PALT/LRF, VNIRS, and TIRS for asteroid characterisation.	C (§6.4)
REQ-MIS-12	The returned samples shall contain at least 5 distinct REEs.	Ana + RoD	Analyse expected REE speciation in the leachate against the five-element target; review the assay/curation plan.	C (§6.1)
REQ-MIS-13	The mission shall return $\geq$5 g of processed and unprocessed asteroid regolith to Earth.	Ana + Test	Analyse sample capacity/mass; test capture and retention.	C (§6.3)
REQ-MIS-14	The mission shall ensure mass compatibility with the Ariane 62 launcher.	Analysis	Verify payload & spacecraft mass against Ariane 62 capacity.	PC (§8.2)
REQ-MIS-15	The mission shall ensure volume compatibility with the Ariane 62 launcher.	Insp + RoD	Verify spacecraft volume against Ariane 62 fairing and rideshare allocation.	C (§8.2)
REQ-MIS-16	The bioreactor containment system shall prevent any release of biological material to the asteroid environment under all credible failure modes.	Ana + Test + RoD	Analyse, test, and review all containment failure modes; containment continuity verified at the payload integration gate (Section 3.3).	C (§6.1)
REQ-MIS-17	The cell culture health shall be continuously monitored during bioprocessing operations.	Insp	Review culture health sensors and monitoring chain.	C (§6.2)
REQ-MIS-18	The selected microbial culture shall be classified at BSL-1.	Insp	Organism selection reviewed by ESA safety officer.	C (§6.1)
System				
REQ-SYS-01	The spacecraft shall have a final launch mass of $M_{\text{launch}} \leq 1300\,\text{kg}$.	RoD	Verify the system mass budget against the 1300 kg launch-mass cap (including margin).	C (§8.2)
REQ-SYS-02	In stowed configuration, the spacecraft shall occupy a volume of $V_{\text{stowed}} \leq 8.8\,\text{m}^3$.	Insp + RoD	Check the stowed envelope against the $8.8\,\text{m}^3$ volume allocation (including margin).	C (§8.2)
REQ-SYS-03	The system shall enable interfacing between all subsystems of the spacecraft.	RoD	Review the inter-subsystem data, power, and mechanical interfaces against the system architecture, closed by CDH requirements.	C (§7.3)

Continued on next page

Table 9.1 – *Continued from previous page*

Req ID	Requirement	Method	Description	Check
REQ-SYS-04	The system shall be capable of performing a sample-return mission to and proximity operations at asteroid 25143 Itokawa.	RoD	Review the integrated mission, trajectory, and proximity-operations design against the sample-return objective at Itokawa.	C (§5)
REQ-SYS-05	The system shall enable the fulfilment of the mission's science objectives.	RoD	Closed by REQ-PAY-01 to 04 and the BIO, HMS, RSI & SRC requirements.	C (§6)
REQ-SYS-06	The system shall perform satisfactory thermal management to enable mission operations.	RoD	Closed by REQ-TCS-01 to 05 & REQ-TCS-DER-01 to 07.	C (§7.5)
REQ-SYS-07	The system shall enable transmission and reception of data by the spacecraft from and to Earth.	RoD	Closed by TT&C requirements.	C (§7.2)
Payload				
REQ-PAY-01	The payload shall contain a spent-medium bioreactor.	RoD	Review bioreactor type, volume, and mass in payload design.	C (§6.1)
REQ-PAY-02	The payload shall enable asteroidal characterisation.	Ana + RoD	Analyse instrument FOV, resolution, and SNR against objectives.	C (§6.4)
REQ-PAY-03	The payload shall include a sample return mechanism.	RoD + Test	Review return mechanism design; test capture, containment, and seal functions at the SRC mate (Section 3.3).	C (§6.3)
REQ-PAY-04	The payload shall only contain microorganisms classified at BSL-1.	Insp	Organism selection reviewed by ESA safety officer.	C (§6.1)
Bioreactor				
REQ-BIO-01	The bioreactor shall ensure the *P. simplicissimum* are kept dormant until phase 6 of the mission.	Ana + Test	Analyse storage conditions; demonstrate dormancy and revival under transit simulation.	C (§6.1)
REQ-BIO-02	The bioreactor shall germinate the dormant *P. simplicissimum* to start phase 6 of the mission.	Test	Demonstrate controlled germination/activation of the dormant culture.	C (§6.1)
REQ-BIO-03	The bioreactor shall implement a closed, contamination-controlled fluid and gas exchange system.	Insp + Test	Review fluid/gas design; test leaks/barriers; inspect interfaces at the payload leak- and sterility-verification gate (Section 3.3).	C (§6.1)
REQ-BIO-04	The bioreactor shall sustain microbe activity for the duration of bioprocessing operations.	Ana + Test	Model viability against environment; run full-duration ground bioreactor demo.	C (§6.1)
REQ-BIO-05	The bioleaching process shall achieve a REE/PGE enrichment factor of ≥50× relative to unprocessed feedstock.	Ana + Test	Test bioleaching enrichment against unprocessed feedstock.	C (§6.1)
REQ-BIO-DER-01	The bioreactor shall maintain a sample flow rate of 5–20 μL/min with ≤100 μL per cycle for LMC_{OOL} operation.	Ana + Test	Verify the sample flow rate and per-cycle volume for LMC_{OOL}. operation.	C (§6.2)
Health Monitoring				
REQ-HMS-01	The health state of the *P. simplicissimum* shall be monitored continuously throughout all active bioreactor phases.	Insp + Test	Review and test continuous health monitoring across active bioreactor phases.	C (§6.2)
REQ-HMS-02	The system shall provide sufficient information on the microorganism state for autonomous C&DH decision-making.	Ana + Test	Verify the health-state data products support autonomous C&DH decision-making.	C (§6.2)
REQ-HMS-03	The cellular integrity of the *P. simplicissimum* shall be monitored primarily using LMC_{OOL} chips.	RoD + Test	Review and test cellular-integrity monitoring using the LMC_{OOL} chips.	C (§6.2)
REQ-HMS-04	The system shall detect and assess potential indications of life in asteroid samples using LMC_{OOL} chips.	Test	Test life-marker detection sensitivity of the LMC_{OOL} chips on representative samples.	C (§6.2)
REQ-HMS-05	The system shall provide information on the containment status of the microorganism.	Insp + Test	Verify containment-status sensing and reporting.	C (§6.2)

Continued on next page

Table 9.1 – *Continued from previous page*

Req ID	Requirement	Method	Description	Check
REQ-HMS-06	The system shall characterise the effects of prolonged cosmic radiation exposure on the microorganism.	Ana + Test	Analyse and test the microorganism response to prolonged cosmic-radiation exposure.	PC (§6.2)
REQ-HMS-07	The system shall implement redundancy for all instruments including LMC_{OOL} chips to ensure data reliability.	RoD	Review the redundancy architecture for all health-monitoring instruments.	C (§6.2)
Remote Sensing				
REQ-RSI-01	The remote sensing suite shall provide a morphology characterisation of Itokawa's surface accurate to 1 m.	Ana + Sim	Analyse the AFC pixel scale and SPC shape-model accuracy at the mapping altitude.	C (§6.4)
REQ-RSI-02	The remote sensing suite shall provide grain-size magnitude on Itokawa's surface down to 5×5 m patches.	Analysis	Analyse the TIRS thermal-inertia resolution and regional grain-size discrimination.	C (§6.4)
REQ-RSI-03	The remote sensing suite shall measure relative surface phosphate abundance from the 10.3 μm P–O band.	Ana + Test	Analyse TIRS SNR and band depth at 10.3 μm; perform calibration tests.	C (§6.4)
REQ-RSI-04	The remote sensing suite shall measure relative surface carbonate abundance from the 3.4 μm band.	Ana + Test	Analyse VNIRS SNR and band depth at 3.4 μm; perform calibration tests.	C (§6.4)
Sample Return Capsule				
REQ-SRC-01	The SRC shall tolerate acceleration $\geq 40 g_0$.	Ana + Test	Analyse and test the SRC structure under the design acceleration.	C (§6.5)
REQ-SRC-02	The SRC shall tolerate heating from a re-entry velocity of 12.9 km/s.	Ana + RoD	Analyse entry heating, size the heat shield, and review heritage. Heat-shield qualification by similarity to Stardust/OSIRIS-REx per the long-lead plan (Table 3.1).	C (§6.5)
REQ-SRC-03	The SRC shall have a touch-down speed ≤5 m/s.	Analysis	Size the descent system and compute touchdown velocity.	C (§6.5)
REQ-SRC-04	The SRC shall return ≥5 g of processed and unprocessed asteroidal material to Earth.	Ana + RoD	Analyse sample capacity/mass; review Hayabusa2/OSIRIS-REx heritage.	C (§6.5)
Power				
REQ-EPS-01	The EPS shall provide continuous, uninterrupted power to all spacecraft subsystems throughout all operational modes for the full mission lifetime.	Analysis	Compute the power budget across all operational modes against EPS generation and storage capacity.	C (§7.7)
REQ-EPS-02	The solar arrays shall deliver sufficient power at 1.7 AU EOL to sustain simultaneously ion propulsion and spacecraft housekeeping operations with a 20% system margin.	Analysis	Compute EOL array output at 1.7 AU against the combined propulsion and housekeeping demand including the 20% margin.	C (§7.7)
REQ-EPS-03	The battery shall sustain safe mode operations for a minimum of 2 h following launch, prior to solar array deployment and power generation.	Ana + Test	Analyse battery capacity against the 2 h safe-mode load; confirm by discharge test.	C (§7.7)
REQ-EPS-04	Battery depth of discharge shall not exceed 30% in any operational scenario to preserve cycle life and maintain adequate contingency capacity.	Analysis	Verify the depth of discharge against the 30% limit across all operational load cases.	C (§7.7)
REQ-EPS-05	The EPS shall accommodate the full throttle range of the ion propulsion system.	Insp + Test	Review EPS monitoring/telemetry and the command interface with C&DH.	C (§7.7)
REQ-EPS-06	The main power bus shall be regulated at 28 V, whilst a dedicated high-voltage bus shall be provided to the PPU to support propulsion requirements.	Insp + RoD	Review the bus architecture and inspect the regulated 28 V and dedicated high-voltage PPU rails.	C (§7.7)
Propulsion				

Continued on next page

Table 9.1 – *Continued from previous page*

Req ID	Requirement	Method	Description	Check
REQ-PROP-01	The propulsion shall generate a $\Delta V \geq 3800\,\mathrm{m/s}$ with the primary ion thruster.	Analysis	Compute ΔV budget from trajectory including 25% margin; size propellant via Tsiolkovsky.	C (§5.8)
REQ-PROP-02	The propulsion subsystem shall provide necessary thrust for transit.	Analysis	Analyse thruster I_{sp} and thrust against burn durations and timeline.	C (§7.4)
REQ-PROP-04	The propulsion subsystem shall provide thrust between **80** and **120** mN during cruise.	Ana + Test	Define cruise thrust range; confirm thruster range via functional test.	C (§7.4)
REQ-PROP-DER-01	The ion propulsion PPU shall accept a variable input across the range 500–9000 W and shall not demand more than 3000 W for the ion propulsion.	Ana + RoD	Review the PPU input-power range and verify ion-propulsion power draw against the EPS interface across the throttle profile.	PC (§7.4)
REQ-PROP-DER-02	The propulsion subsystem shall be capable of operating across a throttle range consistent with array power varying between ~4000 W at 1.7 AU EOL and ~12.1 kW at 1 AU BOL.	Analysis	Analyse the thruster throttle range against the array-power envelope from 1.7 AU EOL to 1 AU BOL.	C (§7.4)
ADCS				
REQ-ADCS-01	The ADCS shall generate a $\Delta V \geq 600\,\mathrm{m/s}$ with the RCS.	Analysis	Compute RCS ΔV budget against proximity operations and manoeuvre needs.	C (§7.6)
REQ-ADCS-02	The ADCS subsystem shall provide 3-axis stabilisation.	Ana + Sim	Analyse actuator/sensor layout; simulate 3-axis control authority.	C (§7.6)
REQ-ADCS-03	The RCS thrusters shall be positioned to produce no disturbance torques during the main chemical burn.	Analysis	Analyse RCS placement and torque budget during the main burn.	C (§7.6)
REQ-ADCS-DER-01	The ADCS shall provide pointing control $\leq 0.008°$ about each axis during Phase 4.	Ana + Sim	Simulate the GN&C loop in the proximity environment and assess pointing control.	C (§7.6)
REQ-ADCS-DER-02	The ADCS shall provide pointing knowledge of the bus $\leq 0.005°$ during Phase 4.	Ana + Sim	Assess star-tracker attitude knowledge against the reconstruction requirement.	C (§7.6)
REQ-ADCS-DER-03	The ADCS shall provide control jitter $\leq 0.004°/\mathrm{s}$ during Phase 4.	Ana + Sim	Simulate control jitter under proximity disturbances.	C (§7.6)
REQ-ADCS-DER-04	The ADCS shall provide the SRC with 15 RPM.	Ana + Test	Analyse and test the SRC spin-up provision.	C (§6.5)
REQ-ADCS-DER-05	The ADCS shall maintain solar array pointing to within 10° of the sun vector during all cruise and thrust modes.	Ana + Sim	Simulate array-drive and bus pointing to confirm sun-vector tracking within 10° across cruise and thrust modes.	C (§7.6)
Structure				
REQ-STRUC-01.1	The structure shall withstand longitudinal launch loads $\geq 6 g_0$.	Ana + Test	Perform FEM analysis under launch loads; conduct vibration testing per the MAIP environmental campaign (Section 3.3).	C (§7.1)
REQ-STRUC-01.2	The structure shall withstand lateral launch loads $\geq 2 g_0$.	Ana + Test	Perform FEM analysis under launch loads; conduct vibration testing.	C (§7.1)
REQ-STRUC-02	The structure shall be able to provide **TBD** radiation protection for the payload.	Ana + Test	Model radiation in SPENVIS; analyse and test shielding thickness.	PC (§7.1)
REQ-STRUC-05	The structure shall enable compatibility with the payload adapter of the Ariane 62 launcher.	Insp	Review the separation interface against the Ariane 62 payload adapter.	C (§7.1)
REQ-STRUC-DER-01	The primary structure shall provide mounting interfaces for two deployable solar array wings, each with a deployed area of 19 m^2 and mass of no more than ~57 kg per wing.	RoD	Review the primary-structure mounting provisions and mass allocation for the two deployable array wings.	PC (§7.1)

Continued on next page

Table 9.1 – *Continued from previous page*

Req ID	Requirement	Method	Description	Check
REQ-STRUC-DER-02	The spacecraft structure shall accommodate the stowed solar array envelope within the available launch vehicle fairing volume.	Insp	Check the stowed array envelope against the Ariane 62 fairing and rideshare volume allocation.	C (§7.1)
REQ-STRUC-DER-03	The spacecraft structure shall accommodate MLI covering around the whole spacecraft.	Insp	Check the surface area and accommodate the MLI around it.	C (§7.1)
Thermal				
REQ-TCS-01	The TCS shall keep the bioreactor within specified temperature bounds.	Ana + Test	Build TMM for worst-cases; conduct thermal vacuum testing.	C (§7.5)
REQ-TCS-02	The TCS shall keep instruments within specified temperature bounds.	Ana + Test	Compute TMM for instrument zones; conduct TVAC testing.	C (§7.5)
REQ-TCS-03	The growth medium shall remain >0°C in all phases.	Ana + Test	Build TMM; verify the growth medium against its cold limit across all phases.	C (§7.5)
REQ-TCS-04	The battery shall be charged at +10 to +30°C with a 0°C floor.	Analysis	Verify battery thermal limits across charge and worst-case cold cases.	C (§7.5)
REQ-TCS-05	The TCS shall keep the spacecraft bus within specified temperature bounds.	Ana + Test	Worst-case bus thermal model and TVAC verification.	C (§7.5)
REQ-TCS-DER-01	The TCS shall ensure 20°C propellant-tank conditioning.	Analysis	Verify propellant-tank conditioning against the 20°C set point.	C (§7.5)
REQ-TCS-DER-02	The TCS shall ensure the bioreactor operates within the 20–30°C range.	Ana + Test	Verify bioreactor operating temperature by TMM and TVAC test.	C (§7.5)
REQ-TCS-DER-03	The NIRS3 detector must consistently be held at -85°C at all times.	Ana + Test	Model and test the NIRS3 detector radiator chain against its operating-temperature limit.	C (§7.5)
REQ-TCS-DER-04	The MERTIS detector temperature must consistently be held at 20±10°C at all times.	Ana + Test	Verify MERTIS detector-temperature stability and the calibration reference.	C (§7.5)
REQ-TCS-DER-05	The MERTIS detector temperature must consistently be held at 20±10°C, deviating at most by ±10 mC during operations.	Ana + Test	Verify TCS ability to maintain temperature stability in a simulated near-asteroid environment.	C (§7.5)
REQ-TCS-DER-06	The TCS shall provide heat-rejection capacity sufficient to dissipate PPU waste heat across the full throttle input-power range of 500–9000 W.	Ana + Test	Size the PPU radiator and verify waste-heat rejection across the full throttle input range.	PC (§7.5)
REQ-TCS-DER-07	The TCS shall maintain the fermenter at 2 °C to 10 °C during the cruise phase.	Ana + Test	Verify the fermenter cruise-storage temperature by TMM and TVAC test.	C (§7.5)
Telecommunications				
REQ-TELE-01	The mission shall have a downlink data rate of (≥8 kbps) with either the HGA throughout the mission.	Analysis	Compute downlink budget using antenna gain, transmit power, modulation, and path loss.	C (§7.2)
REQ-TELE-02	The TT&C subsystem shall close the downlink with a link margin of at least +3 dB at the maximum Itokawa–Earth range.	Analysis	Compute full link budget: gain, power, path/pointing losses, noise, and coding.	C (§7.2)
REQ-TELE-03	The mission shall have an uplink data rate of 320 bps.	Analysis	Compute uplink budget using ground EIRP, receiver sensitivity, and path loss.	C (§7.2)
Command & Data Handling				
REQ-CDH-01	The C&DH subsystem shall receive and buffer ≥ 16 Gbit of campaign data to the SSR.	Ana + Test	Verify SSR capacity and buffering against the proximity-campaign data volume.	C (§7.3)
REQ-CDH-02	The C&DH subsystem shall enable interfacing between all spacecraft subsystems.	RoD + Test	Review data bus architecture and command/telemetry interfaces to each subsystem; test end-to-end data handling across integrated system.	C (§7.3)
REQ-CDH-DER-01	The C&DH subsystem shall provide command and telemetry interfaces to the PCDU for load switching, fault-protection triggers, and propulsion throttle-level management.	RoD	Review the C&DH–PCDU command and telemetry interface design.	C (§7.3)

Continued on next page

Table 9.1 – *Continued from previous page*

Req ID	Requirement	Method	Description	Check
RAMS				
REQ-RAMS-01	End-to-end mission reliability (returning ≥5 g without containment breach) shall be $R_{mission} \geq 0.75$.	Analysis	Construct the end-to-end reliability model for the return objective.	PC (§12.6)
REQ-RAMS-02	The propulsion subsystem shall have a 1+1 cold-redundant architecture.	RoD	Review the propulsion redundancy architecture.	C (§7.4)
REQ-RAMS-03	The propulsion subsystem shall make use of pyrotechnic isolation valves.	Insp + RoD	Review the propulsion isolation-valve design.	C (§7.4)
REQ-RAMS-04	The C&DH subsystem shall have a 1+1 cold-redundant architecture.	RoD	Review the C&DH redundancy architecture.	C (§7.3)

9.2. Compliance Assessment

The compliance status of every requirement is recorded in the *Check* column of Table 9.1 and assessed against the current Phase 0 baseline. A grade of **C** (Compliant) means the baseline closes the requirement by the cited analysis or review, with any test-based verification deferred to the qualification phase, **PC** (Partially Compliant) flags a defined architecture for which a margin is tight, a value remains TBD, or an internal inconsistency is still open, finally, **NC** (Non-Compliant) denotes a baseline that does not satisfy the requirement. Of the 112 requirements in the matrix, 107 are Compliant, 5 are Partially Compliant, and none are Non-Compliant.

Payload and thermal verification dependent on hardware-level data: Three items are architecturally defined but not yet quantitatively closed: the payload radiation shielding thickness **(REQ-STRUC-02)** is a TBD pending the dose analysis, the characterisation of prolonged galactic-cosmic-ray exposure on the culture **(REQ-HMS-06)** is deferred to dedicated testing under risk ASS-HMS-11, and the MERTIS detector ±10 mK stability **(REQ-TCS-DER-05)**, the tightest thermal requirement in the system, awaits the transient thermal model with modulating VCHP conductance, which is the principal open thermal analysis.

End-to-end mission reliability **(REQ-RAMS-01)**: The reliability of the current Phase 0 baseline is 0.55, short of the 0.75 target. It reaches 0.754 only after the assumed maturation of the space-bioreactor chain to TRL 6 and the LMC_{OOL} instrument to TRL 7 by the planned 2032 production start. As the report identifies this maturation, dominated by the need for an extended-duration microgravity bioreactor demonstration, as a significant programmatic risk, the requirement is graded Partially Compliant on the strength of the maturation plan.

Power, Propulsion, and Thermal PPU Integration **(REQ-STRUC-DER-01, REQ-PROP-DER-01, REQ-TCS-DER-06)**: Three interdependent platform requirements remain Partially Compliant pending further design maturation. Structurally, the mounting provisions and mass allocations for the two deployable solar array wings must be reviewed and finalized **(REQ-STRUC-DER-01)**. For propulsion, the Power Processing Unit (PPU) input-power range must be verified against the EPS interface across the 500–9000 W throttle profile **(REQ-PROP-DER-01)**. Consequently, the Thermal Control System (TCS) must be explicitly sized to ensure sufficient heat-rejection capacity for the PPU waste heat across this variable throttle range **(REQ-TCS-DER-06)**.

10
Design Sensitivity

To establish the feasibility of the Silicon Shepherd architecture prior to the next design phase, a Centralized Monte Carlo simulation (10,000 iterations) was conducted. Unlike isolated subsystem analyses, this coupled model evaluates the integrated system's response to interacting uncertainties to verify applied margins. The analysis focuses on four critical interdependent drivers: (1) **Mass Growth:** System mass margins varied around a nominal 20% against the 1300 kg Ariane 62 rideshare limit. (2) **Trajectory Execution Errors:** Departure ΔV dispersions (±150 m/s) and Flight Path Angle (γ) variations (±0.2°) against the 40 g structural limit of the Sample Return Capsule (SRC). (3) **EPS and Trajectory Coupling:** Solar array degradation (up to 5% variance) and engine throttling against a 3000 W target and 400-day maximum cruise duration. (4) **Microgravity Bioleaching Efficiency:** Payload extraction efficiency varied (50%–75%) against the strict 120-day operational timeline.

10.1. Sensitivity Results Analysis

To evaluate system-level impacts, the Monte Carlo outputs were aggregated into a centralized dashboard (Figure 10.1), detailing architectural vulnerabilities and validations.

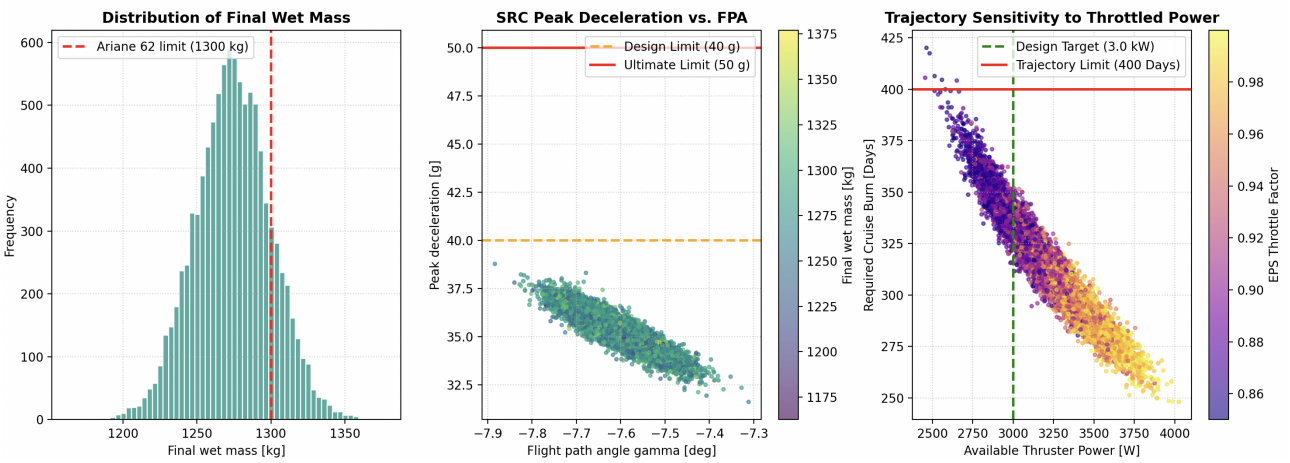

Figure 10.1: Centralized Monte Carlo distribution outputs. Left: Final spacecraft wet mass against the Ariane 62 limit. Center: SRC peak deceleration vs. Flight Path Angle (γ). Right: Trajectory sensitivity mapping available thruster power against required cruise duration.

10.1.1. Mass Sensitivity and SRC Re-entry Dynamics

Because the architecture relies on a staged propulsion strategy, the final wet mass is highly sensitive to dry mass growth via the Tsiolkovsky cascade, as the chemical system must accelerate both the unmargined dry mass and the required electric propellant. As demonstrated in Figure 10.1 (left), compounding dry mass margins push the system over the launch vehicle limit, resulting in a 15.66% probability of launch vehicle rejection under expected uncertainty bounds (mean wet mass: 1273.81 kg). To confidently proceed, a strict mass-reduction campaign must be implemented on the base dry mass to ensure it can absorb a 20% margin without violating the 1300 kg constraint.

Conversely, the return trajectory architecture was stress-tested against the structural limits of the SRC by coupling Itokawa departure ΔV errors with γ navigation uncertainties (Figure 10.1, center). The scatter plot demonstrates a tight, linear clustering of peak decelerations around the 35.2 g nominal baseline. While navigation uncertainties induce a spread in the entry corridor, the steepest simulated angles fail to generate enough aerodynamic drag to threaten the 40 g yield limit, returning a 0.00% probability of structural failure. This extreme robustness proves the heritage-based capsule architecture possesses a massive built-in structural

buffer, validating the design and offering a prime target for future mass-optimization to alleviate the launch mass constraint.

10.1.2. Coupled Power, Trajectory, and Operational Timelines

The stochastic model evaluated the interdependency between electrical degradation and astrodynamics, mapping the non-linear relationship where electrical degradation inversely stretches the fixed ΔV transfer time (Figure 10.1, right). Simulating up to a 5% radiation degradation variance on the 3994 W arrays revealed an 18.85% probability of dropping available thruster power below the 3000 W nominal design point (mean power: 3219.0 W). However, because the thruster is designed to safely throttle down to a 500 W floor, the system seamlessly trades electrical power for burn duration. This confirms an extremely low 0.06% trajectory failure rate against the 400-day maximum cruise envelope (mean duration: 314.0 days), proving the array sizing is highly resilient even under severe off-nominal throttling.

Evaluating the biomining process against the strict 120-day nominal hardware timeline, however, exposed a severe operational vulnerability: a 100.00% probability of schedule failure. The chosen timeline requires a perfect 75% microbial efficiency; any degradation simulated by the microgravity environment (modelled between 50%–75%) inherently extends the required batch processing time. To ensure mission closure, a minimum schedule margin of 60 days must be formally allocated to the proximity operations phase.

10.1.3. Volume and Cost Sensitivities

While mass, power, and schedule act as critical architectural drivers, volume and cost are significantly less sensitive. The fully stowed spacecraft—including the 38 m^2 folded arrays, propulsion tanks, and the MISAR bioreactor—fits comfortably within the 8.8 m^3 Ariane 62 rideshare allocation. Consequently, moderate volumetric growth across internal subsystems can be safely absorbed without risking launch vehicle incompatibility. Similarly, financial sensitivities are buffered by the mission's procurement strategy: payload development is assumed to be subsidized by external scientific stakeholders, and the spacecraft bus heavily leverages high-TRL heritage components. Therefore, technical and schedule robustness remain the definitive priorities for the upcoming design phase.

10.2. Conclusion on Design Robustness

The Centralized Monte Carlo analysis successfully transitioned the design from a deterministic baseline to a robust stochastic model. By evaluating inter-subsystem couplings, the analysis uncovered critical design sensitivities obscured by isolated reviews—specifically the mass cascading effect and the severe rigidity of the biological timeline.

While astrodynamics, re-entry physics, and the decoupled propulsion strategy possess exceptional margins, the system is critically constrained by dry mass growth and possesses zero schedule margin for the biological payload. To safely proceed into the next phase, the following actionable steps must be prioritised:

- **Initiate Mass-Reduction:** The total unmargined dry mass must be optimized to confidently secure the Ariane 62 rideshare slot. The over-engineered SRC presents the primary target for safely shedding parasitic mass.
- **Inject Schedule Margin:** A minimum of 60 days must be added to the nominal 120-day bioleaching timeline, or parallel R&D must be accelerated to stabilize microbial efficiency limits in microgravity.
- **Lock Propulsion Firmware:** Section 10.1.2 demonstrates that the 400-day return trajectory is secured even when EPS degradation forces the system to throttle down to a 500 W hardware floor. However, as identified in the Phase 0 compliance assessment (REQ-TCS-DER-06), PPU heat rejection across this extreme throttle range remains partially compliant. Therefore, the propulsion firmware must enforce a throttle minimum that satisfies both the safe trajectory transit times and the finalized TCS heat-rejection capacity, preventing thermal instability at low-power states while permanently securing the return window.

Provided these corrective actions are implemented, the Silicon Shepherd architecture is validated and conditionally robust for subsequent development.

11
Sustainable Development Strategy

This chapter closes the sustainability case at the detailed design level. Planetary protection, space-debris mitigation, comparative energetic-cost against terrestrial rare-earth-element (REE) extraction, and scalability were inherited at Baseline (REQ-STK-11, REQ-STK-10, REQ-STK-06, REQ-STK-14) and flowed down to nine REQ-SUS-XX.Y verification requirements. The chapter covers the mission's footprint—how sustainability shaped the design (Section 11.1, Section 11.2), and its handprint, how the flight system advances sustainable practice (Section 11.3).

11.1. Designing for Sustainability

A screening-tier life-cycle assessment (LCA) per the ESA LCA Handbook [173] tracks CED, GWP, ADP, and freshwater use. Phase-level energy decomposition confirms baseline results: the Ariane 62 embedded manufacturing-and-launch energy dominates by two to three orders of magnitude over spacecraft-internal contributions. Thus, the most effective sustainability levers lower launched mass and remove process hazards rather than trimming in-flight power.

Three key design decisions were updated. First, electric primary propulsion (the RIT-2X gridded-ion thruster on 110 kg of xenon, Section 7.4) keeps the chemical propellant fraction low, reducing manufacturing burden and allocated launch energy. Second, chemical reaction-control moved from classical hydrazine bipropellant to ADN-based green monopropellant LMP-103S on Bradford ECAPS HPGP thrusters (Section 7.6). LMP-103S is less toxic, insensitive to air/water vapour, and carries PRISMA and SkySat heritage [174, 175], eliminating MMH/MON handling and casualty exposure. Third, the bus primary structure uses CFRP unidirectional-tape facesheets over an aluminium-3003 honeycomb core (Section 7.1). Composite facesheets lower structural mass and launch-energy charge—despite higher embedded manufacturing energy—while the aluminium core retains a mature recycling stream. Remaining subsystems fall below the screening threshold. Per REQ-SUS-14.1, sustainability acted as an explicit 10 % trade-off criterion, driving the electric-primary and green-monopropellant selections.

11.2. Planetary Protection and End-of-Life

Silicon Shepherd is a COSPAR Category V unrestricted Earth-return mission [176]. Targeting an S-type asteroid means only documentary requirements apply outbound. However, self-imposed requirements (REQ-STK-11, REQ-MIS-18b, REQ-MIS-19b, REQ-MIS-23, REQ-MIS-24b) are enforced to comply with the COSPAR rationale (Section 12.6.4). The primary planetary protection constraint governs sample return: returned material must be sterile to preclude contamination. The SRC follows Stardust and OSIRIS-REx heritage (PICA thermal protection, passive entry) and is recovered at Woomera under full Category V handling (Section 6.5).

Debris mitigation (REQ-STK-10) is satisfied via the disposal architecture. Post-SRC release, the bus executes an Earth-avoidance divert onto a stable heliocentric trajectory and passivates (venting lines, isolating batteries, cutting RF power) per ESA guidelines [178]. Because the bus never enters a bound orbit, it places no objects into protected LEO/GEO regions. Returning only the inert SRC to a licensed range bounds on-ground casualty risk well below the 10^{-4} threshold. Table 11.1 summarises closure status.

11.3. Mission Contribution to Sustainability

11.3.1. Comparative Energetic Cost

The comparative energetic-cost analysis (REQ-STK-06) uses a functional unit of $\mathrm{MJ\,kg^{-1}}$ of elemental REE delivered, mirroring the baseline cradle-to-product boundary. On the space side, the launcher dominates: Ariane 62 embedded energy is $\sim 10^7$ MJ, whereas the closed propellant inventory (Section 7.4), cruise, and payload operating energy total 10^4 MJ to 10^6 MJ. Charging full launcher energy to a rideshare represents a strict upper bound, yielding $E_{\mathrm{sys}} \approx 10^7$ MJ.

Table 11.1: Planetary-protection and debris-mitigation closure status against the detailed design (parents REQ-STK-11 and REQ-STK-10).

Obligation	Source	Detailed-design provision	Status
Backward contamination	COSPAR PPP, ECSS-U-ST-20C [177]	In-flight inactivation of the culture, inert return manifest	Closed (arch.)
SRC re-entry survival	COSPAR PPP	PICA TPS, Stardust/OSIRIS-REx heritage, Woomera recovery under Category V handling	By analysis
Bus disposal	ESSB-ST-U-007 [178]	Non-Earth-intersecting heliocentric divert; no insertion into protected LEO/GEO regions	Closed
Passivation	ESSB-ST-U-007 [178]	Propellant lines vented, batteries drained and isolated, RF cut	Closed (concept)
On-ground casualty $\leq 10^{-4}$	ESSB-ST-U-007 [178]	Only the inert SRC reaches ground, at a licensed range, bus never re-enters	By design

Returned elemental REE mass remains the primary uncertainty. Treating the 5 g processed-regolith return at baseline contents of 1 to 10 ppm with the 50× enrichment of REQ-PAY-15 gives $m_{\mathrm{REE}} \approx 0.5\,\mathrm{mg} = 5\times10^{-7}\,\mathrm{kg}$. The demonstration-scale energetic cost is therefore $e_{\mathrm{space}} = \frac{E_{\mathrm{sys}}}{m_{\mathrm{REE}}} \approx \frac{10^{7}\,\mathrm{MJ}}{5\times10^{-7}\,\mathrm{kg}} \approx 2\times10^{13}\,\mathrm{MJ\,kg^{-1}}$-REE, with a 10^{12} to 10^{14} band driven by return yield uncertainty. Compared to terrestrial LCAs—$\sim 10^{3}\,\mathrm{MJ\,kg^{-1}}$ for light REEs [179] and $\sim 10^{5}\,\mathrm{MJ\,kg^{-1}}$ for heavy REEs [180, 181], this is eight to ten orders of magnitude more intensive. This is expected for small sample-returns like OSIRIS-REx and Stardust, whose value was never bulk mass. The figure quantifies the gap the mission begins to close: reaching parity with terrestrial mining requires scaling up to return $\sim 100\,\mathrm{kg}$ of REE per mission.

11.3.2. Scalability Pathway

Scalability (REQ-STK-14) provides the demonstration's sustainability value via three levers that scale the architecture from grams to the hundred-kilogram regime: stacking bioleaching modules to scale reactor capacity without redesign, amortising launch energy across a fleet, and transitioning the return leg toward a partially closed-loop vehicle. While technically feasible, this exceeds the ESA F-class envelope, prompting the demonstration to verify the process at the smallest credible scale. Independent of space-flight economics, the bioreactor and autonomous control loop transfer directly to terrestrial processing of low-grade ores, mine tailings, and electronic waste, currently limited to laboratory scale [40]. Flight-qualifying an unattended reactor directly advances this terrestrial pathway.

11.3.3. Societal and Economic Alignment

The mission aligns with three UN SDGs [182]: SDG 9 (Industry, Innovation, Infrastructure) by maturing closed-loop bioleaching to flight; SDG 12 (Responsible Consumption/Production) by demonstrating an extraction pathway whose terrestrial counterpart generates $\sim 2000\,\mathrm{t}$ of tailings and 1 t to 1.4 t of radioactive waste per tonne of refined REE; and SDG 15 (Life on Land) by displacing terrestrial deforestation and groundwater contamination at the margin. Strategically, it addresses the critical supply concentration driving the EU Critical Raw Materials Act [7], given that 69 % of mined REE output and nearly 90 % of refining capacity sit within a single country. While the financial value of the 5 g reference return is negligible (Section 8.5), the mission delivers the first in-situ bioleaching dataset from real asteroidal regolith in deep space, securing a strategic option for future resource diversification.

12
Technical Risk Assessment

Silicon Shepherd couples flight-proven bus hardware to a biological payload chain with almost no flight heritage, and most of the mission's technical risk originates there. This chapter identifies, scores, and treats those risks. Section 12.1 ties the assessment to the top-level requirements, and Section 12.2 sets the likelihood and severity scales, adapted to span the gap between deep-space heritage and a TRL-5 payload. The technical risk register and its mitigation then drive the residual-risk picture, after which the contingency and FDIR concept defines the reactive response to events that occur anyway. Finally, the RAMS analysis treats reliability, availability, maintainability, and safety.

12.1. Success Criteria

Technical risks are assessed by their impact on mission success criteria. The criteria are listed by domain to ensure direct traceability to top-level requirements, encompassing the payload, bus, and programmatic architectures.

Payload: REQ-MIS-01, REQ-MIS-13, REQ-MIS-21, REQ-PAY-14, REQ-PAY-15, REQ-STK-04, and REQ-STK-05 dictate the nature and primary capabilities derived from the science instruments, the biological extraction phase, and the physical sample return over the mission lifetime.

Spacecraft Bus: Overarching system-level constraints dictate that the platform subsystems must successfully perform deep-space transit, proximity navigation, and Earth-return targeting while maintaining necessary power, thermal, and telemetry margins to ensure payload survivability.

Programmatic & Compliance: REQ-MIS-23, REQ-STK-07, REQ-STK-10, and REQ-STK-11 ensure Silicon Shepherd's adherence to stringent ESA F-class budget constraints, space debris mitigation guidelines, and COSPAR planetary protection mandates.

12.2. Methodology

Risks are characterised by the magnitude and likelihood of separate outcomes. While the evaluation framework follows ESA risk management methodology [183], the likelihood scale is adapted to accommodate the extreme disparity between flight-proven spacecraft heritage and the novel biological payload.

Table 12.1 defines the unified assessment criteria. Likelihood probability brackets are mapped to corresponding Technology Readiness Levels (TRL) to provide accurate differentiation for early-phase architectures, while severity is defined by the extent of the risk's impact upon the overarching payload, bus, and programmatic success criteria.

12.2.1. Risk Index and the Severity 5 Override

The magnitude of a risk is quantified by calculating the risk index: multiplying the numerical severity score ($1 - 5$) by the numerical likelihood score (where A=1, B=2, C=3, D=4, E=5). The resulting risk index dictates the acceptability of the risk (Table 12.2).

Crucially, a severity score of 5 (Catastrophic) acts as a systemic override. Regardless of its mathematical likelihood, any catastrophic risk is immediately elevated to a minimum index of 10 to ensure mandatory technical handling.

Table 12.1: Unified Risk Assessment Criteria: Likelihood (TRL mapped) and Severity Definitions.

Likelihood (L)			Severity (S)		
Sc.	**Prob.**	**TRL & Heritage Mapping**	**Sc.**	**Level**	**System-Level Consequence**
E	> 20%	Unproven concept (TRL 1–3); feasibility unknown in space.	**5**	Catastrophic	Total loss of spacecraft or payload, irrecoverable Cat V safety breach, or project cancellation.
D	10 – 20%	Lab validation only (TRL 4); requires major redesign.	**4**	Critical	Baseline success unmet, loss of major operational subsystem, or severe cost overrun exceeding reserves.
C	2 – 10%	Relevant env. validation (TRL 5); e.g., ISS-tended payloads.	**3**	Major	Loss of secondary science objectives, loss of critical hardware redundancy, or mandatory mission descoping.
B	0.1 – 2%	Flight-proven architecture (TRL 6–8) with minor mods.	**2**	Marginal	Minor operational anomalies or data reductions absorbable within redundant chains and nominal margins.
A	< 0.1%	Extensive deep-space flight heritage (TRL 9) or COTS.	**1**	Negligible	No observable impact on science return, platform operations, budget, or safety.

Table 12.2: Risk Index and Mandatory Handling Strategies.

Index Score	Magnitude & Acceptability	Handling Strategy
20 – 25	**Maximum (Unacceptable)**	Maximum disruption of project plan; maximum threat to project success. Implement new process or change baseline plan.
10 – 16	**High (Unacceptable)**	Large threat to project success. Implement new process or change baseline plan. (Note: All Severity 5 risks default here).
5 – 9	**Medium (Acceptable)**	Some threat to project success. Aggressively manage, consider alternative process.
3 – 4	**Low (Acceptable)**	Little threat to project success. Some management actions necessary.
1 – 2	**Minimum (Acceptable)**	No threat to project success. Current approach is sufficient.

12.3. Technical Risk Register

Table 12.3 centralizes the overarching system-level threats and the functional failures associated with the Silicon Shepherd mission.

Table 12.3: Unmitigated System Technical Risk Register.

ID	Risk Event	Cause	Consequence	L	S	Idx
Payload						
PAY-01	Radiation microbial death	Insufficient shielding against deep-space radiation during transit.	Total loss of biological payload viability.	D	5	20
PAY-02	Regolith toxicity	Unknown asteroid regolith is toxic to the selected microbe.	Fails to reach the ≥ 50× REE enrichment target.	D	4	16
PAY-03	Reduced bio-leaching yield	Space environment lacks convective mixing for nutrient transport.	Significant degradation of enrichment yield or diversity.	D	3	12
PAY-04	Microbial mutation	Deep-space radiation induces detrimental mutations in strain.	Strain loses bio-leaching efficiency or becomes non-viable.	C	4	12
PAY-05	Extreme Solar Particle Event	Unexpected massive solar flare exceeding F-class shielding.	Acute radiation sterilization of the biological payload.	A	5	5*
PAY-06	Payload integration failure	Automated transfer mechanism fails to move regolith into bioreactor.	Inability to begin the primary science operations phase.	D	5	20
PAY-07	LMC_{00L} clogging	Asteroid particulates bypass physical filters and enter micro-channels.	Loss of real-time microbe monitoring and telemetry.	C	4	12
PAY-08	Bioreactor mechanical failure	Internal stirring or fluid loop fails during continuous operation.	Inability to maintain homogeneous bio-leaching environment.	C	4	12
PAY-09	Target mineral non-detection	TIRS fails to resolve 10.3 μm phosphate absorption band.	Inability to locate host minerals, preventing collection.	C	4	12

PAY-10	Microgravity Drift	Long-duration exposure to space radiation and microgravity de-calibrates the solid-state ion sensors.	False or missed detection of metal ion concentrations, compromising Tier 2 culture state assessment.	C	3	9
PAY-11	Thermal-Inertia Mis-calculation	S-type asteroid thermal inertia models fail to accurately map to the targeted 0.5-5 mm grain size.	Selection of an incompatible sampling site, jamming the pneumatic feed with oversized blocks.	C	4	12
Spacecraft Bus						
BUS-01	Asteroid collision	Sensor failure or unmapped local debris field during descent.	Severe damage or total loss of the spacecraft.	C	5	15
BUS-02	TCS failure during eclipse	Primary heater circuits fail to maintain payload bay temps.	Culture enters unplanned dormancy, draining batteries.	C	3	9
BUS-03	Optical suite occlusion	Chemical RCS thruster exhaust kicks up abrasive regolith dust.	Complete loss of navigation visibility and site mapping.	D	4	16
BUS-04	Chemical RCS valve degradation	Deep-space exposure induces thermal breakdown in propellant lines.	Loss of critical control authority prior to asteroid arrival.	C	5	15
BUS-05	X-band link degradation	Radiation degrades the primary X-band transponder over lifetime.	Severe degradation of telemetry and command budgets.	C	4	12
BUS-06	Solar Array Deployment Jamming	Mechanical hinges fail to lock symmetrically post-launch.	Critical power deficit prevents bioreactor thermal regulation.	C	5	15
BUS-07	Xenon Supercritical Phase Transition	Localised heater underperformance or MLI degradation drops the COPV temperature below 16.6°C.	Xenon drops into a two-phase regime, causing fluid slosh, CoM shifts, and severe ADCS instability.	C	4	12
BUS-08	Array Degradation via Plume Impingement	Uncharacterised ion impingement from the RIT-2X thrusters onto the solar array surfaces over multi-year burns.	Accelerated degradation of the GaAs cells, reducing EOL power below the 466.8 W required.	C	4	12
BUS-09	VCHP Cold-Lockout Failure	The Ammonia Variable Conductance Heat Pipe fails to properly lock out during cold-cruise or safe mode.	Unintended parasitic heat leak to the OSR radiator, overwhelming survival heaters and draining the battery.	C	4	12
BUS-10	Honeycomb Core Delamination	Acoustic and vibrational loads from Ariane 62 ascent exceed the facing-to-core adhesive peel strength.	Structural yielding of the primary vertical walls, potentially compromising the payload envelope.	B	5	10*
Programmatic & Compliance						
PRG-01	ERC impact containment breach	Structural yield exceeded or crush pads fail during hard landing.	Biosphere exposure to unsterilised asteroidal material.	B	5	10*
PRG-02	Payload Contamination	Inadequate pre-launch sterilization allows Earth microbes to survive.	Rogue microbes outcompete the bio-mining strain.	A	5	5*
PRG-03	EOL disposal failure	Spacecraft fails to execute deflection manoeuvrer or vent propellants.	Uncontrolled s/c becomes a long-term orbital debris hazard.	B	4	8
PRG-04	Project cost overrun > 15%	Underestimation of complex bioreactor space-qualification costs.	Exceeds ESA F-class budget cap of 205M€.	D	4	16

12.4. Mitigation Strategies and Residual Risk

To ensure mission viability, proactive mitigation strategies are implemented to reduce the likelihood or severity of unacceptable outcomes. Table 12.5 outlines how the highest-impact drivers are reduced to acceptable levels.

Table 12.5: Risk Mitigation, Derived Requirements, and Residual Risk.

ID	Detailed Mitigation Strategy	Owner	L	S	Idx
PAY-01	Incorporate radiation shielding sized to the mission environment.	Thermal & Rad Chief	A	5	5*
PAY-02	Conduct extensive laboratory tests using simulated regolith.	Bio Engineering Chief	B	4	8
PAY-05	Accepted as residual hazard to optimize system mass parameters.	Thermal & Rad Chief	A	5	5*
PAY-06	Execute rigorous vacuum life-testing of the transfer mechanism.	Structures Chief	A	5	5*
PAY-11	Design sampling head for versatile grain capture; utilize radiometric ground observations prior to arrival.	Payload Chief	B	4	8
BUS-01	FDIR cross-checks LiDAR altitude with WAC stereoscopic ranging.	Astro-dynamics Chief	A	5	5*
BUS-02	Implement cold redundancy for critical payload heater circuits.	Thermal Chief	A	3	3
BUS-03	Integrate mechanical dust covers on optics and sequence RCS pulses.	Bio Engineering Chief	B	4	8

BUS-04	Redundant active heater chains along RCS lines with latch valves.	Propulsion Chief	A	5	5*
BUS-06	Utilise single-fault tolerant hinge mechanisms from heritage platforms.	Structures Chief	A	5	5*
BUS-07	Redundant localised COPV patch heaters and passive MLI tenting to guarantee > 16.6°C threshold and use of anti-sloshing tank to reduce perturbations.	Thermal Chief	A	4	4
BUS-08	Optimize RIT-2X thruster cant angle and integrate localized plume shields on solar array yokes.	Propulsion Chief	A	4	4
BUS-09	Implement a parallel cold-biased survival heater loop on the VCHP.	Thermal Chief	B	4	8
BUS-10	Perform rigorous acoustic/vibration testing on a structural qualification model with oversized potting.	Structures Chief	A	5	5*
PRG-01	Dual ground-commandable heat and chemical sterilization loops.	Payload Chief	A	5	5*
PRG-02	Minimum likelihood achieved via cleanroom integration. Accepted.	Bio Engineering Chief	A	5	5*
PRG-03	Allocate dedicated ΔV margin strictly for EOL disposal.	Propulsion Chief	A	4	4
PRG-04	Implement strict design-to-cost (DTC) philosophy, utilizing heritage bus components and establishing clear descoping paths.	Project Manager	B	4	8

12.4.1. Risk Visualization

To visualise the technical risk landscape, a side-by-side heat map profile maps the identified elements before and after engineering controls. The background gradient computes the mathematical multiplication constraint spanning from a base score of 1 to a maximum index threshold of 25.

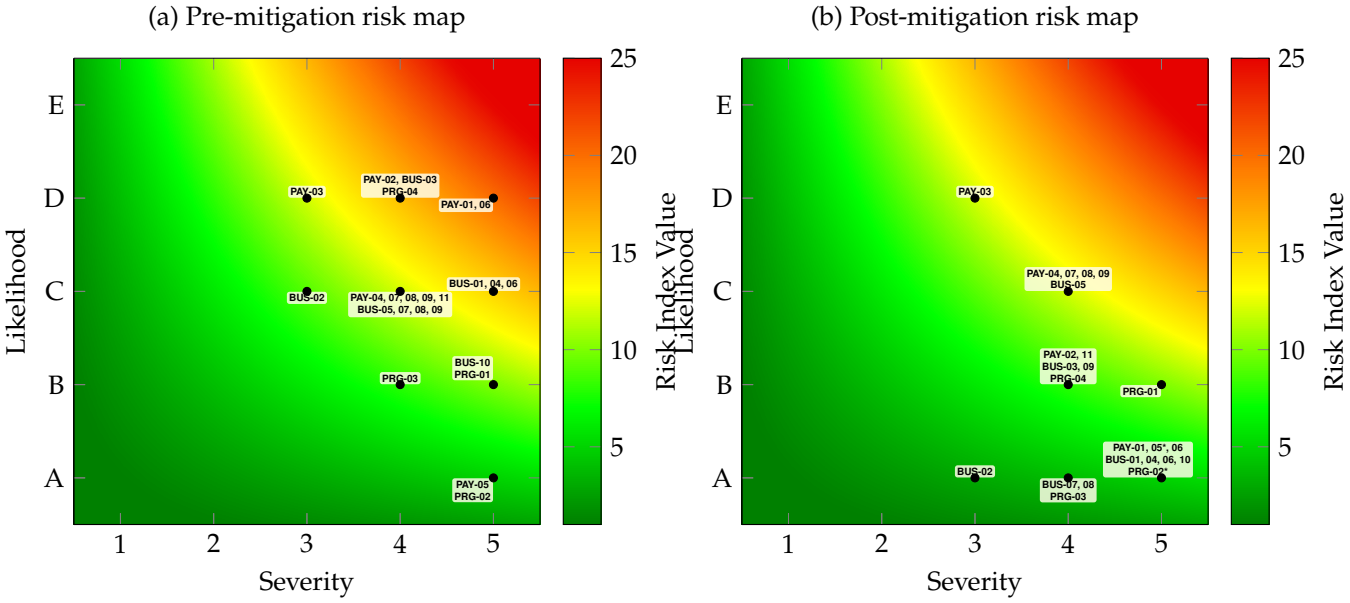

Figure 12.1: Comparative Pre- and Post-Mitigation Technical Risk Heat Maps reflecting the direct evaluation of the multiplication index. Asterisks (*) denote Severity 5 accepted overrides.

The comparative visualization illustrates a systemic mitigation flow driving the core vehicle vulnerabilities toward the acceptable operational green zones. Initial profiles highlight a dense concentration of subsystem hazards within critical regions ($S \geq 4$), stemming directly from proximity trajectory dynamics and the low baseline maturity of unrefined mechanical transfer components. By verifying autonomous cross-strapping along the chemical RCS lines and assigning isolated backup heater loops, the final operational profile pushes the critical mission nodes cleanly toward the minimum likelihood boundary. Environmental elements beyond physical spacecraft protection architectures, such as the catastrophic Carrington-class particle flare event (PAY-05), are explicitly isolated and maintained as accepted residual indices to optimise system mass parameters.

12.5. Contingency and FDIR Concept

Contingency planning provides the reactive system-level response to hazardous events that manifest despite planned mitigations. This section utilizes the Generic Architecture for FDIR Engineering (GAFE) methodology to translate feared events into trigger-isolate-recover sequences.

12.5.1. Contingency Margins and Reserved Buffers

A strict distinction is drawn between sizing margins (which absorb estimation uncertainty) and contingency reserves (locked buffers held against off-nominal events).

Table 12.7: Baseline contingency reserves, additional to nominal sizing margins.

Resource	Reserve	Released for	Basis
Propellant (ΔV)	25%	TAG aborts, site diversion, EOL (PAY-09, PAY-11, BUS-01, PRG-03)	[2, 14]
Battery DoD	ops capped at 80% nominal	Heater override, safe-mode (BUS-02, BUS-07, BUS-09)	[147]
Array generation	15% oversize	Array degradation, load shed (BUS-08)	[2]
Thermal	single-fault-tolerant heater chain	Primary/VCHP heater loss (BUS-02, BUS-07, BUS-09)	TCS-REQ-003
Bio consumables	≥1 re-inoculation + 1 buffer flush	Microbial death/toxicity (PAY-01, PAY-02)	[8]
ADCS hardware	4-of-3 Wheel pyramid + fall-back	Wheel wear / Momentum management	[147]
TT&C hardware	HGA + cross-strapped LGAs	HGA failure (BUS-05)	[14]
Navigation	2× Star tracker + IMU + Sun sensor	Tracker blinding / Dust occlusion (BUS-03)	[184]
Containment	Two commandable sterilisation paths	Loss-of-containment (PRG-01)	[185]

12.5.2. Contingency Action Plan

Table 12.8 maps the highest-priority residual risks to a trigger-isolate-recover sequence.

Table 12.8: Contingency Action Plan based on Hardware FDIR logic.

ID	Detection	Reserve Consumed	Isolate & Recover	Owner
PAY-01	LMC_{00L} biomarker viability drops.	Spare microbial culture.	Suspend leaching, flush loop, re-inoculate fermenter.	Bio Eng. Chief
PAY-02	Fluid pH or oxygen levels out-of-bounds.	Sterile buffer fluid.	Stop feed, flush reactor with buffer fluid and retry.	Bio Eng. Chief
PAY-05	DSN solar weather alert & viability loss.	N/A (Unrecoverable).	Abandon bioleaching. Repurpose to purely return regolith.	Project Manager
PAY-08	Flow-meter registers zero flow in loop.	Backup fluid pump.	Isolate primary pump, activate redundant pump.	Bio Eng. Chief
PAY-09	TIRS fails to detect 10.3 μm phosphate.	ΔV reserve.	OBC autonomous TAG abort, propulsive divert to backup site.	Propulsion Chief
PAY-11	WAC imagery identifies oversized grains.	ΔV margin & Safe mode.	Autonomous TAG abort during descent; divert to backup site.	Astro-dynamics
BUS-01	LiDAR/WAC divergence limit exceeded.	ΔV margin and safe mode.	Abort descent, fire retreat thrusters, hold Sun-pointing.	Astro-dynamics
BUS-02	Payload bay temp drops suddenly.	Backup heater & battery.	OBC sheds non-essentials, powers secondary heater.	Thermal Chief
BUS-03	Brightness drop across NAC/WAC sensors.	Inertial drift fallback.	Command cover override, switch baseline to IMU/Star Trackers.	Payload Chief
BUS-04	Pressure drop in chemical RCS lines.	Backup latch valves.	Isolate leaking branch, re-route via cross-strap.	Propulsion Chief
BUS-05	X-band carrier signal strength drops.	Backup LGA antenna.	Fallback to secondary transponder, switch to LGA.	Electronics Chief

BUS-07	COPV thermistors drop below 17°C.	Battery reserve.	Load shed non-essentials, force-activate secondary patch heaters, anti-sloshing tank reduces total calibration needed by ADCS.	Thermal Chief & ADCS Chief
BUS-08	Array power generation drops off nominal curve.	15% Array oversize.	Ground-commanded load shedding and re-optimized thrust schedule.	EPS Chief
BUS-09	VCHP temperature drops during eclipse.	Survival heater margin.	Trigger secondary survival heaters to overcome parasitic heat leak.	Thermal Chief
PRG-01	Sensors indicate ERC structural breach.	Active sterilization paths.	Command dual heat/chemical sterilization loops.	Payload Chief

12.6. RAMS

This section establishes a detailed analysis of Reliability, Availability, Maintainability, and Safety treatment for the Silicon Shepherd.

12.6.1. Reliability

The numerical reliability target of mission succes is defined:

> **REQ-RAMS-01:** The end-to-end mission reliability, defined as the probability of returning $\geq 5\,\text{g}$ of processed asteroidal material to Earth without containment breach, shall be $R_{\text{mission}} \geq 0.75$.

This target is calibrated against the historical record of deep-space sample-return missions rather than ECSS allocation tables, because no published mission-level reliability allocation exists in this class. Of the five flown deep-space sample-return missions to date, three (Stardust, Hayabusa2, OSIRIS-REx) returned samples successfully, one (Hayabusa) returned samples after multiple severe in-flight failures, and one (Genesis) suffered a parachute-deployment failure with partial sample loss [13, 186, 105]. The raw historical success rate is therefore ~ 0.8 for the heritage sample-return architecture alone, before accounting for the additional novelty of an autonomous biological payload chain at TRL 5. A target of 0.75 reflects this base rate with a small allowance for planned TRL maturation of the payload chain between PDR and launch.

To determine reliabilities of different system phases, either heritage is taken, or reliability is estimated using TRL to reliability mapping by Nasa, as shown in Table 12.9. For component estimation, parallel redundancies are calculated via $R_{\text{parallel}} = 1 - (1 - r)^n$, while series components are evaluated as $R_{\text{series}} = \prod_{i=1}^{n} r_i$.

Table 12.9: NASA TRL to Estimated Reliability Mapping for Small Satellites

Technology Readiness Level (TRL)	Description	Est. Reliability Range
TRL 1	Basic principles observed	0.4
TRL 2	Technology concept formulated	0.5
TRL 3	Experimental proof-of-concept	0.6
TRL 4	Component validated in lab / functional verification	0.7
TRL 5	Component validated in relevant environment	0.8
TRL 6	System/subsystem demonstrated in relevant environment	0.89
TRL 7	System prototype in operational environment	0.95
TRL 8	System flight-qualified through test and demonstration	0.97
TRL 9	Actual system flight-proven through mission operations	0.99

First, the reliabilities as they stand at current phase 0 are taken and the reliabilities determined, as shown in Table 12.10 and Table 12.11:

The mission logic is decomposed into seven phases. Series logic is taken conservatively, as no quantitative redundancy between phases exist. For bus components, heritage reliabilities are assigned from small-spacecraft busses [1]. For both rendezvous and proximity operation a of TRL 8 is assigned, TRL 9 for sampling and transfer, as the technology used is proven by the TAGSAM mechanism on OSIRIS-REX [21]. The bioleaching payload (MISAR and HMS) are modelled by the technologies used in series: electrodialysis in space (TRL 9)[187], microbe culture herding (TRL 5)[3], fluid handling in space (TRL 9)[188] and 2 LMC_{OOL} (TRL 4) in parralel. LMC_{OOL}, which refers here to the combination of technologies used on the LMC_{OOL} chip, has been

Table 12.10: Pre maturation reliability allocation

Phase	Critical chain	r basis	$R_{\mathbf{ph}}$
Launch & sep.	Ariane 62 + sep. mech.	Heritage	0.97
Bus (cruise)	EPS, TT&C, OBC, ADCS	Heritage (0.90-0.95)	0.93
RPO	ADCS+GN&C, prop., nav.	TRL 8 · TRL 8	0.95
Sampling	Sampler · transfer	TRL 9 · TRL 9	0.98
Bioleach.	MISAR Bioreactor & HMS	TRL 9·5·9·(4)×2	0.713
Remote sens.	Instrument suite	TRL 8	0.97
SRC re-entry	SRC TPS, parachute, crumple	H2/O-REx	0.93
Product			**0.55**

Table 12.11: Post maturation reliability allocation

Phase	Critical chain	r basis	$R_{\mathbf{ph}}$
Launch & sep.	Ariane 62 + sep. mech.	Heritage	0.97
Bus (cruise)	EPS, TT&C, OBC, ADCS	Heritage (0.90-0.95)	0.95
RPO	ADCS+GN&C, prop., nav.	TRL 9, $r = 0.98$	0.98
Sampling	Sampler · transfer	TRL 9 · TRL 9	0.98
Bioleach.	MISAR Bioreactor & HMS	TRL 9·6·9·(7)×2	0.87
Remote sens.	Instrument suite	TRL 9	0.99
SRC re-entry	SRC TPS, parachute, crumple	H2/O-REx/TW-3	0.99
Product			**0.754**

conservatively assigned TRL 4, as it is only validated in a lab. A case could be made for TRL 5 since it has been tested under relavent environment (microgravity, vacuum), but this was in a controlled setting. Bioreactor technology was assigned TRL 5 since the critical functions are shown by BioRock and BioAsteroid, but they are different systems than the MISAR instrument. The **0.55** system reliability falls short of the **0.75** requirement, necessitating a technological maturation analysis prior to production in May 2032.

Technological maturation Technological maturation is required to comply with **REQ-RAMS-01**. With time, bus reliability is expected to improve to 0.95. By 2032 Tianwen-3 [189] and MMX[184] are expected to complete their sample acquisition missions, hence the TRL of rendezvous & proximity ops is expected to improve, reaching 9. By the maturation of the sensing suite outlined in Section 6.4.5, it is considered to improve to TRL 9, and so is the SRC with the Tianwen-3 [189] and MXX [184] missions.

The main driver of the low reliability is the bioleaching payload, consisting of the MISAR instrument and HMS. LMC_{OOL} technology is expected to mature to at least TRL 7-8. As the launch window of Silicon Shepherd overlaps with the LMC_{OOL}'s planned inclusion on a cube-sat mission, maturing the technology to TRL 8. Conservatively, a TRL of 7 is selected. The reliability without improveming the bioreactor technology is 0.67. Specifically, testing a *P.simplicissimum* packed-bed reactor for >120 days in microgravity would achieve TRL 6, satisfying the 0.75 target.

Maturing space bioreactors requires extended microgravity testing achievable only in space. Given the system's mass (Table 6.5) and the ISS's planned deorbit [190], this could prove a significant challenge. The scientific community must prioritise these experiments for the mission to be completed, or plan them for post-ISS space stations. Conversely, Silicon Shepherd offers a flight-proving opportunity for space bioreactors and LMC_{OOL}, accelerating LMC_{OOL} to TRL 9 ahead of ESA's L4 Enceladus mission [191].

With maturation of LMC_{OOL} and space bioreactor technology, the reliability requirement **REQ-RAMS-01** is feasible. Adding redundancies in other phases than the HMS is considered unfavourable, as this would add significant weight. To improve reliability further, for increased chance of mission succes, more effort should be taken to mature the technologies utilised.

12.6.2. Availability

For a one-shot deep-space mission, availability is not a continuous service metric but applies at the specific moments when a critical function is needed. Five such moments dominate Silicon Shepherd: sample collection (TAG maneuvre of 20 minutes) the bioleaching at the asteroid (continuous bioreactor operation for 105 days), Deep Space Network passes (scheduled), and the Earth-return capsule release (a single narrow window). A fourth critical moment is the Touch-and-Go sampling operation, which concerns proximity dynamics,

dust exposure, and regolith-transfer readiness. Availability across all four moments is backed by single or double-fault-tolerant hardware as detailed in the safety-critical functions of Section 12.6.4

12.6.3. Maintainability

No physical maintenance is possible after launch. Maintainability for Silicon Shepherd, therefore, reduces to two mechanisms: the spacecraft's ability to recover from faults autonomously, fully covered by the FDIR architecture and contingency reserves established in the baseline[1], and the ability to correct software faults via ground uplink. In accordance with deep-space mission operational practice, all on-board software memory shall be patchable via ground command through the MOC, ensuring corrective software maintenance capability throughout the mission lifetime.

12.6.4. Safety

Safety is of primary concern for the Silicon Shepherd mission. Silicon Shepherd is a COSPAR Category V unrestricted Earth-return mission. Because S-type asteroids lack indigenous life [176], outbound Phase I applies with no formal requirements. However, biosafety requirements are enforced to comply with the COSPAR rationale: *The Earth must be protected from extraterrestrial matter carried by returning spacecraft (backward planetary protection)* [176]. The requirements put in place are shown in Table 12.12:

ID	Requirement
REQ-STIK-11	The mission shall comply with COSPAR planetary protection requirements.
REQ-MIS-18b	In case of deposition of biological material on the asteroidal environment through failure modes, documentation of extend and nature of contamination shall be made and shared with space science community.
REQ-MIS-19b	The bioreactor shall prevent deposition of life microbes on the return sample
REQ-MIS-23	The selected microbial culture shall be classified at BSL-1.
REQ-MIS-24b	The sample return capsule shall prevent release of biological material under all credible failure modes.

Table 12.12: Biosafety requirements for the SILICON:SHEPHERD mission

Additional to the biosafety requirements by Cospar, the mission has to oblige by ESA debris mitigation [**ESSB-ST-U-007**]. Table 12.13 lists the functions whose failure produces either biosafety requirements breach or a launcher/debris non-compliance event, each with an allocated fault-tolerance level and a heritage anchor.

Table 12.13: Safety-critical functions and allocated fault tolerance. FT = fault tolerance; 1-FT = single-fault tolerant.

Function	Failure consequence	FT	Mitigation	Heritage anchor
Alicanto disintegration on Itokawa	Contamination of space body	1-FT	Documentation of asteroid operations	No heritage with life microbes
Containment at sample transfer interface	Internal contamination, science loss	1-FT	Hermetic transfer mechanism, backup feed path	Baseline O-02 mitig.
Sample return capsule structural integrity at reentry	REQ-MIS-24b breach	2-FT	Passive crumple zone + heat shield + sealed canister (Genesis-informed)	Hayabusa2/OSIRIS-REx SRC [2, 186]
Parachute deployment	SRC hard impact, possible breach	1-FT	Redundant initiators; crumple zone tolerates non-deployment	Genesis lesson [105]
End-of-life spacecraft disposal	Long-term debris, NEA-pop. contam.	1-FT	Heliocentric divert with margin; passive disposal as fallback	OSIRIS-REx APEX precedent

A 2-FT approach for sample return capsule structural integrity prevents an irrecoverable REQ-MIS-24b breach. This fits F-class constraints because COSPAR planetary protection (derived from the Outer Space Treaty) applies regardless of mission class [185], and the mitigation requires no novel hardware or significant mass penalty. Mission-critical functions whose failure ends the mission but causes no safety event (propulsion, ADCS, TT&C, etc.) are instead held to single-fault tolerance (1-FT), accepting one failure with degraded but recoverable consequences, consistent with the failure-tolerance philosophy of Baseline. The mission therefore adopts a two-tier redundancy posture: 2-FT for containment-critical functions, 1-FT for mission-critical functions.

References

[1] Roy et al. Cavalini. *SILICON SHEPHERD: BASELINE REPORT*. AE3200 Design Synthesis Exercise, Group 03. TU Delft, 2026.

[2] Takeshi Oshima, Fuyuto Terui, and Yuichi Tsuda. "Chapter 3 - Spacecraft system design of Hayabusa2". In: *Hayabusa2 Asteroid Sample Return Mission*. Ed. by Masatoshi Hirabayashi and Yuichi Tsuda. Elsevier, 2022, pp. 25–48. DOI: 10.1016/B978-0-323-99731-7.00003-9.

[3] Rosa et al. Santomartino. "Microbial biomining from asteroidal material onboard the international space station". In: *npj Microgravity* 12.1 (2026). DOI: 10.1038/s41526-026-00567-3.

[4] U.S. Geological Survey. *Mineral Commodity Summaries 2025*. Tech. rep. USGS, 2025. DOI: 10.3133/mcs2025.

[5] International Energy Agency. *Global Critical Minerals Outlook 2025*. Tech. rep. IEA, 2025.

[6] European Court of Auditors. *Special Report 04/2026: Critical Raw Materials for the Energy Transition*. Tech. rep. European Court of Auditors, 2026.

[7] European Parliament and Council. *Regulation (EU) 2024/1252 establishing a framework for ensuring a secure and sustainable supply of critical raw materials*. Official Journal of the European Union. 2024.

[8] C. S. et al. Cockell. "Space station biomining experiment demonstrates rare earth element extraction in microgravity and Mars gravity". In: *Nature Communications* 11.1 (2020), p. 5523. DOI: 10.1038/s41467-020-19276-w.

[9] Ismar Borges De Lima and Walter Leal Filho, eds. *Rare Earths Industry: Technological, Economic, and Environmental Implications*. Elsevier, 2016. DOI: 10.1016/C2014-0-01863-1.

[10] Milan Grohol and Constanze Veeh. *Study on the Critical Raw Materials for the EU 2023 – Final Report*. Tech. rep. European Commission, 2023. DOI: 10.2873/725585.

[11] R. Santomartino, L. Zea, and C. S. Cockell. "The smallest space miners: principles of space biomining". In: *Extremophiles* 26.1 (2022), p. 7.

[12] A. Schippers et al. "Biomining: Metal Recovery from Ores with Microorganisms". In: *Geobiotechnology I*. Vol. 141. Advances in Biotechnology. Springer, 2013, pp. 1–47.

[13] Yuichi Tsuda et al. "Hayabusa2 mission status: Landing, roving and cratering on asteroid Ryugu". In: *Acta Astronautica* 171 (2020), pp. 42–54. DOI: 10.1016/j.actaastro.2020.02.035.

[14] D. S. et al. Lauretta. "OSIRIS-REx: Sample Return from Asteroid (101955) Bennu". In: *Space Science Reviews* 212.1-2 (2017), pp. 925–984. DOI: 10.1007/s11214-017-0405-1.

[15] Ghislaine Crozaz and Ernst Zinner. "Ion probe determinations of the rare earth concentrations of individual meteoritic phosphate grains". In: *Earth and Planetary Science Letters* 73.1 (1985), pp. 41–52. DOI: 10.1016/0012-821x(85)90033-0.

[16] M. et al. Ebihara. "Chemical and mineralogical compositions of two grains recovered from asteroid Itokawa". In: *Meteoritics & Planetary Science* 50.2 (2015), pp. 243–254. DOI: 10.1111/maps.12418.

[17] ECSS. *Space Engineering – Verification*. Tech. rep. ECSS-E-ST-10-02C Rev.1. ECSS, 2018.

[18] European Space Agency. *ESA F2 ARRAKIHS Phase 2 Report*. Public Release v0.9.2. ESA, 2023. URL: https://www.cosmos.esa.int/documents/7423467/7423486/ESA-F2-ARRAKIHS-Phase-2-PUBLIC-v0.9.2.pdf.

[19] Agnieszka Krakos. "Lab-on-chip technologies for space research—current trends and prospects". In: *Microchimica Acta* 191.1 (2024), p. 31. DOI: 10.1007/s00604-023-06084-4.

[20] R. W. et al. Gaskell. "Characterizing and Navigating Small Bodies with Imaging Data". In: *Meteoritics & Planetary Science* 43.6 (2008), pp. 1049–1061. DOI: 10.1111.

[21] CEOS EOPortal Directory. *OSIRIS-REx*. Committee on Earth Observation Satellites (CEOS), 2024. URL: https://directory.eoportal.org/satellite-missions/osiris-rex.

[22] "INVESTIGATION ON THE INITIATION OF CULTURES OF PENICILLIUM SPP AND THEIR RESPONSE TO THE PRESENCE IN THE CULTURE MEDIUM OF VARIOUS CONCENTRATIONS OF BORAX". In: *Analele Universităţii din Oradea, Fascicula Protecţia Mediului* XVIII (2012). ISSN: 1224-6255. DOI: 10.5555/20133214121.

[23] Alireza Esmaeili et al. “Simultaneous leaching of Cu, Al, and Ni from computer printed circuit boards using Penicillium simplicissimum”. In: *Resources, Conservation and Recycling* 177 (2022), p. 105976. ISSN: 0921-3449. DOI: 10.1016/j.resconrec.2021.105976.

[24] Kerry A. Trumble et al. “Postflight Aerothermal Analysis of the Stardust Sample Return Capsule”. In: *Journal of Spacecraft and Rockets* 47.5 (2010), pp. 765–774. DOI: 10.2514/1.41514.

[25] Robert A. et al. Williams. “OSIRIS-REx Entry, Descent, and Landing Performance”. In: *AIAA SCITECH 2025 Forum*. AIAA, 2025. DOI: 10.2514/6.2025-2424.

[26] JAXA/ISAS. *Hayabusa2 Reentry Capsule Recovery Operations, Woomera*.

[27] Arianespace. *Ariane 6 User’s Manual*. Issue 2, Revision 0. Arianespace. 2021.

[28] ESA. *Ariel: Spacecraft*. 2020.

[29] Matthew M. Knight. *Comet Interceptor Team Telecon*. Presentation to the Small Bodies Assessment Group. June 2019.

[30] s. Bayon and I. Roma. *CDF STUDY REPORT: COMET INTERCEPTOR Assessment of Mission to Intercept a Long Period Comet or Interplanetary Object*. Tech. rep. ESA, 2019. URL: https://sci.esa.int/documents/34923/36148/CometInterceptor_CDF_Study_Report.pdf.

[31] G. H. et al. Jones. “The Comet Interceptor Mission”. In: *Space Science Reviews* 220.9 (2024). DOI: 10.1007/s11214-023-01035-0.

[32] Jet Propulsion Laboratory and National Aeronautics and Space Administration. *Stardust Sample Return Press Kit*. Press Kit. NASA Jet Propulsion Laboratory, Jan. 2006. URL: https://www.jpl.nasa.gov/news/press_kits/stardust-return.pdf.

[33] Zahra et al. Ghasemi Monfared. “Effect of particle irregularity and particle size distribution on the morphology of packed beds”. In: *Scientific Reports* 15 (2025), p. 15086. DOI: 10.1038/s41598-025-99495-7.

[34] Air Liquide. *Gasflessen en frames*. Air Liquide, 2026. URL: https://nl.airliquide.com/levering/gasflessen-en-frames.

[35] Aamer Ali et al. “Membrane technology in renewable-energy-driven desalination”. In: *Renewable and Sustainable Energy Reviews* 81 (2018), pp. 1–21. ISSN: 1364-0321. DOI: 10.1016/j.rser.2017.07.047.

[36] Roy et al. Cavalini. *SILICON SHEPHERD: MIDTERM REPORT*. AE3200 Design Synthesis Exercise, Group 03. TU Delft, 2026.

[37] P. et al. Rasoulnia. “Fungal leaching of valuable metals from a power plant residual ash using *Penicillium simplicissimum*”. In: *Waste Management* 52 (2016), pp. 309–317.

[38] G. Andrews. “Fluidized-bed bioreactors”. In: *Biotechnology and Genetic Engineering Reviews* 6.1 (1988), pp. 151–178. DOI: 10.1080/02648725.1988.10647847.

[39] M. et al. Kuure-Kinsey. “Modeling and predictive control of a rotating disk bioreactor”. In: *Proceedings of the American Control Conference* 5 (2005), 3259–3264 vol. 5. DOI: 10.1109/ACC.2005.1470474.

[40] Claire-Marie et al. Loudon. “BioRock: new experiments and hardware to investigate microbe–mineral interactions in space”. In: *International Journal of Astrobiology* 17 (2018), pp. 303–313. DOI: 10.1017/S1473550417000234.

[41] M et al. Taghavi. “The international space station packed bed reactor experiment: capillary effects in gas-liquid two-phase flows”. In: *npj Microgravity* 9.55 (2023). DOI: 10.1038/s41526-023-00302-2.

[42] J. N. Warnock, K. Bratch, and M. Al-Rubeai. “Packed Bed Bioreactors”. In: *Bioreactors for Tissue Engineering*. Springer, 2005, pp. 87–113. DOI: 10.1007/1-4020-3741-4_4.

[43] Monika et al. Grzegorczyk. “The effect of lyophilization and storage time on the survival rate and hydrolytic activity of Trichoderma strains”. In: *Folia Microbiologica* 63.4 (July 2018), pp. 433–441. ISSN: 1874-9356. DOI: 10.1007/s12223-017-0581-0.

[44] Patrick Gervais, Jean-Philippe Fasquel, and Paul Molin. “Water relations of spore germination”. In: *Applied Microbiology and Biotechnology* 29 (Jan. 1988), pp. 586–592. DOI: 10.1007/BF00260989.

[45] Richard Fike. “Nutrient Supplementation Strategies for Biopharmaceutical Production Part 1: Identifying a Formulation”. In: *BioProcess International* 7 (2008).

[46] Mohammad et al. Jafari. “Acidophilic bioleaching: A Review on the Process and Effect of Organic–inorganic Reagents and Materials on its Efficiency”. In: *Mineral Processing and Extractive Metallurgy Review* 40.2 (2018), pp. 87–107. DOI: 10.1080/08827508.2018.1481063.

[47] Muling Sheng et al. "A Review of the Application of Oxalic Acid in Hydrometallurgical Processes". In: *Separations* 13.2 (2026). ISSN: 2297-8739. DOI: 10.3390/separations13020066.

[48] Ruberlan Gomes Silva et al. "Selective Precipitation of High-Quality Rare Earth Oxalates or Carbonates from a Purified Sulfuric Liquor Containing Soluble Impurities". In: *Mining, Metallurgy & Exploration* 36.5 (Oct. 2019), pp. 967–977. ISSN: 2524-3470. DOI: 10.1007/s42461-019-0090-6.

[49] Ahmad Nawab, Xinbo Yang, and Rick Honaker. "Parametric study and speciation analysis of rare earth precipitation using oxalic acid in a chloride solution system". In: *Minerals Engineering* 176 (2021), p. 107352. DOI: 10.1016/j.mineng.2021.107352.

[50] Nofriady Aziz et al. "Chemical kinetics of Rare Earth Element (REE) separation by precipitation method". In: *Journal of the Indian Chemical Society* 102.11 (2025), p. 102062. ISSN: 0019-4522. DOI: 10.1016/j.jics.2025.102062.

[51] William M. Haynes, ed. *CRC Handbook of Chemistry and Physics*. 103rd. Boca Raton, FL: CRC Press, 2022. ISBN: 978-1-032-27776-2.

[52] James S. Elliot and Israel N. Rabinowitz. "Calcium Oxalate Crystalluria: Crystal Size in Urine". In: *The Journal of Urology* 123.3 (1980), pp. 324–327. ISSN: 0022-5347. DOI: 10.1016/S0022-5347(17)55918-2. URL: https://www.sciencedirect.com/science/article/pii/S0022534717559182.

[53] Xuzheng Ji et al. "Advances in particulate matter filtration: Materials, performance, and application". In: *Green Energy & Environment* 8.3 (2023), pp. 673–697. ISSN: 2468-0257. DOI: 10.1016/j.gee.2022.03.012.

[54] et al. Lingbo Zhou. "Effect of particle size on the leaching of a weathered crust elution-deposited rare earth ore". In: *Hydrometallurgy* 222 (2023), p. 106200. ISSN: 0304-386X. DOI: 10.1016/j.hydromet.2023.106200.

[55] Scientific Glass Laboratories Ltd. *Physical Properties of Borosilicate Glass 3.3*. n.d. URL: https://www.scientificglass.co.uk/contents/en-uk/d115_Physical_Properties_of_Borosilicate_Glass.html (visited on 05/06/2026).

[56] D. P. Glavin et al. "Abundant ammonia and nitrogen-rich soluble organic matter in samples from asteroid (101955) Bennu". In: *Nature Astronomy* 9.2 (2025), pp. 199–210.

[57] Piet Bergveld. "Thirty years of ISFETOLOGY: What happened in the past 30 years and what may happen in the next 30 years". In: *Sensors and Actuators B: Chemical* 88.1 (2003), pp. 1–20. DOI: 10.1016/S0925-4005(02)00301-5.

[58] Hamilton Company. *GlucoSense Sensor*. 2023. URL: https://www.hamiltoncompany.com/sensors/glucose-sensors/glucosense#specifications.

[59] J. Svenson and I. A. Nicholls. "On the thermal and chemical stability of molecularly imprinted polymers". In: *Analytica Chimica Acta* 435.1 (2001), pp. 19–24.

[60] K. Kumar, Albert J. Jr. Fornace, and Shubhankar Suman. "8-OxodG: A Potential Biomarker for Chronic Oxidative Stress Induced by High-LET Radiation". In: *DNA* 4.3 (2024), pp. 221–238. DOI: 10.3390/dna4030015.

[61] Ja Young Hahm et al. "8-Oxoguanine: from oxidative damage to epigenetic and epitranscriptional modification". In: *Experimental & Molecular Medicine* 54 (2022), pp. 1350–1360. DOI: 10.1038/s12276-022-00822-z.

[62] Qin Chen et al. "Detection of 8-oxo-2'-deoxyguanosine, a marker of oxidative DNA damage, in culture medium from human mesothelial cells exposed to crocidolite asbestos". In: *Carcinogenesis* 17.11 (1996), pp. 2525–2527. DOI: 10.1093/carcin/17.11.2525.

[63] Haotian Cao and Lei et al. Wang. "Hypoxanthine as a Potential Biomarker of Energy Metabolism and Cellular Stress". In: *Metabolites* 9.11 (2019), p. 267. DOI: 10.3390/metabo9110267.

[64] Tomas Lindahl. "Instability and Decay of the Primary Structure of DNA". In: *Nature* 362.6422 (1993), pp. 709–715. DOI: 10.1038/362709a0.

[65] Jean Cadet, Thierry Douki, and Jean-Luc Ravanat. "DNA Base Damage by Reactive Oxygen Species, Oxidizing Agents, and UV Radiation". In: *Cold Spring Harbor Perspectives in Biology* 4.2 (2012), a012559. DOI: 10.1101/cshperspect.a012559.

[66] Hiroshi Kasai. "Analysis of a form of oxidative DNA damage, 8-hydroxyguanine, as a marker of cellular oxidative stress". In: *Mutation Research* 407.1–2 (1998), pp. 1–10.

[67] Kassahn et al. "ATP in the extracellular environment". In: *Cell Stress & Chaperones* 19 (2014), pp. 37–49. DOI: 10.1007/s12192-013-0432-2.

[68] D. E. Atkinson and A. G. Chapman. “Adenylate energy charge in metabolism and cell regulation”. In: *Journal of Bacteriology* 127.1 (1976), pp. 137–144.

[69] D. E. Atkinson. “Energy charge of the adenylate pool as a regulatory parameter”. In: *Nature* 228 (1970), pp. 1299–1300.

[70] Jos H. M. Schippers and Teun Munnik. “NAD(P)H as a central hub in cellular redox regulation”. In: *Journal of Experimental Botany* 67 (2016), pp. 5931–5942. DOI: 10.1093/jxb/erw352.

[71] Graham Noctor, Amna Mhamdi, and Christine H. Foyer. “The roles of reactive oxygen metabolism in plant cells: NADPH and NADH as central redox cofactors”. In: *Plant, Cell & Environment* 33 (2010), pp. 1–17. DOI: 10.1111/j.1365-3040.2009.02046.x.

[72] Sensirion AG. *SLF3x Liquid Flow Sensor — Datasheet*. 2023. URL: https://www.sensirion.com/products/catalog/SLF3S-0600F/.

[73] Honeywell Sensing and Productivity Solutions. *MIPAN Series Miniature Amplified Pressure Sensor — Datasheet*. 2022. URL: https://eu.mouser.com/ProductDetail/Honeywell/MIPAN2XX150PAAAX.

[74] Figaro Engineering Inc. *TGS Gas Sensor Series — Product Specification*. 2022. URL: https://www.figaro.co.jp/en/product/entry/tgs2600.html.

[75] Hamilton Company. *EasyFerm Plus Arc pH Sensor — Datasheet*. 2023. URL: https://www.hamiltoncompany.com/process-analytics/sensors/ph-sensors/easyferm-plus-arc.

[76] Hamilton Company. *VisiFerm DO Arc Dissolved Oxygen Sensor — Datasheet*. 2023. URL: https://www.hamiltoncompany.com/process-analytics/sensors/dissolved-oxygen-sensors/visiferm-do-arc.

[77] Hamilton Company. *CO2NTROL Dissolved CO_2 Sensor — Datasheet*. 2023. URL: https://www.hamiltoncompany.com/process-analytics/sensors/dissolved-co2-sensors/co2ntrol.

[78] Omega Engineering. *Industrial RTD Temperature Sensor with IO-Link/Switch and 4 to 20 mA Outputs*. 2023. URL: https://assets.dwyeromega.com/spec/PRTXI_Specs.pdf.

[79] Kistler Instrumente AG. *Piezoresistive Pressure Sensor Type 4017A — Datasheet*. 2022. URL: https://www.kistler.com/NL/en/cp/miniature-absolute-pressure-sensors-4017a/P0001211.

[80] Aquila Biolabs GmbH. *CGQ BioR Cell Growth Quantifier — Datasheet*. 2023. URL: https://aquila-biolabs.de/wp-content/uploads/2020/09/200914-CGQ-BioR-EN.pdf.

[81] H. et al. Balsiger. “ROSINA — Rosetta Orbiter Spectrometer for Ion and Neutral Analysis”. In: *Space Science Reviews* 128 (2007), pp. 745–801. DOI: 10.1007/s11214-006-8335-3.

[82] Sandra Siljeström et al. “ExoMars Mars Organic Molecule Analyzer (MOMA) Laser Desorption/Ionization Mass Spectrometry (LDI-MS) Analysis of Phototrophic Communities from a Silica-Depositing Hot Spring in Yellowstone National Park, USA”. In: *Astrobiology* 21.12 (2021), pp. 1515–1525. DOI: 10.1089/ast.2020.2368.

[83] NASA. *NASA’s OSIRIS-REx Mission to Asteroid Bennu*. 2026.

[84] B. Gundlach and J. Blum. “A New Method to Determine the Grain Size of Planetary Regolith”. In: *Icarus* 223.1 (2013), pp. 479–492. DOI: 10.1016/j.icarus.2012.11.039.

[85] H. et al. Sierks. “The Dawn Framing Camera”. In: *Space Science Reviews* 163.1–4 (2011), pp. 263–327. DOI: 10.1007/s11214-011-9745-4.

[86] Paolo Martino. *Hera Mission Status Update*. Presentation to the Space Mission Planning Advisory Group (SMPAG). Jan. 2024. URL: https://www.cosmos.esa.int/documents/336356/336472/Hera+mission+update_SMPAG.pdf.

[87] Takahiro Iwata, Kohei Kitazato, and Masanao et al. Abe. “NIRS3: The Near Infrared Spectrometer on Hayabusa2”. In: *Space Science Reviews* 208 (2017), pp. 317–337. DOI: 10.1007/s11214-017-0341-0.

[88] G. et al. Peter. “Developing of MERTIS as an advanced process from the study up to the flight model”. In: *Infrared Remote Sensing and Instrumentation XXI*. Vol. 8867. SPIE. 2013, p. 886707. DOI: 10.1117/12.2024375.

[89] Amy A. et al. Simon. “Widespread carbon-bearing materials on near-Earth asteroid (101955) Bennu”. In: *Science* 370.6517 (2020). DOI: 10.1126/science.abc3522.

[90] Tatsuaki Okada and Tetsuya et al. Fukuhara. “Highly Porous Nature of a Primitive Asteroid Revealed by Thermal Imaging”. In: *Nature* 579.7800 (2020), pp. 518–522. DOI: 10.1038/s41586-020-2102-6.

[91] B. Rozitis and A. J. et al. Ryan. “Asteroid (101955) Bennu’s Weak Boulders and Thermally Anomalous Equator”. In: *Science Advances* 6.41 (2020), eabc3699. DOI: 10.1126/sciadv.abc3699.

[92] D. C. et al. Reuter. "The OSIRIS-REx Visible and InfraRed Spectrometer (OVIRS): Spectral Maps of the Asteroid Bennu". In: *Space Science Reviews* 214.2 (2018), p. 54. DOI: 10.1007/s11214-018-0482-9.

[93] William H. Willcockson. "Stardust Sample Return Capsule Design Experience". In: *Journal of Spacecraft and Rockets* 36.3 (1999), pp. 470–474. DOI: 10.2514/2.3468.

[94] Robert A. Mitcheltree et al. "Aerodynamics of Stardust Sample Return Capsule". In: *Journal of Spacecraft and Rockets* 36.3 (1999), pp. 429–435. DOI: 10.2514/2.3463.

[95] Prasun N. Desai et al. "Entry, Descent, and Landing Operations Analysis for the Stardust Re-Entry Capsule". In: *AIAA/AAS Astrodynamics Specialist Conference and Exhibit*. American Institute of Aeronautics and Astronautics, Aug. 2006. URL: https://ntrs.nasa.gov/citations/20060028186.

[96] NOAA, NASA, and US Air Force. *U.S. Standard Atmosphere, 1976*. Tech. rep. NOAA-S/T 76-1562. Washington, D.C.: U.S. Government Printing Office, 1976.

[97] Michael E. Tauber and Kenneth Sutton. "Stagnation-Point Radiative Heating Relations for Earth and Mars Entries". In: *Journal of Spacecraft and Rockets* 28.1 (1991), pp. 40–42. DOI: 10.2514/3.26206.

[98] R. A. Mitcheltree et al. *An Earth Entry Vehicle for Returning Samples from Mars*. Technical Report NTRS 20010078926. NASA Langley Research Center, 2001.

[99] Kenneth Sutton and Randolph A. Graves. *A General Stagnation-Point Convective-Heating Equation for Arbitrary Gas Mixtures*. Tech. rep. TR R-376. Washington, D.C.: NASA, 1971.

[100] M. A. Covington. "Performance of a Light-Weight Ablative Thermal Protection Material for the Stardust Mission Sample Return Capsule". In: *Proceedings of the 6th International Planetary Probe Workshop*. 2007. URL: https://ntrs.nasa.gov/citations/20070014634.

[101] Huy K. Tran et al. "Phenolic Impregnated Carbon Ablators (PICA) for Discovery Class Missions". In: *31st AIAA Thermophysics Conference*. AIAA Paper 96-1911. 1996. DOI: 10.2514/6.1996-1911.

[102] David Olynick, Yih-Kanq Chen, and Michael E. Tauber. "Aerothermodynamics of the Stardust Sample Return Capsule". In: *Journal of Spacecraft and Rockets* 36.3 (1999), pp. 442–462. DOI: 10.2514/2.3466.

[103] Iain D. Boyd, Kerry A. Trumble, and Michael J. Wright. "Modeling of Stardust Entry at High Altitude, Part 1: Flowfield Analysis". In: *Journal of Spacecraft and Rockets* 47.5 (2010), pp. 708–717. DOI: 10.2514/1.37360.

[104] Peter L. Conley. *Space Vehicle Mechanisms: Elements of Successful Design*. New York: John Wiley & Sons, 1998. ISBN: 978-0-471-14821-4.

[105] Genesis Mishap Investigation Board. *Genesis Mishap Investigation Board Report, Volume I*. Mishap Investigation Report. National Aeronautics and Space Administration (NASA), 2005.

[106] Swedish Space Corporation. *Esrange Space Center User's Manual*. Tech. rep. SSC, 2022.

[107] G. et al. Palermo. "Space Rider: Europe's Reusable Space Transport System". In: *Acta Astronautica* 180 (2021), pp. 483–492.

[108] European Space Agency. *ESA International Relations and Legal Framework for Extra-European Operations*. 2023.

[109] E. et al. Bierhaus. "The OSIRIS-REx Spacecraft and the Touch-and-Go Sample Acquisition Mechanism (TAGSAM)". In: *Space Science Reviews* 214 (Sept. 2018). DOI: 10.1007/s11214-018-0521-6.

[110] M. Verdant and G.H. Schwehm. *The International Rosetta Mission*. Tech. rep. European Space Agency, 1998. URL: https://www.esa.int/esapub/bulletin/bullet93/VER.pdf.

[111] Hexcel Composites. *HONEYCOMB SANDWICH DESIGN TECHNOLOGY*. Hexcel Composites. 2000.

[112] M. et al. Tariq. "Evaluating the mechanical behavior of carbon composites with varied ply-thicknesses using acoustic emission measurements". In: *Journal of Composite Materials* 59 (2 2024). DOI: 10.1177/00219983241297561.

[113] James R Wertz, David F Everett, and Jeffery J Puschell. *Space Mission Engineering: The New SMAD*. Hawthorne, CA: Microcosm Press, 2011.

[114] Michel Bousquet Gerard Maral. $Satellite_{C}ommunications_{S}ystems$. 4th. Hoboken, NJ, USA: John Wiley & Sons, 2002. ISBN: 0 471 49654.

[115] Masanao Abe, Masahiko Arakawa, and Julie et al. Bellerose. *Hayabusa2 Asteroid Sample Return Mission*. 1st ed. Amsterdam, Netherlands: Elsevier, 2022. ISBN: 978-0-323-99731-7.

[116] C. et al. Zeitlin. "Measurements of Energetic Particle Radiation in Transit to Mars on the Mars Science Laboratory". In: *Science* 340.6136 (2013), pp. 1080–1084. DOI: 10.1126/science.1235989.

[117] Dan M Goebel and Ira Katz. *Fundamentals of Electric Propulsion: Ion and Hall Thrusters*. Hoboken, NJ: John Wiley & Sons, 2008.

[118] Manuel Martinez-Sanchez and James E Pollard. "Spacecraft electric propulsion—an overview". In: *Journal of Propulsion and Power* 14.5 (1998), pp. 688–699.

[119] V.-G. Tirila, A. Demairé, and C. N. Ryan. "Review of alternative propellants in Hall thrusters". In: *Acta Astronautica* 212 (2023), pp. 284–306. DOI: 10.1016/j.actaastro.2023.07.047.

[120] T. F. Munro-O'Brien and C. N. Ryan. "Performance of a low power Hall effect thruster with several gaseous propellants". In: *Acta Astronautica* 206 (2023), pp. 257–273. DOI: 10.1016/j.actaastro.2023.01.033.

[121] N. Fazio. *ALTERNATIVE PROPELLANTS FOR GRIDDED ION ENGINES*. Tech. rep. University of Southampton, n.d.

[122] P. Savelev, A. Pashaev, and A. Shumeiko. "Numerical simulation of thermo-throttle for iodine flow rate control in multidirectional plasma thruster". In: *Nuclear Science and Technology Open Research* 1 (2023), p. 12. DOI: 10.12688/nuclscitechnolopenres.17411.1.

[123] ArianeGroup. *Electric Propulsion Systems and Components: Radiofrequency Ion Propulsion for Orbit Raising, Station Keeping and Deep Space Missions*. Tech. rep. ArianeGroup, n.d.

[124] QinetiQ Space. *Electric Propulsion: T5 and T6 Systems*. Tech. rep. QinetiQ, n.d.

[125] J. S. Snyder et al. "Performance Evaluation of the T6 Ion Engine". In: *Journal of Propulsion and Power* 28.2 (2012), pp. 371–379.

[126] John R Brophy et al. "Performance of the NSTAR ion propulsion system on the Deep Space One mission". In: *36th AIAA/ASME/SAE/ASEE Joint Propulsion Conference and Exhibit*. 2000, p. 3816.

[127] John R Brophy et al. "The Dawn spacecraft ion propulsion system". In: *39th AIAA/ASME/SAE/ASEE Joint Propulsion Conference and Exhibit*. 2003, p. 4542.

[128] Kazutaka Nishiyama et al. "Development and Testing of the Hayabusa2 Ion Engine System". In: *34th International Electric Propulsion Conference, Kobe, Japan*. 2015, IEPC–2015–333.

[129] Michael J. Patterson. *NEXT Ion Propulsion System Development Status and Performance*. Tech. rep. NASA/TM-2008-214986. NASA Glenn Research Center, 2008.

[130] Bradford ECAPS. *22N HPGP Thruster Datasheet*. https://satcatalog.s3.amazonaws.com/components/863/SatCatalog_-_Bradford_Space_-_22N_HPGP_-_Datasheet.pdf.

[131] Saft. *Lithium-ion batteries for space*. https://saft.com/en/market-sectors/aerospace-performance/space. 2024.

[132] D. Prevot, Y. Borthomieu, and E. et al. Ligneel. "Performances of Saft Lithium-Ion Cells in LEO Cycling". In: *E3S Web of Conferences* 16 (2017), p. 06005. DOI: 10.1051/e3sconf/20171606005.

[133] Shingo Kameda, Hidehiko Suzuki, and Tomokatsu et al. Takamatsu. "Preflight Calibration Test Results for Optical Navigation Camera Telescope (ONC-T) Onboard the Hayabusa2 Spacecraft". In: *Space Science Reviews* 208 (2017), pp. 17–31. DOI: 10.1007/s11214-015-0227-y.

[134] Eri Tatsumi, Toru Kouyama, and Hidehiko et al. Suzuki. "Updated inflight calibration of Hayabusa2's optical navigation camera (ONC) for scientific observations during the cruise phase". In: *Icarus* 325 (2019), pp. 153–195. DOI: 10.1016/j.icarus.2019.01.015.

[135] Frontgrade Gaisler. *GR712RC Dual-Core LEON3-FT SPARC V8 Processor — Data Sheet*. https://www.gaisler.com/products/gr712rc. 2023.

[136] Authors. *Supercritical Xe as Propellant in Satellite Electric Propulsion System: Experimental Study on Thermal Physical Properties*. 2019.

[137] J. et al. Lehec. *Cryogenic liquid storage system for a spacecraft*. Patent US 8,893,514 B2. 2014.

[138] Ryan P. Gilligan and Thomas M. Tomsik. *Modeling Xenon Tank Pressurization Using One-Dimensional Thermodynamic and Heat Transfer Models*. Tech. rep. NTRS 20170004518. NASA Glenn Research Center, 2017.

[139] Jena-Optronik. *Autonomous Star Sensor ASTRO APS*. Data Sheet. Jena-Optronik GmbH, 2015.

[140] José Meseguer, Isabel Pérez-Grande, and Angel Sanz-Andrés. *Spacecraft Thermal Control*. Cambridge, UK: Woodhead Publishing, 2012. ISBN: 978-1-84569-996-3.

[141] David G. Gilmore, ed. *Spacecraft Thermal Control Handbook*. 2nd. Vol. 1. Reston, VA: AIAA, 2002.

[142] M. M. et al. Joybari. "Cooling of air using heptadecane phase change material in shell and tube arrangement: Analytical and experimental study". In: *Energy and Buildings* (2014). DOI: 10.1016/j.enbuild.2014.09.018.

[143] Exail. *Astrix NS – IMU: High Accuracy 6-axis Space Fiber-Optic Gyroscope IMU*. Data Sheet V002. Exail, 2025.

[144] Bradford Engineering. *Coarse Sun Sensor*. Data Sheet. Bradford Engineering BV, 2017.

[145] JAXA. *Hayabusa2 Information Fact Sheet*. Fact Sheet. JAXA, 2018.

[146] Bradford Space. *Reaction Wheel Unit W18*. 2025.

[147] B. T. C. Zandbergen. *Spacecraft Design: Reader AE1222-II*. TU Delft, 2020.

[148] Navid S. Fatemi et al. "Performance of High-Efficiency Advanced Triple-Junction Solar Panels for the LILT Mission Dawn". In: *Conference Record of the Thirty-first IEEE Photovoltaic Specialists Conference*. 2005, pp. 818–821. DOI: 10.1109/PVSC.2005.1488260.

[149] Sei-ichiro et al. Watanabe. "Hayabusa2 Mission Overview". In: *Space Science Reviews* 208 (2017), pp. 3–16. DOI: 10.1007/s11214-017-0377-1.

[150] Benkhoff et al. "BepiColombo: Mission Overview and Science Goals". In: *Space Science Reviews* 217.8 (2021), p. 90. DOI: 10.1007/s11214-021-00861-4.

[151] Niels F.W. Ligterink. *SILICON SHEPHERD: HERDING MICROBES TO MINE THE SOLAR SYSTEM - Project Guide*. Design Synthesis Exercise Issue 6. TU Delft, 2026.

[152] European Space Agency. *Q & A — Call for Fast (F) Mission 2018*. ESA Cosmos. 2018. URL: https://www.cosmos.esa.int/web/call-for-fast-mission-2018/q-a.

[153] NASA. *Space Systems Engineering: Cost Estimating Module, version 1.0*. NASA Space Systems Engineering / SSRI Knowledge Base. URL: https://s3vi.ndc.nasa.gov/ssri-kb/static/resources/18.%20Cost_Module_V1.0.pdf.

[154] European Space Agency. *Hera — ESOC Operations Portal*. ESA ESOC. 2020. URL: https://esoc.esa.int/content/hera.

[155] Jeff Foust. *Falcon 9 launches ESA's Hera asteroid mission*. SpaceNews. 2024. URL: https://spacenews.com/falcon-9-launches-esas-hera-asteroid-mission/.

[156] Howard E. McCurdy. *Low-Cost Innovation in Spaceflight: The Near Earth Asteroid Rendezvous (NEAR) Shoemaker Mission*. Tech. rep. NASA SP-2005-4536. NASA, 2005. URL: https://ntrs.nasa.gov/citations/20050159707.

[157] JHU/APL. "NEAR Program Cost: Faster, Better, Cheaper in Practice". In: *Proc. AIAA/USU Conference on Small Satellites*. 1996. URL: https://digitalcommons.usu.edu/smallsat/1996/all1996/75.

[158] Joan Pau et al. Sánchez. "ESA F-Class Comet Interceptor: Trajectory Design to Intercept a Yet-to-be-discovered Comet". In: (2021). URL: https://www.researchgate.net/publication/353544654.

[159] Wikipedia. *Ariane 6*. 2024. URL: https://en.wikipedia.org/wiki/Ariane_6.

[160] European Spaceflight. *ESA Spent €82 Million to Launch Sentinel-1D Satellite on Ariane 6*. 2026. URL: https://europeanspaceflight.com/esa-spent-e82-million-to-launch-sentinel-1d-satellite-on-ariane-6/.

[161] SRE-PA and D-TEC staff. *Margin Philosophy for Science Assessment Studies*. Technical Note SRE-PA/2011.097, Issue 1 Revision 3. European Space Agency, June 2012.

[162] William F. McDonough and S.-s. Sun. "The composition of the Earth". In: *Chemical Geology* 120.3–4 (1995), pp. 223–253. DOI: 10.1016/0009-2541(94)00140-4.

[163] Argus Media. *Argus Rare Earths Monthly Outlook, Issue 24-6*. Tech. rep. Argus Media Group, 2024.

[164] Dante S. Lauretta and Harold C. Jr. Connolly. "Asteroid (101955) Bennu in the laboratory: Properties of the sample collected by OSIRIS-REx". In: (2024). DOI: 10.1111/maps.14227.

[165] Grand View Research. *Rare Earth Elements Market Size, Share & Trends Analysis Report, 2025–2030*. 2025. URL: https://www.grandviewresearch.com/industry-analysis/rare-earth-elements-market.

[166] Fact.MR. *Rare Earth Elements Market – Global Market Analysis Report 2026–2036*. 2026. URL: https://www.factmr.com/report/rare-earth-elements-market.

[167] Spherical Insights & Consulting. *Global Asteroid Mining Market Size, Forecast 2025–2035*. 2025. URL: https://www.sphericalinsights.com/reports/asteroid-mining-market.

[168] The Business Research Company. *Asteroid Mining Global Market Report 2026*. 2026. URL: https://www.thebusinessresearchcompany.com/report/asteroid-mining-global-market-report.

[169] ISO. *ISO 16290:2013 Space systems — Definition of the Technology Readiness Levels*. Standard. ISO, 2013.

[170] U.S. Government Accountability Office. *Technology Readiness Assessment Guide: Best Practices for Evaluating the Readiness of Technology for Use in Acquisition Programs and Projects*. Tech. rep. GAO-20-48G. GAO, 2020. URL: https://www.gao.gov/products/gao-20-48g.

[171] European Space Agency. *ESA Space Resources Strategy*. Tech. rep. ESA, 2019. URL: https://sci.esa.int/documents/34161/35992/1567260390250-ESA_Space_Resources_Strategy.pdf.

[172] Ollama. *Qwen3-Coder Library Page*. URL: https://ollama.com/library/qwen3-coder.

[173] ESA. *Space System Life Cycle Assessment (LCA) Handbook, Issue 2*. Tech. rep. ESSB-HB-U-005, Issue 2. ESA, 2026.

[174] Kjell Anflo and Robert Möllerberg. "Flight demonstration of new thruster and green propellant technology on the PRISMA satellite". In: *Acta Astronautica* 65.9–10 (2009), pp. 1238–1249. DOI: 10.1016/j.actaastro.2009.03.056.

[175] Mathias Persson, Kjell Anflo, and Peter Friedhoff. "Flight Heritage of Ammonium Dinitramide (ADN) Based High Performance Green Propulsion (HPGP) Systems". In: *Propellants, Explosives, Pyrotechnics* 44.9 (2019), pp. 1073–1080. DOI: 10.1002/prep.201900248.

[176] European Space Agency (ESA). *ECSS Planetary Protection Standard*. Standard. European Space Agency, 2024. URL: https://technology.esa.int/upload/media/ECSS-Planetary-Protection-Standard-ECSS-U-ST-20C.pdf.

[177] ECSS. *Space Engineering — Electrical and Electronic*. Tech. rep. ECSS-E-ST-20C. ECSS, 2008.

[178] ESA Space Debris Mitigation Working Group. *ESA Space Debris Mitigation Requirements*. Tech. rep. ESSB-ST-U-007, Issue 1 Rev.1. ESA, 2025.

[179] Pavel Koltun and Ambalavanar Tharumarajah. "Life Cycle Impact of Rare Earth Elements". In: *International Scholarly Research Notices* 2014 (2014), p. 907536. DOI: 10.1155/2014/907536.

[180] Ehsan Vahidi, Julie Navarro, and Fu Zhao. "An initial life cycle assessment of rare earth oxides production from ion-adsorption clays". In: *Resources, Conservation and Recycling* 113 (2016), pp. 1–11. DOI: 10.1016/j.resconrec.2016.05.006.

[181] Andrea Schreiber, Josefine Marx, and Petra Zapp. "Life cycle assessment studies of rare earths production – Findings from a systematic review". In: *Science of the Total Environment* 791 (2021), p. 148257. DOI: 10.1016/j.scitotenv.2021.148257.

[182] UN General Assembly. *Transforming Our World:* tech. rep. A/RES/70/1. United Nations, 2015.

[183] ECSS. *Space project management - Risk management*. Standard ECSS-M-ST-80C. ESA Requirements and Standards Division, 2008.

[184] Stefano et al. Campagnola. "Mission analysis for the Martian Moons eXploration (MMX) mission". In: *Acta Astronautica* (2021).

[185] COSPAR Panel on Planetary Protection. *COSPAR Policy on Planetary Protection*. Tech. rep. COSPAR, 2024.

[186] C. E. et al. Mario. "Autonomous Navigation Performance Using Natural Feature Tracking during the OSIRIS-REx Touch-and-Go Sample Collection Event". In: *The Planetary Science Journal* 3.5 (2022), p. 114. DOI: 10.3847/PSJ/ac5183.

[187] NASA. "ICES 2021 - Article". In: NASA Technical Reports Server (NTRS). 2021. URL: https://ntrs.nasa.gov/citations/20210010411.

[188] N. et al. "Microfluidics and Macrofluidics in Space: ISS-Proven Fluidic Transport and Handling Concepts". In: *Frontiers in Space Technologies* 2 (2022), p. 9696. URL: https://ui.adsabs.harvard.edu/abs/2022FrST...2.9696N/abstract.

[189] Zengqian et al. Hou. "In search of signs of life on Mars with China's sample return mission Tianwen-3". In: *Nature Astronomy* 9.6 (2025), pp. 783–792. DOI: 10.1038/s41550-025-02572-0.

[190] Abbey A. et al. Donaldson. *NASA Selects International Space Station US Deorbit Vehicle*. NASA, June 2024. URL: https://tinyurl.com/mw35b8bm.

[191] TU Delft. *Kleine chip, grootse missie: op zoek naar tekenen van buitenaards leven*. Delft University of Technology, Apr. 2022. URL: https://tinyurl.com/u97xsxh4.